Sample Preparation Methodologies for MALDI MS Imaging and Related Topics

Caroline Jane Earnshaw

A thesis submitted in partial fulfilment of the requirements of Sheffield Hallam University for the degree of Doctor of Philosophy

May 2009

Acknowledgements

I would like to take this opportunity to thank my supervisor, Professor Malcolm Clench, for his support throughout my Ph.D. and the rest of the mass spectrometry group at Sheffield Hallam University both past and present for the fantastic three and a half years that I have had.

I would also like to express my gratitude to the charitable organisations responsible for my funding; EPSRC and RSC.

I feel privileged to have attended numerous conferences both nationally and internationally and would like to thank the BMSS and ASMS for their generous travel grants.

I would also like to extend my thanks to Dr Klaus Dreisewerd, University of Münster, Germany, Dr Peter Marshall, GSK, Dr Don Richards, Pfizer, Dr Alan Barnes, Shimadzu, Dr Marten Snel and Emmanuelle Claude, Waters, Professor Nicola Woodroofe, Sheffield Hallam University and Dr Chris Bolton, Queen Mary, University of London for useful scientific discussions.

And finally, I would like to thank my family and friends for their love, encouragement and support.

Abstract

The diverse applications of MALDI MSI are explored in this thesis with an emphasis on the sample preparation procedure and method development for small molecule analysis for a range of samples. The two main themes that have been focussed on are the pharmaceutical and metabolomic applications of this state of the art technique.

MALDI MSI has been evaluated as a technique for the detection and imaging of anti-asthmatic compounds in lung tissue. Four compounds were assessed initially with conventional MALDI MS experiments, followed by both direct and indirect tissue imaging experiments.

Pharmaceutical tablet formulations have also been assessed using MALDI MSI to map the active component throughout the excipients contained within the tablet providing information that is critical to the manufacturing process such as the homogeneity of the active pharmaceutical ingredient (API) throughout the tablet.

MALDI MSI has been applied to the relatively new addition to the 'omics sciences, metabolomics. A non-targeted metabolomics approach has been used to study both plant and animal tissue in an attempt to gain a greater understanding of the complex biological processes that occur within both types of tissue.

Wheat grain was used as the model system to conduct the experiments and evaluate the application of both UV MALDI MS and IR LDI MS for plant metabolomics. These techniques provided complementary information to published literature, however the novel aspect of this study was the incorporation of imaging experiments for UV MALDI MS; this allowed the metabolites to be visualised in the wheat grain section.

MALDI MSI was also used to explore the differences between mice with chronic relapsing experimental autoimmune encephalomyelitis; the animal model of multiple sclerosis alongside healthy controls. Spinal cord samples were analysed and the main difference was tentatively attributed to choline levels.

CONTENTS

LIST OF FIGURES

Chapter 1

Chapter 2

Chapter 3

Chapter 4

Chapter 5

LIST OF TABLES

Chapter 4

Chapter 5

Abbreviations

3-HPA	3-Hydroxypicolinic acid
9-AA	9-aminoacridine
α-CHCA	Alpha-cyano-4-hydroxycinnamic acid
μE	MicroEinstein
ABH	Antibody high
amu	Atomic mass unit
APCI	Atmospheric pressure chemical ionisation
API	Active pharmaceutical ingredient
AR	Analytical reagent
ATP	Adenosine triphosphate
CFA	Complete Freund's adjuvant
CI	Chemical ionisation
CID	Collision induced dissociation
CMC	Carboxymethyl cellulose
CNS	Central Nervous System
COPD	Chronic obstructive pulmonary disease
CREAE	Chronic relapsing experimental autoimmune encephalomyelitis
CTAB	Cetrimonium bromide
Da	Dalton
DESI	Desorption electrospray ionisation
DHB	2, 5-Dihydroxybenzoic acid
DIOS	Desorption/ionisation on silicon
DNA	Deoxyribose nucleic acid
DPA	Days post anthesis

EI	Electron ionisation
Er:YAG	Erbium:Yttrium aluminium garnet
ESI	Electrospray ionisation
EtOH	Ethanol
F20TPP	5, 10, 15, 20-Tetrakis (pentafluorophenyl) porphyrin
FA	Ferulic acid
FAB	Fast atom/ion bombardment
FDA	Food and Drug Administration
FP	Fluticasone propionate
FWHM	Full-width-at-half-maximum
GC-MS	Gas chromatography mass spectrometry
GM	Genetically modified
GSK	GlaxoSmithKline
H&E	Haematoxylin and eosin
HPLC	High performance liquid chromatography
Hz	Hertz
ICS	Inhaled corticosteroids
IFA	Incomplete Freund's adjuvant
IR	Infrared
IUPAC	International union of pure and applied chemistry
KEGG	Kyoto encyclopedia of genes and genomes
LC-MS	Liquid chromatography mass spectrometry
LDI MS	Laser desorption ionisation mass spectrometry
LMI	Liquid metal ions
M	Molar
MALDI	Matrix-assisted laser desorption/ionisation

Mb	Megabase
MFX	Micro-focus X-ray
MRI	Magnetic resonance imaging
mRNA	Messenger ribose nucleic acid
MRS	Magnetic resonance spectroscopy
MS/MS	Tandem mass spectrometry
MSI	Mass spectrometry imaging
m/z	Mass-to-charge ratio
NADH	Nicotinamide adenine dinucleotide
Nd:YAG	Neodymium:Yttrium aluminium garnet
NIR	Near infra red
NMR	Nuclear magnetic resonance
OCT	Optimum cutting temperature
oTOF MS	Orthogonal time-of-flight mass spectrometry
PAT	Process analytical technology
PBS	Phosphate buffered saline
PCA	Principal component analysis
PET	Positron emission tomography
ppm	Parts per million
QTOF	Quadrupole time of flight
r.f.	Radio frequency
SA	Sinapinic acid
SIMS	Secondary ion mass spectrometry
TDC	Time-to-digital converter
TFA	Trifluoroacetic acid
TiO_2	Titanium dioxide

TOF MS	Time-of-flight mass spectrometry
UHQ	Ultra High Quality
UV	Ultra violet

Chapter 1

Introduction

1.1 Introduction to Mass Spectrometry

Mass spectrometry is an analytical technique that is used to measure the masses of individual molecules or atoms by the determination of the mass to charge ratio (m/z). There are three fundamental parts to a mass spectrometer: the ionisation source; the analyser and the detector. Initially the sample is introduced into the ionisation source either directly or indirectly. The ions formed are then subjected to electrostatic and / or magnetic fields that direct the ions into the mass analyser where they are separated according to their m/z values [1]. The detector converts ion energy into electrical signals; these signals are subsequently transmitted to a computer and information regarding m/z values and their corresponding relative abundances are collected and presented in the form of a mass spectrum. The mass spectrometer operates under high vacuum of ~ 10^{-4} – 10^{-8} Torr to enable the ions to travel without interference from air molecules [2]. In recent years, technological improvements have made it possible to analyse a multitude of diverse samples and it is for this reason that mass spectrometry is such an invaluable technique in the biomedical sciences. Mass spectrometry has a prominence in many areas of science; the scope of which encompasses physics, biology, chemistry, material science and environmental sciences. The hallmarks of mass spectrometry include excellent sensitivity, molecular specificity and versatility.

1.2 Ionisation Sources

There are many methods of ionisation available to produce ions in the gas phase: electron ionisation (EI) [3]; chemical ionisation (CI) [4]; fast atom/ion bombardment (FAB) [5]; secondary ion mass spectrometry (SIMS) [6]; electrospray ionisation (ESI) [7]; nanoelectrospray ionisation (nanoESI) [8]; atmospheric pressure chemical ionisation (APCI) [9]; desorption/ionisation on silicon (DIOS) [10]; desorption electrospray ionisation (DESI) [11] and matrix-assisted laser desorption/ionisation (MALDI) [12, 13].

In the past, mass spectrometry was primarily carried out using EI as the ionisation source; however, a major limitation was that researchers were only able to detect

small molecules [14]. This encouraged researchers to develop alternative ionisation sources (examples include FAB, MALDI and ESI) that could enable them to study a range of biomolecules. The advent of ESI and MALDI ionisation techniques have permitted the analysis of biomolecules with unprecedented accuracy and speed; leading to this type of mass spectrometry being an integral part of biochemistry and medicine. MALDI and ESI are now the ionisation sources of choice for the majority of biomedical applications.

1.2.3 Spray Ionisation Techniques

Spray techniques were introduced to enable the direct sampling of solutions such as biological fluids and eluents from chromatographic techniques coupled to the mass spectrometer as liquids are not suited to the vacuum in the mass spectrometer.

1.2.3.1 Atmospheric Pressure Chemical Ionisation (APCI)

APCI can be used for the analysis of non-volatile samples without the requirement to first convert them to a gaseous state; analysis of liquids is achieved by the spraying of the samples directly into the ion source. The ionisation is similar to CI whereby gas-phase ion-molecule charge transfer reactions take place with the reagent gas ions and the analyte molecules [9]. The analyte solution is vaporised using heat and desolvated before interacting with the corona discharge; this results in ion formation [15]. At atmospheric pressure ions can be involved in more ion-molecule collisions, and therefore APCI is a more sensitive technique than that of CI.

1.2.3.2 Electrospray Ionisation (ESI)

ESI, a concept introduced in the late 1960's by Dole *et al.* [7], is an atmospheric ionisation technique that can be used for the analysis of biomolecules and is often the ionisation interface used in conjunction with liquid chromatography. In the mid-1980's ESI was coupled to mass spectrometry by Fenn *et al.* [16]; this was applied to

the analysis of biomolecules in 1989 [17]. The liquid sample is injected into a capillary and on exiting the capillary a fine mist of charged droplets is produced brought about by the potential difference between the capillary tip and the surrounding atmospheric pressure area. Nitrogen gas is present near the ESI interface to facilitate the evaporation of solvent from the charged droplets. Prior to mass analysis the ions enter a region under high vacuum and are desolvated.

1.2.4 Desorption Ionisation Techniques

Desorption ionisation techniques were introduced due to the limitations with both electron ionisation and chemical ionisation as these types of ionisation are not suitable for compounds that are thermally labile. Biological samples contain a diverse array of compounds that are often thermally labile and non volatile. Thus the introduction of desorption ionisation techniques has allowed for the analysis of many more biomolecules beyond the 100,000Da mass range [12].

1.2.4.1 Secondary Ion Mass Spectrometry (SIMS)

SIMS is a surface analysis technique where the sample surface is irradiated with a high energy primary ion beam such as liquid metal ions (LMI), for example Ga^+ or In^+ [18, 19]. This results in the ejection of atomic secondary ions and molecular fragments from the sample surface. The secondary ions are then mass analysed. Good lateral resolution can be achieved using this technique. The introduction of cluster ion beams and time-of-flight (TOF)-MS analysers has widened the scope for SIMS applications [20].

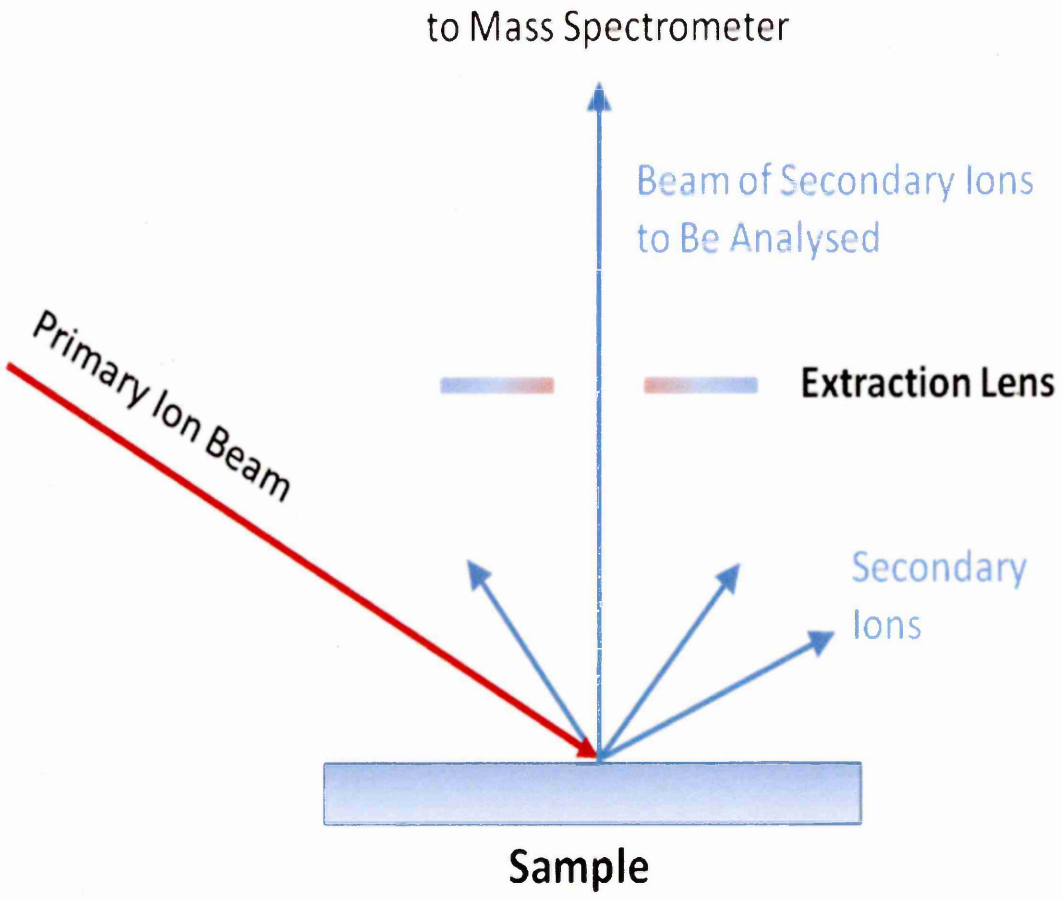

Figure 1.1: Schematic Diagram of the SIMS Ionisation Process. The primary ion beam irradiates the sample surface resulting in the formation of atomic secondary ions and molecular fragments being ejected from the surface of the sample. Adapted from [21].

1.2.4.2 Fast Atom/Ion Bombardment (FAB)

Developed and pioneered by Barber and co-workers in the 1980's [5] FAB originated from SIMS [6]. FAB differs from SIMS in three ways; first, samples to be analysed are dissolved in a matrix, for example glycerol, in order to prolong the sample current duration, secondly, a beam of high energy atoms is used instead of ions – this change enabled FAB to be used with magnetic sector mass spectrometers, and, thirdly, it is considered to be a softer ionisation technique than SIMS. It has been likened to MALDI as it incorporates a matrix and produces intact protonated and deprotonated molecules [22].

A FAB gun utilises inert gas atoms (Ar or Xe) to generate the fast beam of atoms used to bombard the sample; the ions produced are then extracted, accelerated and mass analysed [23, 24].

1.2.4.3 Desorption/Ionisation On Silicon (DIOS)

Suizdak *et al.* introduced DIOS [10] in an attempt to avoid interfering matrix background signals that are apparent in MALDI analysis. This technique replaces the conventional mixing of the matrix and sample; instead samples are placed directly onto a modified porous silicon surface and are then bombarded with a laser beam [25]. This method of desorption has been used for the analysis of carbohydrates [26], peptides [27, 28] and small drug molecules [29]. The presence of high concentrations of salts is not detrimental to analysis.

1.2.4.4 Desorption Electrospray Ionisation (DESI)

Pioneered by Cooks and co-workers [11], DESI is a relatively new ionisation technique whereby samples can be investigated rapidly (within seconds) in their native environment requiring minimal sample preparation. The DESI process involves charged droplets generated by electrospray ionisation being directed onto the sample surface, where on impact with the sample surface results in the ejection of

charged particles that can be measured by the mass spectrometer producing mass spectra similar in appearance to those generated by ESI [11]. DESI has been used to investigate a variety of pharmaceutical samples such as tablets [30, 31, 32] and illicit tablets [33], and plant material [34].

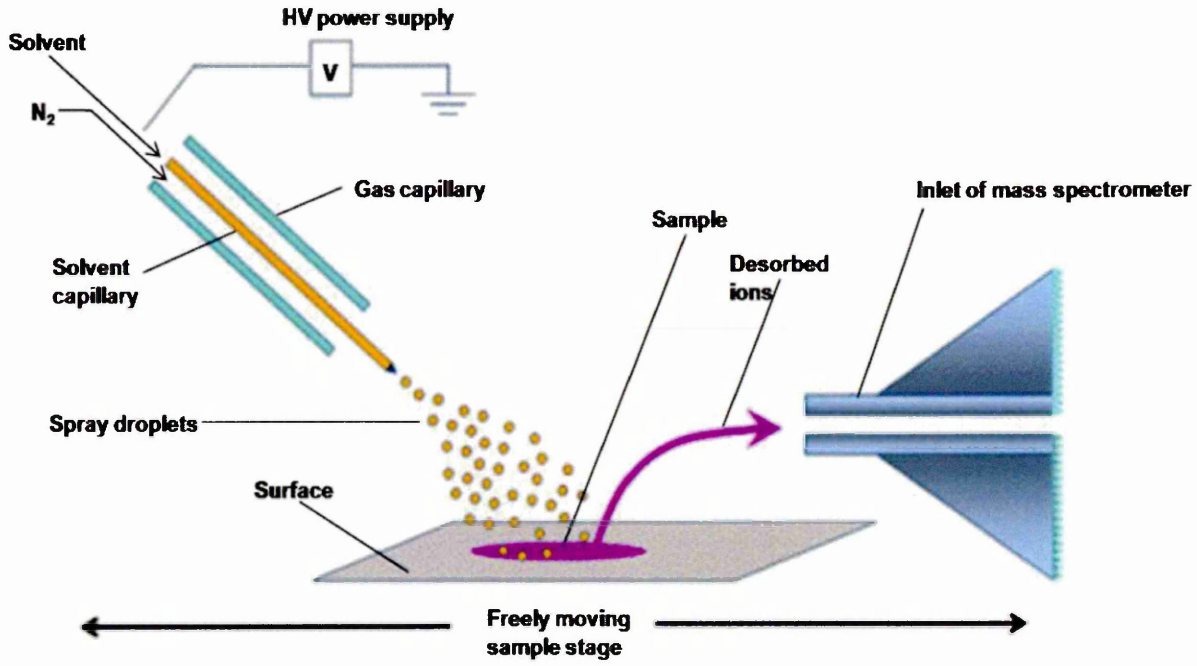

Figure 1.2: Schematic Diagram of the DESI Instrumentation. The charged droplets from the DESI emitter are directed onto the sample surface; the resulting impact causes the ejection of charged particles that are extracted via the sampling capillary [35].

1.2.4.5 Matrix-Assisted Laser Desorption Ionisation (MALDI)

Matrix-Assisted Laser Desorption Ionisation Mass Spectrometry, a soft ionisation technique, was developed in the late 1980's through the work conducted by Tanaka [12] and Hillenkamp [13]. This method of ionisation improved on former laser mass spectrometry techniques by incorporating a laser-absorbing matrix to minimise fragmentation that was observed with laser desorption ionisation mass spectrometry (LDI MS) [36]. The use of a chemical matrix facilitates the energy transfer between the matrix and the analyte. Despite the extensive use and acceptance of MALDI within the scientific community, the underlying ionisation mechanisms are still not well understood and many different theories have been put forward; however, it is sufficient to say that no one mechanism can explain all the ions formed in a MALDI experiment [37]. The proposed mechanisms are discussed in section 1.3.

The first stage in MALDI MS is to select a matrix to enable analysis to be performed on the compound of interest. A matrix usually consists of small organic molecules in a solvent solution and its role is to absorb energy at the laser wavelength. The matrix can be applied to the analyte in many different ways and analysis can be performed once the matrix has co-crystallised with the analyte, resulting in a solid deposit of analyte molecules embedded in the matrix.

During MALDI analysis the laser fires at the sample and irradiates the crystals causing rapid heating of the crystals to occur which leads to localised sublimation. This results in a plume of gaseous phase matrix containing the intact analyte and it is during this process that ionisation occurs. The three most important processes for ion formation to occur are: the close contact of the matrix and analyte molecules; analyte desorption from the sample surface; and, finally, efficient ionisation [38].

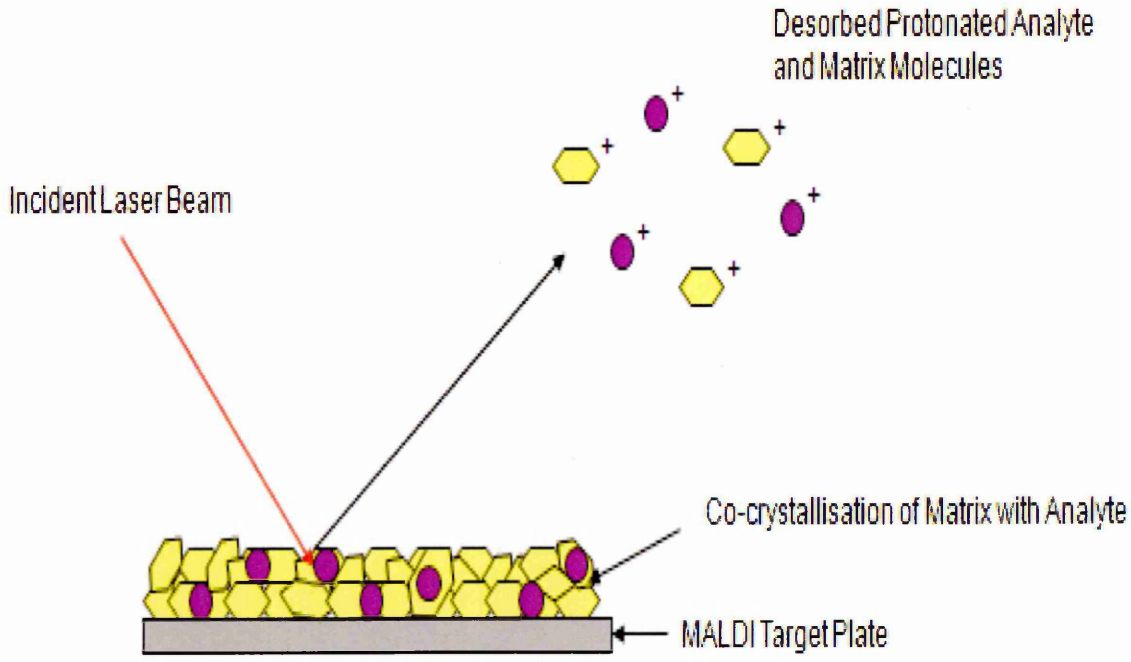

Figure 1.3: Schematic Diagram of the MALDI Process in Positive Ion Mode. The laser irradiation of the sample results in the desorption of molecules, generating the gas plume where it is thought ionisation occurs.

1.3 Ion Formation Mechanisms in UV-MALDI

The ion formation mechanisms associated with ultra violet (UV)-MALDI have been investigated and some of the theories may also apply to infra red (IR)-MALDI.
The underlying mechanisms require further investigation in order to develop more standardised methodologies that take into account all the variables that affect the results obtained in relation to sensitivity and reproducibility [39].

The main variables are as follows:

- Matrix selection
- Physical and chemical analyte characteristics
- Concentrations of both the matrix and the analyte
- Sample preparation methodology
- Features associated with the laser
- Local environment, for example temperature

There are many different theories regarding the reactions that occur in ion formation in the MALDI process. There is an increasing consensus amongst researchers that a two-step model exists, where there is a primary ionisation event followed by extensive secondary reactions in the plume.
The foremost primary ionisation steps include cluster reactions with preformed ions and pooling mediated photoionisation of the matrix. Although the exact reaction mechanisms associated with MALDI are not yet fully understood, there have been many proposed theories [39]. The importance of secondary reactions is highlighted by the fact that many molecules present themselves in spectra in their protonated form [40, 41].

1.3.1 Primary Ion Formation

1.3.1.1 The Cluster Model

Introduced by Karas *et al.*[42], this model assumes that large protonated analyte clusters are preformed in the chemical matrix [43].

The concept behind the cluster model is that post-irradiation of the sample by the laser, the clusters are desorbed and in the gas phase neutral matrix molecules are desolvated and analyte ions are created.

1.3.1.2 Multiphoton Ionisation

This is the simplest explanation for ion formation brought about by the transfer of energy from the matrix to the sample; it can be represented by the following equation whereby a matrix cation radical is formed [36]:

$$M \xrightarrow{n(h\nu)} M^{+\cdot} + e^{-}$$

M = Matrix Molecule

$M^{+\cdot}$ =Radical cation

e^{-} = electron

h = Planck's constant (the proportionality constant between the photon energy (E) and the frequency of the corresponding radiation frequency)

v = radiation frequency (electromagnetic wave)

1.3.1.3 Gas-phase Proton Transfer

Reactions between matrix molecules do occur in the plume; the formation of reaction intermediates may be a fundamental requirement for the protonation of analytes [40].

Protonated matrix formation:

$$M^{+\cdot} + M \longrightarrow MH^{+} + (M - H)^{\cdot}$$

The radical formed in the above reaction can be converted into $(M - H)^{-}$ if it reacts with a free electron:

$$(M - H)^{\cdot} + e^{-} \longrightarrow (M - H)^{-}$$

Reactions can also occur between the matrix and the analyte; very often these reactions produce protonated species. These are thought to occur after secondary proton transfer reactions have taken place in the plume:

$$MH^{+} + A \longrightarrow M + AH^{+}$$

The creation of ions by gas phase reactions has been reported as a feasible mechanism for ionisation by Wang *et al.* [44].

1.3.1.4 Energy Pooling

This details the role of MALDI matrix excitation states and explains the energetic processes underpinning a 'diffusely excited solid'. The internal energy of two or more excited state matrix molecules combine ('pool' together, as represented in the equation as M*M*) to form one matrix radical cation ($M^{+\cdot}$) [39].

This approach is conceivable as clusters often form in MALDI plumes; the following equations detail the process:

$$MM \xrightarrow{2h\nu} M^{*}M^{*} \longrightarrow M + M^{+\cdot} + e^{-}$$

$$M^{*}M^{*} + A \longrightarrow MM + A^{+\cdot} + e^{-}$$

1.3.1.5 Excited-State Proton Transfer

This is a popular theory that involves one photon where a single excited matrix molecule (M*) can efficiently transfer a labile proton to the analyte / matrix molecule in the ground state [45].

The following equations detail this theory:

$$M + h\nu \longrightarrow M^*$$

$$M^* + A \longrightarrow (M - H)^- + AH^+$$

$$M^* + M \longrightarrow (M\text{-}H)^- + MH^+$$

1.3.1.6 Disproportionation Reactions

It is proposed that disproportionation reactions may hold the key to the fact that some matrices perform better in positive ion mode and others in negative ion mode [46, 47]. The following equation displays this theory:

$$2M \xrightarrow{nh\nu} (MM)^* \longrightarrow (M - H)^- + MH^+$$

1.3.1.7 Desorption of Preformed Ions

Another proposal is that the ions are preformed and that the laser pulse liberates them resulting in their desorption [48].

1.3.1.8 Thermal Ionisation

Thermal ionisation is a very likely mechanism when particle suspension matrices have been utilised in the experiment. This is because this particular type of matrix is composed of fine particles and these particles do not possess a chromophore or have the ability to co-crystallise with the analyte. Thermal ionisation can occur in two

ways: at the particle surface as expressed using the Saha-Langmuir equation [49] or via a disproportionation reaction that incorporates the electron affinity of the matrix. It has also been inferred that laser-induced damage on the crystalline surface, approximately 1 μm in thickness, causes desorption of ions to occur. When an IR laser is used the laser penetrates much deeper into the sample [39, 50].

1.3.2 Secondary Ion Formation

1.3.2.1 Electron Transfer

A feasible reaction in the plume may involve electron transfer; this process is detailed in the following equation whereby reactions are thought to occur between the matrix radical cation and an analyte molecule:

$$M^{+\cdot} + A \leftrightarrow M + A^{+\cdot}$$

Electron transfer has been put forward as a possible mechanism that is thought to occur when the compounds of interest have low ionisation energies [50].

1.3.2.2 Proton Transfer

Gas phase proton transfer reactions with neutral matrix and neutral analyte molecules, when the primary ions are radical cations, have been reported [41].
The free energy change (ΔG) of matrix-analyte and analyte-analyte reactions in the plume can be selected in the mass spectrum.

$$\Delta G = -RT\ln(K)$$

K: calculated from the relative abundances of ions in the mass spectrum that are thought to be involved in charge transfer reactions in the plume [39, 50].

1.3.2.3 Cationisation

Cationisation is the term given to the process where the analyte is primarily ionised by forming metal ion adducts. This has been shown to be a process commonly observed with carbohydrates and synthetic polymers [51, 52].

Gas-phase cationisation has been an observed reaction in a number of publications along with other gas-phase reactions [53-56].

Zhang *et al.* have investigated the role of the matrix in the cationisation process [56].

1.3.3 Ion Suppression Effects

Matrix suppression of the analyte, brought about by secondary ion reactions, is the most common type of suppression that occurs during the MALDI process [57].

Donegan and co-workers successfully managed to reduce the matrix suppression effect on small molecules by spray coating the MALDI target plate with a solution containing nitrocellulose and alpha-cyano-4-hydroxycinnamic acid (α-CHCA ~1-2mg/mL in acetone); however, the experiments performed were limited to conventional MALDI analysis. This technique was a different slant on the dried-droplet technique, but this method has not been documented for the analysis of tissue samples [57].

1.4 The Desorption Process

As with the mechanisms for ionisation, there are many theories put forward as to how the desorption process occurs. The thermal spike model details how low laser fluence irradiation of the sample results in heating of the sample, causing the sublimation of matrix molecules. However, if the laser intensity is increased beyond a certain point a rapid increase in desorption efficiency is observed [58]. Another desorption hypothesis that has been put forward is the pressure-pulse theory. This is based on the pressure gradient that is observed normal to the surface where the desorption of large molecules is enhanced by colliding them with high speed matrix

molecules [59]. More recently, the Quasi thermal model was introduced by Hillenkamps' research group where the co-crystallised analyte/matrix combination undergoes pressure related decomposition, forming smaller particles. The smaller particles (clusters and /or single molecules) are desorbed via thermal effects exerted thus creating the MALDI plume where these particles undergo collisions, resulting in the formation of the matrix and analyte gas phase species by expansion cooling [60, 61]. An important factor in promoting efficient desorption is thought to be reliant on the thermodynamic properties of the matrix. The MALDI response has been shown to be affected by sample morphology [62]; this could potentially alter the desorption/ablation process.

1.5 The Mass Analyser

There are many different types of mass analyser that operate under high vacuum conditions to prevent ions colliding with air molecules.

Nominal-mass analysers have a resolution of approximately 1:1000-2000; specificity, however, can be enhanced by the use of high resolution mass spectrometers where the resolution can be as high as 1:100 000 giving mass accuracy under 1ppm [63].

1.5.1 The Time-of-Flight Mass Analyser

Developed in the late 1940's by Cameron and co-workers [64], time-of-flight mass spectrometry (TOF-MS) is a type of mass spectrometry in which an electric field of known strength is used to accelerate the ions. Improvements in mass resolution led to the first commercial instrument being introduced in 1955 by Wiley and McLaren [65].

More recently, TOF-MS has been coupled to MALDI and ESI ionisation methods and has been utilised in the development of high resolution instruments such as the quadrupole time-of-flight (QTOF) and in other instruments with TOF-TOF capabilities. The main features associated with TOF-MS include high sensitivity, theoretically unlimited mass range and rapid analysis time [66].

Unlike the quadrupole mass analyser, all the ions of differing m/z values enter the time-of-flight at the same time and therefore selected ion monitoring does not significantly increase the sensitivity.

1.5.1.1 The Theory Underpinning Time-of-Flight Mass Spectrometry

Time-of-flight separates ions based on their velocity, the time taken to reach the detector. Ions with a higher mass travel more slowly than ions of a lower mass and multiply charged ions travel faster than singly charged ions [67].

The theory behind the mass analysis is post-acceleration of the ions occurs to a constant kinetic energy. The velocity of the ions is an inverse function of the square root of their m/z values; the following equation demonstrates this principle:

$$v = \left(\frac{2zV}{m}\right)^{1/2}$$

v = velocity
zV = constant kinetic energy
z = charge on the ion
V = accelerating potential
m = mass
t = time
L = length of flight tube

Mass analysis of ions can be achieved by calculating their time of arrival at the detector placed at the end of the flight tube as shown in the following equation:

$$t = \frac{L}{v} = L\left(\frac{m}{2zV}\right)^{1/2}$$

1.5.1.1.1 Linear TOF-MS

The ions pass along the field free drift zone and where they are separated according to their m/z values. The attainable mass resolution is lower using linear TOF than that of reflectron TOF instrumentation; this arises from differences in the velocities of ions with the same m/z value [68].

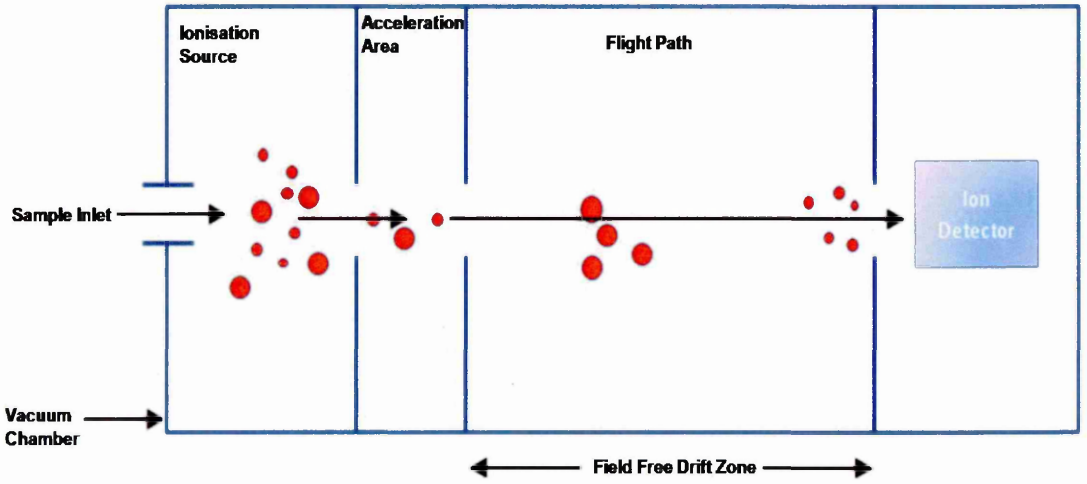

Figure 1.4: Schematic Diagram of the Linear Time-of-Flight Instrument Arrangement. Ions are separated based on their m/z ratio with lighter ions travelling faster than heavier ions and multiply charged ions travelling faster than singly charged ions (adapted from [1]).

1.5.1.1.2 Reflectron TOF-MS

The reflectron TOF, developed in 1973 by Mamyrin and co-workers [69], can be used to correct and compensate for the kinetic energy distribution of ions. The ions are directed towards a detector by an electrostatic field and ions that possess more kinetic energy penetrate deeper into the reflectron that is located at the end of the flight tube and have a slightly longer path to travel to reach the detector and the opposite of this is true for ions with less kinetic energy. As demonstrated by the diagram in figure 1.5 the ions are turned approximately 180° by a fixed potential gradient and then reaccelerated back through the reflectron and focussed towards the detector [70].

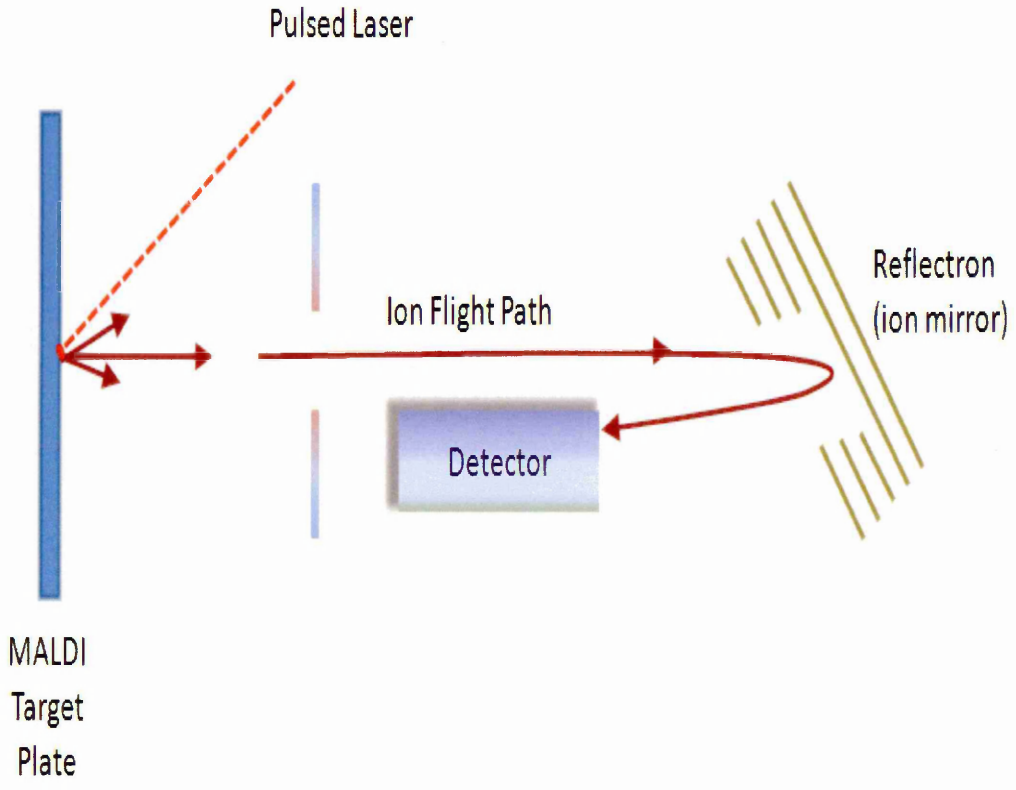

Figure 1.5: Schematic Diagram of the Reflectron Time-of-Flight Arrangement (adapted from [1])

1.5.2 The Quadrupole Time-of-Flight Mass Analyser

The quadrupole time-of-flight mass analyser, as its name suggests, is a combination of the quadrupole mass analyser with the time-of-flight mass analyser [71].

The instrument is comprised of three quadrupoles: Q0; Q1 and Q2 and a reflectron TOF mass analyser. The QqTOF tandem mass spectrometer can be thought of as a triple quadrupole with the last quadrupole (Q2) being replaced with a TOF mass analyser. This instrumentation can be interfaced with ESI, APCI and as figure 1.6 illustrates a MALDI ion source. The main advantage of the quadrupole time-of-flight mass analyser is the ability to record all ions in parallel accompanied with high resolution and mass accuracy. The purpose of Q0 is for collisional cooling and for the focusing of the ions; both Q0 and Q2 are only operated in the radio frequency (r.f.) mode.

To obtain TOF-MS data Q1 is operated in r.f. mode; MS/MS data is obtained by the Q1 being in mass filter mode to enable only the precursor ion of interest to be selected.

Q2 is where collision induced dissociation (CID) takes place with gas molecules such as nitrogen and argon. Once ions have left the collision cell (Q2) they are re-accelerated and focussed using ion optics that enters the ion modulator of the TOF mass analyser.

A pulsed electric field is used to push the ions orthogonal to their original trajectory into the accelerating column. Ions then move into the field free drift zone where they are separated based on their mass to charge ratio in the time-of-flight mass analyzer. A time-to-digital converter (TDC) is used to record all mass spectra [71].

The higher sensitivity and improved resolution achieved with QTOF instrumentation has been demonstrated for the analysis of phosphopeptides by Steen *et al.*[72].

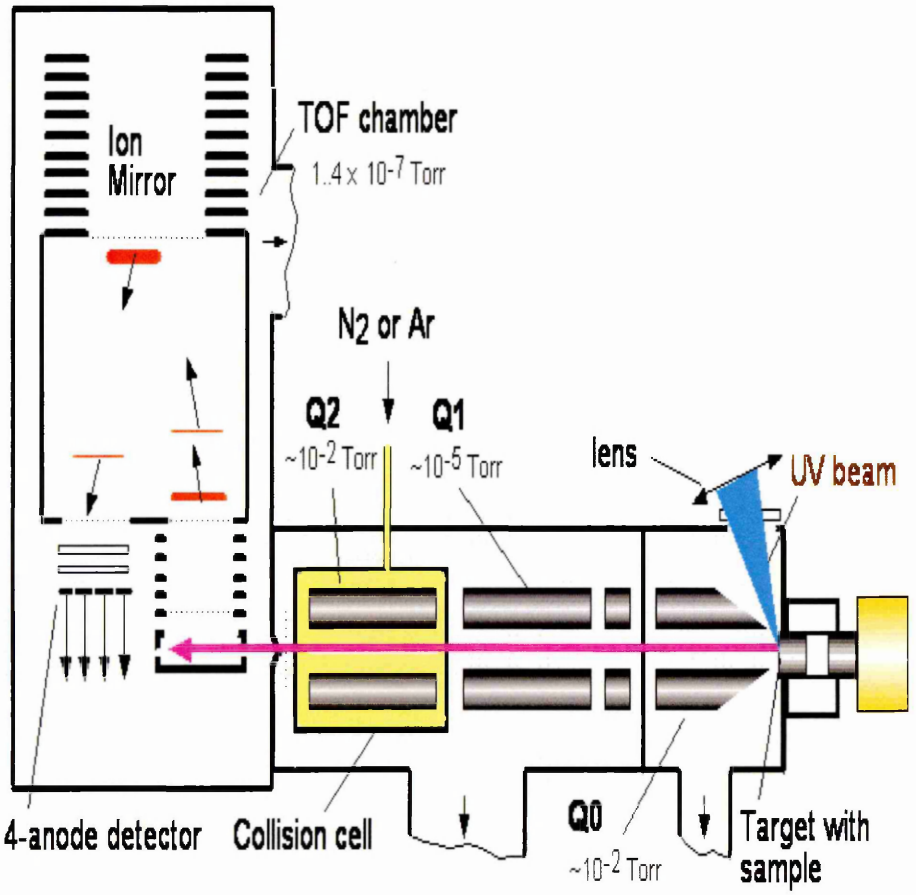

Figure 1.6: Schematic Diagram of a Hybrid Quadrupole Time-of-Flight Instrument with an Orthogonal MALDI Ion Source. Image supplied by Dr J. Wingate, Applied Biosystems/MDS Sciex, taken from the oMALDI Server users Manual, MDS Sciex, 2003 [73].

1.6 Tandem Mass Spectrometry

Tandem mass spectrometry more commonly referred to as MS/MS was first implemented in the late 1960's [74]. MS/MS involves the coupling of two mass spectrometers in time and space to obtain more information relating to a sample of interest. It can be used to deduce the structure of unknown compounds, for the identification of compounds from complex mixtures and to investigate collision induced dissociation pathways. The three stages in MS/MS are: mass selection; fragmentation via collisions with neutral gas atoms and mass analysis. The four main types of scan that can be used for MS/MS analysis are: product ion scans; precursor ion scans; constant neutral loss scans and selected reaction monitoring. To obtain structural information the product ion scan is the most widespread mode whereby the spectrum of the product ions can be obtained from the dissociation of a mass-selected precursor [75].

1.7 Mass Spectrometry Imaging Techniques

Molecular imaging techniques such as magnetic resonance imaging (MRI) [76] and positron emission tomography (PET) [77] are long established; however, the direction that the biomedical sciences are taking towards biomarker discovery makes the existing techniques somewhat unsuitable. This is mainly because they require molecular probes in order to detect a compound of interest; therefore there is not the capacity to simultaneously detect many different biomolecules that may be present within the sample. In recent years mass spectrometry imaging techniques have entered a league of their own in terms of sensitivity, mass accuracy, high-throughput and the ability to be used for many different chemically diverse compounds from a variety of samples. There are many applications of mass spectrometry imaging techniques that encompass the 'omics' revolution with a particular emphasis on proteomics [78], lipidomics [79, 80] and metabolomics [81].

1.7.1 SIMS Imaging

The earliest mass spectrometry imaging technique was based on SIMS.

SIMS imaging is performed by rastering a focussed narrow diameter primary ion beam across the sample surface generating a mass spectrum for each location where the beam strikes the sample. With imaging software the culmination of these data can be used to produce molecular ion maps by selecting the ion masses of interest [20]. This type of mass spectrometry analysis is also referred to in the literature as microprobe imaging [82]; this type of imaging is common to both SIMS imaging and MALDI MSI.

The sensitivity of SIMS imaging is restricted by the narrow diameter of the primary ion beam as this limits the number of secondary ions that can be generated at each increment of the analysis [20]. The attainable resolution is determined by the spot size of the primary ion beam; 50nm spot sizes are commercially available [83].

SIMS imaging is well-suited for the analysis of small molecules (under 1000Da); however, as the m/z value increases the generation of secondary ions decreases. It has unparalled spatial resolution in comparison with other mass spectrometry imaging techniques and SIMS imaging with subcellular resolution has been reported [84, 85]. Monroe *et al.* have used SIMS imaging to investigate endogenous compounds within spinal cord tissue sections [86]. The localisation of lipids in the aortic wall has also been imaged using TOF-SIMS [87].

1.7.2 DESI Imaging

DESI Imaging is a relatively new concept where molecular images can be obtained while the sample is in ambient conditions without the need for matrix application.

To obtain images using DESI the sample is mounted onto a target such as a microscope slide and is moved under a stationary fixed spray nozzle, generating a mass spectrum for each location on the sample. A two-dimensional image is obtained when all the data for individual locations are accumulated for selected ion (s) [88]. DESI Imaging mass spectrometry has been used to obtain images for the distribution of clozapine and its metabolites in a range of rat tissue [89], to study the

distribution of phospholipids in rat brain sections [90] and liver adenocarcinoma [91]. More recently, Kertesz *et al.* [92] have reported improved imaging resolution of approximately 40μm by optimising the most influential parts of the analysis such as the distance from the spray tip to the sample and the solvent flow rate.

1.7.3 Matrix-Assisted Laser Desorption Ionisation Mass Spectrometry Imaging (MALDI MSI)

MALDI MSI involves firing the laser (pulsed UV of the MALDI ion source), usually a nitrogen (337nm) or Nd: YAG (355nm, triple frequency) at increments along the sample of interest in a raster pattern and every time the laser fires at a particular location on the sample a mass spectrum is generated. The accumulation of these data allows many different images to be observed by the selection of different mass to charge ratios. The coupling of MALDI with a TOF mass analyser allows for a theoretically unlimited mass range to be achieved [66].

1.7.3.1 Microprobe Mode

The conventional approach to MALDI MSI is using microprobe mode where as previously described in section 1.7.3 a laser is used to raster over the sample surface at set increments and once the imaging experiment has run to completion images can be generated and individual spectra from each laser spot can be viewed. The achievable image resolution with MALDI MSI is a current limitation of the technique. Factors that limit such a resolution in microprobe mode include the laser spot size and the sample stage movement [93]. This has prompted researchers such as Heeren *et al.* to investigate ways to improve spatial resolution; this was done using the MALDI mass microscope [83, 93].

1.7.3.2 Microscope Mode

Microscope mode in contrast to microprobe mode utilises a two-dimensional detector to generate magnified images of the ion distributions in discrete areas within a sample. With this mode of mass spectrometry the spatial resolution is determined by the quality of the ion optics and the resolving power of the detector rather than the laser spot size as with microprobe analysis.

Luxembourg *et al.* have succesfully demonstrated the concept of MALDI in the microscope mode for the analysis of peptide and protein distributions [93]. The achievable resolution with this approach is significantly better than with the more accepted conventional approach of MALDI in microprobe mode. A lateral resolution of 4μm has been reported for the analysis of peptides and proteins [93].

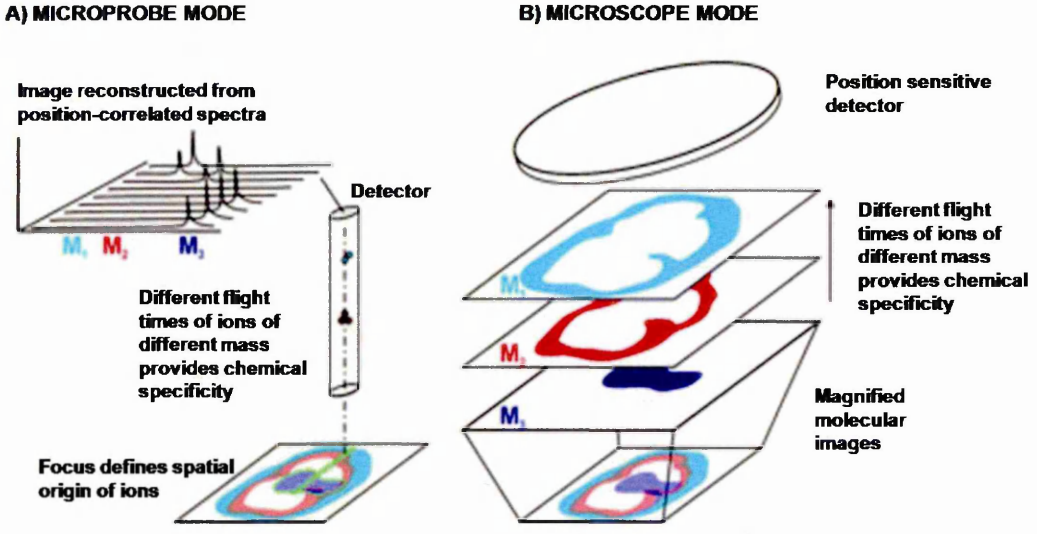

Figure 1.7: Schematic Diagram of the Microprobe and Microscope Modes of Analysis [82].

1.8 Practical Aspects of MALDI MSI

1.8.1 Instrumentation

The application of MALDI MSI to protein profiling experiments can be achieved using conventional MALDI-TOF-MS instrumentation; however, for small molecules this is not the instrumentation of choice due to the limitations brought about by the instrument configuration. The conventional MALDI-TOF-MS instruments are of axial configuration in contrast to instrumentation used for small molecule analysis; orthogonal MALDI ion sources on hybrid quadrupole time of flight (QqTOF) instruments with tandem MS capabilities. Orthogonal MALDI ion sources ensure that the ions are introduced at an angle that is perpendicular to the time-of-flight tube; therefore, unevenness in the surface topography of the sample does not affect the mass accuracy [94]. With the conventional MALDI-TOF-MS instrumentation the time of flight of an ion can be affected by the surface topography and charging effects of the sample. For problems relating to the charging effect, sputter coating with metals such as gold has greatly improved the data generated [95]. The QqTOF with an orthogonal MALDI ion source offers good mass measurement stability and the potential to perform tandem MS experiments.

1.8.2 UV Lasers for MALDI MSI

The most widely incorporated lasers in MALDI are Nitrogen (N_2, λ=337nm) and frequency tripled Neodymium: Yttrium Aluminium Garnet (Nd: YAG, λ=355nm). The N_2 laser is the most commonly used laser for MALDI analysis; this is probably due to the low cost associated with this type of laser. The incorporation of solid state lasers such as the Nd: YAG into MALDI instrumentation has become more popular due to the higher repetition rates associated with the laser; for example, up to 1kHz is achievable with an Nd:YAG laser in comparison with 20Hz on a standard N_2 laser [96]. The wavelength at which the nitrogen laser operates makes it more amenable to a wider selection of matrices than the frequency tripled Nd: YAG. However, the higher repetition rates associated with the Nd:YAG laser have made it a popular choice. Investigations conducted by Holle *et al.* have shown that the narrow

gaussian beam profile can result in reduced sensitivity. They have overcome this problem by modifying the frequency tripled Nd: YAG laser to a structured beam profile [97].

1.8.3 IR Lasers

1.8.3.1 IR MALDI MS

In contrast to UV MALDI, where the laser energy deposition proceeds through electron excitation, IR MALDI operates through vibration mechanisms [98].

The first published result of using an IR laser for MALDI was by Overberg *et al.* [99]. The matrices of choice for this type of laser are liquids such as glycerol. This is because more sample is consumed by each laser shot than in UV MALDI; thus the application of a solid matrix to the sample surface would somewhat limit the amount of data that could be generated. IR MALDI is not as sensitive as UV MALDI; this was demonstrated in the work conducted by Berkenkamp *et al.* [100]. The IR lasers are also considerably more expensive to implement than the commonly incorporated N_2 lasers in UV MALDI [101].

1.8.3.2 Infrared Laser Desorption Ionisation (IR LDI)

A recent review article by Peterson [102] highlighted the fact that many researchers are looking into ways that efficient ionisation from complex biological samples may be achieved without the use of a chemical matrix. This is particularly important for small molecule analysis as the matrix background signals can hinder the interpretation of the data. The use of infrared lasers has abolished the requirement of the matrix for the analysis of certain samples, for example some plant material as this type of tissue contains residual water. Erbium: Yttrium aluminium garnet (Er:YAG) lasers are infrared lasers that emit light with a wavelength of 2.94μm. The frequency of the Er: YAG laser overlaps with the resonant band of water O-H vibrations. Therefore, this type of laser is good for samples that contain residual water as the

water takes the role of the matrix in absorbing the laser energy and thus promoting the ionisation. A major advantage of using the Er: YAG laser is the elimination of interfering matrix peaks. IR LDI MS has been used for the molecular profiling of rat brain tissue sections [103], seeds, fruits and whole oils [104].

1.8.4 Sample Preparation Strategies for MALDI MSI

In the last decade, advances have been made in MALDI MSI; however, there are still some fundamental issues that need to be addressed with the main emphasis being on the sample preparation procedure. The sample preparation procedure, storage and handling of samples are some of the most important factors in MALDI MSI and controlling these variables is more likely to generate analytical results that are reproducible.

There are many different techniques and methods used for sample preparation but these can vary for individual compounds. Hence, to achieve the highest quality, reproducible results the sample preparation procedure must be optimized for each analyte of interest.

1.8.4.1 Tissue Preparation for Direct and Indirect Analyses

In order to achieve good, reproducible results tissue should be stored and prepared in a suitable manner [105, 106].

The majority of imaging experiments have been conducted on biological tissue samples – either to study endogenous compounds, for example the study of diseased tissue and for the identification of biomarkers related to diseased state tissue [107], or for the detection of a particular compound such as an administered pharmaceutical compound [108].

The removal and storage of tissue are important factors in maintaining the spatial resolution of compounds. Tissue samples need to be removed in such a way that the native shape of the tissue is preserved as much is possible; this is usually achieved by snap freezing the sample using nitrogen-cooled isopentane.

The most important factors in tissue sectioning are tissue thickness, temperature and the use of fixing media [105, 109]. Cryosectioning is performed to obtain a tissue section that is suitable for analysis. Fixing media such as optimum cutting temperature (OCT) [105] are used to mount the sample onto the sample stage prior to sectioning. OCT has been reported to cause ion suppression effects in MALDI and should be avoided where possible [105, 110]. The use of carboxymethyl cellulose (CMC) has been demonstrated to be a good embedding media that does not interfere with MALDI analysis [111]. The environmental conditions within the cryostat should be optimized for the type of tissue; for example, fatty tissues tend to require a lower temperature to obtain better quality sections. Tissue thickness has been shown to be an influential factor; thicker tissue sections are easier to cut and handle but are less electrically conductive in the mass spectrometer. The opposite of this is true for thinner sections. It has been found that for MALDI Imaging the optimum tissue thickness for direct analysis is ~10-20μm - this thickness is sufficient to expose the intracellular contents of the cells within the tissue [112]. Research has shown that thin sections are also required for the optimal ionisation of both the analyte and matrix [105]. After sectioning, the tissue should be mounted on a surface which is electrically conductive such as an aluminium plate or directly onto the MALDI target plate for analysis. Tissue sections should be mounted quickly and stored at -80°C prior to analysis as allowing the sample to warm has been reported to have a substantial impact on the data generated and its reproducibility [107]. It is important that when transferring the tissue to the plate that the native shape of the tissue is maintained and that the tissue is not torn or distorted in any way.

1.8.4.1.1 Direct Tissue Analysis

Direct tissue analysis is usually performed to maintain the spatial resolution of compounds. It is advantageous in comparison with indirect tissue analysis as there is minimal handling of the sample, and therefore less room for error or analyte losses. An example of direct tissue analysis can be seen in the research of Hsieh *et al.* [113]. They conducted a study to measure Clozapine in rat brain tissue using sinapinic acid as a matrix as this crystallises better over tissue than α-CHCA.

Direct tissue analysis can be problematic when using organic matrices as the co-crystallisation between the analyte of interest and the matrix may be hindered due to the presence of endogenous compounds within the tissue or by a high salt content.

1.8.4.1.2 Indirect Tissue Analysis - Blotting Methods

To overcome the problems that are associated with direct tissue analysis, a blotting method, a form of indirect tissue analysis, can be adopted.

Research by Chaurand *et al.* [114] has shown that carbon-filled polyethylene membranes were suitable for use in MALDI as they showed good electrical conductivity and the ability to blot proteins due to their hydrophobic surfaces without loss of spatial resolution. Nylon [115], nitrocellulose [116] and more recently cellulose [117] have been investigated as potential blotting membranes.

Bunch *et al.* (2004) [117] investigated pharmaceutical compounds in skin indirectly using MALDI by using a blotting method that involved the coating of cellulose membranes with the matrix and then blotting the treated skin sample onto the membrane. In order to get the highest quality image the blotting membrane and the matrix must be suited to the analyte. More recently, Prideaux *et al.* have reported the imaging of xenobiotic compounds in skin by indirect MALDI MSI [118].

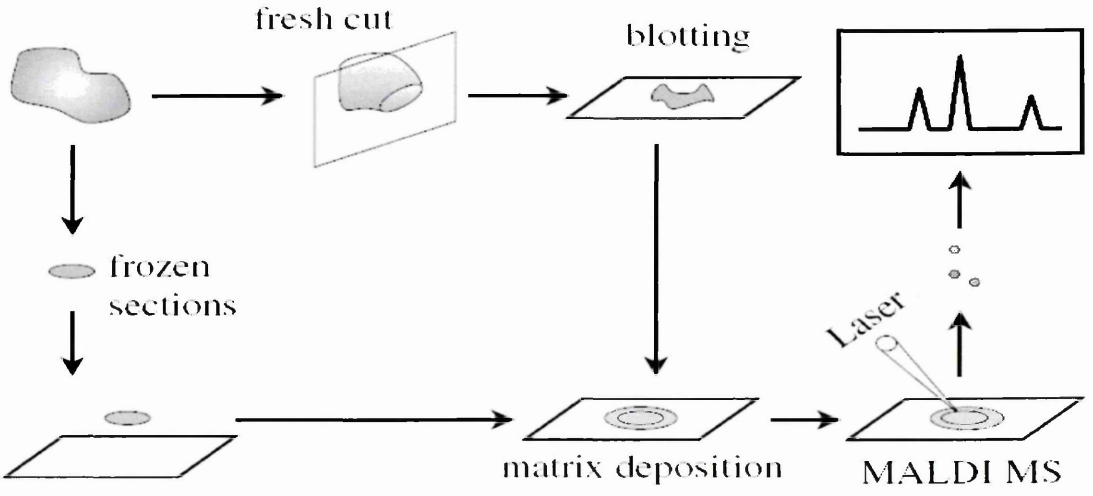

Figure 1.8: Schematic Diagram of the Blotting and Direct Tissue Procedures. Adapted from Todd *et al.* [119].

1.8.4.2 Matrix Selection

Selection of the most suitable matrix is imperative to obtain high quality results with MALDI in conjunction with the optimisation of sample preparation; these are essentially the most important parameters of MALDI analysis.

Due to the majority of MALDI matrices having low molecular weights, most MALDI analyses until recently concentrated on large molecules, typically >1500Da. Cohen and Gusev [120] conducted a series of experiments to assess the suitability of MALDI for small molecule analysis. They recommended the selection of a matrix that does not directly interfere in the same mass region of the spectrum as the analyte or alternatively the use of a high molecular weight or inorganic matrix. However, these approaches are only valid for when the analyte information is already known and would still pose problems for analyses such as metabolomic applications. The main requirements of a MALDI matrix is co-crystallisation (organic matrices) with the analyte; the matrix must be soluble in the solvent in which the analyte is dissolved in, absorb at the laser wavelength, be stable under vacuum and ultimately promote ionisation At present there are no protocols as to how to select the best matrix for a particular application. Zenobi *et al.* [50] proposed guidelines for matrix selection based on ion formation mechanisms; however, research is still being conducted into matrix crystallisation and the analyte incorporation process. In the past, many different compounds were empirically tested for their suitability to act as a MALDI matrix. However, at present there are relatively few matrices available that yield reproducible, high quality mass spectra. The most common MALDI matrices are the cinnamic and benzoic acid derivatives; these were documented as good MALDI matrices for proteins in the late 1980's [121].

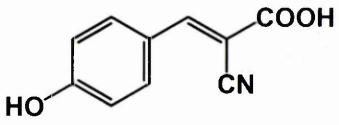

α-Cyano-4-hydroxycinnamic acid (α-CHCA)

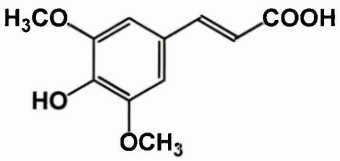

Sinapinic Acid (SA)

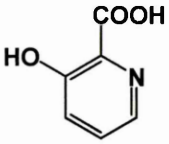

3-Hydroxypicolinic acid (3-HPA)

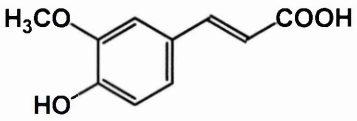

Ferulic Acid (FA)

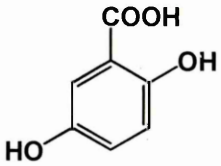

2, 5-Dihydroxybenzoic acid (DHB)

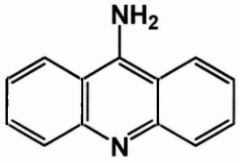

9-aminoacridine (9-AA)

Figure 1.9: The Chemical Structures of Established MALDI Matrices.

The organic acid matrices depicted in figure 1.9 all contain chromophores and it is this part of the organic compound that absorbs the laser energy. Organic acid matrices are good for positive ion mode MALDI; this is because they have acidic properties and thus are characterised as proton donors. As most analyses are performed in this mode, this type of matrix has become a popular choice.

Organic acids such as 2, 5-dihydroxybenzoic acid (DHB), alpha-Cyano-4-hydroxycinnamic acid (α-CHCA) and sinapinic acid (SA) are routinely used in the analysis of proteins. α-CHCA, characterised by its ability to form small homogenous crystals has also proven a good matrix for the analysis of small compounds such as pharmaceutical products. 3-hydroxypicolinic acid (3-HPA) is good for oligonucleotide analysis and ferulic acid (FA) is good for peptide/protein analysis [122]. The concentration of matrices is based on the solubility of the matrix and the efficiency of the matrix to promote ionisation. Organic matrices are typically made to a concentration of ~10-25mg/mL in a suitable solvent that the matrix and analyte will be soluble in. However, the main disadvantage associated with the use of organic acid matrices is that they produce lots of background noise in the low mass region due to matrix clusters and fragment ions leading to interfering peaks, which can sometimes make it difficult to isolate the peaks of interest associated with the analyte. For most organic matrices, the background noise from the matrix peaks occurs in the low mass region [123] which can coincide with compounds such as pharmaceutical products and metabolites as these often have low molecular weights.
For compounds that are not suited to positive ion analysis, negative ion mode MALDI can be performed. 9-aminoacridine (9-AA) is a matrix that has been reported to be a good matrix for negative ion mode MALDI as it contains one basic group and it has a conjugated ring system. As 9-AA is a strong base it accepts protons, resulting in the formation of $[M-H]^-$ ions. This chemical feature makes it a good matrix for the analysis of compounds in negative ion mode and superseded the conventional organic acid matrices for this application. 9-AA has been used to analyse proteins [124] and for the metabolomic analysis of eukaryotic tissue [125]. Edwards and Kennedy detected 105 metabolites using this matrix in negative ion mode and they achieved good detection limits for the standards (in the nanomolar to micromolar range) [125].

Although MALDI MSI has emerged as an excellent molecular imaging technique its use in biological tissue analysis is somewhat hindered by the lack of suitability of the matrix and the crystallisation processes on tissue surfaces that contain endogenous salts. Different matrices form different types of crystals and the choice of matrix is dependent on the analyte as not all matrices have the same capacity to instigate the ionisation of a particular analyte. The choice of solvent that the matrix is dissolved in is also important; the solvent is usually selected based on the solubility of the matrix and the analyte.

To overcome these problems tissue washing to remove endogenous compounds such as salts has been reported; this washing procedure is generally accepted for large molecules such as peptides and proteins. However, for small molecule analysis, this could cause significant translocation of the compounds of interest or if the compound is soluble in the washing solvent, it could be lost altogether. If the conventional solid organic matrices are not suitable for a particular type of analysis due to interfering peaks in the area of interest, the potential of ionic liquid matrices along with particle suspension matrices has been investigated in an attempt to offer an alternative solution. Ionic liquid matrices are prepared by mixing an acidic MALDI matrix and an organic base in equimolar concentrations [126, 127]. They are compatible with both polar and non polar analytes [120] and they do not produce areas with high signal intensity (hotspots). However, their use is correlated with poor ionization efficiency and interfering peaks and low mass resolution [128]. Liquid matrices are commonly incorporated into IR MALDI MS methods [129].

1.8.4.2.1 Particle Suspension Matrices

First introduced by Tanaka *et al.* in 1988 [12], particle suspension matrices are composed of metal particles that are suspended in solution. More recently particle suspensions have been re-evaluated for their potential role in MALDI analyses [130-132]. Their mode of action is different from that of organic acids in that co-crystallisation does not occur between the matrix and the analyte. It is thought that particle suspension matrices work by a thermal ionisation mechanism. In positive ion mode, graphite-based matrices induce strong cationisation of sodium, and

potassium, hence the formation of sodium and potassium adducts is more prevalent than the formation of the molecular ion species. The potential limitation with particle suspension matrices is that the matrix is thought to promote increased fragmentation of the analyte and lower sensitivity [63]. However, it is important to stress that the choice of matrix is influenced by the nature of the sample. Thus if the conventional matrices are unsuitable, a compromise has to be reached.

Crecelius *et al.* [132] investigated the use of particle suspension matrices for the analysis of tetracycline antibiotics utilising concentrations of approximately 10mg/mL in a solvent solution in which the particles will form a suspension, for example ethanol. The particle suspension mix incorporated ethylene glycol to act as a dispersant and an acid such as trifluroacetic acid (TFA) is often added to enhance the ionisation of the analyte. More recently Black *et al.* [133] have done some research into the use of pencil lead as a matrix and as an internal calibrant, and for the analysis of peptides and polymers.

1.8.4.2.2 Matrix Application

The deposition of the chemical matrix is a critical factor in achieving reproducible data using MALDI MSI [134]. There are many different ways that the matrix can be applied to the sample and, depending on which method of application is chosen, this also affects the concentration of the matrix to be prepared. The matrix can be applied either to coat the entire surface of the sample or in an ordered array of discrete spots across the surface.

Endogenous compounds contained within samples can promote adduct formation, poor crystallisation of the matrix and ion suppression effects. The type of sample to be analysed may also affect the spectral quality from spot to spot due to the heterogeneity within the tissue i.e. in some parts of the tissue suppression effects may be more evident due to a higher concentration of endogenous compounds.

For biological tissue analysis, it is important to have the matrix homogenously distributed on the surface of the tissue in order to ensure that the results obtained

reflect the biological characteristics of the sample and not uneven matrix coverage [135].

1.8.4.2.3 Manual Spotting

The matrix can be deposited in discrete spots by manually pipetting a small amount (1μL) directly onto the tissue surface [105, 112].

1.8.4.2.4 Airspray Deposition

This method employs an airbrush that is connected to a compressor, thus allowing the pressure at which the matrix is applied to be controlled. The matrix application process with this particular device is controlled manually; therefore the operator has to make a judgement as to whether the matrix coverage is homogenous and this is prone to human error. It is very important to minimise sample wetting when applying the matrix as this can cause migration of the analytes within the tissue section and therefore not provide reliable data when imaging experiments are performed [117].

Electrospray matrix deposition has also been reported where the matrix crystal formation and size were influenced by the spray voltage and the distance from the sample [136]. Oscillating capillary nebulisers have also been reported to produce homogenous matrix coverage [134].

It is thought that the droplet size of the matrix from manual spraying is much larger than what can be achieved with an automated spray, giving rise to poorer crystal formation [135].

1.8.4.2.5 Automated Matrix Spotters

Automated matrix spotters were introduced to combat the potential human error and sample wetting associated with applying the matrix manually. However, the major

limitation to the implementation of some of these instruments into laboratories is the expense; this has led some researchers, for example Baluya *et al.* [137], to modify inexpensive commercial inkjet printers. These printers have shown to be an improvement on the manual techniques still employed by many laboratories. A potential problem associated with this type of modification is the compatibility of the solvents used to prepare matrices with the plastic containers contained within the printer; plasticiser contamination is an impending problem.

A few examples of commercially available automated matrix spotters that have been used in MALDI MSI experiments are the Shimazdu Chip, Bruker image Prep, Suncollect and Labcyte Portrait 630. The Shimadzu Chip uses piezoelectric technology to deliver pico-litre volumes of matrix onto preselected regions of the sample surface without contact with the sample [138]. The Bruker ImagePrep system also uses piezoelectric technology to create a matrix aerosol with an achievable droplet size of 20μm. The matrix application process is controlled by a light scattering sensor [139].

The Suncollect system operates using a needle to deposit pre-determined quantities onto the sample surface; however, the limitation with this type of instrument includes having to use lower concentrations of matrix to avoid blocking of the needle and the fact that matrix can crystallise around the needle and thus interfere with matrix deposition. The Suncollect matrix deposition device also can be adapted to spray coat the samples - this is more beneficial for imaging experiments than for profiling experiments [140]. The Labcyte Portrait 630 avoids these problems by employing a unique acoustic technology in which sound energy is used to transfer very small droplets of matrix to the sample. This ensures that there is no contact with the sample on transferral of the matrix and the matrix concentration can be varied as there is no needle to become blocked. The benefits of this type of sample preparation include prevention of the movement of biomolecules, the ability to control the drying time of the matrix and the number of passes of matrix. The user therefore has the ability to calculate how much matrix has been deposited in one position and the enhanced crystal formation and spot size produce more reliable and reproducible mass spectra [134].

1.9 Applications of MALDI MSI

MALDI MSI is an emerging technique for investigating molecular distributions within biological systems through the analysis of thin tissue sections and hundreds of compounds can be measured in a single MALDI imaging experiment. The first major application of MALDI MS was for the analysis of proteins and peptides. Caprioli *et al.* introduced MALDI MSI in 1997 with their work detailing the direct profiling of analytes within tissue sections [141]. MALDI in contrast to many other techniques is tolerant of contaminants such as buffers and salts, gives good sensitivity and produces relatively simple spectra with most ions being singly charged, sodiated or potassiated. Since the introduction of MALDI MSI, research has moved towards biomedical applications, for example mapping disease biomarkers, and in pharmaceutical research, for example mapping pharmaceutical compounds in tissue [142]. This is because spatial information on the distribution of pharmaceutical compounds in tissue is a very important aspect in assessing drug efficiency. Conventionally this was done using a combination of autoradioluminography and metabolite data obtained from techniques such as liquid chromatography (LC)/MS. The main problem associated with this technique is that the compound must be radiolabelled and current technology does not allow for the differentiation between the compound of interest and its metabolites. MALDI MSI has been investigated by Stoekli *et al.* as a potential technique to complement whole-body autoradioluminography. MALDI MSI allows for the detection of both the compound of interest and its metabolites without the need for a radiolabelled compound [111]. The fast analysis time and the specificity of MALDI analysis make it an ideal technique for such analysis. Hsieh *et al.* [142] have also conducted research into mapping pharmaceutical compounds in tissue using MALDI MSI. High performance liquid chromatography HPLC-MS/MS is a common technique used in drug analysis applications; however, this technique does not provide information relating to the distribution of the compound in tissues and organs, unlike MALDI MSI.

MALDI MSI has been demonstrated as a suitable technique for a diverse range of samples; xenobiotic compounds in skin have been analysed using indirect MALDI

MSI by Prideaux *et al.*[118] and MALDI MSI has also been applied to plant science to investigate agrochemicals (Mesotrione and Azoxystrobin) in soya plants [143].

1.10 Data Interpretation and Analysis

Specialised software packages are commercially available for MALDI MSI; the software is responsible for both the control of the instrument and the processing of the data once it has been successfully acquired.

MALDI MSI analyses often generate large complex datasets where an image can consist of thousands of spectra; the ion intensities can vary in each spectrum along with the masses observed. The data generated by MALDI MSI can contain a wealth of valuable information. Conventionally MALDI MSI experiments have focussed on the analysis of known compounds of scientific interest. However, for studies where there may be subtle differences, for example a comparison between healthy and diseased tissues, there needs to be established methodology to analyse such complex datasets in which these differences can be pinpointed and accounted for. The most common statistical approaches include hierarchical cluster analysis and principal component analysis. Hierarchical cluster analysis is a technique where the mass spectra are clustered on the basis of their similarity and are presented in the form of a dendrogram; this has been applied to MALDI MSI data for the analysis of human cancer tissue sections [144].

Principal Component Analysis (PCA) is used for the simplification and reduction of multidimensional datasets [145] in which a new coordinate system is created for the dataset based on a linear transformation; the first principal component (this is the greatest variance) is found on the first axis and the second largest variance on the second axis and so forth. Data are presented in the form of a scores plot and a loadings plot. The scores plot assigns a score, in this example the detected m/z value along with its corresponding ion intensity imported into the software, that represents the weighting each principal component has within the sample. The loadings plot presents data with respect to its own influence in each principal component allocation. PCA is a more sophisticated way of looking at large datasets generated

by MALDI MSI with the major goal being the identification of trends in the dataset that are not obvious without this type of analysis [146].

1.11 Aims of Thesis

The overall aim of the work reported in this thesis was to develop methodologies and sample preparation strategies for the application of MALDI MSI for small molecule analysis from a range of samples. This includes:

Pharmaceutical Compound Analysis:

- Evaluation of MALDI MSI sample preparation procedures for the analysis of anti-asthmatic compounds in lung tissue.
- To investigate the application of MALDI MSI for the evaluation of pharmaceutical dosage forms. Tablets have been directly analysed in order to assess the homogeneity of the active drug component throughout the excipients. This can provide important information that relates back to the formulation process.

Metabolomics:

- Evaluation of MALDI MSI for metabolomic studies in plant tissue using wheat as the model system. The endogenous compounds within wheat grain sections were analysed and imaged in order to gain a greater understanding of the complex biological processes.
- To establish methodology for the study of Chronic Experimental Allergic Encephalomyelitis; the animal model of multiple sclerosis. The mouse model was investigated; spinal cord analysis of diseased tissue alongside control tissue was analysed for potential biomarkers related to the disease pathogenesis.

1.12 References

[1] El-Aneed A., Chen A., Banoub J. Mass Spectrometry, Review of the Basics: Electrospray, MALDI and Commonly Used Mass Analyzers. Applied Spectroscopy Reviews, 2009, 44, 210-230.

[2] Dass C. Principles and Practice of Biological Mass Spectrometry. Wiley Interscience, 2001.

[3] Dempster A. J. A. A New Method of Positive Ray Analysis. Physics Review, 1918, 11, 316-324.

[4] Munson M. S. B., Field F. H. Chemical Ionization Mass Spectrometry. I. General Introduction. Journal of the American Chemical Society, 1966, 88, 2621-2630.

[5] Barber M., Bordoli R. S., Sedgwick R. D., Tyler A.N. Fast Atom Bombardment of Solids (FAB) - A New Ion-Source for Mass Spectrometry. Journal of the Chemical Society, Chemical Communications, 1981, 325-327.

[6] Benninghoven A., Rudenauer F. G., Werner H. W. Secondary Ion Mass Spectrometry - Basic Concepts, Instrumental Aspects, Applications and Trends, Wiley, New York 1987.

[7] Dole M, Mack L. L., Hines R.L. Molecular beams of macroions. Journal of Chemical Physics, 1968, 49, 2240-2249.

[8] Wilm M., Neubauer G., Mann M. Parent ion scans of unseparated peptide mixtures, Analytical Chemistry, 1996, 68, 527-533.

[9] Dzidic I., Carroll D. I., Stillwell R. N., Horning E. C. Atmospheric pressure ionisation (API) mass spectrometry. Formation of phenoxide ions from chlorinated aromatic compounds. Analytical Chemistry, 1975, 47, 1308-1312.

[10] Wei J., Buriak J. M., Siuzdak G. Desorption/Ionization Mass Spectrometry on Porous Silicon. Nature, 1999, 399, 243-246.

[11] Takats, Z., Wiseman J. M., Cologan B., Cooks R. G. Mass Spectrometry Sampling Under Ambient Conditions with Desorption Electrospray Ionisation. Science, 2004, 306, 471-473.

[12] Tanaka K., Hiroaki W., Ido Y., Akita S., Yoshida Y., Yoshida T. Protein and Polymer Analyses up to m/z 100 000 by Laser Ionisation Time-of-Flight Mass Spectrometry. Rapid Communications in Mass Spectrometry, 1988, 2, 151-153.

[13] Karas M., Hillenkamp F. Laser Desorption ionisation of proteins with molecular masses exceeding 10,000 daltons. Journal of Analytical Chemistry, 1988, 60, 2299-2301.

[14] Schiller J., Sub R., Arnhold J., Fuchs B., LeBig J., Muller M., Petkovic M., Spalteholz H., Zschornig O., Arnold K. Matrix-assisted laser desorption and ionization time-of-flight (MALDI-TOF) mass spectrometry in lipid and phospholipid research. Progress in Lipid Research, 2004, 43, 449-488.

[15] Vestal M. L. Methods of Ion Generation. Chemical Reviews, 2001, 101, 361-376.

[16] Yamashita M., Fenn J. B. Negative ion production with the electrospray ion source. Journal of Physical Chemistry, 1984, 88, 4671-4675.

[17] Fenn J. B, Mann M., Meng C. K., Wong S. F., Whitehouse C.M. Electrospray ionisation for mass spectrometry of large biomolecules. Science, 1989, 246, 64-71.

[18] Barofsky B. F., Giessmann U., Swanson L. W., Bell A. E. Molecular SIMS with a liquid metal field ion point source. International Journal of Mass Spectrometry and Ion Physics, 1983, 46, 495-497.

[19] Gutharay S. K., Douglass S., Orloff J. High-resolution primary ion beam probe for SIMS. Applied Surface Science, 2004, 231, 926-929.

[20] Belu A. M., Graham D. J., Castner D. G. Time-of-flight secondary ion mass spectrometry: techniques and applications for the characterization of biomaterial surfaces. Biomaterials, 2003, 24, 3635-3653.

[21]http://serc.carleton.edu/images/research_education/geochemsheets/techniques/SIMS4.JPG.v2.jpg
Last accessed 10th May 2009.

[22] Tomer K. B. The development of fast atom bombardment combined with tandem mass spectrometry for the determination of biomolecules. Mass Spectrometry Reviews, 1989, 8, 445-482.

[23] Huang Q. W., Wu G-L., Tang H-T. Formation mechanisms of secondary ions in fast-atom bombardment mass spectrometry. International Journal of Mass Spectrometry and Ion Processes, 1986, 70, 145-152.

[24] Schuetzle D., Riley T. L., de Vries J. E., Prater T. J. Applications of high-performance mass spectrometry to the surface analysis of materials. Mass Spectrometry Reviews, 2005, 3, 527-585.

[25] Kraj A., Dylag T., Gorecka-Drzazga A., Bargiel S., Dziuban J., Silberring J. Desorption/ionization on silicon for small molecules: a promising alternative to MALDI TOF. Acta Biochimica Polonica, 2003, 50, 783-787.

[26] Compton B. J., Siuzdak G. Mass spectrometry in nucleic acid, carbohydrate and steroid analysis. Spectroscopy, 2003, 17, 699-713.

[27] Lewis W. G., Shen Z., Finn M. G., Siuzdak G. Desorption/ionization on silicon (DIOS) mass spectrometry: background and applications. International Journal of Mass Spectrometry, 2003, 226, 107-116.

[28] Thomas J. J., Shen Z., Crowell J. E., Finn M. G., Siuzdak G. Desorption/ionization on silicon (DIOS). A diverse mass spectrometry platform for protein characterization. Proceedings of the National Academy of Sciences of the United States of America, 2001, 98, 4932-4937.

[29] Go E. P., Prenni J. E., Wei J., Jones A., Hall S. C., Witkowska E., Shen Z., Siuzdak G. Desorption/ionization on silicon Time-of-Flight/Time-of-Flight Mass Spectrometry. Analytical Chemistry, 2003, 75, 2504-2506.

[30] Chen H., Talaty N. N., Takats Z., Cooks R. G. Desorption Electrospray Ionisation Mass Spectrometry for High-Throughput Analysis of Pharmaceutical Samples in the Ambient Environment. Analytical Chemistry, 2005, 77, 6915-6927.

[31] Weston D. J., Bateman R., Wilson I. D., Wood T. R., Creaser C. Direct Analysis of Pharmaceutical Drug Formulations Using Ion Mobility Spectrometry/Quadrupole-Time-of-Flight Mass Spectrometry Combined with Desorption Electrospray Ionisation. Analytical Chemistry, 2005, 77, 7572-7580.

[32] Williams J. P., Scrivens J. H. Rapid accurate mass desorption electrospray ionisation tandem mass spectrometry of pharmaceutical samples. Rapid Communications in Mass Spectrometry, 2005, 19, 3643-3650.

[33] Leuthold L. A., Mandscheff J.-F., Fathi M., Giroud C., Augsburger M., Varesio E., Hopfgartner G. Desorption electrospray ionisation mass spectrometry: direct toxicological screening and analysis of illicit Ecstacy tablets. Rapid Communications in Mass Spectrometry, 2006, 20, 103-110.

[34] Rodriguez-Cruz S. E. Rapid analysis of controlled substances using desorption electrospray ionisation mass spectrometry. Rapid Communications in Mass Spectrometry, 2006, 20, 53-60.

[35] http://www.prosolia.com/image/DESI.gif
Last accessed 10th May 2009.

[36] Brown T., Clipston N. L., Simjee N., Luftmann H., Hungerbuhler H., Drewello T. Matrix-assisted laser desorption/ionisation of amphiphilic fullerene derivatives. International Journal of Mass Spectrometry, 2001, 210, 249-263.

[37] Kuger R., Fournier I., Gluckmann M., Karas M. Analyte incorporation and ionization in Matrix-Assisted Laser Desorption Ionization Visualized by pH indicator molecular probes. Analytical Chemistry, 2001, 73, 5812-5821.

[38] Zenobi R., Knochenmuss R. Ion Formation in MALDI Mass Spectrometry. Mass Spectrometry Reviews, 1998, 17, 337-366.

[39] Knochenmuss R. Ion formation mechanisms in UV-MALDI. Analyst, 2006, 131, 966-986.

[40] Ehring H., Karas M., Hillenkamp F. Role of photoionisation and photochemistry in ionisation processes of organic molecules and relevance for matrix-assisted laser desorption/ionisation mass spectrometry. Organic Mass Spectrometry, 1992, 27, 427-480.

[41] Karas M., Gluckmann M., Schafer J. Ionisation in matrix-assisted laser desorption/ionisation: singly charged molecular ions are the lucky survivors. Journal of Mass Spectrometry, 2000, 35, 1-12.

[42] Karas M., Kruger R. Ion formation in MALDI: the cluster ionisation mechanism. Chemical Reviews, 2003,103, 427-439.

[43] Liao P.-C., Allison J. Ionisation processes in matrix-assisted laser desorption/ionisation mass spectrometry: matrix dependent formation of [M+H]+ and [M+Na]+ ions of small peptides and some mechanistic comments. Journal of Mass Spectrometry, 1995, 30, 408-423.

[44] Wang B.H., Dreisewerd K., Bahr U., Karas M., Hillenkamp F. Gas-phase cationization and protonation of neutrals from MALDI. Journal of the American Society for Mass Spectrometry, 1993, 4, 393-398.

[45] Karbach V., Knochenmuss R. Do single matrix molecules generate primary ions in ultraviolet matrix-assisted laser desorption/ionisation. Rapid Communications in Mass Spectrometry, 1998, 12, 968-974.

[46] Busch K. L. Desorption-ionisation mass spectrometry. Journal of Mass Spectrometry, 1995, 30: 230-240.

[47] Breuker K., Knochenmuss R., Zenobi R. Gas-phase basicities of deprotonated matrix-assisted laser desorption/ionisation molecules. International Journal of Mass Spectrometry, 1999, 184, 25-38.

[48] Lehmann E., Knochenmuss R., Zenobi R. Ionisation mechanisms in matrix-assisted laser desorption/ionisation mass spectrometry: contribution of pre-formed ions. Rapid Communications in Mass Spectrometry, 1997, 11, 1483-1492.

[49] Lidgard R., Duncan M. W. Utility of MALDI-TOF mass spectrometry for the analysis of low molecular weight compounds. Rapid Communications in Mass Spectrometry, 1995, 9, 128-132.

[50] Knochenmuss R., Stortelder A., Breuker K., Zenobi R. Secondary ion-molecule reactions in matrix-assisted laser desorption/ionisation. Journal of Mass Spectrometry, 2000, 35, 1237-1245.

[51] Nielen M. W. F. MALDI Time-of-Flight Mass Spectrometry of Synthetic polymers. Mass Spectrometry Reviews, 1999, 18, 309-344.

[52] Harvey D. J. Matrix assisted laser desorption ionisation mass spectrometry of oligosaccharides and glycoconjugates. Journal of Chromatography A, 1996, 720, 429-446.

[53] Wong C. K. L., Chan T-W. D. Cationization Processes in Matrix-assisted Laser Desorption/Ionization Mass Spectrometry: Attachment of Divalent and Trivalent Metal Ions. Rapid Communications in Mass Spectrometry, 1997, 11, 513-519.

[54] Bogan M. J, Agnes G. R. Time-of-flight mass spectrometric analysis of ions produced from adjacent sample spots irradiated simultaneously by a single 337 nm laser. Rapid Communications in Mass Spectrometry, 2003, 17, 2557-2562.

[55] Erb W. J., Hanton S. D., Owens K. G. A study of gas-phase cationisation in matrix-assisted laser desorption/ionisation time-of-flight mass spectrometry. Rapid Communications in Mass Spectrometry, 2006, 20, 2165-2169.

[56] Zhang J., Zenobi R. Matrix-dependent cationisation in MALDI mass spectrometry. Journal of Mass Spectrometry, 2004, 39, 808-816.

[57] Donegan M., Tomlinson A. J., Nair H., Juhasz P. Controlling matrix suppression for matrix-assisted laser desorption/ionisation analysis of small molecules. Rapid Communications in Mass Spectrometry, 2004, 18, 1885-1888.

[58] Vertes A., Levine R. D. Sublimation vs fragmentation in matrix-assisted laser desorption. Chemical Physics Letters, 1990, 171, 284-290.

[59] Johnson R. E., Sundquist B. U. R. Laser pulse ejection of organic molecules from a matrix - lessons from fast-ion induced ejection. Rapid Communications in Mass Spectrometry, 1991, 5, 574-578.

[60] Dreisewerd K., Shurenverg M., Karas M., Hillenkamp F. Influence of the laser intensity and spot size on the desorption of molecules and ions in matrix-assisted laser desorption ionisation with a uniform beam profile. International Journal of Mass Spectrometry and Ion Processes, 1995, 14, 127-148.

[61] Schurenberg M., Dreisewerd K., Kamanabrou S., Hillenkamp F. Influence of the sample temperature on the desorption of matrix molecules and ions in MALDI. International Journal of Mass Spectrometry and Ion Processes, 1998, 172, 89-94.

[62] Dreisewerd K. The Desorption Process in MALDI. Chemical Reviews, 2003, 103, 395-426.

[63] Villas-Boas S., Nielsen J., Smedsgaard J., Hansen M. A. E., Roessner-Tunali U. Metabolome Analysis An Introduction Wiley publication 2007.

[64] Cameron A. E., Eggers R. An ion ''Velocitron''. Review of Scientific Instruments, 1948, 19, 605-607.

[65] Wiley W. C., McLaren I. H. Time-of-Flight Mass Spectrometer with Improved resolution. Review of Scientific Instruments 1955, 26, 1150-1157.

[66] Guilhaus M., Mlynski V., Selby D. Perfect timing: Time-of-Flight Mass Spectrometry. Rapid Communications in Mass Spectrometry, 1997, 11, 951-962.

[67] Guilhaus M. Principles and Instrumentation in Time of Flight Mass Spectrometry. Physical and Instrumental Concepts, Journal of Mass Spectrometry, 1995, 30, 1519-1532.

[68] Glish G. L., Vachet R. W. The Basics of Mass Spectrometry in the Twenty First Century. Nature Reviews, 2003, 2, 140-150.

[69] Mamyrin, B. A., Karatajev, V. J., Shmikk D. V., Zagulin V. A. The mass-reflectron, a new nonmagnetic time-of-flight mass spectrometer with high resolution. Journal of Experimental and Theoretical Physics, 1973, 37, 45-48.

[70] Cotter R. J. Time-of-Flight Mass Spectrometry for the Structural Analysis of Biological Molecules. Analytical Chemistry, 1992, 64, 1027A-1039A.

[71] Chernushevich I. V., Loboda A. V., Thomson B. A. An Introduction to quadrupole-time-of-flight mass spectrometry. Journal of Mass Spectrometry, 2001, 36, 849-865.

[72] Steen H., Kurster B., Mann M. Quadrupole time-of-flight versus triple qaudrupole mass spectrometry for the determination of phosphopeptides by precursor ion scanning. Journal of Mass Spectrometry, 2001, 36, 782-790.

[73] oMALDI Server users Manual, MDS Sciex, 2003.

[74] Jennings K. R. Collision induced decompositions of aromatic molecular ions. International Journal of Mass Spectrometry and Ion Physics, 1968, 1, 227-235.

[75] de Hoffman E. Tandem Mass Spectrometry: Fundamentals and Instrumentation. Enclyclopedia of Analytical Chemistry. Meyers R. A. (Editor) Wiley Publications, 2006, 1-22.

[76] Lauterbur P. C. Image Formation by Local Interactions: Examples of Employing Nuclear Magnetic Resonance. Nature, 1973, 242, 190-191.

[77] Ter-Pogossian M. M., Raichle M. E., Sobel B. E. Positron Emission Tomography. Scientific American, 1980, 243, 170-181.

[78] MacAleese L., Stauber J., Heeren R. M. A. Perspectives for imaging mass spectrometry in the proteomics landscape. Proteomics, 2009, 9, 819-834.

[79] Brunelle A., Laprevote O. Lipid imaging with cluster time-of-flight secondary ion mass spectrometry. Analytical and Bioanalytical Chemistry, 2009, 393, 31-35.

[80] Hou W., Zhou H., Elisma F., Bennett S.A.L., Figeys D. Technological developments in lipidomics. Briefings in functional genomics and proteomics, 2008, 7, 395-409.

[81] Bedair M., Sumner L. W. Current and emerging mass spectrometry technologies for metabolomics. Trends in Analytical Chemistry, 2008, 27, 238-250.

[82] Luxembourg S. L., Mize T. H., McDonnell L. A., Heeren R. M. A. High-Spatial Resolution Mass Spectrometric Imaging of Peptide and Protein Distributions on a Surface. Analytical Chemistry, 2004, 76, 5339-5344.

[83] McDonnell L. A., Heeren R. M. A. Imaging Mass Spectrometry. Mass Spectrometry Reviews, 2007, 26, 606-643.

[84] Colliver T. L., Brummel C. L., Pacholski M. L, Swanek F. D., Ewing A.G., Winograd N. Atomic and molecular imaging at the single-cell level with TOF-SIMS. Analytical Chemistry, 1997, 69, 225-2231.

[85] Sjovall P., Lausmaa J., Nygren H., Carlsson L., Malmberg P. Imaging of membrane lipids in single cells by imprint-imaging time-of-flight secondary ion mass spectrometry. Analytical Chemistry, 2003, 75, 3429-3434.

[86] Monroe E. B., Annangudi S. P., Hatcher N. G., Gutstein H. B., Rubakhin S. S., Sweedler J. V. SIMS and MALDI MS imaging of the spinal cord. Proteomics, 2008, 8, 3746-3754.

[87] Malmberg P., Borner K., Chen Y., Friberg P., Haganhoff B., Mansson J-E., Nygren H. Localization of lipids in the aortic wall with imaging TOF-SIMS. Biochimica et Biophysica Acta, 2007, 1771, 185-195.

[88] Ifa D. R., Wiseman J. M., Song Q., Cooks R. G. Development of capabilities for imaging mass spectrometry under ambient conditions with desorption electrospray ionization (DESI). International Journal of Mass Spectrometry, 2007, 259, 1, 8-15.

[89] Wiseman J. M., Ifa D. R., Zhu Y., Kissinger C. B., Manicke N. E., Kissinger P. T., Cooks R. G. Desorption electrospray ionisation mass spectrometry: Imaging

drugs and metabolites in tissues. Proceedings of the National Academy of Sciences, 2008, 105, 18120-18125.

[90] Wiseman J. M., Ifa D. R., Song Q., Cooks R. G. Tissue Imaging at Atmospheric Pressure Using Desorption Electrospray Ionisation (DESI) Mass Spectrometry. Angewandte Chemie International Edition, 2006, 45, 7188-7192.

[91] Wiseman J. M., Puolitaival S. M., Takats Z., Cooks R. G., Caprioli R. M. Mass Spectrometric Profiling of Intact Biological Tissue by Using Desorption Electrospray Ionization. Angewandte Chemie International Edition, 2005, 44, 7094-7097.

[92] Kertesz V., Van Berkel G. J. Improved imaging resolution in desorption electrospray ionization mass spectrometry. Rapid Communications in Mass Spectrometry, 2008, 22, 2639-2644.

[93] Luxembourg S. L., Vaezaddeh A.R., Amstalden E. R., Zimmerman-Ivol C. G, Hochstrasser D. F., Heeren R. M. A. The molecular scanner in microscope mode. Rapid Communications in Mass Spectrometry, 2006, 20, 3435-3442.

[94] Guilhaus M., Selby D., Mlynski V. Orthogonal acceleration time-of-flight. Mass Spectrometry Reviews, 2000, 19, 65-107.

[95] Scherl A., Zimmerman-Ivol C. G., Di Dio J., Vaezzadeh A. R., Binz P-A., Amez-Droz M., Cochard R., Sanchez J-C., Gluckmann M., Hochstrasser D. F. Gold coating of non-conductive membranes before matrix-assisted laser desorption/ionization tandem mass spectrometric analysis prevents charging effect. Rapid Communications in Mass Spectrometry, 2005, 19, 605-610.

[96] Griffiths W. J. (Editor). Metabolomics, Metabonomics and Metabolite Profiling. Royal Society of Chemistry Publishing, 2008.

[97] Holle A., Haase A., Kayser M., Hohndorf J. Optimizing UV laser focus profiles for improved MALDI performance. Journal of Mass Spectrometry, 2006, 41, 705-716.

[98] Klochkov D.V., Kotkovskii G. E., Nalobin A. S., Tananina E. S., Chistyakov A. A. Ion formation upon water excitation by IR laser radiation in the range of OH

stretching vibrations. Journal of Experimenatl and Theretical Physics Letters, 2002, 75, 20-22.

[99] Overberg A., Karas M., Bahr R., Kaufmann R., Hillenkamp F. Matrix-Assisted Infrared-Laser (2.94-MU-M) Desorption Ionization Mass-Spectrometry of Large Biomolecules. Rapid Communications in Mass Spectrometry, 1990, 4, 293-296.

[100] Berkenkamp S., Menzel C., Karas M., Hillenkamp F. Performance of infrared matrix-assisted laser desorption/ionization mass spectrometry with lasers emitting in the 3μm wavelength range. Rapid Communications in Mass Spectrometry, 1997, 11, 1399-1406.

[101] Dreisewerd K., Berkenkamp S., Leisner A., Rohlfing A., Menzel C. Fundamentals of matrix-assisted laser desorption/ionisation mass spectrometry with pulsed infrared lasers. International Journal of Mass Spectrometry, 2003, 226, 189-209.

[102] Peterson D. S. Matrix-Free Methods for Laser Desorption/Ionisation Mass Spectrometry. Mass Spectrometry Reviews, 2007, 26, 19-34.

[103] Dreisewerd K., Lemaire R., Pohlentz G., Salzet M., Wisztorski M., Berkenkamp S., Fournier I. Molecular Profiling of Native and Matrix-Coated Tissue Slices from Rat Brain by Infrared and Ultraviolet Laser Desorption/Ionization Orthogonal Time-of-Flight Mass Spectrometry. Analytical Chemistry, 2007, 79, 2463-2471.

[104] Dreisewerd K., Draude F., Kruppe S., Rohlfing A., Berkekamp S., Pohlentz G. Molecular Analysis of Native Tissue and Whole Oils by Infrared Laser Mass Spectrometry. Analytical Chemistry, 2007, 79, 4514-4520.

[105] Schwartz S. A., Reyzer M. L., Caprioli R. M. Direct tissue analysis using matrix-assisted laser desorption/ionisation mass spectrometry: practical aspects of sample preparation. Journal of the American Society for Mass Spectrometry, 2003, 38, 699-708.

[106] Goodwin R. J. A., Dungworth J. C., Cobb S. R., Pitt A. R. Time-dependent evolution of tissue markers by MALDI MS imaging. Proteomics, 2008, 8, 3801-3808.

[107] Rohner T. C., Staab D., Stoeckli M. MALDI mass spectrometric imaging of biological tissue sections. Mechanisms of Ageing and Development, 2004, 126, 177-185.

[108] Reyzer M. L., Hsieh Y., Ng K., Korfmacher W. A., Caprioli R. M. Direct Analysis of drug candidates in tissue by matrix-assisted laser desorption/ionisation mass spectrometry. Journal of Mass Spectrometry, 2003, 38, 1081-1092.

[109] Chaurand P., Norris J. L., Cornett D. S., Mobley J. A., Caprioli R. M. New developments in profiling and imaging of proteins from tissue sections by MALDI mass spectrometry. Journal of Proteome Research, 2006, 5, 2889-2900.

[110] Kruse R., Sweedler J. V. Spatial profiling of invertebrate ganglia using MALDI MS. Journal of the American Society for Mass Spectrometry, 2003, 14, 752-759.

[111] Stoekli M., Staab D., Schweitzer A. Compound and metabolite distribution measured by MALDI Mass spectrometric imaging in whole-body tissue sections. International Journal of Mass Spectrometry 2007, 260, 195-202.

[112] Crossman L., McHugh N. A, Hsieh Y., Korfmacher W. A, Chen J. Investigation of the profiling depth in matrix-assisted laser desorption/ionization imaging mass spectrometry. Rapid Communications in mass Spectrometry, 2006, 20, 284-290.

[113] Hsieh Y., Casale R., Fukuda E., Chen J., Knemeyer I., Wingate J., Morrison R., Korfmacher W. Matrix-assisted laser desorption/ionization imaging mass spectrometry for direct measurement of clozapine in rat brain tissue. Rapid Communications in Mass Spectrometry, 2006, 20, 965-972.

[114] Chaurand P., Sanders M. E., Jensen R. A., Caprioli R. M. Proteomics in Diagnostic Pathology: Profiling and Imaging Proteins Directly in Tissue Sections. American Journal of Pathology, 2004, 165, 1057-1068.

[115] Zaluzec E. J., Gage D. A., Allison J., Watson J. T. Direct matrix assisted laser desorption ionisation mass spectrometric analysis of proteins immobilised on nylon based membranes. Journal of the American Society for Mass Spectrometry, 1994, 5, 230-237.

[116] Preston L. M., Murray K. K., Russell D. H. Reproducibility and quantification of MALDI MS; Effects of nitrocellulose on peptide ion yields. Biological Mass Spectrometry, 1993, 22, 544-550.

[117] Bunch J., Clench M. R., Richards D. S. Determination of pharmaceutical compounds in skin by imaging matrix-assisted laser desorption/ionisation mass spectrometry. Rapid Communications in Mass Spectrometry, 2004, 18, 3051-3060.

[118] Prideaux B., Atkinson S. J., Carolan V. A., Morton J., Clench M. R. Sample preparation and data interpretation procedures for the examination of xenobiotic compounds in skin by indirect imaging MALDI-MS. International Journal of Mass Spectrometry, 2007, 260, 243-251.

[119] Todd P. J., Schaaf G., Chaurand P., Caprioli R. M. Organic ion imaging of biological with secondary ion mass spectrometry and matrix-assisted laser desorption/ionisation. Journal of Mass Spectrometry, 2001, 36, 355-369.

[120] Cohen L. H., Gusev L. H. Small molecule analysis by MALDI mass spectrometry. Analytical and Bioanalytical Chemistry, 2002, 373, 571-586.

[121] Beavis R. C., Chait B. T. Factors affecting the ultraviolet laser desorption of proteins. Rapid Communications in Mass Spectrometry 1989, 3, 233-237.

[122] Chaurand P., Cornett D. S., Caprioli R. M. Molecular imaging of thin mammalian tissue sections by mass spectrometry. Current Opinion in Biotechnology, 2006, 17, 1-6.

[123] Soltzberg L. J., Patel P., Small molecule matrix-assisted laser desorption/ionization time-of-flight mass spectrometry using a polymer matrix. Rapid Communications in Mass Spectrometry, 2004, 18, 1455-1458.

[124] Vermillion-Salsbury R. L., Hercules D. M. 9-aminoacridine as a matrix for negative mode matrix-assisted laser desorption/ionisation. Rapid Communications in Mass Spectrometry, 2002, 16, 1575-1581.

[125] Edwards J. L., Kennedy R. T. Metabolomic Analysis of Eukaryotic Tissue and Prokaryotes Using Negative Mode MALDI Time-of-Flight Mass Spectrometry. Analytical Chemistry, 2005, 77, 2201-2209.

[126] Zabet-Moghaddam M., Heinzle E., Thorley A. Qualitative and quantitative analysis of low molecular weight compounds by ultraviolet matrix-assisted laser desorption/ionization mass spectrometry using ionic liquid matrices. Rapid Communications in Mass Spectrometry, 2004, 18, 141-148.

[127] Armstrong D. W., Zhang L.-K,. He L., M. L. Gross. Ionic liquids as matrixes for matrix-assisted laser desorption/ionization mass spectrometry. Analytical Chemistry, 2001, 73, 3679-3686.

[128] Cramer R., Burlingame A. L. Employing target modifications for the investigation of liquid infrared matrix-assisted laser desorption/ionization mass spectrometry. Rapid Communications in mass Spectrometry, 2000, 14, 53-60.

[129] Berkenkamp S., Menzel C., Hillenkamp F., Dreisewerd K. Measurements of mean initial velocities of analyte and matrix ions in infrared matrix-assisted laser desorption ionization mass spectrometry. Journal of the American Society for Mass Spectrometry, 2002, 13, 209-220.

[130] Dale R., Knochenmuss R., Zenobi R. Two-phase matrix-assisted laser desorption/ionization: Matrix selection and sample pretreatment for complex anionic analytes. Rapid Communications in Mass Spectrometry, 1997, 11, 136-142.

[131] Kraft P., Alimpiev S., Dratz E., Sunner J. Infrared surface-assisted laser desorption ionization mass spectrometry on frozen aqueous solutions of proteins and

peptides using suspensions of organic solids. Journal of the American Society for Mass Spectrometry, 1998, 9, 912-924.

[132] Crecelius A., Clench M. R., Richards D. S., Parr V. Thin-layer chromatography-matrix-assisted laser desorption ionisation-time-of-flight mass spectrometry using particle suspension matrices. Journal of Chromatography A, 2002, 958, 249-260.

[133] Black C., Poile C., Langley J., Herniman J. The use of pencil lead as a matrix and calibrant for matrix-assisted laser desorption/ionisation. Rapid Communications in Mass Spectrometry, 2006, 20, 1053-1060.

[134] Chen Y., Allegood J., Liu Y., Wang E., Cachn-Gonzlez B., Cox T. M., Merrill A. H., Sullards M. C. Imaging MALDI Mass Spectrometry Using an Oscillating Capillary Nebulizer Matrix Coating System and Its Application to Analysis of Lipids in Brain from a Mouse Model of Tay-Sachs/Sandhoff Disease. Analytical Chemistry, 2008, 80, 2780-2788.

[135] Aerni H-R., Cornett D. S., Caprioli R.M. Automated Acoustic Matrix Deposition for MALDI Sample Preparation. Analytical Chemistry, 2006, 78, 827-834.

[136] Wei H., Nolkrantz K., Powell D. H., Woods J. H., Ko M-C., Kennedy R. T. Electrospray sample deposition for matrix-assisted laser desorption/ionization (MALDI) and atmospheric pressure mass spectrometry with attomole detection limits. Rapid Communications in Mass Spectrometry, 2004, 18, 1193-1200.

[137] Baluya D. L., Garrett T. J., Yost R. A. Automated MALDI Matrix Deposition Method with Inkjet Printing for Imaging Mass Spectrometry. Analytical Chemistry, 2007, 79, 6862-6867.

[138] http://www.ssi.shimadzu.com/products/product.cfm?product=chip

[139] Schuerenberg M., Shi G., Muller R., Deninger S. O, Suckau D. A New Sensor-Controlled Preparation technique for MALDI Tissue Imaging. Poster Presentation, ABRF 2008, Poster V44-M, Convention Centre, Salt Lake City, Utah.

(http://www.bdal.com/fileadmin/PDF/literature2008/abrf-poster2008/ABRF2008-V44-M-ImagePrep.pdf) Last accessed 10th May 2009.

[140] http://www.sunchrom.de/pdf/SunChrom%20SunCollect_english.pdf Last accessed 10th May 2009.

[141] Caprioli R. M., Farmer T. B., Gile J. Molecular imaging of biological samples: Localization of peptides and proteins using MALDI TOF MS. Journal of Analytical Chemistry, 1997, 69, 4751-4760.

[142] Hsieh Y., Chen J., Korfmacher W. A. Mapping Pharmaceuticals in tissues using MALDI imaging mass spectrometry. Journal of Pharmacological and Toxicological Methods, 2006, 55, 193-200.

[143] Mullen A. K., Clench M. R., Crosland S., Sharples K. R. Determination of agrochemical compounds in soya plants by imaging matrix-assisted laser desorption/ionisation mass spectrometry. Rapid Communications in Mass Spectrometry, 2005, 19, 2507-2516.

[144] Deininger S-O., Ebert M. P, Utterer A. F, Gerhard M., Rocken C. MALDI Imaging Combined wtih Hierarchical Clustering as a New Tool for the Interpretation of Complex Human Cancers. Journal of Proteome Research, 2008, 7, 5230-5236.

[145] Van de Plas V., Ojeda F., Dewil M., Van Den Bosch L., De Moor B., Waelkens E. Prospective Exploration of Biochemical Tissue Composition Via Imaging Mass Spectrometry Guided by Principal Component Analysis. Pacific Symposium on Biocomputing, 2007, 12, 458-469.

[146] McCombie G., Staab D., Stoekli M., Knochenmuss R. Spatial and spectral correlations in MALDI mass spectrometry images by clustering and multivariate analysis Analytical Chemistry, 2005, 77, 6118-6124.

Chapter 2

Evaluation of MALDI MSI Sample Preparation Procedures for the Analysis of Anti-Asthmatic Compounds in Lung Tissue

2.1 Introduction

Asthma is a chronic disease that causes inflammation in the airways particularly in the lungs. In the UK alone there are 5.4 million people currently receiving treatment for asthma, therefore it is of great interest to the pharmaceutical industry to develop better medications to relieve the symptoms [1]. During an asthma attack, the muscles around the airways constrict, causing the airways to become narrower; the lining of the airways become inflamed and mucus starts to accumulate in the airways further constricting airflow [1].

Asthma drugs have to be inhaled in order to be effective and this is usually achieved by the use of pressurised metered inhalers or nebulisers, which create a fine mist of the drug. Inhaled corticosteroids (ICS) such as Budesonide and Fluticasone Propionate are crucial in the management of asthma as they play a key role in reducing inflammation and ultimately improving the function of the lungs. The clinical effectiveness of corticosteroids is brought about by their ability to block the multiple inflammatory pathways that characterise asthma and other chronic inflammatory airway diseases [2, 3]. Inhaled corticosteroids are also used in the treatment of chronic obstructive pulmonary disease (COPD) [4]. Long acting beta 2 adrenergic receptor agonists, for example Salmeterol, are often used in conjunction with the corticosteroid drugs. When inhaled, Salmeterol causes the smooth muscle in the airways to relax leading to bronchodilation and provides some relief from the asthma attack [5]. The use of combination therapies incorporating the use of a corticosteroid with a bronchodilator is becoming increasingly common in the treatment of asthma, for example Seretide, a combination of Fluticasone Propionate with Salmeterol. Once inhaled, there are many factors that can affect the drug's efficacy such as its half-life, its lipophilicity and the distribution of the drug in the lungs [6].

The aim of inhaled drug therapies is to attain high local concentrations in the lungs and limit systemic exposure. The distribution of inhaled asthma drugs in the lung can be related to how effective the drug is in having its therapeutic effect. There are many factors that can affect drug distribution in the lungs such as the type of

compound inhaled, the way in which the compound was inhaled and the condition of the airways.

In addition to the actual drug distribution another important factor is how quickly the drug is cleared from the lung after bringing about its therapeutic effect.

Techniques that are commonly employed for drug distribution studies include PET [7], MRI [8] and autoradiography. PET and MRI are techniques that can be used *in vivo* although the achievable spatial resolution is only in the range of millimeters. However, for PET there is a requirement for the compound of interest to be radiolabelled. Autoradiography has better resolution than PET and MRI (in the range of micrometers); however, there is still a requirement for the compound of interest to be radiolabelled. Whole body autoradiography [9] has been demonstrated; however, the main drawback with this technique is the cost and, as it is the radioactive label that is measured, it can be difficult to differentiate between the drug and its metabolites.

Stoeckli *et al.* [10] have compared autoradiography with MALDI MSI; the sensitivity and speed of a MALDI imaging experiment and the ability to differentiate between a compound and its metabolites have made MALDI MSI complementary to existing techniques. A comparison has also been reported between DESI MS and autoradiography, where the distribution of Propanolol was measured in a range of organs [11].

Methods that have previously been used to assess drug distribution in the lungs include gamma scintigraphy [12] and LC-MS/MS which has been used to study the pulmonary disposition of three compounds used in the treatment of asthma by measuring the levels of drug in the perfusate [13].

In this chapter methodology is detailed for the direct and indirect analysis of anti-asthmatic compound in lung tissue. The indirect analysis of pharmaceutical compounds in tissue has been previously described by Bunch *et al.* for the analysis of pharmaceutical compounds in skin [14].

In the work reported in this chapter the potential of MALDI MSI has been investigated for the study of a number of compounds. The following sections detail these.

2.1.1 Budesonide

Budesonide has been reported to undergo rapid and reversible intracellular esterification with long chain fatty acids in the airway tissue in animal studies [15] and also in human studies [16] using radioactively labelled Budesonide. It was reported in the animal studies that 80% of the administered radioactively labelled Budesonide was found as esters, predominatly as Budesonide Oleate [15]. It is thought that this fatty acid conjugation explains why the effects of Budesonide are long lasting.

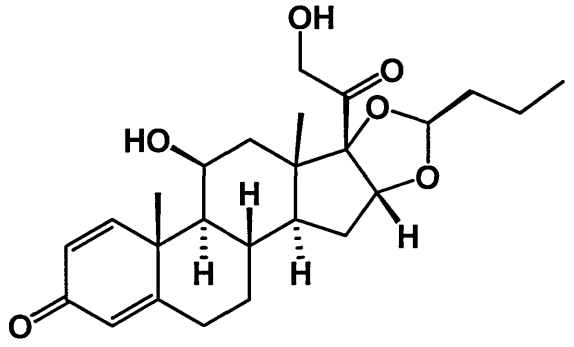

Figure 2.1: The Chemical Structure of Budesonide

IUPAC name: 16,17-(butylidenebis(oxy))-11,21-dihydroxy-, (11-β,16-α)-pregna-1,4-diene-3,20-dione

Formula: $C_{25}H_{34}O_6$

RMM: 430.24

2.1.2 Fluticasone Propionate

Unlike Budesonide, Fluticasone Propionate does not undergo esterification. Undissolved Fluticasone Propionate particles have been reported in the airway lumen at periods up to 22 hours after inhalation [16]. Clearly the undissolved particles are

not going to bring about a pharmacological effect; this is because the drug is not accessible to intracellular glucocorticoid receptors [16].

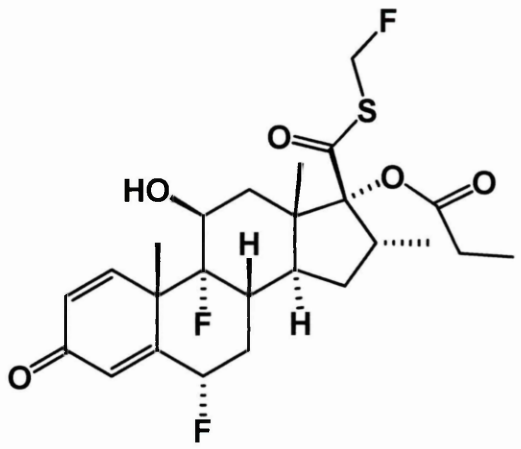

Figure 2.2: The Chemical Structure of Fluticasone Propionate.

IUPAC name: S-(fluoromethyl)-6α,9-difluoro-11β, 17-dihydroxy-16α-methyl-3-oxoandrosta-1, 4-diene-17β-carbothioate, 17-propionate

Formula: $C_{25}H_{31}F_3O_5S$

RMM: 500.18

2.1.3 Salmeterol

Salmeterol has a long half life of approximately 12 hours; this is related to its chemical structure in that it has a lipophilic tail that facilitates its binding and resulting accumulation in the cytoplasmic membrane, thus bringing about a prolonged β_2 receptor stimulation [17].

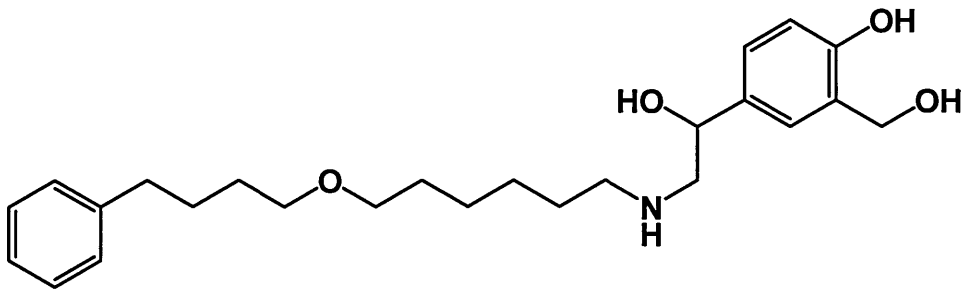

Figure 2.3: The Chemical Structure of Salmeterol.

IUPAC name: 2-(hydroxymethyl)-4-{1-hydroxy-2-[6-(4-phenylbutoxy) hexylamino]ethyl}phenol

Formula: $C_{25}H_{37}NO_4$

RMM: 415.27

2.1.4 GSK256066B

The test compound was supplied by GlaxoSmithKline (GSK). The structure of this chemical compound is confidential.

2.2 Experimental

2.2.1 Materials

Budesonide, Salmeterol, Fluticasone Propionate (FP) and GSK256066B were supplied by GlaxoSmithKline (GSK), Stevenage, UK. α-cyano-4-hydroxycinnamic acid (α-CHCA), titanium dioxide (TiO_2) and graphite, ethylene glycol, ethanol and trifluoroacetic acid (TFA) were purchased from Sigma Aldrich, Dorset, UK

2.2.2 Methodology

2.2.2.1 Preliminary Matrix Investigations

Preliminary MALDI MS experiments were conducted using the conventional dried droplet technique to assess each of the drugs with different matrices in order to select the most appropriate matrix for each compound. This was achieved by mixing 1μL of the drug compound with 1μL of the matrix solution and then spotting 1μL of the combined solution onto a MALDI spot target for analysis. Each drug compound was prepared in the following concentrations using 95% ethanol: 1mg/mL, 0.1mg/mL and 0.01mg/mL. This range of concentrations was used to assess the different levels of detection for each drug compound. The matrices tested were dissolved in the same solvent as the drug to aid the co-crystallisation process. α-CHCA was made to a concentration of 25mg/mL in 95% ethanol containing 0.1% TFA.

Particle suspension matrices were also investigated in the same way and were optimised for the direct tissue experiments. The optimum particle suspension matrix was found to be a mixture of TiO_2 and graphite made to a total concentration of 10mg/mL (6mg TiO_2 and 4mg graphite) containing 0.1% TFA and 0.01% ethylene glycol. The TFA was added to enhance the formation of protonated species and the ethylene glycol was added as a dispersant. The matrix was applied using an airbrush as detailed in section 2.2.2.4.

2.2.2.2 Preparation of Rat Lung Tissue

Laboratory rats (male Wistar rats, supplied by Biological Services, University of Sheffield, Beech Hill Road, Sheffield, S10 2RX) were sacrificed by the schedule one method of the Home Office, UK regulations. Immediately after the animals had been sacrificed the lung tissue was dissected out and immediately frozen using isopentane and liquid nitrogen. A cryostat (Leica CM1510) with chamber temperature: -20°C was used to section the lung tissue to a thickness of 20μm and then the sections were thaw mounted onto aluminium plates. This was followed by the spiking of the tissue for all the compounds investigated and matrix application.

2.2.2.3 Methods for Drug Analysis on Lung Tissue

2.2.2.3.1 Direct Analysis

1μL of each of the different concentrations drug solutions prepared as stated in 2.2.2.1 was applied to separate lung tissue sections prepared as stated in 2.2.2.2. Once the drug spots had dried, the matrix was applied (refer to section 2.2.2.4). The drug compounds were applied to different regions of the lung tissue section to evaluate potential regional suppression effects. Total drug concentrations equate to 1μg, 100ng and 10ng on the tissue surface.

2.2.2.3.2 Indirect Analysis

Fresh lung tissue was spiked with each of the different concentrations of the drug compounds and left on the tissue for approximately two hours, after which time a cellulose blot was taken by pressing the cellulose membrane against the tissue surface for a 40 second period. This was found to be the optimal blotting time for efficient analyte transfer from the tissue onto the cellulose membrane. This membrane was then coated with matrix (refer to section 2.2.2.4). Total drug concentrations equate to 1μg, 100ng and 10ng on the tissue surface; however, the total amount of drug recovered is dependent on the efficiency of the blotting procedure.

2.2.2.4 Matrix Application

Matrix was applied using an airspray deposition technique; one coating cycle comprised 5 sprays over the surface of the tissue with a spray distance of approximately 10 inches from the tissue surface. Five cycles were needed to achieve a homogenous layer of matrix over the tissue surface.

Some of the tissue samples described in this chapter were sputter coated with gold in an attempt to increase sensitivity (refer to section 2.3.2). Approximately 5nm of gold was deposited directly after matrix application using an Emitech SC7620 mini sputter coater (Materials and Engineering Institute, Sheffield Hallam University).

2.2.3 Instrumentation

All analyses were performed in positive ion mode on an Applied Biosystems/MDS Sciex hybrid quadrupole time-of-flight mass spectrometer (Q-Star Pulsar-*i*) with an orthogonal MALDI ion source and a high repetition Nd: YAG laser (1 kHz). The Nd: YAG laser has an elliptical spot size of 100x150µm. Images were obtained at a resolution of 150 x 150µm. The laser fired at a power of 30% (3.2µJ) at each location for 2 seconds.

2.3 Results and Discussion

2.3.1 Budesonide

The mass spectrum in figure 2.4 represents the initial data obtained from conventional MALDI MS experiments.

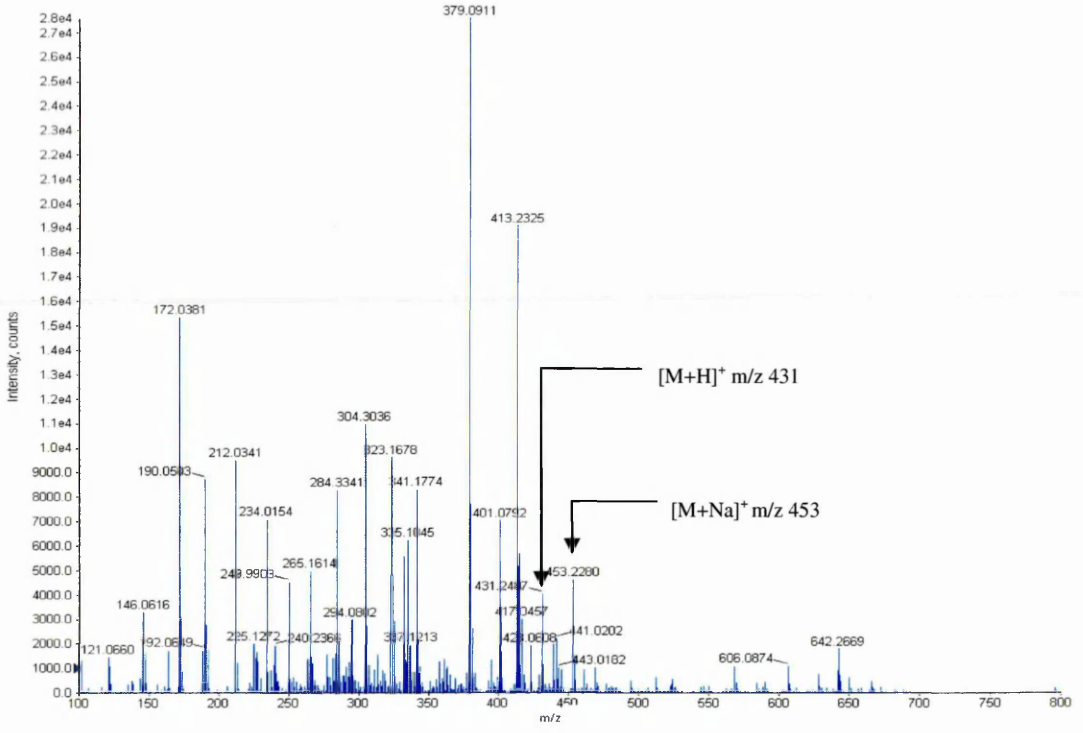

Figure 2.4: MALDI Mass Spectrum of Budesonide. A representative full scan positive ion MALDI mass spectrum for Budesonide (500ng on the MALDI target plate) with α-CHCA showing the protonated molecule at m/z 431 and sodiated molecule at m/z 453.

The direct imaging of Budesonide from lung tissue could not be achieved using either organic matrices such as α-CHCA or inorganic particle suspension matrices such as TiO_2/graphite. Therefore, an indirect blotting method was incorporated into the analysis to investigate if the drug could be detected from the surface of the lung tissue. The lung tissue contains sufficient moisture to aid the transfer of the drug compound to the blotting medium. This allows organic acid matrices to be used as the endogenous compounds are not present in sufficient quantity to prevent matrix crystallisation or suppress ionisation of the drug compound.

The results of this procedure can be seen in figure 2.5. In this example, the data were normalised with the corresponding protonated matrix peak at m/z 190. The total drug concentration in the image shown in figure 2.5 is 1µg. The circled area shows the presence of the drug although there is some evidence of lateral diffusion of the drug. This may have occurred during the transfer of the drug from the tissue onto the membrane or during matrix application.

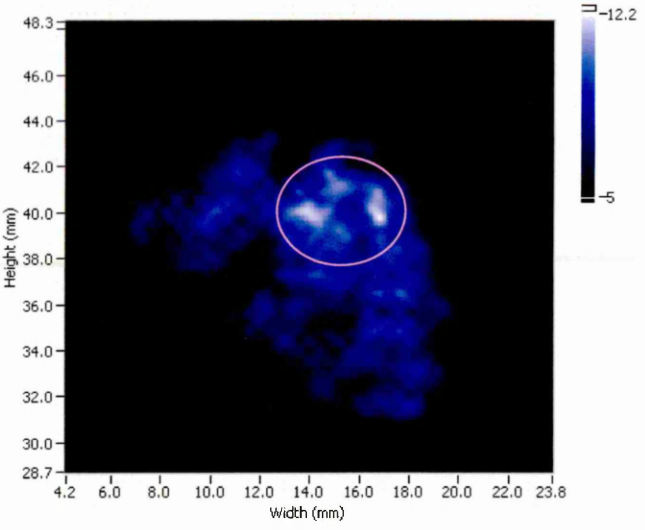

Figure 2.5: Indirect MALDI MS Image of Budesonide.

The amount of the drug on the tissue surface is 1µg. The $[M+H]^+$ at m/z 431 of Budesonide was normalised with the $[M+H]^+$ of α-CHCA at m/z 190. The circled area shows the drug spiked area. The scale on the right hand side of the image shows the intensity with white being the most intense (i.e. accounting for more ions) and the darker colour accounting for fewer ions.

2.3.2 Fluticasone Propionate

As previously mentioned in section 2.1.2 there has been evidence reported to support the fact that Fluticasone Propionate remains in the lung in its particle form [15]. Attempts to image Fluticasone Propionate are reported in this section. Initially the TiO_2/Graphite matrix was used for the analysis of Fluticasone Propionate in lung tissue. The results are presented in figure 2.6 where the spots are labelled 1, 2 and 3. Spots 1 and 2 are not as clearly defined as spot 3; this could be due to regional suppression effects within the lung tissue. There is evidence of lateral diffusion; this could be due to the choice of solvent used to dissolve the drug but the matrix application procedure can also cause the diffusion of analytes on tissue samples [18].

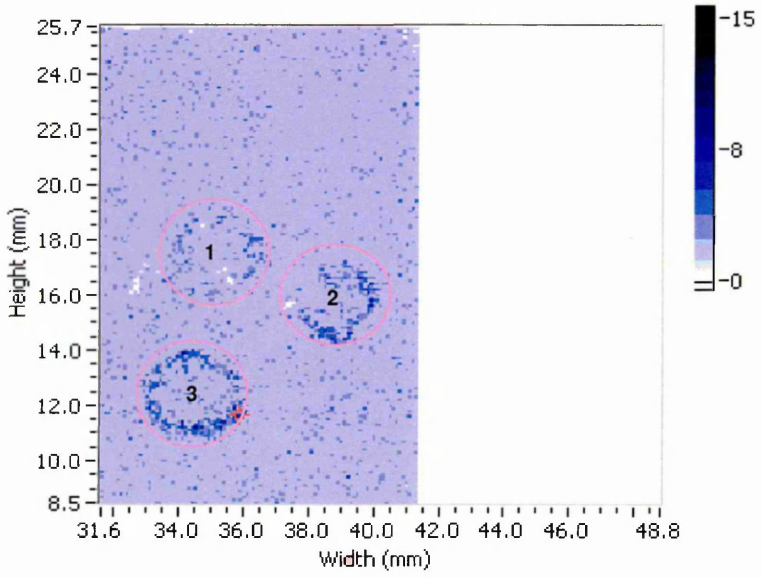

Figure 2.6: Direct MALDI MS Image of Fluticasone Propionate on Lung Tissue. The drug concentration of each spot is 1µg. The potassiated molecule is the most predominant ion at m/z 539. The matrix used was TiO_2/Graphite prepared as stated in 2.2.2.1. The image shows evidence of lateral diffusion within the drug spiked areas highlighted in the image. The scale on the right hand side of the image shows the intensity with dark blue being the most intense (i.e. accounting for more ions) and lighter blue/white accounting for fewer ions.

The same experiment was repeated and incorporated sputter coating of gold across the sample surface on top of the matrix layer in an attempt to increase the sensitivity.

The results from this analysis are presented in figure 2.7. When figures 2.6 and 2.7 are compared it is clear that the sputter coated gold has increased the sensitivity and the image is much clearer. The perimeter of the tissue section can be seen along with the three spots of FP. The total drug amount of each spot is 1µg. Although 10ng could be detected with conventional MALDI dried droplet experiments, imaging experiments on the lung tissue could not be obtained at levels less than 1µg; this is probably due to the presence of endogenous compounds that are suppressing the ionisation of the drug off the tissue surface.

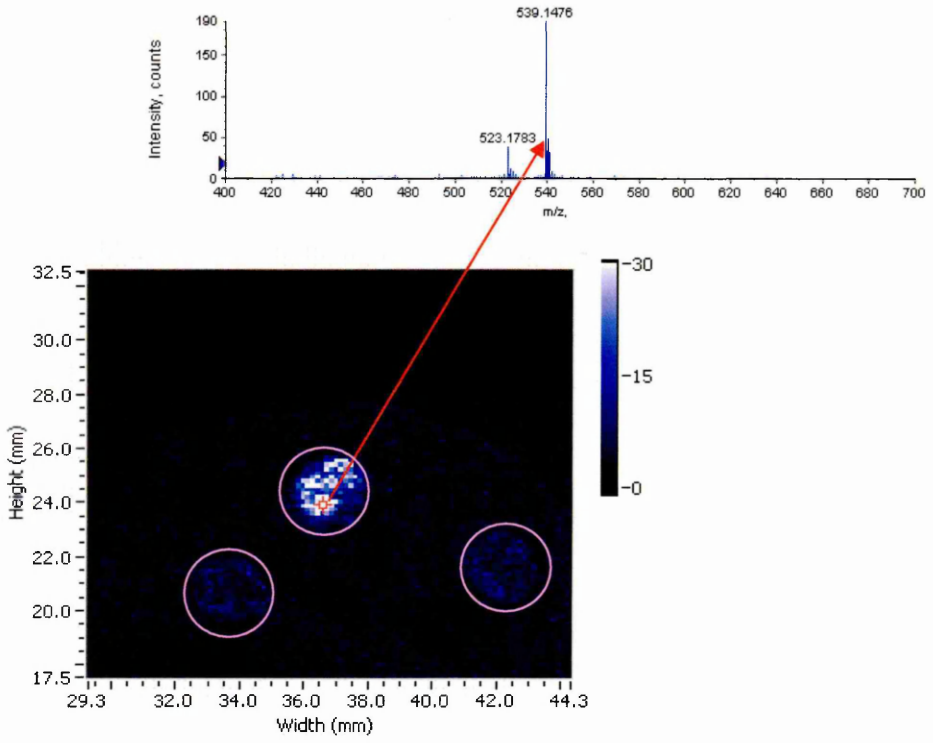

Figure 2.7: Direct MALDI MS Enhanced Image of Fluticasone Propionate on Lung Tissue. Image shows the distribution of $[M+K]^+$ at m/z 539. The sample was prepared exactly as detailed for figure 2.6 where the tissue was spiked with three 1µL spots of Fluticasone Propionate; the drug concentration of each spot was 1µg. The matrix used was TiO_2/Graphite prepared as stated in 2.2.2.1. After the matrix had been applied to the surface of the tissue the sample was sputter coated with gold.
The scale on the right hand side of the image shows the intensity with white being the most intense (i.e. accounting for more ions) and the darker colour accounting for fewer ions.

2.3.3 Salmeterol

The data in figure 2.8 was obtained from conventional MALDI-MS analysis.

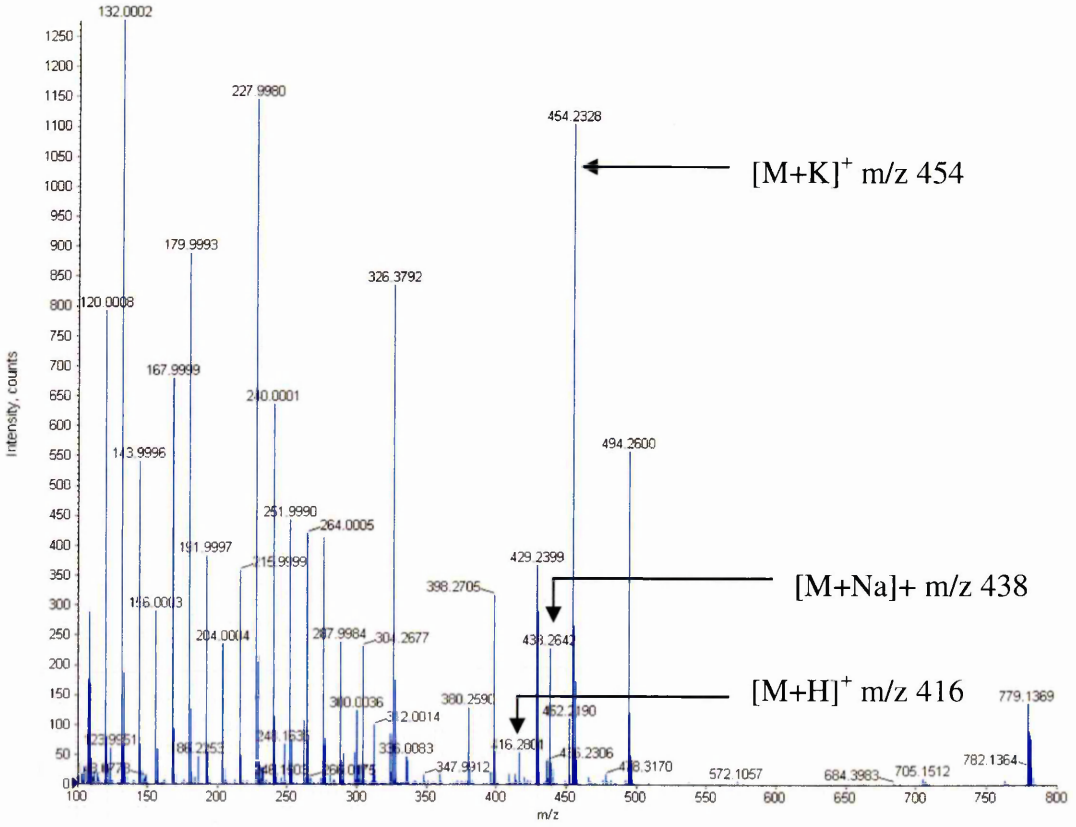

Figure 2.8: MALDI Mass Spectrum of Salmeterol. MALDI mass spectrum of the potassium adduct of Salmeterol at m/z 454 its predominant form. The sodium adduct at m/z 438 and the protonated molecule at m/z 416 are also present. This spectrum was obtained from conventional MALDI MS analysis of the drug, Salmeterol, with the particle suspension matrix TiO_2/Graphite.

Experiments were conducted to try to image this compound in lung tissue; however, results could not be obtained even at the 1µg level. Possible reasons for this include suppression of Salmeterol ionisation by the carbon cluster peaks present in the low mass region under m/z 400. This drug could also not be detected from indirect imaging experiments.

2.3.4 GSK256066B

GSK256066B is a compound that ionises very well in MALDI as can be seen in figure 2.9; the protonated, sodiated and potassiated species can be clearly seen and appear to suppress the matrix peaks, in particular the carbon cluster peaks. This is an example of analyte suppression of the matrix.

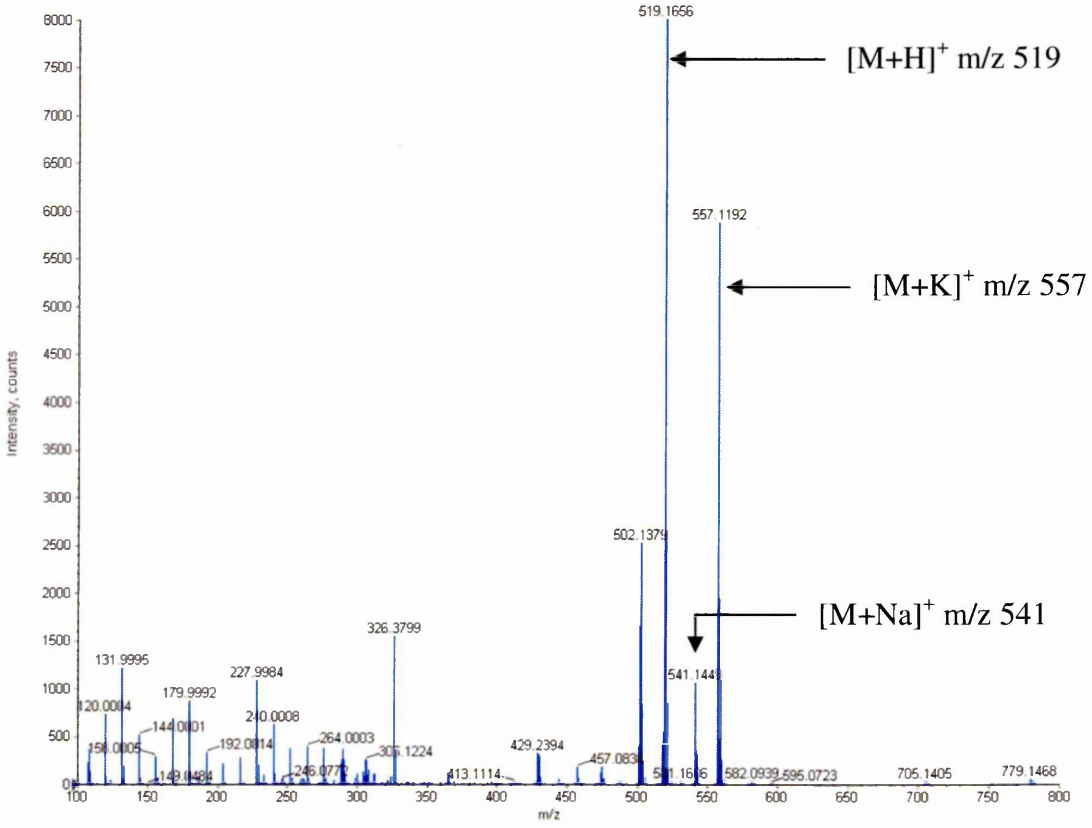

Figure 2.9: MALDI Mass Spectrum of GSK256066B. A representative MALDI mass spectrum to show detection at the 1µg level of GSK256066B using particle suspension containing graphite and TiO_2 from a conventional positive ion MALDI MS experiment.

The spectrum shown in figure 2.9 shows clearly the $[M+H]^+$ at m/z 519, $[M+Na]^+$ at m/z 541 and $[M+K]^+$ at m/z 557.

It appears that the protonated molecule is suppressing the matrix peaks (i.e. the peaks under m/z 400).

2.3.4.1 Direct Analysis of GSK256066B On Lung Tissue

Direct tissue analysis was performed in order to maintain the spatial resolution of the drug compound on the tissue.

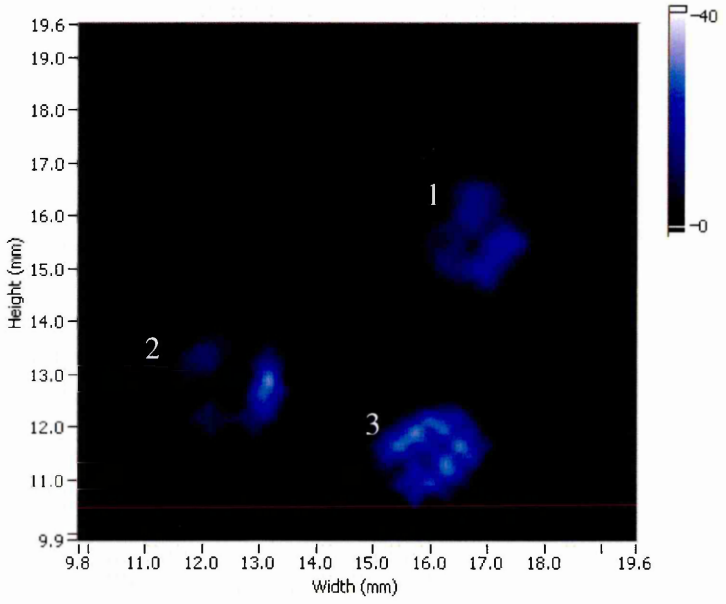

Figure 2.10: MALDI MS Image of the Distribution of $[M+H]^+$ at m/z 519 of GSK256066B. Each spot represents a total drug concentration of 1µg. The matrix used was TiO_2/graphite. The scale on the right hand side of the image shows the intensity with white being the most intense (i.e. accounting for more ions) and the darker colour accounting for fewer ions.

The three spiked regions of drug are visible in the image; however, the intensity of the spot labelled number 3 in the image appears slightly more intense that the other two spots labelled 1 and 2 in the image. This may be due to differing levels of endogenous compounds and salts across the tissue surface leading to variations in suppression effects. In an attempt to overcome these observed suppression effects an indirect blotting approach was investigated.

2.3.4.2 Indirect Blotting Analysis of GSK256066B

As this compound ionises particularly well an indirect blotting approach was used to try to detect drug concentrations of less than 1µg off the surface of the lung tissue. The three drug spiked concentrations on the lung tissue were 1µg, 100ng and 10ng. The cellulose membrane was pressed against the tissue for 40 seconds which was considered an efficient transfer time as can be seen from the results in figure 2.11.

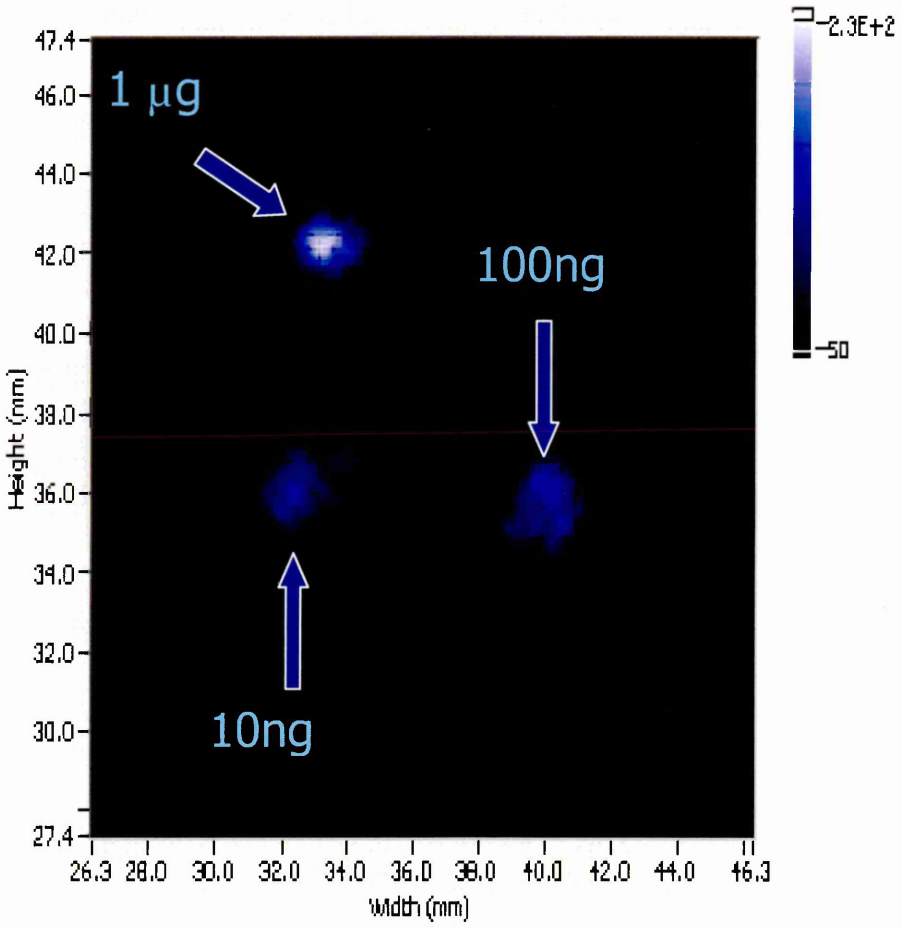

Figure 2.11: Indirect MALDI MS Image of the Distribution of $[M+H]^+$ at m/z 519 of GSK256066B. The cellulose blotting method was successful with the three spiked drug concentrations being clearly visible on the image. The scale on the right hand side of the image shows the intensity with white being the most intense (i.e. accounting for more ions) and the darker colour accounting for fewer ions.

This data can also be represented as a 3D plot as shown in figure 2.12.

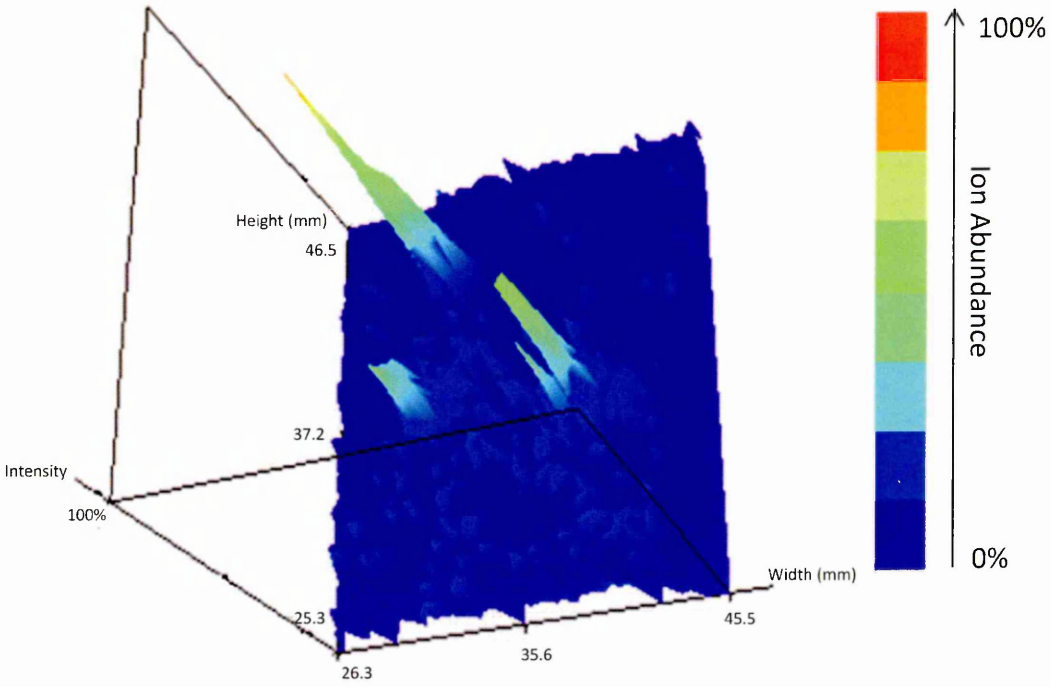

Figure 2.12: 3D plot of GSK256066B MALDI MSI Data. The colour scale on the right hand side of the plot relates to ion intensity, with red being the most intense (i.e. accounting for more ions) than the blue colour. The plot corresponds to figure 2.11.

2.4 Conclusion

The initial MALDI dried droplet experiments showed that all the drugs could be detected; however, drug detection directly from lung tissue is much more complex. This is due to the presence of endogenous compounds within the tissue which can interfere with the mass spectrometry analysis, for example by suppressing the ionisation of the drug compound and affecting/inhibiting the matrix co-crystallisation process. Initial experiments showed that a range of matrices were potentially suitable for the analysis of the four pharmaceutical compounds; however, this highlights the importance of matrix selection and the optimisation of the matrix on the tissue. For example, it was found that although α-CHCA generated good conventional MALDI MS data, its use was limited with the tissue imaging experiments. Problems were encountered as this matrix would not co-crystallise on the surface of the lung tissue when direct tissue experiments were conducted. α-CHCA was used successfully for the indirect blotting experiments.

The results show that the GSK256066B, Budesonide and Fluticasone Propionate can be detected in lung tissue; however, although Salmeterol can be detected with conventional MALDI dried droplet analysis, it cannot be detected in lung tissue. This is thought to be due to endogenous compounds within the lung tissue suppressing the ionisation of Salmeterol because Salmeterol does not appear to ionise as well as the other pharmaceutical compounds reported in this chapter. Suggestions for future work include further optimisation of methods to achieve greater sensitivity that will permit additional studies in analysing lung tissue dosed with drug *in vivo*. The optimisation would have to take into account the level at which the animal had been dosed and possible derivatisation of compounds in order to image the distribution. For example, studies have shown that up to 80% of administered Budesonide converts into Budesonide Oleate [15] so optimisation could be achieved by the esterification of Budesonide into its fatty acid conjugate. If this could be detected it is reasonable to assume that it could be detected from animals that had been dosed with this drug. The dosages given to animals may vary from animal to animal as rats and mice are commonly used to study lung diseases. It may also vary depending on whom a drug is aimed at. For example, paediatric doses differ from

adult doses. Tissue blotting has shown to be an effective way to analyse the drug distribution as shown in figure 2.11. Whilst this did method did not work well for all the compounds studied it worked particularly well for GSK256066B. However, this compound has previously been shown to ionise very well (refer to figure 2.9).

Endogenous compounds within lung tissue also present problems that are difficult to overcome. The lungs could be perfused, however, this could lead to the translocation of compounds, and therefore any image would not reflect the true distribution. Tissue washing steps have been reported using graded ethanol solutions to remove endogenous salts from the tissue surface, thus decreasing any observed suppression effects. This could potentially result in the translocation of the compound or loss of compound if it is soluble in the washing solvent.

2.5 References

[1] http://www.asthma.org.uk/

[2] Umland S. P., Schleimer R. P., Johnston S. L. Review of the molecular and cellular mechanisms of action of glucocorticoids for use in asthma. Pulmonary Pharmacology and Therapeutics, 2002, 15, 35-50.

[3] Pelaia G., Vatrella A., Cuda G., Maselli R., Marsico S. A. Molecular mechanisms of corticosteroid actions in chronic inflammatory airway diseases. Life Sciences, 2003, 72, 1549-61.

[4] Calverley P. M. A. Inhaled Corticosteroids are Beneficial in Chronic Obstructive Pulmonary Disease. American Journal of Respiratory and Clinical Care Medicine, 2000, 161, 341-344.

[5] O'Connell E. J. Review of the Unique Properties of Budesonide. Clinical Therapeutics, 2003, 25, C42-C60.

[6] National Asthma Education Prevention Program (NAEPP). Expert Panel Report: guidelines for the diagnosis and management of asthma - update on selected topics. Journal of Allergy and Clinical Immunology, 2002, 110, S141-S219.

[7] Bergstrom M., Grahnen A., Langstrom B. Positron emission tomography microdosing: a new concept with application in tracer and early clinical drug development, 2003, 59, 357-366.

[8] Craig Richardson J., Bowtell R. W., Mader K., Melia C. D. Pharmaceutical applications of Magnetic Resosnance Imaging (MRI). Advanced Drug Delivery Reviews, 2005, 57, 1191-1209.

[9] Solon E. G., Balani S. K., Lee F. W. Whole-body autoradiography in drug discovery. Current Drug Metabolism, 2002, 3, 451-462.

[10] Stoeckli M., Staab D., Schweitzer A. Compound and metabolite distribution measured by MALDI mass spectrometric imaging in whole-body tissue sections. International Journal of Mass Spectrometry, 2007, 260, 195-202.

[11] Kertesz V., Van Berkel G. J., Vavrek M., Koeplinger K. A., Schneider B. B., Covey T. R. Comparison of Drug Distribution Images fro Whole-Body Thin Tissue Sections Obtained Using Desorption Electrospray Ionisation Tandem Mass Spectrometry and Autoradiography. Analytical Chemistry, 2008, 80, 5168-5177.

[12] Newman S. P. Can lung deposition data act as a surrogate for the clinical response to inhaled asthma drugs? British Journal of Clinical Pharmacology, 2000, 49, 529-537.

[13] Ewing P., Eirefelt S. J., Andersson P., Blomgren A., Ryrfeldt A., Gerde P. Short Inhalation Exposures of the Isolated and Perfused Rat Lung to Respirable Dry Particle Aerosols; the Detailed Pharmacokinetics of Budesonide, Formoterol and Terbutaline. Journal of Aerosol Medicine and Pulmonary Drug Delivery, 2008, 21, 169-180.

[14] Bunch J., Clench M. R., Richards D. S. Determination of pharmaceutical compounds in skin by imaging matrix-assisted laser desorption/ionisation mass spectrometry. Rapid Communications in Mass Spectrometry, 2004, 18, 3051-3060.

[15] Miller-Larson A., Mattsson H., Hjertberg E., Dahlback M., Tunek A., Brattsand R. Reversible fatty acid conjugation of budesonide: novel mechanism for prolonged retention of topically applied steroid in airway tissue. Drug Metabolism and Disposition, 1998, 26, 623-630.

[16] Maassen van den Brink K. I., Boorsma M., Jeske Staal-van den Brekel A., Edsbacker S., Wouters E. F. Thorsson L. Evidence of the in vivo esterification of budesonide in human airways. British Journal of Clinical Pharmacology, 2008, 66, 27-35.

[17] Clark R. B., Allal C., Friedman J., Johnson M., Barber R. Stable activation and desensitization of beta 2-adrenergic receptor stimulation of adenylyl cyclase by salmeterol: evidence for quasi-irreversible binding to an exosite. Molecular Pharmacology 1996, 49, 182-189.

[18] Stoeckli M., Staab D., Schweitzer A. Compound and metabolite distribution measured by MALDI mass spectrometric imaging in whole-body tissue sections. International Journal of Mass Spectrometry, 2007, 260, 195-202.

Chapter 3

Analysis of Pharmaceutical Tablet Formulations using MALDI MSI

3.1 Introduction

Tablets are compacted pharmaceutical dosage forms that contain active ingredients and excipients such as bulking agents, lubricants and disintegrants. There are many different tablet formulations and pharmaceutical manufacturing techniques that can be used to produce them. The manufacturing process can vary depending on the chemical properties of the active pharmaceutical ingredient (API). It is of extreme importance to the pharmaceutical industry to evaluate the outcomes of the drug formulation process, and in particular for solid dosage formulations, i.e. tablets, to study the distribution of constituents within them. Examining the finished product is one way to achieve this and is vital for slow release formulations where the distribution of the active ingredient throughout the excipients can affect how effective the tablet is post-administration [1].

The introduction of the process analytical technology (PAT) initiative by the American Food and Drug Administration [2] has made pharmaceutical companies even more aware of the need to improve manufacturing efficiency and finished product quality [2]. Imaging techniques have formed part of this initiative and have already been used to investigate tablet formulations. Techniques used include magnetic resonance imaging (MRI) [4], Raman, Micro-Focus X-ray [1] (MFX) and Near Infrared (NIR) imaging [5-6]. Raman spectroscopy, in particular, has had a vital role in the analysis of solid pharmaceutical products owing to the minimal sample preparation required. APIs tend to give a good Raman response and there is less spectral overlap in Raman spectra than is observed with NIR. It is possible to use Raman spectroscopy to map APIs in pharmaceutical tablet formulations and this has been successfully demonstrated by Šašić [7]. However, due to the complexity of the data and the lack of imaging software, this can be a difficult process.

A range of mass spectrometry techniques have also been utilised in the study of pharmaceutical formulations. Secondary Ion Mass Spectrometry (SIMS) is a surface ionisation technique where secondary ions are generated by focussing a pulsed primary ion beam on the sample surface. The secondary ions that are generated are usually analysed using a Time of Flight (TOF) mass spectrometer [8]. Prestidge *et al.* have demonstrated the use of TOF SIMS for the characterisation of solid-state

pharmaceutical products [9]. SIMS can be used with imaging software to study the distribution of the analyte of interest within a sample.

Non-imaging techniques such as Desorption Electrospray Ionisation Mass Spectrometry (DESI-MS) have also been used for the analysis of pharmaceutical drug formulations. DESI is a technique where charged droplets created by an electrospray source are concentrated onto a solid sample, resulting in surface interaction creating secondary ions that can be detected using mass spectrometry [10]. DESI has been used to study pharmaceutical drug formulations [11-12] and for the screening of illicit Ecstasy tablets [13]. Whilst DESI requires no sample preparation, it is relatively fast and is a soft ionisation technique, but at present there is no commercial imaging software available for this application. Therefore only profiles (i.e. surface mass spectra) can be obtained. It should be noted, however, that quite often profiling experiments provide the user with enough information regarding the sample of interest.

MALDI MS has been applied previously to the analysis of clandestine tablets [14], where the tablets were ground into a fine powder and dissolved in methanol in order to permit spot target analysis to be performed using a combination of α-CHCA and cetrimonium bromide (CTAB) in a water:acetonitrile solution (50:50 v/v).

The work presented in this chapter demonstrates the first use of MALDI MSI to study tablets. The overall aim of this work was to map the distribution of the active drug throughout all the excipients contained within the tablets. MALDI-MSI has been assessed as a potential technique to directly image the distribution of the active drug throughout the tablet and to also provide some quantitative information in relation to the manufactured dose of the tablet.

The following tablets were obtained for MALDI MSI analysis: a confidential tablet formulation, tablet X (placebo, 1mg, 3mg and 6mg dosage forms); Sildenafil citrate (Viagra 25mg); Paracetamol (500mg); Aspirin (75mg); Anadin Extra (a mixture of aspirin (300mg), Paracetamol (200mg) and Caffeine (45mg), and Solpadeine (a mixture of Paracetamol (500mg) and Caffeine (65mg).

Principal Component Analysis (PCA) software is used to simplify multidimensional datasets. PCA has been previously incorporated into the interpretation of MALDI MSI data to discriminate between different regions in mammalian tissue sections [15-

[17] and to evaluate data from the analysis of porcine skin that had been treated with hydrocortisone [18]. In this chapter it is demonstrated how PCA can be used to differentiate between the active component and the excipients contained within the tablet.

3.2 Experimental

3.2.1 Materials

α-cyano-4-hydroxycinnamic acid (α-CHCA), ethanol (EtOH, HPLC grade) and trifluoroacetic acid (TFA, HPLC grade) were purchased from Sigma Aldrich, Dorset, UK. The following tablets were purchased commercially from a local pharmacy: Paracetamol 500mg (Wallis Laboratory Limited, Bedfordshire, UK), Aspirin 75mg (M & A Pharmachem Ltd, Greater Manchester, UK), Anadin Extra (Wyeth Consumer Healthcare, Berkshire, UK) and Solpadeine (Glaxosmithkline Dungarvan Ltd, Co Waterford Ireland). Sildenafil citrate (Viagra) 25 mg dosage form and Tablet X in placebo, 1mg, 3mg and 6mg dosage forms were supplied by Pfizer, Kent, UK. The tablet cutter used was purchased commercially, PillCutter, PillMate®, Shantys Ltd, Essex, UK.

3.2.2 Sample Preparation Methods

3.2.2.1 Preparation of Tablets for Conventional MALDI Dried Droplet Experiments

In order to asses the suitability of a range of matrices for the analysis of pharmaceutical tablet formulations, different tablets were dissolved in 2mL of ethanol and sonicated for approximately 15 minutes. 1μL of drug solution was combined with 1μL of matrix and spotted onto a stainless steel MALDI target plate. It was found that α-CHCA was the best choice of matrix for these studies as the drugs ionise well with this matrix.

3.2.2.2 Preliminary Studies into Tablet Preparation for MALDI MSI

Tablets are manufactured in many different shapes and sizes and therefore there is a requirement to optimise the sample preparation procedure for each tablet as this ultimately affects the data generated and image quality. The preliminary studies began with tablet X; a series of small tablets with convex surfaces. The underside of the tablet was filed using an emery board as a flat surface was required for the mounting of the tablet section onto the recessed MALDI target plate; this was followed by matrix application (α-CHCA 25mg/mL in EtOH containing 0.1% TFA) applied using an airspray deposition method. The results in section 3.4.1 demonstrate the problems encountered with this sample preparation method. In order for improved MALDI MSI analysis on tablets to be performed the sample preparation method was optimised further (refer to section 3.4.2).

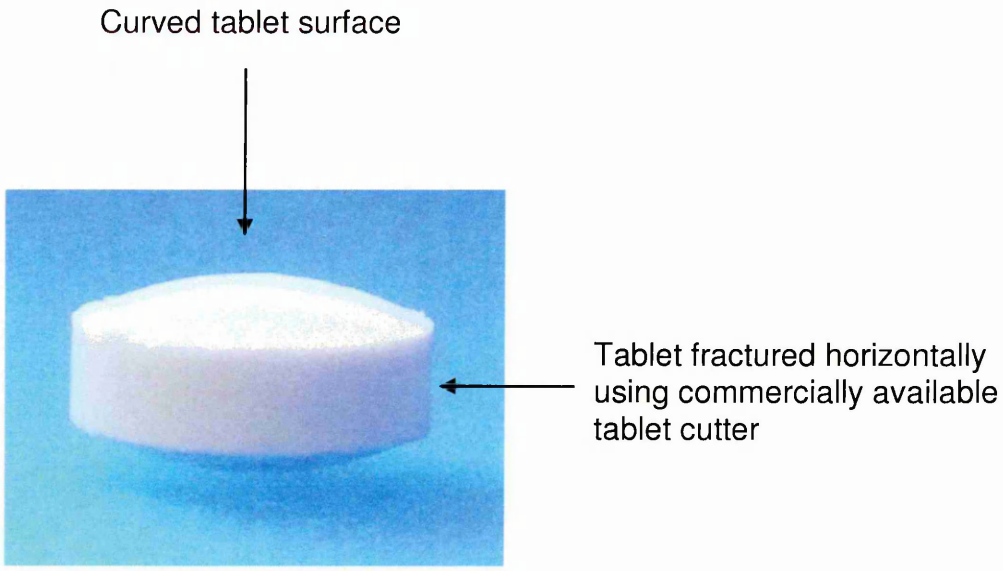

Figure 3.1: The Curved Surface of Tablet X. Photograph of tablet X showing the curved surface of the tablet and the position at which the horizontal section was obtained using a commercially available tablet cutter.

3.2.2.2.1 Optimisation of the Tablet Preparation Procedure

Tablet sections approximately 1mm in thickness were created using a tablet cutter to fracture the tablet, thus exposing the surface of the tablet. (Note, this procedure was not necessary for the Paracetamol and aspirin tablets as they already had flat surfaces). The underside of the tablet was filed down in order to ensure that it would fit into a recessed MALDI target plate.

3.2.2.3 Matrix Selection and Application

Preliminary experiments were conducted to assess the suitability of different matrices and solvents. Compound X and the other tablets studied in this chapter were soluble in ethanol and ionised efficiently using α-CHCA dissolved in ethanol containing 0.1% TFA.

The matrix was applied using an airbrush that required manual operation. Important parameters to control include the amount of matrix that is applied to the sample and wetting of the sample caused by applying the matrix too quickly should be avoided. Sample wetting can be avoided by optimising the distance between the airbrush and the sample, the pressure at which the matrix is applied and choosing a suitable solvent such as acetone or ethanol that evaporates very quickly. Approximately 1.5mL of matrix was applied to each tablet at a spray distance of about 10 inches away from the sample surface.

Figure 3.2: The Flat Surface of Tablet X. A photograph showing the flat surface of the tablet section obtained with the optimised sample preparation method and affixed to the MALDI target plate.

3.3 Instrumentation

3.3.1 Mass Spectrometric Analysis

All analyses were performed in positive ion mode on an Applied Biosystems/MDS Sciex hybrid quadrupole time-of-flight mass spectrometer (Q-Star Pulsar-*i*) with an orthogonal MALDI ion source and a high repetition Nd: YAG laser (1 kHz). The Nd: YAG laser has an elliptical spot size of 100x150µm. The laser scanned over the sample in a raster pattern and acquired data at 100µm increments. The laser fired at a power of 30% (3.2µJ) at each location for 2 seconds.

3.3.2 Visualisation Software

oMALDI server software version 5 (Applied Biosystems/MDS Sciex) was used to generate images from the acquired mass spectral data.

3.3.3 Principal Component Analysis (PCA)

PCA was performed using the "Markerview" software package (Applied Biosystems/MDS Sciex). Five random locations from the tablet image data were taken and these data were entered this data into Markerview. Supervised PCA was performed using Pareto scaling. This type of scaling calculates the square root of the standard deviation and uses this information as a scaling factor [19]. This in turn reduces any major intensity changes that are sometimes observed within the sample and also with the matrix peaks.

3.4 Results and Discussion

3.4.1 Preliminary Tablet X Data Prior to Optimisation of Sample Preparation

There are many tablets that are commercially available that have a convex tablet surface.

It was found that one of the most important aspects of the sample preparation procedure was to produce a flat surface. The image presented in Figure 3.3 demonstrates the importance of the sample preparation procedure. As can be seen there is a doughnut effect in which it appears that the highest concentration of compound X is around the edges of the tablet with less drug in the middle of the tablet. This is hypothesised to be a laser-induced effect resulting in the distortion of the image; the laser may be too close to the centre of the tablet due to its convex nature and too far away from the edges as explained diagrammatically in figure 3.4.

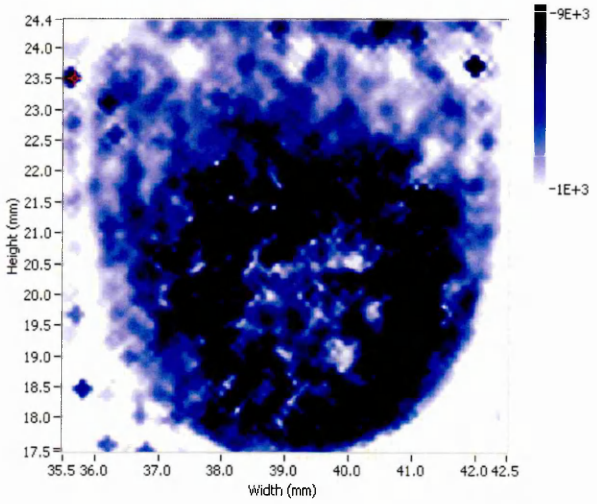

Figure 3.3: MALDI MS Image of Tablet X. Tablet X (3mg) with a convex surface exposed for MALDI MSI analysis. The scale on the right hand side of the image shows the ion intensity with the dark blue colour being the most intense (i.e. accounting for more ions) and the lighter blue/white colour accounting for fewer ions.

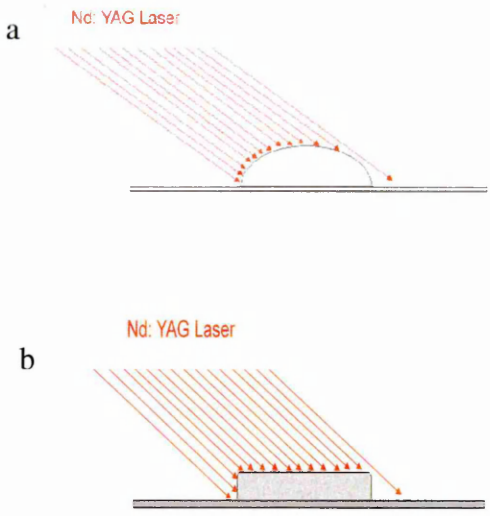

Figure 3.4: Schematic Diagram of Proposed Laser Position. A proposed schematic diagram to explain the image distortion by way of laser position: (a) shows how the laser may be too close to the curved tablet surface and too far away from the edges of the tablet; (b) shows that the laser is consistently at the same distance to the tablet section surface; the edge of the tablet where the laser misses could explain the 'flattening' effect observed in some of the tablet images.

3.4.2 Tablet X (placebo, 1mg, 3mg and 6mg tablets) Post-Optimisation of Sample Preparation Method

Figure 3.5 is a collection of representative spectra for the analysis of Tablet X: (a) placebo; (b) 1mg tablet; (c) 3mg tablet and (d) 6mg tablet. In figure 3.5 b-d the protonated molecule ($[M+H]^+$ = m/z 507) of the active drug is clearly visible. The full scan spectra show a relative increase in ion counts when the concentration of the active increases. The ion counts for the matrix peaks decrease as the ion intensity for the active compound increases. With higher concentrations of this particular drug it is observed that the matrix peaks are suppressed. This is because the active drug in this case ionises very well. Figure 3.6 shows the corresponding images showing the distribution of m/z 507 throughout the tablet sections. These have been normalised against the corresponding matrix peak ($[M+H]^+$ at m/z 190). The intensity scale on each of the images represents ion intensity/abundance for m/z 507; thus the deeper the colour, the more of the active pharmaceutical ingredient there is in that particular location.

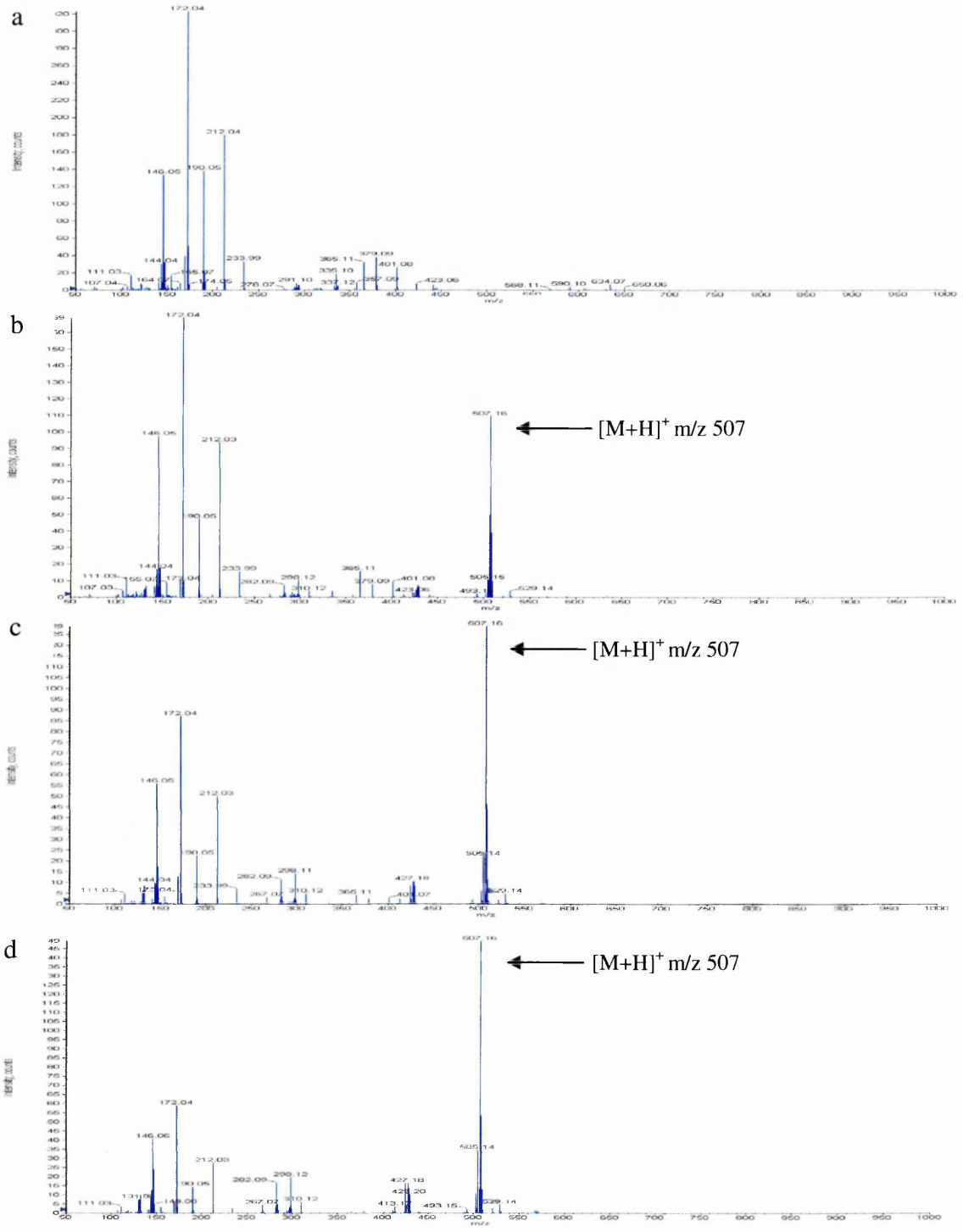

Figure 3.5: MALDI Mass Spectra of the Different Tablet X Concentrations. Full scan spectra for placebo (a), 1mg tablet (b), 3mg tablet (c) and 6mg tablet (d). The matrix peaks are clearly visible on the placebo spectrum; however, as the compound X (m/z 507.16) concentration increases suppression of the matrix peaks is observed.

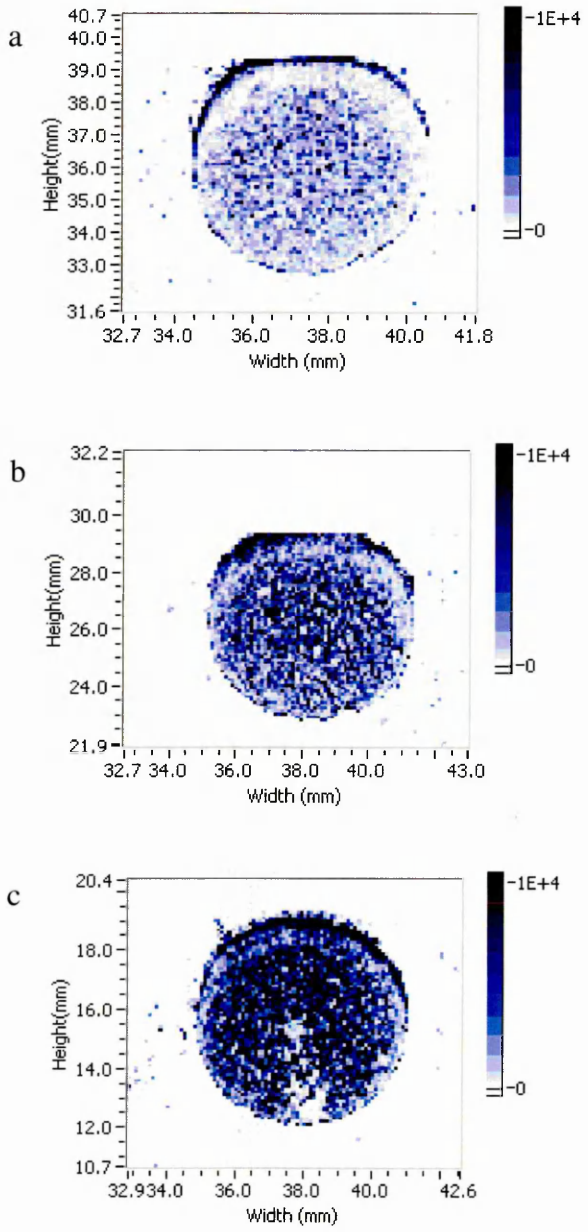

Figure 3.6: MALDI MS Images of Tablet X at a Range of Drug Concentrations. Images show the protonated molecule (m/z 507.16) normalised against the corresponding protonated matrix peak (m/z 190.05). The images show that the active component (compound x) is relatively homogenously distributed throughout the tablet at different concentrations a) 1mg, b) 3mg and c) 6mg. The scale on the right hand side of the image shows the ion intensity with the dark blue colour being the most intense (i.e. accounting for more ions) and the lighter blue/white colour accounting for fewer ions.

3.4.2.1 Quantitative Aspects of Tablet X Analysis

MALDI MSI can provide quantitative information. Five spectra obtained from each imaging run were randomly selected and a plot of the intensities of m/z 507/190 is shown in figure 3.7.

PCA analysis was performed to discriminate between the tablets containing compound X and the placebo and between the different concentrations of compound X in the tablets. PCA was used to explore how the four tablets (placebo, 1mg, 3mg and 6mg) differ in composition statistically. Figure 3.8 shows the results from the PCA analysis and shows the following information:

- The scores plot shows significant grouping for the three different dose tablets and a separate grouping for the placebo.
- The corresponding loadings plot confirms that the more active ingredient the tablet contains, the more it groups towards m/z 507. As the placebo doesn't contain any active compound, it groups furthest away from m/z 507.

The matrix peaks were not excluded from this analysis, in order to illustrate further that when the tablets contain a readily ionisable active compound, it suppresses the matrix signal. As the placebo does not contain a component that is readily ionisable the matrix peaks suppress the excipient peaks. Therefore, it is an interesting observation that although one would expect the grouping for the placebo to be furthest away from the m/z 507 ion from the active compound; this is also where the matrix peaks are located in the loadings plot (m/z 146.05, m/z 172.03, m/z 190.05, m/z 212.03). PCA supports the quantitative aspect of this investigation and it may also provide information on matrix suppression.

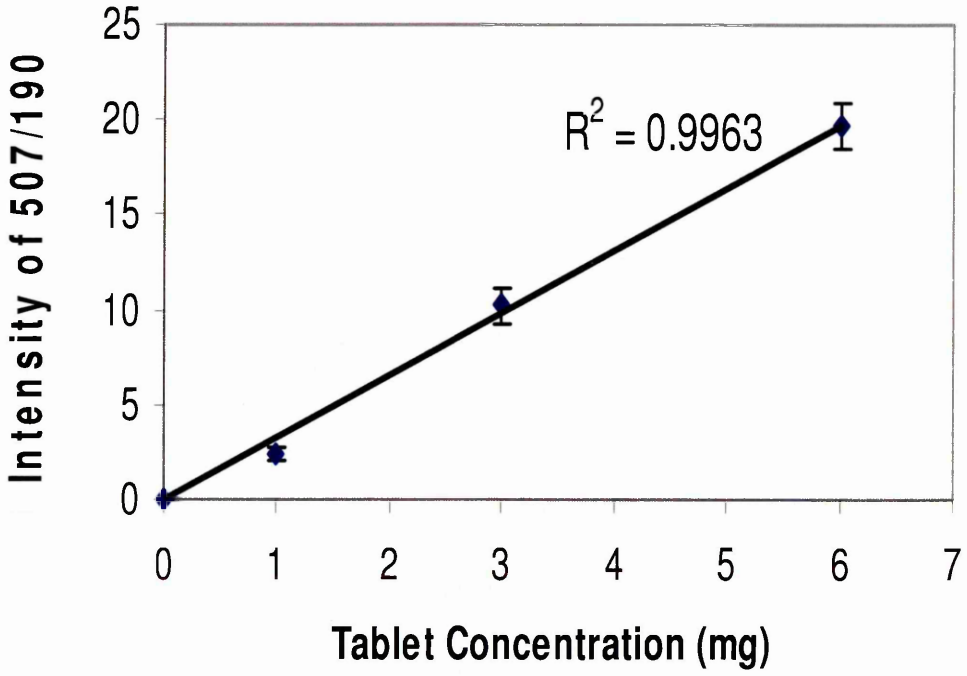

Figure 3.7: Graph of Increasing Tablet X Concentrations. A graph to show the normalised increase in intensity observed as the concentration of the active pharmaceutical ingredient was increased in the tablet formulations. Five spectra were randomly selected and the mean value was plotted. The error bars represent the standard deviation. The correlation coefficient, R^2, was computed using Excel 2003. The range for R^2 values is between 0 and 1 where 0 represents no statistical correlation and 1 is the highest achievable correlation. The R^2 value of 0.9963 shows that there is a statistical correlation between the normalised intensity on the y axis and tablet concentration on the x axis.

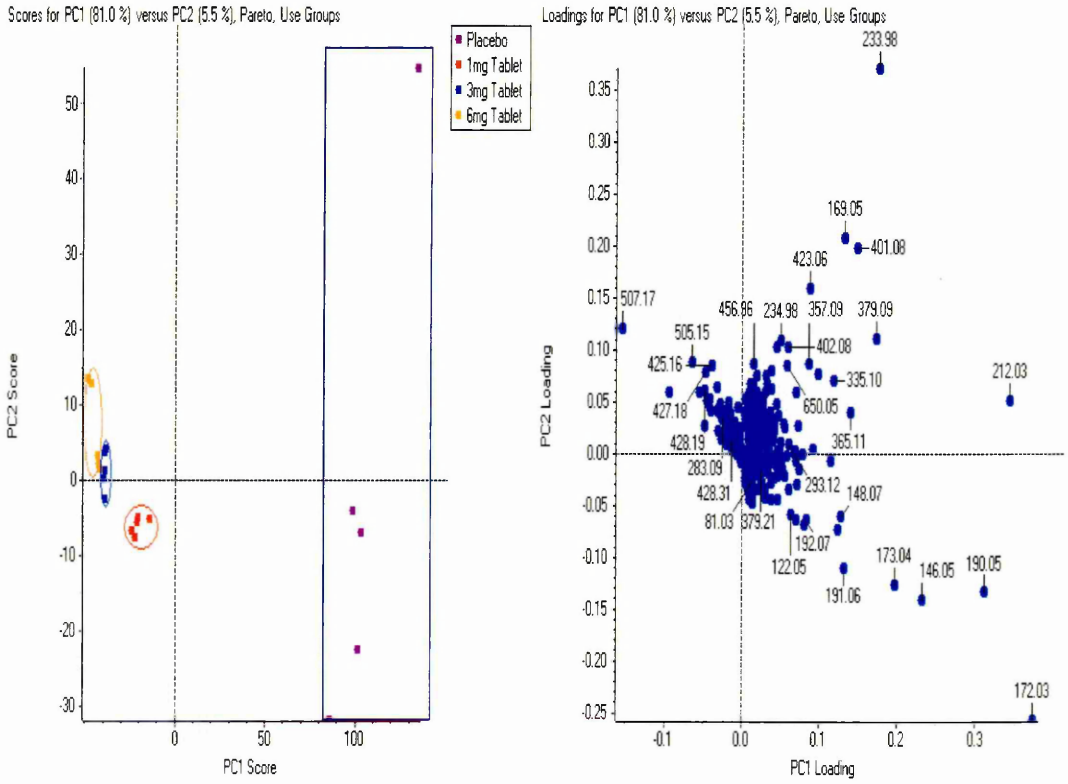

Figure 3.8: PCA Analysis of Tablet X. The same five spectra used to produce the graph in figure 3.7 were entered into the Markerview software and supervised PCA analysis was performed using Pareto scaling. There is clear separation between the placebo and the tablets containing the active component compound X. The tablets containing the active drug are grouped closely together as can be seen in the scores plot and group according to their drug concentration.

3.4.3 Sildenafil Citrate (Viagra 25mg)

Sildenafil citrate (Viagra) is a drug developed by Pfizer, used to treat erectile dysfunction and pulmonary arterial hypertension.

The distribution of m/z 475 (the Sildenafil base $[M+H]^+$) throughout a section of a Viagra tablet can be seen in figure 3.10. The image data has been normalised against the corresponding matrix peak ($[M+H]^+$ at m/z 190). The full scan spectrum shows that the sildenafil base dominates the spectrum suppressing the ions associated with the matrix. The sodium adduct is also present at m/z 497.

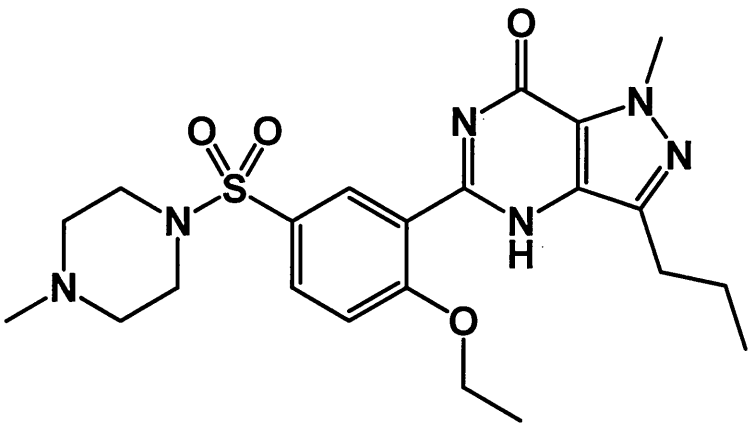

Figure 3.9: The Chemical Structure of Sildenafil base.

IUPAC Name: 5-(2-ethoxy-5-((4-methylpiperazin-1-yl)sulfonyl)phenyl)-1-methyl-3-propyl-1H-pyrazolo[4,3-d]pyrimidin-7-one

Formula: $C_{22}H_{30}N_6O_4S$

RMM: 474.20

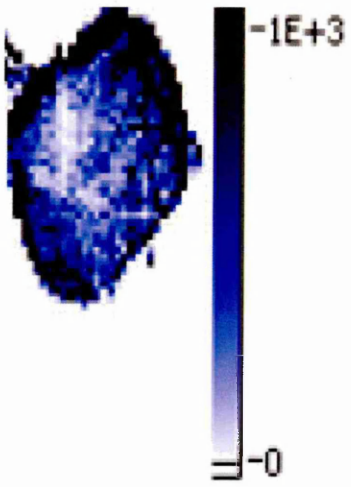

Figure 3.10: MALDI MS Image of Sildenafil. The distribution of $[M+H]^+$ at m/z 475 normalised against the corresponding matrix peak at m/z 190. The scale on the right hand side of the image shows the ion intensity with the dark blue colour being the most intense (i.e. accounting for more ions) and the lighter blue/white colour accounting for fewer ions.

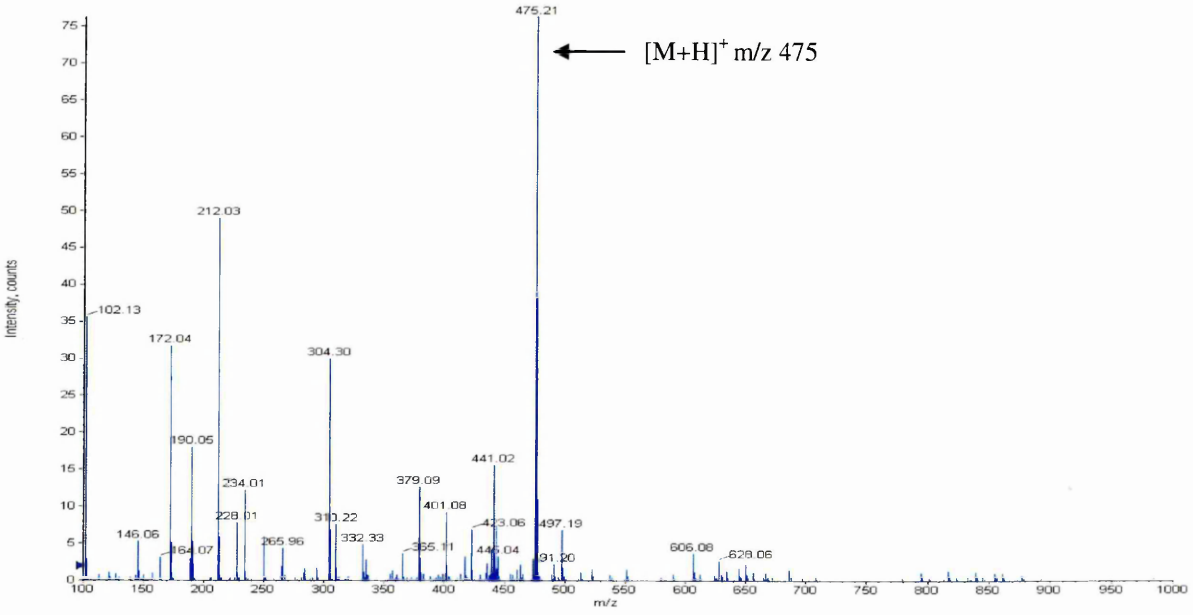

Figure 3.11: MALDI Mass Spectrum of Sildenafil. The full scan mass spectrum of Sildenafil showing the protonated molecule at m/z 475.

3.4.4 Paracetamol (500mg) and Aspirin (75mg)

Images have been obtained for aspirin (acetylsalicylic acid) and paracetamol (acetaminophen) – both drugs have analgesic and antipyretic properties; however, aspirin also acts as an anti inflammatory.

Figure 3.13 shows the distribution of the $[M+H]^+$ of Paracetamol at m/z 152 throughout a tablet section. These data have been normalised against the corresponding matrix peak ($[M+H]^+$ = m/z 190). The image and the corresponding ion intensity scale show that the distribution of Paracetamol is consistent and appears relatively homogenous throughout the section, although the edges of the tablet seem to be brighter indicating a higher concentration of Paracetamol towards the outer edges of the tablet. This is thought to arise through laser focussing effects as discussed in section 3.4.1.

Figure 3.16 shows the distribution of the aspirin sodium adduct ion ($[M+Na]^+$ = m/z 203) throughout a tablet section. These data have been normalised against the corresponding matrix peak ($[M+Na]^+$ = m/z 212). The sodium adduct ion was imaged rather than the lower intensity protonated molecule ($[M+H]^+$ = m/z 181). The image shows that the aspirin appears to be located on the outer parts of the tablet as the ion counts for the middle part of the tablet section suggest that there is less aspirin in the middle. The high concentration of active ingredient at the tablet surface may be due to greater compression at the surface. This may cause an increase in density at the surface when the tablet is pressed. Increased tablet density would increase the spatial concentration of the API without increasing its actual concentration.

3.4.4.1 Paracetamol

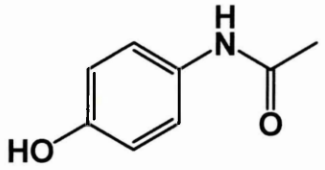

Figure 3.12: The Chemical Structure of Paracetamol.

IUPAC Name: N-(4-hydroxyphenyl) acetamide.

Formula: $C_8H_9NO_2$

RMM: 151.06

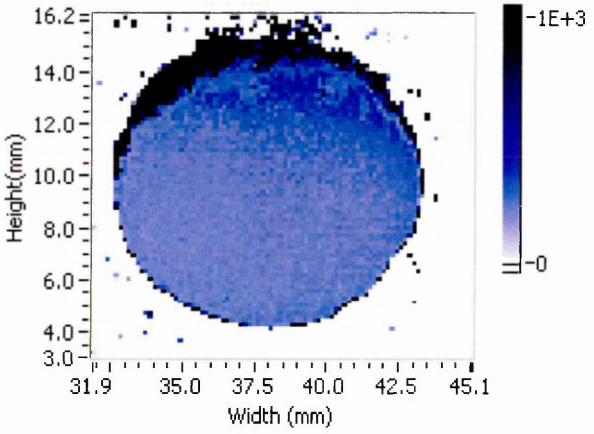

Figure 3.13: MALDI MS Image of Paracetamol. The distribution of $[M+H]^+$ at m/z 152 normalised against the corresponding protonated matrix peak at m/z 190. The scale on the right hand side of the image shows the ion intensity with the dark blue colour being the most intense (i.e. accounting for more ions) and the lighter blue/white colour accounting for fewer ions.

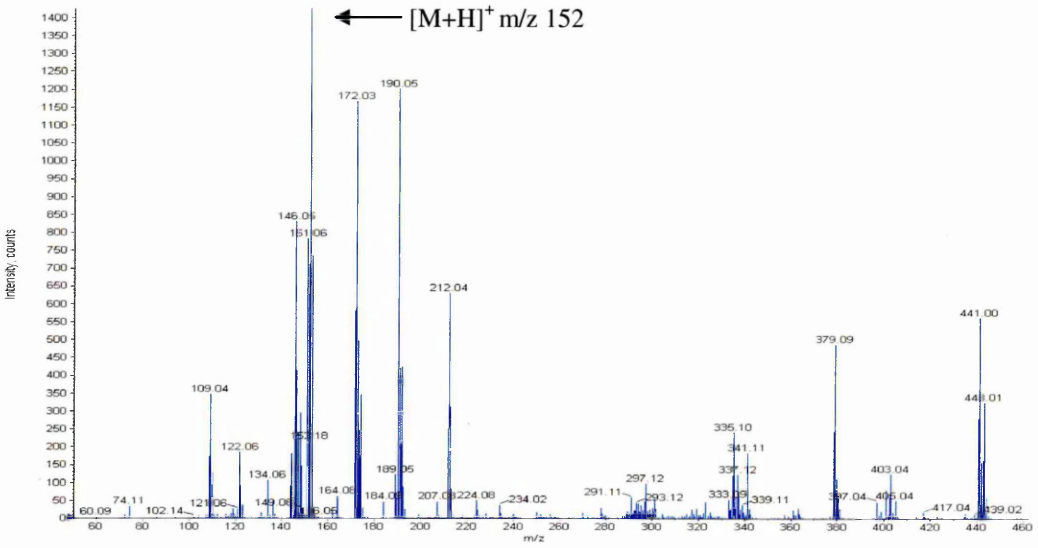

Figure 3.14: MALDI Mass Spectrum of Paracetamol. The full scan MALDI mass spectrum for paracetamol tablet analysis showing the protonated molecule at m/z 152.

3.4.4.2 Aspirin

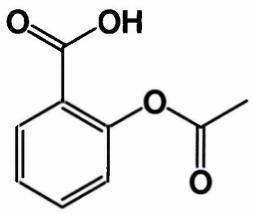

Figure 3.15: The Chemical Structure of Aspirin.

IUPAC Name: 2-acetoxybenzoic acid.

Formula: $C_9H_8O_4$

RMM: 180.04

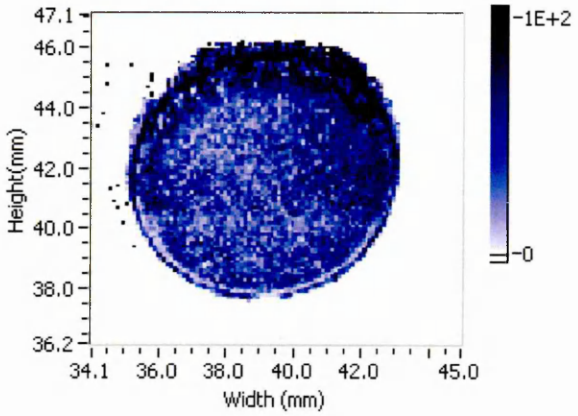

Figure 3.16: MALDI-MS Image of Aspirin. The ion distribution image of m/z 203 normalised against the corresponding matrix ion at m/z 212. The scale on the right hand side of the image shows the ion intensity with the dark blue colour being the most intense (i.e. accounting for more ions) and the lighter blue/white colour accounting for fewer ions.

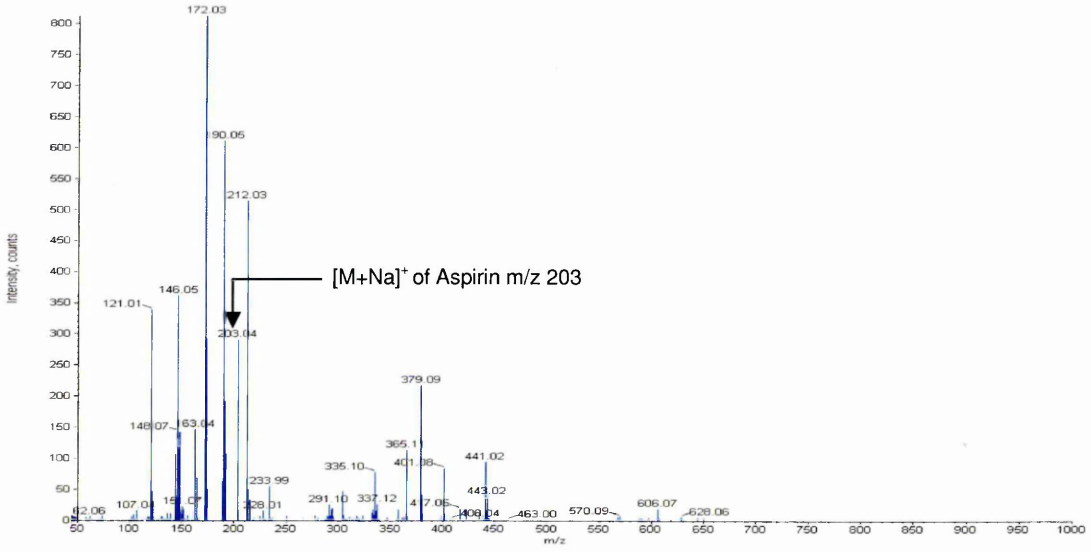

Figure 3.17: MALDI Mass Spectrum of Aspirin. A representative MALDI mass spectrum of Aspirin showing the $[M+Na]^+$ at m/z 203.

3.4.5 Solpadeine and Anadin Extra

Many over the counter pain relief drugs such as Anadin Extra contain a mixture of paracetamol and aspirin and some of these drugs, for example Solpadeine, contain caffeine to accelerate pain relief. Conventional MALDI MS analysis has been applied to Anadin Extra and Solpadeine in an attempt to detect the different drugs contained within each tablet as it was not possible to obtain images for Solpadeine and Anadin Extra. This was due to the consistency of the tablet; the crumbly textures of these tablets don't make them amenable to the sectioning process.

3.4.5.1 Solpadeine

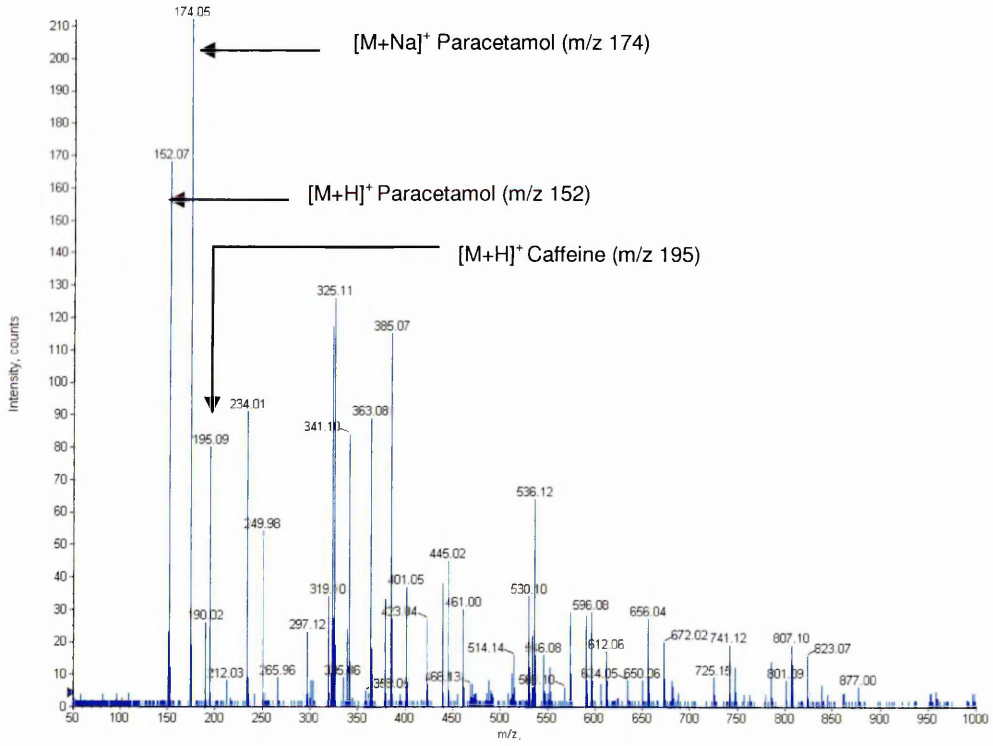

Figure 3.18: MALDI Mass Spectrum of Solpadeine. The protonated Paracetamol can be seen at m/z 152, the sodiated Paracetamol peak dominates the spectrum and the protonated caffeine can be seen at m/z 195.

The Spectrum in figure 3.18 shows the presence of both the protonated and sodiated paracetamol at m/z 152 and m/z 174 respectively. Caffeine was also detected as a protonated molecule at m/z 195. The protonated and sodiated paracetamol (500mg) compared to the quantity of caffeine contained within the tablet (65mg).

3.4.5.2 Anadin Extra

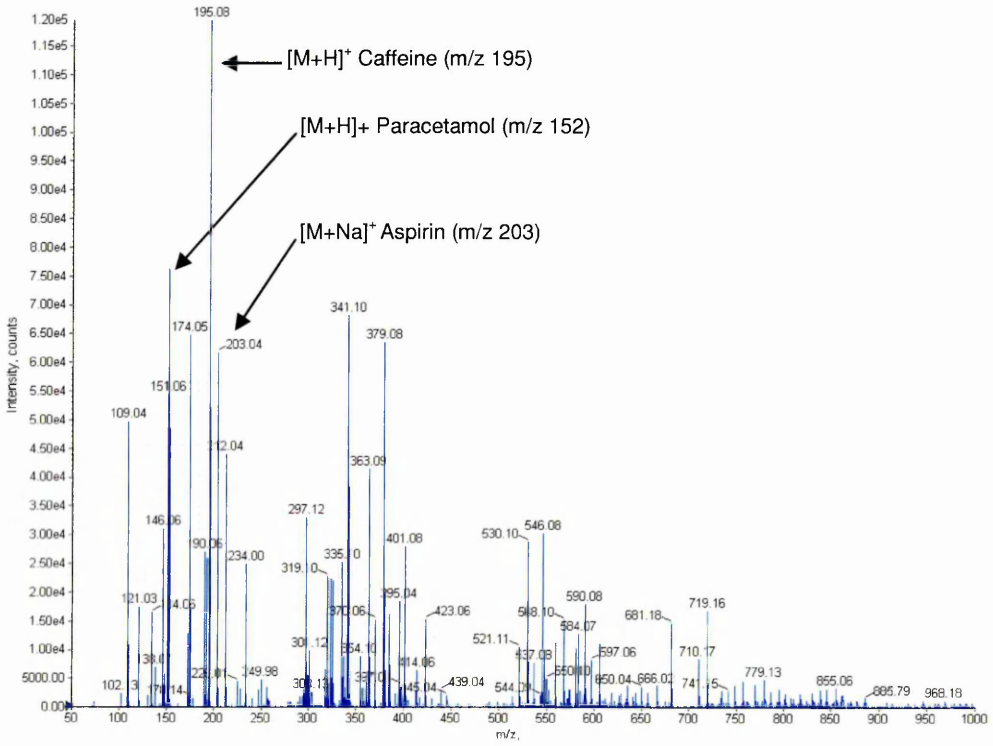

Figure 3.19: MALDI Mass Spectrum of Anadin Extra. The protonated Paracetamol can be seen at m/z 152, the protonated Caffeine at m/z 195 dominates the spectrum and the sodiated Aspirin can be seen at m/z 203.

All the pharmaceutical components (caffeine, paracetamol and aspirin) of Anadin Extra were detected by conventional MALDI analysis as shown in figure 3.19. The ion from sodiated caffeine was the most prominent peak in the MALDI mass spectrum although this was the least abundant drug in the tablet, containing only 45mg.

3.5 Conclusion

A novel approach utilising MALDI MSI for the direct analysis of tablets has been demonstrated in this study. The sensitivity, specificity and rapid analysis time, together with the imaging capabilities make MALDI MSI a valuable technique in many biomedical disciplines. The introduction of MALDI MSI has been invaluable in pharmaceutical analysis both in animal models of drug distribution and in solid pharmaceutical formulations. In this chapter, the importance of being able to visualise the spatial localisation of a compound of interest within a sample, in this case tablet formulations, has been evaluated. Images have been obtained for Tablet X, Viagra, Paracetamol and Aspirin. However, the crumbly nature of Solpadeine and Anadin Extra made it very difficult to obtain tablet sections of ~1mm in thickness and therefore images could not be obtained for these tablets. The shape of the tablet can dictate the sample preparation to some extent. For example, if a tablet had a convex surface this would need to be sectioned in a way that would produce a relatively flat surface - this was required in order to perform MALDI analysis on the Tablet X dosage forms.

The tablet images in figure 3.6 appear to have relatively homogenous distributions of the active compound throughout the excipients. However, the top of the tablet images (most apparent in figure 3.13) initially appear to have a higher concentration of active compound. The charging effect has been reported when the ionization sources are of axial configuration [20]. This can be overcome by sputter coating the sample with a metal over the layer of the matrix [21]. The non-conductive nature of tablet sections of ~1mm thickness could potentially be due to a charging effect. However, this is unlikely as the kinetic energy of the ions is decoupled from the mass analyzer in orthogonal QqTOF instrumentation. A more likely explanation is that the angle of the laser is such that it is firing at the outer edge of the tablet and not at the surface; this is predominantly observed at the top of the tablet sections. Future studies could include re-adjustment of the laser to try to combat such a problem.

3.6 References

[1] Rigby S. P., Van der Walle C. F., Raistrick J. H. Determining drug spatial distribution within controlled delivery tablets using MFX imagaing. Journal of Controlled Release, 2004, 96, 97-100.

[2] Hinz D. C. Process analytical technologies in the pharmaceutical industry: the FDA's PAT initiative. Analytical and Bioanalytical Chemistry, 2006, 384, 1036-1042.

[3] Gowen A. A., O'Donnell C. P., Cullen P. J., Bell S. E. J. Recent applications of Chemical Imaging to pharmaceutical process monitoring and quality control. European Journal of Pharmaceutics and Biopharmaceutics, 2008, 69, 10-22.

[4] Richardson J.C., Bowtell R.W., Mäder K., Melia C.D. Pharmaceutical applications of magnetic resonance imaging (MRI). Advanced Drug Delivery Reviews, 2005, 57, 1191-1209.

[5] Šašić S. An in-depth analysis of Raman and near-infrared chemical images of common pharmaceutical tablets. Applied Spectroscopy, 2007, 61, 239-250.

[6] Hilden L. R., Pommier C. J., Badawy S. I. F., Friedman E. M. NIR chemical imaging to guide/support BMS-561389 tablet formulation development. International Journal of Pharmaceutics, 2008, 353, 283-290.

[7] Šašić S. Raman Mapping of Low-Content API Pharmaceutical Formulations. I. Mapping of Alprazolam in Alprazolam/Xanax Tablets. Pharmaceutical Research, 2007, 24, 58-65.

[8] Belu A. M, Graham D. J, Castner D. G. Time-of-flight secondary ion mass spectrometry: techniques and applications for the characterization of biomaterial surfaces. Biomaterials, 2003, 24, 3635-3653.

[9] Prestidge C. A., Barnes T. J., Skinner W. J. Time-of-Flight secondary-ion mass spectrometry for the surface characterization of solid-state pharmaceuticals. Journal of Pharmacy and Pharmacology, 2007, 59, 251-259.

[10] Takats Z., Wiseman J. M., Cologan B., Cooks R. G. Mass Spectrometry Sampling Under Ambient Conditions with Desorption Electrospray Ionisation. Science, 2004, 306, 471-473.

[11] Weston D. J., Bateman R., Wilson I. D., Wood T. R., Creaser C. S. Direct Analysis of Pharmaceutical Drug Formulations Using Ion Mobility Spectrometry/Quadrupole-Time-of-Flight Mass Spectrometry combined with Desorption Electrospray Ionization. Analytical Chemistry, 2005, 77, 7572-7580.

[12] Williams J. P., Scrivens J. H. Rapid accurate mass desorption electrospray ionisation tandem mass spectrometry of pharmaceutical samples. Rapid Communications in Mass Spectrometry, 2005, 19, 3643-3650.

[13] Leuthold L. A., Mandscheff J. F., Fathi M., Giroud C., Augsburger M., Varesio E., Hopfgartner G. Desorption electrospray ionization mass spectrometry: direct toxicological screening and analysis of illicit Ecstasy tablets. Rapid Communications in Mass Spectrometry, 2006, 20, 103-110.

[14] Su A. K., Liu J. T., Lin C. H. Rapid drug-screening of Clandestine tablets by MALDI TOF mass spectrometry. Talanta, 2005, 67, 718-724.

[15] McCombie G., Staab D., Stoeckli M., Knochenmuss R. Spatial and spectral correlations in MALDI mass spectrometry images by clustering and multivariate analysis. Analytical Chemistry, 2005, 77, 6118-6124.

[16] Trim P. J., Atkinson S. J., Princivalle A. P., Marshall P.S., West A., Clench M.R. Matrix-assisted laser desorption/ionisation mass spectrometry imaging of lipids in rat brain tissue with integrated unsupervised and supervised multivariant statistical analysis. Rapid Communications in Mass Spectrometry, 2008, 22, 1503-1509.

[17] Djidja M-C., Carolan V., Loadman P. M., Clench M. R. Method Development for protein profiling in biological tissues by matrix-assisted laser

desorption/ionisation mass spectrometry imaging. Rapid Communications in Mass Spectrometry, 2008, 22, 1615-1618.

[18] Prideaux B., Atkinson S. J., Carolan V. A., Morton J., Clench M. R. Sample preparation and data interpretation procedures for the examination of xenobiotic compounds in skin by indirect imaging MALDI-MS. International Journal of Mass Spectrometry, 2007, 260, 243-251.

[19] Van den Berg R. A., Hoefsloot H. C. J., Westerhuis J. A., Smilde A. K., van der Werf M. J. Centering, scaling and transformations: improving the biological information content of metabolomics data. BMC Genomics, 2006, 7, 142-157.

[20] Scherl A., Zimmermann-Ivol C. G., Di Dio J., Vaezzadeh A. R., Binz P-A., Amez-Droz M., Cochard R., Sanchez J-C., Gluckmann M., Hochstrasser D. F. Gold coating of non-conductive membranes before matrix-assisted laser desorption/ionization tandem mass spectrometric analysis prevents charging effect. Rapid Communications in Mass Spectrometry, 2005; 19, 605-610.

[21] Guittard J., Hronowski X. L., Costello C. E. Direct Matrix-assisted laser desorption/ionization mass spectrometric analysis of glycosphingolipids on thin layer chromatographic plates and transfer membranes. Rapid Communications in Mass Spectrometry, 1999, 13, 1838-1849.

Chapter 4

Metabolite Profiling of Wheat Grain using IR LDI MS and UV MALDI MSI

4.1 Introduction to Plant Metabolomics

Metabolomics is a rapidly expanding area of scientific research and metabolomics-based studies have been applied to many areas of science; examples include studying the effects of genetic manipulation [1], the investigation of diseases such as cancer [2] and diabetes [3], drug discovery [4] and toxicology [5], amongst others. In this chapter, a metabolomics strategy has been used to investigate plant tissue using MALDI MS for the imaging and profiling of developing wheat grains. In recent years, there has been a surge in plant metabolomic studies [6] ranging from investigations into secondary metabolism [7] to gaining a greater understanding of the changes in metabolite levels during abiotic stress [6, 8]. Plant metabolomic analyses have been previously performed predominantly on fruits [9, 10], leaves [11] and tubers [12].

4.1.1 Clarification of Terminology

The terms metabolomics and metabonomics are often used interchangeably to mean the study and characterisation of metabolites, usually small molecule metabolites, in biological systems [13].

The standard definitions that have been established are as follows:

Metabolites: the intermediates of biochemical reactions within cells that are responsible for connecting many pathways providing information on the cellular status of the cell or tissue, thus defining the phenotype of the cell or tissue in response to genetic or environmental changes [14]. Metabolites are compounds that are formed by metabolic processes therefore providing information that complements genomics, transcriptomics and proteomics in relation to gene expression, protein expression and enzyme activity [14].

Metabolome: The identification and quantification of all the intracellular (endometabolome) and extracellular metabolites (exometabolome) that have a molecular mass under 1000Da [15].

Metabolomics: A term used to describe the identification and/or quantification of metabolites contained within cells and tissues [16].

Metabolomics generally utilises chromatographic-mass spectrometry-based techniques to generate data. The approaches and methods are now very similar between metabonomics and metabolomics; however, the term metabonomics often relates more to the analysis of biofluids in biomarker discovery, whereas metabolomics is applied more to tissue analysis, biomarker discovery and gene function analysis [14].

Metabonomics: "the comprehensive and simultaneous systematic profiling of multiple metabolite levels and their systematic and temporal changes caused by factors such as diet, lifestyle, environmental, genetic effects, pharmaceutical effects both beneficial and adverse in whole organisms"[16].

Metabolite Profiling: This approach can encompass either metabonomics or metabolomics and is generally the term given to the detection, identification and/or the quantitation of metabolites in a sample [14].

4.2 The Importance of Plant Metabolomics

Around 20 plant species provide approximately 90% of the world's supply of food: some of the major crops include rice, wheat, barley, potato and soy [17]. In addition to their significant role as food crops, plants and plant material yield numerous products of importance to human sustenance, including wood, vitamins and medicinal drugs with 80% of all medicinal drugs originating from plant material. It is thought that these drugs have been derived from only 2% of the world's entire plant species [17]. Therefore, it is plausible that metabolomics may have a major role in the detection and identification of potential therapeutic agents and significant drug discovery.

As plants are autotrophic organisms there are features that are unique to plant metabolomics such as the photosynthetic process where light is used as the energy

source and adenosine triphosphate (ATP) and nicotinamide adenine dinucleotide (NADH) are used in the synthesis of glucose by carbon dioxide [17].

The metabolism of plants is largely dependent on the amount of light available; however, carbon availability can also have an impact on the metabolic profile [18].

Metabolomics is also of great importance in the investigation of genetically modified (GM) crops and in the elucidation of the genetic modification process; thus metabolomics-based studies are particularly useful to make comparisons between GM crops and non-GM crops for the assessment of crop quality and nutritional value [19].

4.2.1 Plant Metabolism

Metabolism can be separated into primary metabolism and secondary metabolism. Primary metabolites include compounds that are essential to life such as amino acids and sugars. Secondary metabolites are formed by pathways derived from primary metabolism and are characterized by their chemical diversity and often their unknown function, although it is thought they operate in signalling cascades [20].

Due to the dynamic nature of metabolism it is important to ensure that metabolism has been stopped before metabolomic experiments are conducted; this can be achieved by quenching of the sample.

4.2.2 Quenching of Plant Tissue

Quenching refers to the process whereby metabolism is stopped [21]. This process can vary for different biological samples. Once the tissue has been harvested metabolism must be stopped immediately in order to preserve the metabolic status of the sample. The quenching of plant tissues is generally done using liquid nitrogen as this method enables rapid freezing of the sample; samples can then be stored at -80°C prior to analysis as this is thought to preserve sample integrity. Other quenching agents include ice cold methanol or acidic treatments [21]. However, with this method of quenching the sample is not frozen. Therefore, if metabolite

localisation experiments are to be conducted, the use of such solutions could result in metabolite delocalisation, thus interfering with analysis.

Once the plant tissue samples have been quenched the tissue can be stored at -80 °C or alternatively it can be freeze dried. As many metabolomics approaches utilise an extraction step, sample thawing must be avoided or limited in order to ensure that the metabolic status of the sample does not change. Freeze drying is an alternative method of plant tissue storage that preserves the metabolic status of the tissue as enzyme activity cannot occur without the presence of water [22]. However, it has been reported that the freeze drying process can decrease metabolite extraction efficiency due to a potential irreversible problem that may occur where the metabolites adhere to the cell walls and membranes [23].

4.2.3 The Chemical Complexity of Metabolomics

Metabolomics is a dynamic process whereby the metabolites produced by enzyme-catalysed reactions in cells have a finite half life as they are constantly being produced, transformed into other compounds or degraded [17]. These reactions are organised into metabolic pathways that depict the cyclic nature of metabolism. These pathways also show how metabolites can undergo modification reactions in order to serve as a precursor that can be converted into a biologically active compound. The metabolic pathway databases are discussed in more detail in section 4.4.

Type of Modification	Chemical Addition
Hydroxylation	OH
Phosphorylation	PO_4
Reduction	H_2
Amidation	NH_2
Acetylation	CH_3CO

Table 4.1: Common Metabolite Modifications [17].

Metabolites often retain the chemical characteristics of their parent metabolite but they can also form larger chemical compounds. An example of this is the conversion of glucose into storage carbohydrates such as starch [17]. Metabolites may also be converted into smaller compounds; this can occur through oxidation reactions that lead to the loss of water molecules. The synthesis of metabolites is crucial for cell survival as often the metabolites produced have pivotal roles in contributing to the infrastructure of the cell and/or have an energy-related role. Terminology has been developed to summarise these processes; anabolic metabolism is the synthesis of complex molecules for energy storage and catabolism is the degradation of complex molecules for energy release [24].

There are many factors that can cause variability in metabolic profiles. For example, environmental factors can influence the concentrations of metabolites observed [25].

4.3 Techniques Used to Study Metabonomics/Metabolomics

There are many techniques that can be employed to investigate the metabolome. The most widely used techniques include Nuclear Magnetic Resonance (NMR) spectroscopy[26] and hyphenated mass spectrometry techniques such as Liquid Chromatography-Mass Spectrometry (LC-MS) [27] and Gas Chromatography Mass Spectrometry (GC-MS)[28]. NMR is a fast technique and there are no separation steps prior to analysis. The major disadvantage of this technique is the dynamic range over which it operates along with its poor sensitivity.
One of the main problems associated with the use of GC-MS is the need for chemical derivatisation to make the metabolites more volatile [29].

4.3.1 The Role of Mass Spectrometry in Metabolomic Research

Mass Spectrometry based techniques have become increasingly important in the area of metabolomics. Numerous metabolomics approaches utilise a chromatographic separation technique coupled to a mass spectrometer - the combination of chromatography with spectrometry provides good sensitivity and selectivity [30].

The most influential aspects of MS analyses for metabolomic studies are:

- High sensitivity
- High throughput
- Identification of compounds from complex biological samples
- Information relating to metabolite structure can be obtained by fragmentation (MS/MS)
- Quantitative information can be obtained

The two most common hyphenated MS techniques that are used in this area of science are GC-MS [28] and LC-MS [27]. GC-MS has been used to profile plant functional genomics; however, whilst this technique is sensitive it requires time-consuming sample preparation steps, for example the extraction and derivatisation of analytes. GC-MS does not produce rapid results and some particular classes of compounds, for example non-volatile, polar macromolecules cannot be analysed using this technique. At present, LC-MS, in particular LC/ESI-MS, is probably the most widely used technique for metabolite studies. This is because it can detect a range of masses, is reproducible and sensitive, is a soft ionization technique and only requires very basic sample preparation compared with GC-MS [31]. Both GC-MS and LC-MS require an extraction process. This is usually done using liquid extraction where the solvent that is selected is dependent upon the metabolites to be extracted and the analytical technique that is to be used. Thus, the major drawback to extraction-related sample preparation is that it is difficult to locate spatially within the biological sample where the metabolites originated from.

The interpretation of metabolomics data can be rather challenging because a given metabolite may participate in a myriad of biochemical pathways. Due to the complex nature of cell metabolism it is extremely difficult to observe a direct link between metabolomics and genomics.

Metabolites are extremely chemically diverse, both in structure and in their properties such as their polarities, modifications that they may undergo (refer to table 4.1) and the isomeric forms in which they can present themselves. These factors can further complicate analyses for many analytical techniques [17].

A metabolomics technique is desired that can measure, in parallel, many different metabolites in one experiment, can provide reproducible data, is relatively fast in performing analyses and can be automated [32] – Matrix -Assisted Laser Desorption Ionisation Mass Spectrometry Imaging (MALDI MSI) fits all the criteria.

One of the major advantages in using MALDI MSI for metabolomic applications is that this technique boasts good sensitivity. Not only can this technique detect a compound, it also allows for the visualisation of where analytes of interest are spatially located in the tissue section. The spatial resolution of metabolites in complex biological tissues, such as plant tissue, can provide useful information that may be pivotal to the understanding of metabolic processes. There is increasing interest in the use of MALDI MSI for plant science applications – agrochemicals (Mesotrione and Azoxystrobin) have been investigated in soya plants [33]. The use of MALDI MSI to investigate the oligosaccharide distribution in wheat stems has been reported and it was commented that the sensitivity achieved was comparable with what had been achieved in their previous studies carried out using LC-MS [34].

More recently MALDI MS has been applied to the study of temperature-induced stress in wheat [35].

4.4 Metabolomic Databases

Once data has been generated there are many databases available for the tentative identification of the unknowns. Metabolomic databases often contain information on compounds ranging from many different organisms to drug metabolism pathways. These databases demonstrate the extensive work by laboratories and consortia around the world in identifying unknown metabolites and establishing accurate databases that can contain thousands of metabolites. However, there is a lack of complete metabolomic databases. Section 4.4.1 details some of the most established databases.

4.4.1 Spectral Databases

Metlin: This database was a collaborative effort between the Siuzdak and Abagyan research groups at the Scripps Research Institute, La Jolla, USA. Searches can be performed using pre-corrected neutral masses or searched for the loss or gain of a proton; it does not correct for sodiated and or potassiated ions [36].

MassTRIX: MassTRIX is a metabololite search facility that uses the Kyoto Encyclopedia of Genes and Genomes (KEGG) pathways. Masses with their corresponding identities are entered in text format and are matched up with possible metabolites in the Kegg pathway. Mass correction can be performed for the loss or gain of a proton and for sodium adducts. Alternatively neutral masses can be searched for mass corrected data. Specific organisms can be searched by entering the organism of interest before the search is performed [37].

4.4.2 Metabolic Pathway Databases

Metabolic pathway databases contain information based on the information obtained from experimental literature where the biochemical reactions are organised into maps/pathways.

Kyoto Encyclopedia of Genes and Genomes (KEGG): contains in excess of 15 000 compounds from a range of plants, animals and bacteria, 8872 drugs and approximately 11 000 glycan structures. Approximately 93, 000 pathways have been established from 336 reference pathways and are detailed for over 700 organisms. A recent addition to the KEGG database is KEGG Plant containing information relating to plant biosynthetic pathways and phytochemical compounds. The KEGG database is divided into sections that are focussed on a particular area thus making it easier to navigate [38].

MetaCyc: A database that contains over 1200 pathways from more than 1600 organisms that encompasses the pathways of both microorganisms and plants [39].

Metacrop: A database that also contains metabolic pathway information; however, as its name suggest it is more tailored for the analysis of crop plants. It contains information for 6 major crop plants, one of which is wheat and their related biochemical pathways [40, 41].

4.5 Applications of Plant Metabolomics

The first significant plant related publication was by Sauter *et al.* in 1991 [42] using GC-MS to investigate the effects of herbicides on barley plants.

In recent years, metabolomics has been applied to many different areas of science. These include plant biochemistry, testing crop quality and many more [43].

Environmental induced stress has been investigated previously in plant material, for example to study the effects of temperature on Aradopsis thaliana [42, 44]. Another example has been presented where the plant stress was in the form of a deficiency in available nutrients [45].

The integration of all the information obtained in the 'omics sciences is known as systems biology (refer to figure 4.1); however, sophisticated mathematical models are required for the systems biology approach due to the complexity of the data. For example, small changes in the proteome can have a significant impact on the metabolome as enzyme activity is required for many metabolic processes [46].

Metabolomics therefore represents the final stage of systems biology with metabolites representing the end products of gene expression and which can provide complementary information in relation to other 'omics sciences [44].

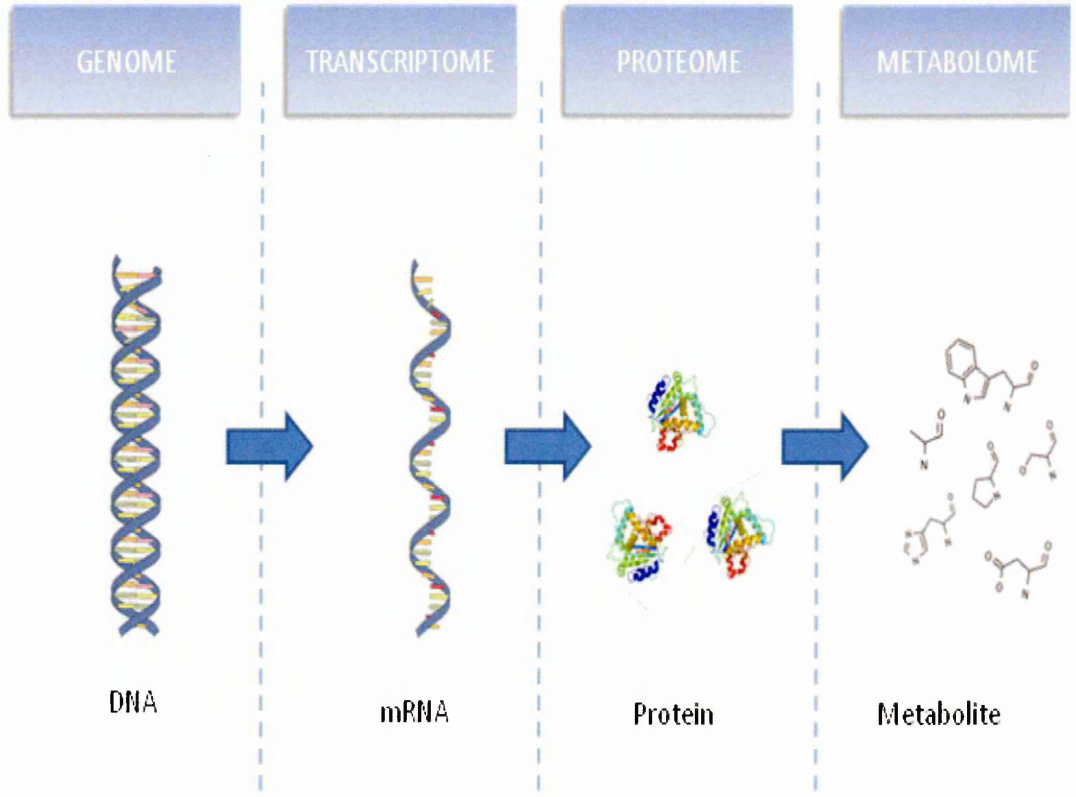

Figure 4.1: Schematic Diagram of the Interactions in the 'Omics': The schematic shows the progression from genomics-based studies to the metabolomic level with metabolites being the end products of gene expression, adapted from [47].

4.5.1 Phenotyping Plant Samples

Metabolomic studies can be very useful for phenotyping experiments, for example phenotyping genetically engineered plants [48]. Metabolomics could also be applied to the study of plants that have been subjected to different environmental conditions, as these changes, whether they are genetic or environmental, will have an impact on the observed metabolic profile. Published results show that starch biosynthesis can be studied in transgenic potato tubers in this way [48].

A comparison has also been made between organic and non-organic crops by investigating the metabolic differences observed [49].

4.6 Limitations of Metabolomics

There has been a movement in recent years to perform non-targeted metabolite studies where an attempt to detect as many metabolites as possible within a sample is performed using a technique such as GC-MS [50]. However, such experiments lead to an abundance of peaks within the mass spectrum generated. It has been estimated that up to 70% of all the detected masses using GC-MS are unknown compounds and that they will remain unknown until metabolomics databases are improved [17].

There are also currently many problems associated with the use of metabolomics databases. These include databases that contain non-biological compounds that have been established for the existing techniques such as NMR and GC-MS. There are limited database resources for the data generated by MALDI as many databases do not take into account the sodiated and potassiated compounds commonly observed with this technique in both plant and animal tissues due to the presence of endogenous salts. Mass correction is therefore a pre-requisite before the data can be entered into the relevant database. Another method of identifying unknown compounds is to obtain standards; however, the main problem associated with this method of compound identification is that many plant metabolites especially those that fall into the secondary metabolite category are not commercially available [9]. At present, the analytical technique that seems the most appropriate taking these two limitations into account is the coupling of LC-MS with NMR due to the achievable high throughput analysis together with chemical selectivity and structure elucidation [51].

4.7 MALDI MS Analysis of Wheat Grain

The increasing demand for high throughput analysis in drug discovery and bioanalysis, where the samples are often complex mixtures that contain contaminants such as salts and buffers, has led researchers to re-evaluate MALDI MS for small molecule analysis [52].

This chapter details the use of UV MALDI MSI and IR LDI MS for the imaging and profiling of plant tissue where wheat grain has been used as the model system. In

particular, a number of different matrix types have been studied and the use of IR LDI MS has been investigated as a matrix-free option

The aim of the work presented in this chapter was to develop methodology for the high-throughput metabolomic analysis of plant samples using wheat grain as the model system. The approach used was non-targeted i.e the method was not optimised to study specific metabolic pathways but to simultaneously detect as many metabolites as possible.

4.7.1 Wheat

The developmental stage of the wheat grain is important as this can affect the metabolic profile; therefore it is important to harvest the crop at similar developmental stages. In wheat this is usually defined by the days post-anthesis. Wheat is a cereal crop that is grown worldwide and on a global scale is one of the most important food grains for human consumption. Therefore, it is of great interest to study which endogenous metabolites wheat grains are comprised of and what makes wheat such a nutritionally important crop. Wheat has a large genome comprising of 16 000Mb; this is in the magnitude of 40 times larger than the rice genome [53]. Poor weather conditions and a movement towards growing 'greener' biofuel crops in place of wheat have previously led to worldwide shortages. Therefore, using metabolomics a greater understanding of the composition of wheat grains can be achieved. This may be of use in the future if there is a need to develop genetically engineered wheat crops to avoid future shortages and protect from crop diseases such as wheat fusarium head blight [55]. A metabolomics approach would also provide information relating to crop quality as this is directly related to the metabolite content of the plant/grain [55].

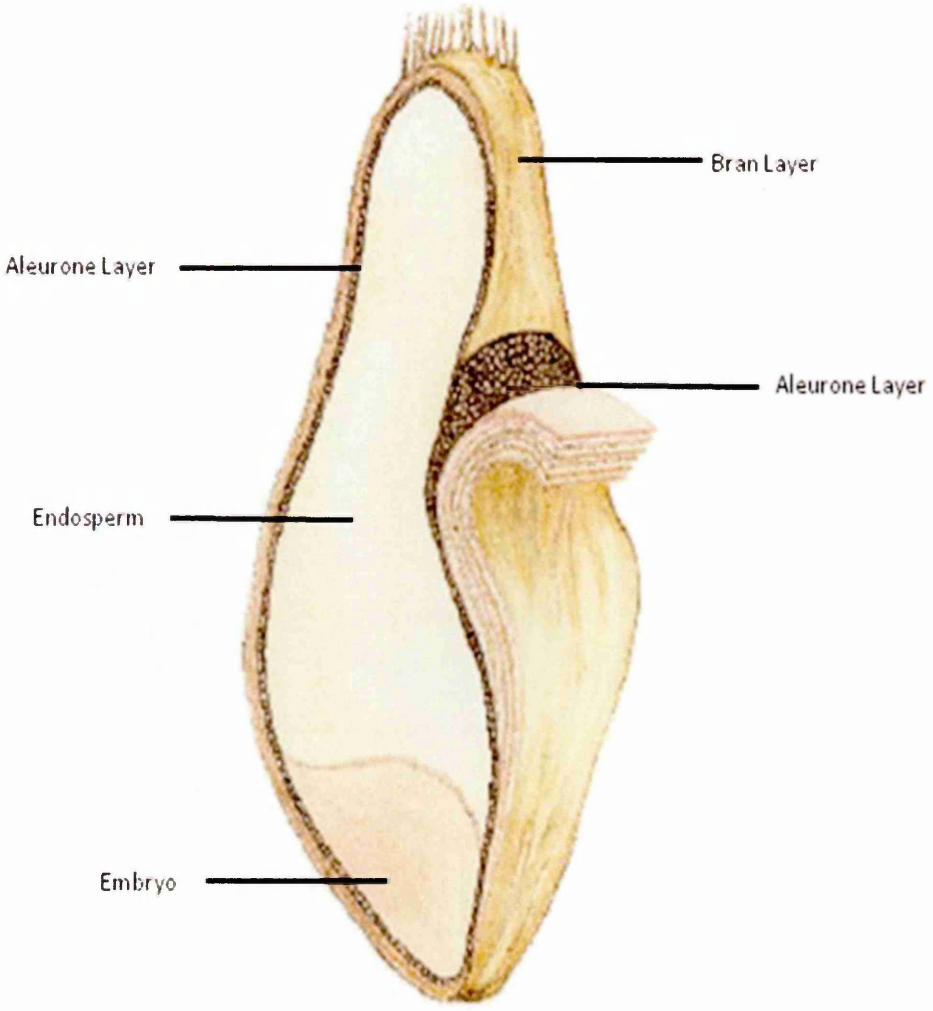

Figure 4.2: Schematic Diagram of a Wheat Grain Cross-Section: The different regions of the wheat grain are annotated on the diagram [56].

4.7.2 Matrix Selection

A range of matrices have been incorporated into MALDI MS analysis in order to assess the potential for metabolomic applications.

Organic matrices have been used in the work described in this chapter namely α-CHCA, 5, 10, 15, 20-tetrakis (pentafluorophenyl) porphyrin (F20TPP) and 9-aminoacridine. The matrix peaks that are observed with α-CHCA occur in the low mass region, interfering with possible metabolites such as amino acids. Therefore F20TPP was tested as the matrix peaks associated with this compound are in the high mass region, and thus there will be less interference where low mass metabolite peaks occur [57].

Inorganic particle suspensions, for example TiO_2, TiO_2/graphite mix, gold and silver nanoparticles, have been investigated as it is thought that they work by a different mode of ionisation – instead of co-crystallising with the analyte it is considered that they work by exerting a thermal effect, passing kinetic energy onto the metabolite to aid ionisation. Kinumi *et al.*[58] have previously reported the use of TiO_2 for small molecule analysis. Particle suspension matrices such as TiO_2 [58] and graphite [59] have been previously used for small molecule analysis.

4.7.3 Experimental

4.7.3.1 Materials

Trifluoroacetic acid (TFA) (AR grade), α-CHCA, 9-aminoacridine, Titanium Dioxide, ethylene glycol, Graphite (1-2 micron, synthetic), F20TPP, acetone and ethanol were purchased from Sigma-Aldrich (Gillingham, UK). Potassium gold (III) chloride ($KAuCl_4$), tetraoctylammonium bromide, dodecanethiol, Gelman Acrodisc CR PTFE 0.2μm, silver nitrate ($AgNO_3$) and sodium borohydride were also obtained from Sigma-Aldrich (Gillingham, UK). Carbon conductive tape (8x20mm) was obtained from TAAB Laboratories Equipment Ltd, Aldermaston, UK. Tape (G304) used to affix the plant tissue for initial experiments with the IR laser was obtained from Plano GmbH, Wetzlar, Germany.

4.7.3.2 Instrumentation

UV MALDI

MALDI MS spectra were acquired using an Applied Biosystems/MDS Sciex (Ontario, Canada) hybrid quadrupole orthogonal time-of-flight instrument (Q-Star Pulsar-i) fitted with a UV MALDI ion source, oMALDI server imaging software and a high repetition (1000Hz) Nd:YAG laser with an elliptical spot size of 100x150μm.

UV MALDI (Ion Mobility)

Ion mobility data was aqcuired using a Waters Corporation Synapt™ HDMS™ orthogonal time-of-flight instrument fitted with a 200Hz Nd: YAG laser (Manchester, UK). Waters MassLynx software was used to process the data.

Matrix Applicator for UV MALDI

Airspray deposition of the matrix onto the wheat grain sections was performed using an Iwata gravity-fed pneumatic air spray gun (Iwata Media Inc., Portland, OR, USA).

IR LDI

IR LDI mass spectra were acquired using a prototype orthogonal time-of-flight mass spectrometer (oTOF MS) equipped with an Er:YAG infrared laser (Speser, Spectrum GmbH, Berlin, Germany) that operates at a wavelength of 2.94 μm.

The full-width-at-half-maximum (FWHM) duration of the laser pulses was ~ 100 μs. The mass range for the experiments conducted using IR LDI MS was limited to by the setting of the quadrupole - the lower cut off was set to m/z 150.

4.7.3.3 Sample Preparation Methodology

Wheat (*Triticum aestivum* L. Var. Axona) plants were grown in Levingtons M3 compost supplemented with Osmacote in a growth room under a day/night regime of 20/16°C, a day length of 16 hours and light intensity of 400μE. The developing wheat grains were harvested at specified times post-anthesis. Once the wheat grains had been harvested, they were instantly frozen using liquid nitrogen to cease any further metabolic activity and were then stored at -80°C prior to analysis. A cryostat (Leica CM1900) was used to section the wheat grains. This was done by embedding the wheat grain in ice to act as a support. Optimum Cutting Temperature embedding medium (OCT) was not used as this is known to suppress MALDI signals [60]. The sections were then attached to double-sided carbon conductive tape and freeze dried; this was followed by matrix application. For IR LDI the wheat grain sections were attached to a different type of double-sided tape [58] and then mounted on a glass slide which was then placed into a custom-made milled-out MALDI target plate. This was required as preliminary experiments showed that the double-sided carbon conductive tape interfered with the analysis, although experiments show that this is not the case for UV MALDI MS. Initial experiments were conducted on freeze-dried wheat grain sections but it was found that were not as suitable for IR LDI as wheat grain sections that had been kept frozen. This is mainly due to the lack of residual water contained within the freeze dried sections. Therefore wheat grains that had been sectioned and kept frozen were used in these experiments.

4.7.3.4 Matrix Application

An airbrush deposition method was used to apply the matrix as homogeneously as possible. The following matrices were studied: α-CHCA, 9-aminoacridine, Titanium dioxide/graphite, Silver nanoparticles, Gold nanoparticles and 5, 10, 15, 20-tetrakis (pentafluorophenyl) porphyrin.

The matrices were prepared as follows:
α-CHCA: 25mg/mL, dissolved in acetone containing 0.1% trifluroacetic acid (TFA),
9-aminoacridine: 10mg/mL, dissolved in acetone.

Titanium dioxide: 5mg/mL suspended in ethanol containing 0.001% ethylene glycol and 0.1% TFA.

Titanium dioxide/graphite mix: 5mg/mL, suspended in ethanol containing 0.001% ethylene glycol and 0.1% TFA.

5, 10, 15, 20-tetrakis (pentafluorophenyl) porphyrin was made to a concentration of 10mg/mL in ethanol.

The gold nanoparticles were synthesised according to the thiol-derivatisation method developed by Brust *et al.* where the gold salt ($KAuCl_4$) was derivatised using dodecanethiol and reduced using sodium borohydride ($NaBH_4$) [61]. The silver nanoparticles were synthesised using the method developed by Munro *et al.* where silver nitrate solution was reduced using $NaBH_4$ [62]. Both the gold and the silver nanoparticles were made to a concentration of 1mg/mL. All the matrices prepared were sonicated for approximately 15 minutes.

4.8 Data Processing

Calibration was performed using the known matrix masses and selected endogenous masses to ensure the mass spectrum was calibrated thoroughly (refer to matrix calibration tables in section 4.9). The calculated mass accuracy for the matrix peaks formed the basis of the permissible mass accuracy criteria for the allocation of masses to potential metabolites. Potential metabolites were detected above these ranges that were logical according to metabolism maps; however, these intermediates of metabolism were probably too low in concentration to give a defined peak and hence the mass accuracy was not as good. In some cases the calibration parameters may also have affected the mass accuracy. Thus fewer metabolites were identified for both 9-aminoacridine data and F20TPP data as there were fewer matrix calibration points that could be used.

4.9 Results and Discussion

4.9.1 Data Analysis

MALDI MSI generates a large amount of data and the interpretation of this data can prove to be challenging.

It has been estimated that there could be around 200 000 metabolites in the plant kingdom [31, 63]. Many metabolite species are very similar in mass or may even have exactly the same mass, and it is difficult to differentiate between isomers. Furthermore, adduct formation is a common trait of MALDI MS analyses, and therefore sodium and potassium adducts must be considered when interpreting data. MS/MS experiments can be beneficially utilised to provide structural information regarding a metabolite of interest; however, MS/MS cannot often differentiate between isomers [64].

In order to interpret the data generated by MALDI MS the following databases were consulted: Metlin [36], MassTrix [37], Kegg [38], MetaCyc [39] and MetaCrop [40]. The detected masses were first converted to neutral masses by subtracting the mass of hydrogen, sodium and potassium. The neutral masses were also calculated for modifications including phosphorylation, hydroxylation and acetylation.
Many metabolites often have similar if not the same masses and trying to assign masses to potential metabolites is not an easy task; however, the accuracy of the instrumentation used must be taken into account and the degree of error calculated. The matrix peaks were used to determine a suitable mass tolerance for the metabolites detected. The wealth of data generated by MALDI MS makes it a difficult and time consuming process to allocate masses detected to potential metabolites; however by including the tables of potential metabolites it is intended to highlight the challenges in mass allocation and the complexities of metabolomics investigations.

4.9.2 UV MALDI MS

A range of UV matrices were investigated (refer to section 4.7.2) in this study to assess how they compare in the ionization of metabolites and whether some matrices were better than others for certain types of metabolites such as oligosaccharides. α-CHCA was the first matrix to be investigated (see figure 4.3) as it is the most widely used matrix in MALDI MSI because it is capable of promoting the ionization of many different compounds.

α-CHCA

Figure 4.3 shows a representative MALDI mass spectrum of a wheat grain obtained using α-CHCA as the matrix. The matrix peaks shown in table 4.2 are dominant in the low mass region (typically under m/z 500) of the MALDI mass spectrum shown in figure 4.3. The intensity of these matrix peaks may be suppressing the ionisation of metabolites present in the plant tissue, especially low abundance metabolites or metabolites may be 'masked' by spectral overlap if the metabolites have the same masses as or similar masses to the matrix ions. The sugars are clearly visible in the MALDI mass spectrum with the mass assignment of the metabolites detected being presented in table 4.3. This table shows the masses that were detected, the theoretical mass, the mass accuracy error in both mDa and ppm, the possible metabolite detected along with the type of ion detected (protonated, sodiated or potassiated) and the possible metabolomic pathways in which the potential metabolite may have a role in; this was established using the databases detailed in section 4.4. The rationale for the mass assignment to potential metabolites was based on the mass accuracy (refer to table 4.2) obtained for the matrix peaks, in this case a mass accuracy of approximately 15ppm. In addition, it has to be biologically feasible that the metabolites will occur in wheat grain; this was also investigated using the metabolomic databases mentioned in section 4.4. Metacrop and MassTrix proved to be very useful as they contain information that is directly related to wheat.

However, the presence of the α-CHCA matrix peaks in the low mass region of the mass spectrum can be problematic both in terms of potential suppression effects

where the matrix ions may be suppressing metabolite ions and in terms of potential spectral overlap of the matrix ion and the metabolite ions. Matrix suppression of metabolites may make the detection of low abundance metabolites virtually impossible. The matrix peaks, however, can be beneficial for the recalibration of the data post acquisition.

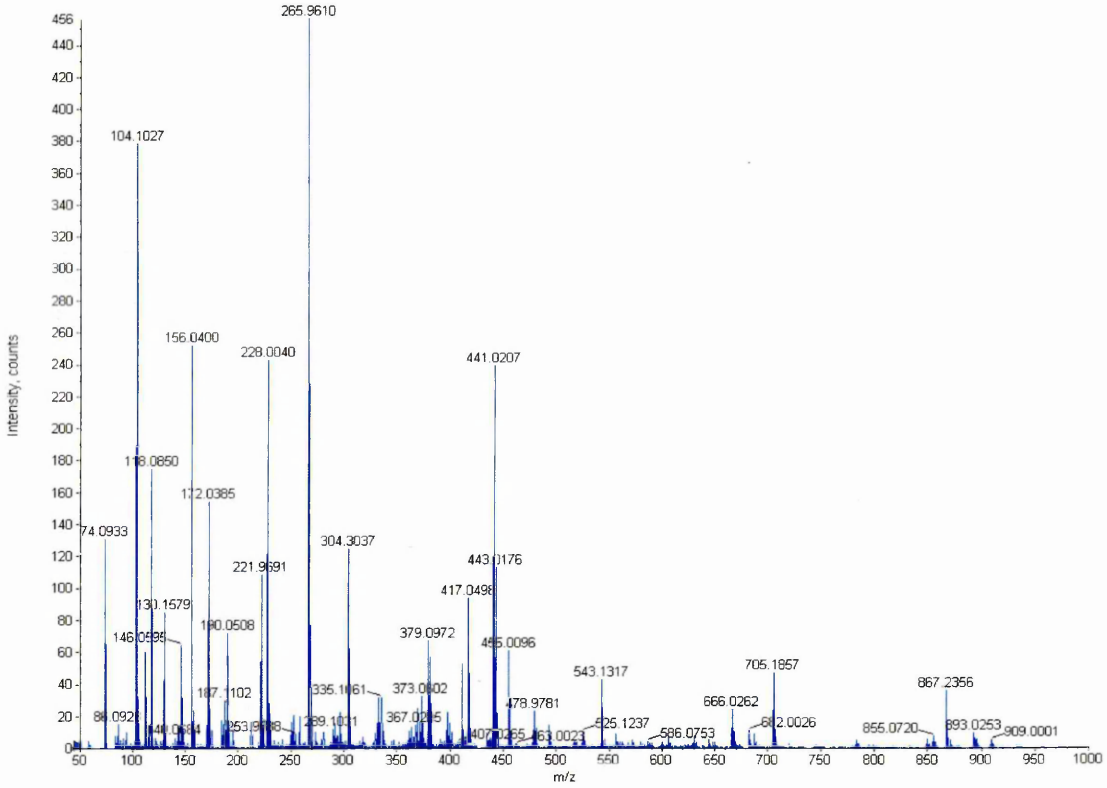

Figure 4.3: MALDI Mass Spectrum of Wheat Grain: A representative full scan spectrum showing the metabolites detected using α-CHCA as the matrix. The dominance of the matrix peaks under m/z 500 can interfere with the metabolic signals via spectral overlap and suppression effects. This can be problematic as quite often in biological tissue there are metabolites that are present in such small quantities.

Mass detected m/z	Theoretical mass	Error (mDa)	Error (ppm)	Ion Detected
172.0385	172.0399	-1.40	-8.14	$[M+H]^+ - H_20$
190.0508	190.0504	0.40	2.11	$[M+H]^+$
212.0354	212.0324	3.00	14.15	$[M+Na]^+$
228.0040	228.0063	-2.30	-10.09	$[M+K]^+$
379.0972	379.0930	4.20	11.08	$[2M+H]^+$
401.0710	401.0750	-4.00	-9.97	$[2M+Na]^+$
417.0498	417.0489	0.90	2.16	$[2M+K]^+$

Table 4.2: Masses obtained for the matrix, α-CHCA.

Mass detected m/z	Theoretical mass	Error mDa	Error ppm	Possible metabolite detected	Ion detected	Possible metabolic pathways
116.0696	116.0711	-1.50	-12.92	Proline	$[M+H]^+$	Arginine and Proline metabolism
118.0850	118.0868	-1.80	-15.24	Valine*	$[M+H]^+$	Valine, leucine and isoleucine degradation
133.0602	133.0613	-1.10	-8.27	Asparagine	$[M+H]^+$	Unknown
138.0547	138.0531	1.60	11.59	Proline	$[M+Na]^+$	Arginine and Proline metabolism
140.0684	140.0688	-0.40	-2.86	Valine*	$[M+Na]^+$	Valine, leucine and isoleucine degradation
173.0425	173.0426	-0.10	-0.58	Ribose	$[M+Na]^+$	
175.1170	175.1195	-2.50	-14.28	Arginine *	$[M+H]^+$	Arginine and proline metabolism
184.0752	184.0738	1.40	7.61	Phosphocholine *	$[M+H]^+$	Phospholipid Synthesis [65]
219.0250	219.0271	-2.10	-9.59	Hex (Glucose)	$[M+K]^+$	Sugar metabolism
258.1090	258.1106	-1.60	-6.20	Glycerophosphocholine*	$[M+H]^+$	Unknown
363.0725	363.0694	3.10	8.54	Amylose	$[M+K]^+$	Sugar metabolism
365.1002	365.1060	-5.80	-15.89	Hex 2 (Sucrose)*	$[M+Na]^+$	Sugar metabolism
381.0796	381.0799	-0.30	-0.79	Hex 2 (Sucrose)	$[M+K]^+$	Sugar metabolism
543.1317	543.1327	-1.00	-1.84	Hex 3 (Raffinose)*	$[M+K]^+$	Sugar metabolism
582.0535	582.0615	-8.00	-13.74	ADP-ribose*	$[M+Na]^+$	Sugar metabolism
588.0820	588.0744	7.60	12.92	GDP-4-Dehydro-6-deoxy-D-mannose	$[M+H]^+$	Sugar metabolism
606.0908	606.0850	5.80	9.57	GDP-D-mannose	$[M+H]^+$	Fructose and Mannose Metabolism
628.0662	628.0670	-0.80	-1.27	GDP-D-Mannose*	$[M+Na]^+$	Fructose and Mannose Metabolism
644.0501	644.0409	9.20	14.29	GDP-D-Mannose	$[M+K]^+$	Fructose and Mannose Metabolism
705.1857	705.1856	0.10	0.14	Hex 4 (Stachyose) *	$[M+K]^+$	Sugar metabolism
867.2356	867.2384	-2.80	-3.23	Hex 5*	$[M+K]^+$	Sugar metabolism

Table 4.3: Potential metabolites detected using α-CHCA as the matrix: Metabolites marked with an asterisk (*) correspond to the images presented in figure 4.4.

Table 4.2 shows the calculated matrix errors of the matrix ions detected. The tabulated data (Table 4.3) of potential metabolites shows the errors in both mDa and in ppm. This was done for data comparison between the data generated herein and the data contained in published literature where the errors are reported in mDa and larger mass accuracy errors are often reported [66]. The metabolites shown in table 4.3 are mostly primary metabolites; these are compounds that are essential to life [20].

4.9.3 Interpretation of MALDI MS Images

Each pixel in the MALDI image relates to the mass spectrum recorded at that point. The brightness of the pixel can be indicative of the relative concentration of the metabolite in that location, although it is important to note that this is not an accurate method of quantification and gives only semi-quantitative information.

Figure 4.4 shows the MALDI images generated using α-CHCA that correspond to some of the metabolites in table 4.3; these are marked with an asterisk (*). Images a and b show the tentative distributions of valine ($[M+H]^+$ and $[M+Na]^+$, respectively) where the images show that valine in its protonated form is more abundant throughout the wheat grain section. Image c is the distribution for m/z 175.12 tentatively assigned to arginine ($[M+H]^+$) and this ion appears to be more abundant at the top of the wheat grain section. The image labelled d shows that there is a relatively homogenous distribution throughout the endosperm regions of the wheat grain section of m/z 184.07; this has been tentatively assigned to the presence of phosphocholine. Image e is the image obtained for m/z 258.11 and shows the ion intensity is greater at the top and centre of the wheat grain section; this mass was tentatively assigned to glycerophosphocholine. Image f is that obtained for m/z 365.10, which has been tentatively assigned to the sodium adduct of sucrose. Image g shows the distribution of 543.13 which has been tentatively assigned to a hexose 3 sugar such as Raffinose; the distribution is similar to that observed for image f. Image h shows the distribution of m/z 582.05 which has been tentatively assigned to ADP-ribose. Images i, j and k, tentatively assigned to the presence of sodiated GDP-D-Mannose, Hex 4 sugar (potassiated), for example Stachyose, and Hex 5 sugar (potassiated), respectively, all appear to be less abundant than in the previous images - this is probably due to the abundance of the ion within the wheat grain section.

a

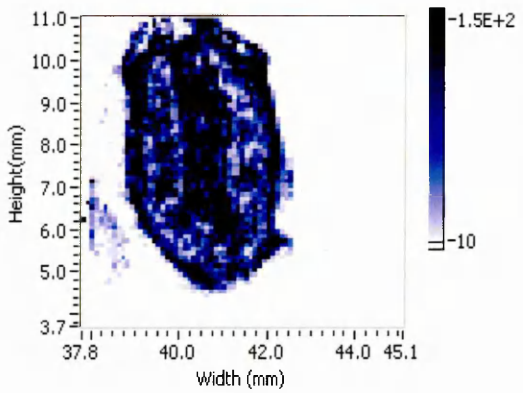
11.0
10.0
9.0
8.0
7.0
6.0
5.0
3.7
Height(mm)
37.8
40.0
42.0
44.0
45.1
Width (mm)
-1.5E+2
-10

b

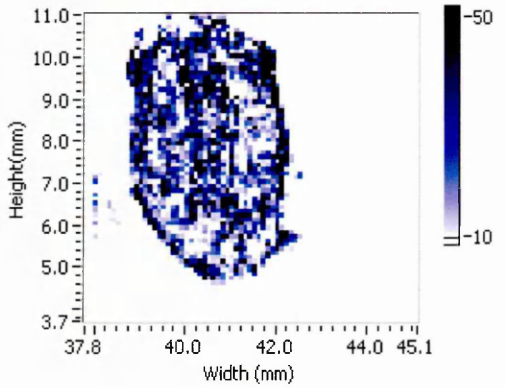
11.0
10.0
9.0
8.0
7.0
6.0
5.0
3.7
Height(mm)
37.8
40.0
42.0
44.0
45.1
Width (mm)
-50
-10

c

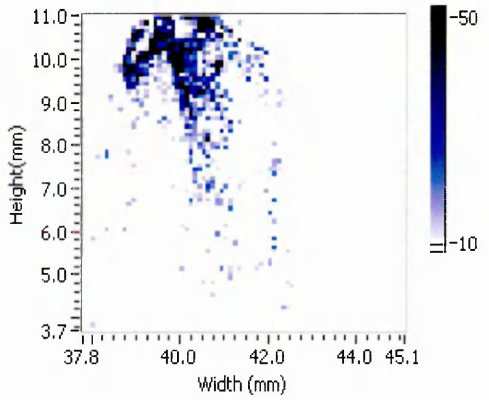
11.0
10.0
9.0
8.0
7.0
6.0
5.0
3.7
Height(mm)
37.8
40.0
42.0
44.0
45.1
Width (mm)
-50
-10

d

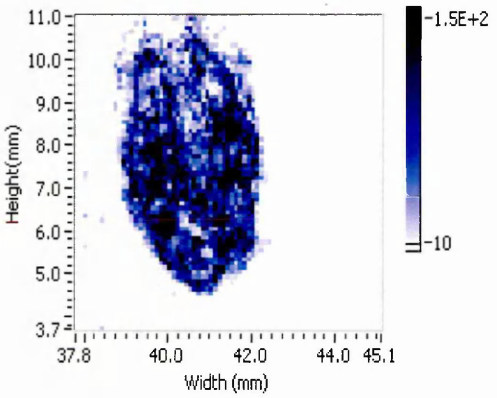
11.0
10.0
9.0
8.0
7.0
6.0
5.0
3.7
Height(mm)
37.8
40.0
42.0
44.0
45.1
Width (mm)
-1.5E+2
-10

e

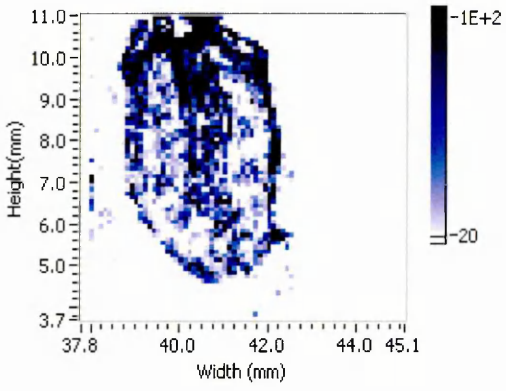
11.0
10.0
9.0
8.0
7.0
6.0
5.0
3.7
Height(mm)
37.8
40.0
42.0
44.0
45.1
Width (mm)
-1E+2
-20

f

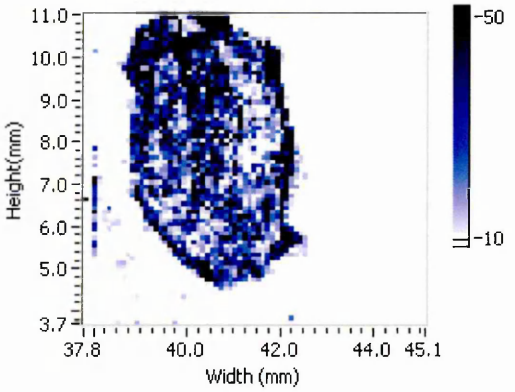
11.0
10.0
9.0
8.0
7.0
6.0
5.0
3.7
Height(mm)
37.8
40.0
42.0
44.0
45.1
Width (mm)
-50
-10

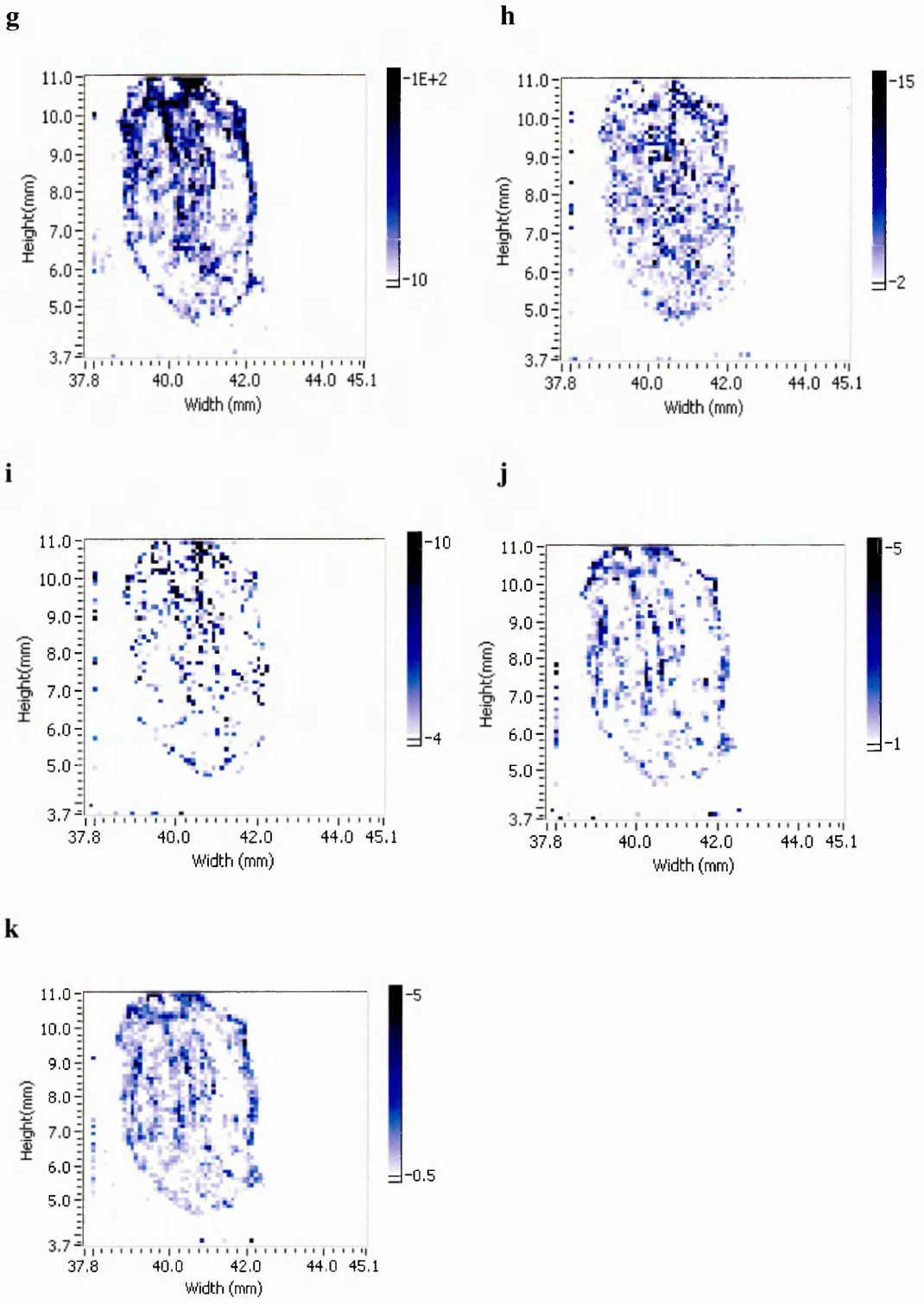

Figure 4.4: MALDI MS Images of Wheat Grain: The accurate MALDI MS images of m/z: (a) 118.09; (b) 140.07; (c) 175.12; (d) 184.07; (e) 258.11; (f) 365.10; (g) 543.13; (h) 582.05; (i) 628.07; (j) 705.19 and (k) 867.24. Images were normalised to the corresponding matrix ion.

F20TPP

Due to the expense of F20TPP this matrix was tested for its use in plant metabolomic analysis by manually spotting the matrix onto the surface of the wheat grain tissue section. Therefore an image for this particular matrix was not generated.

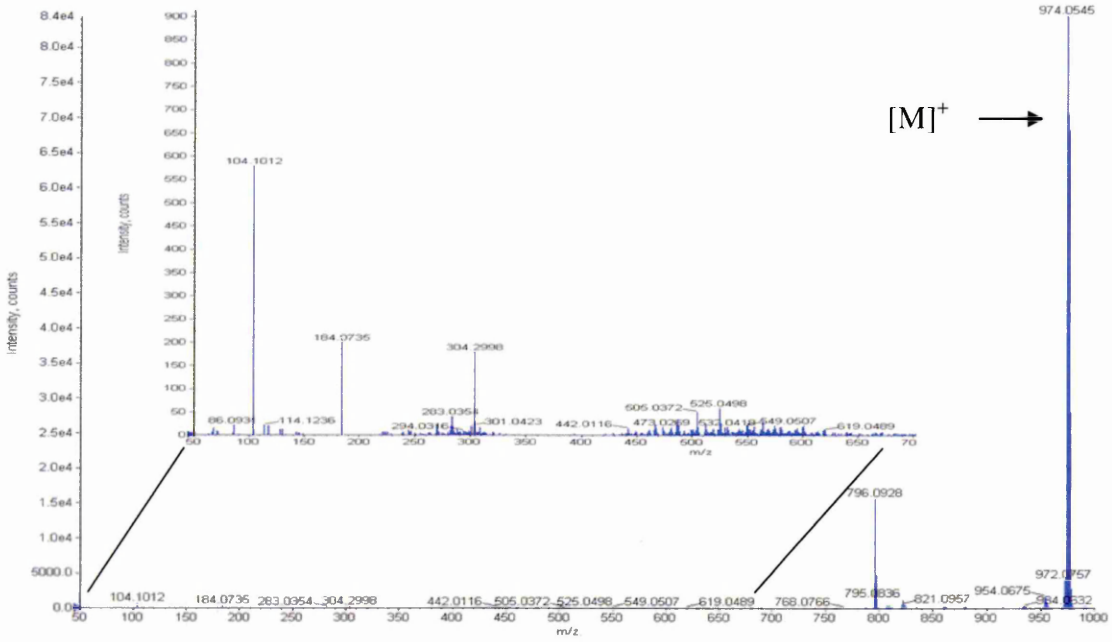

Figure 4.5: MALDI Mass Spectrum of Wheat Grain using F20TPP. A representative full scan MALDI mass spectrum showing the metabolites obtained using F20TPP. As can be seen in the spectrum, the matrix peaks occur at the higher mass end of the spectrum with the main peak for $[M]^+$ occurring at m/z 974.0545.

The masses presented in table 4.4 are related to the mass accuracy of the matrix peaks. As the matrix peaks for F20TPP occur in the high mass region, the peaks used for the calibration included a fragment ion observed at m/z 807.07 and an endogenous peak at m/z 184.07 was used as this peak was common to all the UV MALDI MS experiments conducted in positive ion mode.

The metabolites potentially identified using this particular matrix have errors that are quite large as shown in table 4.5; this was probably due to the lack of calibration

points over a suitable mass range. The metabolites that were tentatively identified appear to be secondary metabolites; these are metabolites that operate in biochemical reactions and in signalling cascades [20]. This is plausible as there are no matrix ions in the low mass region to suppress less abundant secondary metabolites. The databases used as previously described gave an insight into some of the potential pathways associated with these tentatively identified metabolites. The strong intensity for the matrix ion at m/z 974.05 seems to have suppressed the ionisation of the sugars identified previously using α-CHCA as the matrix.

Mass detected m/z	Theoretical Mass	Error mDa	Error ppm	Ion Detected
184.0735	184.0734	0.10	0.54	[Phosphocholine+H]+
807.0711	807.0711	0.00	0.00	[Fragment ion -1R group
974.0545	974.0586	-4.10	-4.21	$[M]^+$

Table 4.4: Masses Obtained for the Matrix F20TPP.

Mass Detected m/z	Theoretical mass	Error mDa	Error ppm	Possible Metabolite	Ion detected	Possible metabolic pathway
184.0735	184.0739	-0.40	-2.17	Phosphocholine	$[M+H]^+$	Phospholipid synthesis [66]
270.0342	270.0379	-3.70	-13.70	N-acetyl-5-glutamyl phosphate	$[M+H]^+$	Arginine biosynthesis
277.0294	277.0325	-3.10	-11.19	6 phosphogluconate	$[M+H]^+$	
289.0379	289.0324	5.50	19.03	3-deoxy-arabino-heptulosonate 7-phosphate	$[M+H]^+$	Shikimate biosynthesis
291.0501	291.0481	2.00	6.87	Sedoheptulose 7-phosphate	$[M+H]^+$	Pentose phosphate pathway/Calvin cycle
309.0435	309.0464	-2.90	-9.38	N1-(5-phospho-D-ribosyl)glycinamide	$[M+Na]^+$	Purine biosynthesis
450.0129	450.0191	-6.20	-13.78	ADP	$[M+Na]^+$	Multiple pathways
455.0805	455.0815	-1.00	-2.20	(S)-2-[5-amino-1-(5-phospho-D-ribosyl)imidazole-4-carboxamido]succinate	$[M+H]^+$	Purine biosynthesis
502.0421	502.0376	4.50	8.96	N6-(1,2-dicarboxyethyl)-AMP	$[M+K]^+$	Purine biosynthesis
505.1736	505.1766	-3.00	-5.94	1-kestose	$[M+H]^+$	Fructan biosynthesis
537.0517	537.0523	-0.60	-1.12	UDP-L-arabinose	$[M+H]^+$	Arabinoxylan, Beta-Glucan, cellulose biosynthesis
582.0556	582.0613	-5.70	-9.79	Phosphoribosyl-AMP	$[M+Na]^+$	Histidine biosynthesis

Table 4.5: Potential Metabolites Detected using F20TPP as the Matrix.

9-aminoacridine

The following MALDI mass spectrum was acquired in negative ion mode using 9-aminoacridine as the matrix.

The most prominent peak in the mass spectrum occurs at m/z 193.07 which is the $[M-H]^-$ of 9-aminoacridine.

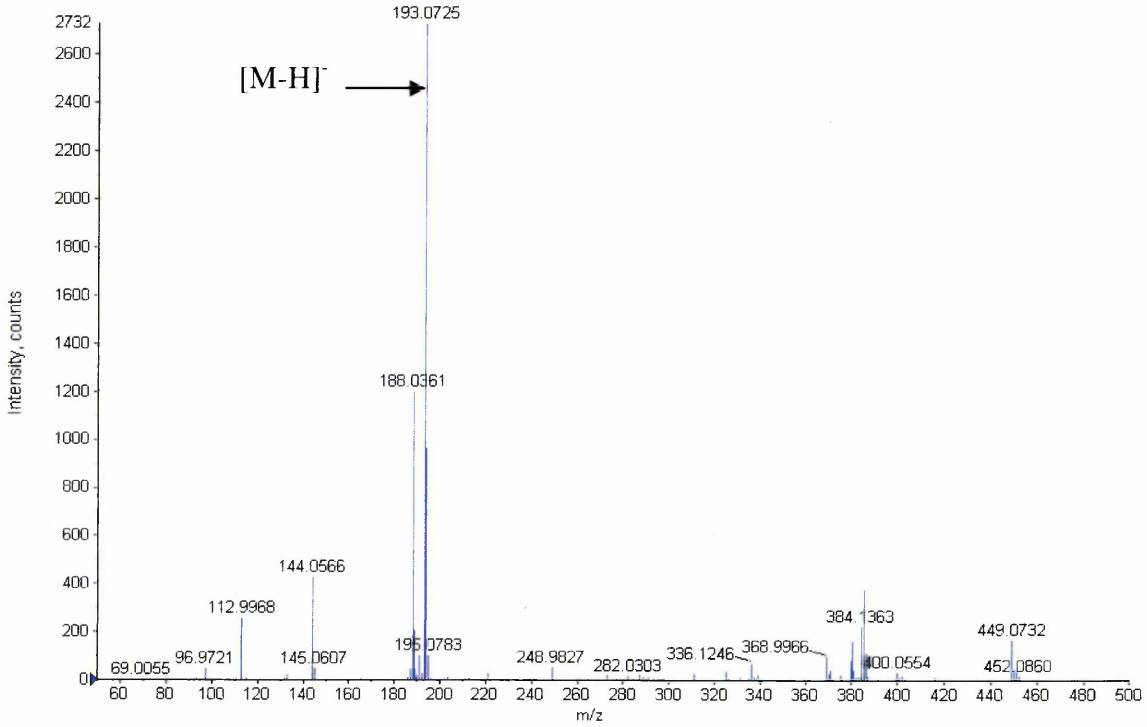

Figure 4.6: MALDI Mass Spectrum of Wheat Grain using 9-aminoacridine: The spectrum shows the metabolites obtained using 9-aminoacridine as a matrix in negative ion mode MALDI. The most prominent matrix peaks can be clearly seen in the spectrum at m/z 193.07. As with other organic matrices these intense matrix signals may have a suppression effect on the metabolites.

The results of the imaging experiments obtained using 9-aminoacridine as the matrix in negative ion mode are shown in figure 4.7. The image on the left is the optical image of the wheat grain section that has been coated with matrix. The MALDI MS images show the tentative distribution of $[M-H]^-$ of sucrose at m/z 341 and $[M-H]^-$ of glucose 6-phosphate at m/z 259, respectively.

Both of the images shown have been normalised to the corresponding matrix mass at m/z 193.07 to account for any potential discrepancies with the matrix coverage of the section.

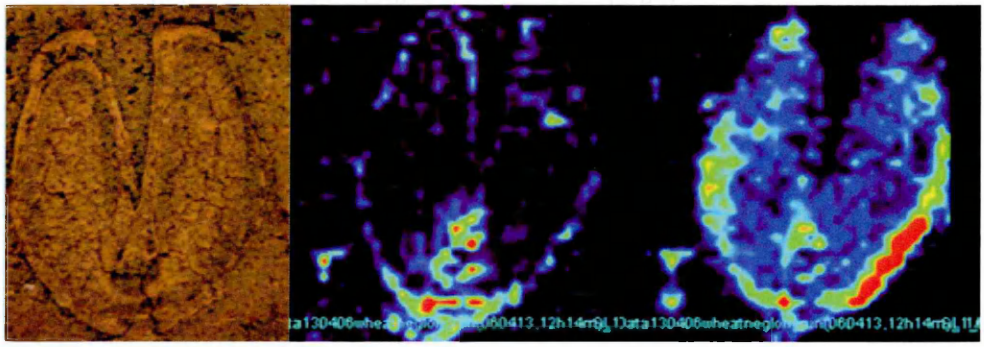

Figure 4.7: MALDI-MS Images of Wheat Grain using 9-aminoacridine: MALDI-MS images of a wheat grain section at 16 dpa obtained in negative ion mode using 9-aminoacridine as the matrix. Images were normalised to the corresponding matrix mass at m/z 193.07. The image on the left is the optical image of the wheat grain section that has been coated with matrix, followed by the MALDI MS images for $[M-H]^-$ of sucrose at m/z 341 and $[M-H]^-$ of glucose 6-phosphate at m/z 259, respectively. The colour intensity of the image represents the abundance of the ion being imaged with red representing the locations at which the ion is most abundant and black representing zero abundance.

Observed m/z	Theoretical m/z	Error mDa	Error ppm	Ion detected
193.0725	193.0766	-4.10	-21.24	$[M-H]^-$
385.1402	385.1453	-5.10	-13.24	$[C26H17N4]^-$

Table 4.6: Masses Obtained for the Matrix 9-aminoacridine.

Observed m/z	Theoretical m/z	Error mDa	Error ppm	Possible Metabolite Detected	Ion Detected	Possible metabolic pathways
145.0607	145.0613	-0.60	-4.14	Glutamine	$[M-H]^-$	Glutamine/Glutamate metabolism
179.0631	179.0556	7.50	41.89	Hexose Sugars	$[M-H]^-$	Sugar metabolism
259.0322	259.0219	10.30	39.77	Glucose 6-phosphate	$[M-H]^-$	Sugar metabolism
341.1297	341.1084	21.30	62.44	Sucrose	$[M-H]^-$	Sugar metabolism

Table 4.7: Potential Metabolites Detected using 9-aminoacridine as the Matrix.

Inorganic Matrices

Other matrices that have been investigated included particle suspension matrices and nanoparticles. These proved to be of limited use; this is probably due to these types of matrix not co-crystallising with the metabolites contained within the wheat grain section.

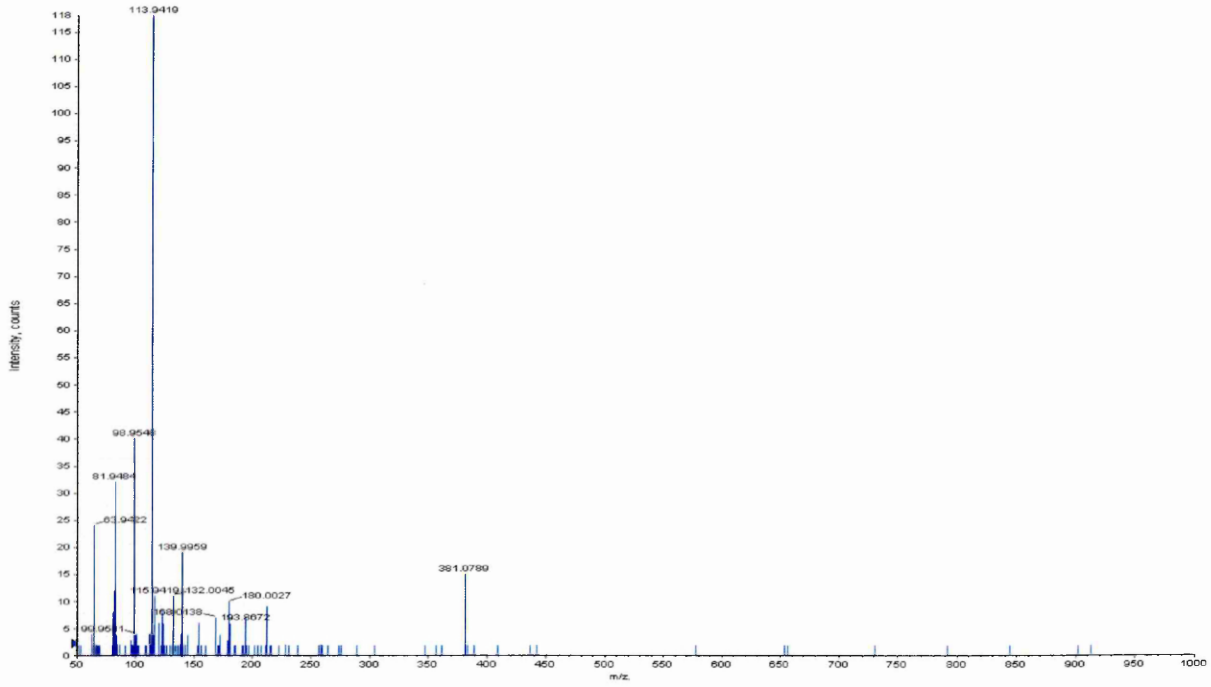

Figure 4.8: MALDI Mass Spectrum of Wheat Grain using TiO_2: The spectrum demonstrates that TiO_2 is a poor matrix for this particular application due to the poor signal intensity.

Gold and silver nanoparticles were also investigated. It was found that these matrices were not as good as conventional MALDI matrices in promoting efficient ionisation of many different types of compounds.

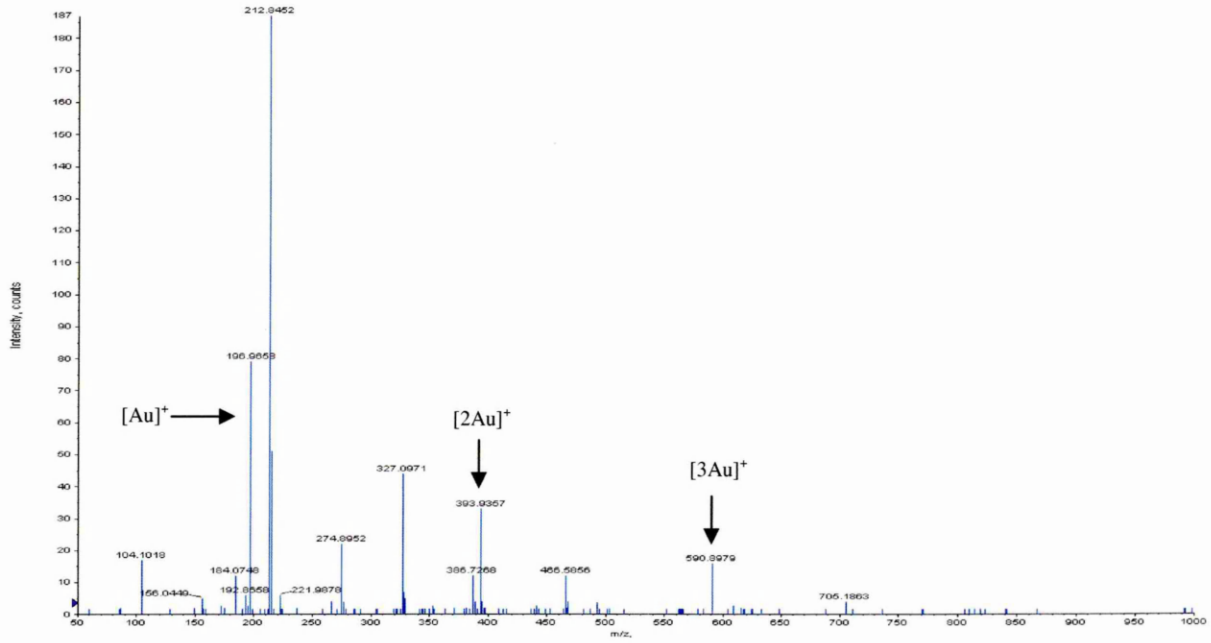

Figure 4.9: MALDI Mass Spectrum of Wheat Grain using Gold Nanoparticles:

As with TiO_2 the signal intensity is poor, therefore few metabolites were detected using this matrix.

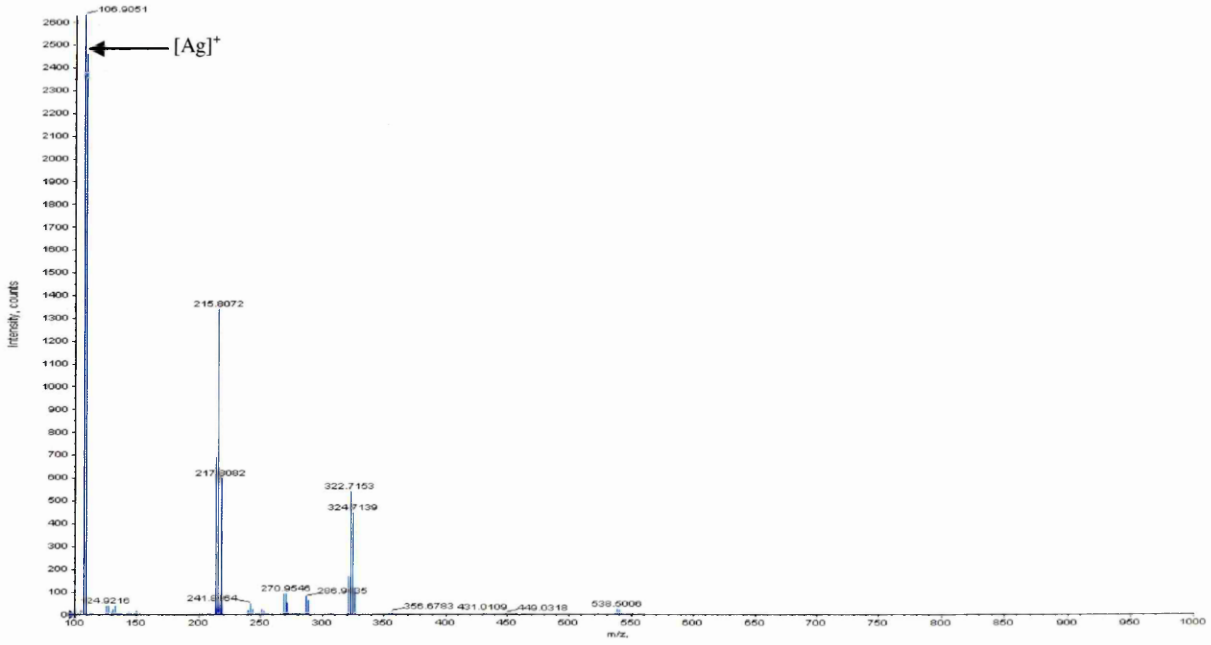

Figure 4.10: MALDI Mass Spectrum of Wheat Grain using Silver Nanoparticles.

4.9.4 Metabolite Profiling in Wheat Grains by MALDI-Ion Mobility Separation Mass Spectrometry

Ion mobility separation combined with MALDI MS was investigated in an attempt to reduce the matrix interference in the low mass region as previously observed in section 4.9.2.

Ions are separated according to their size:charge ratio in a drift tube containing buffer gas under the influence of an electric field. Ions are accelerated through the electric field and undergo collisions with the buffer gas [67]. Once separated on the basis of size the ions enter the time-of-flight where the m/z is measured.

Experiments were conducted using a Waters Corporation Synapt™ HDMS™ instrument [68] fitted with a 200Hz Nd: YAG laser; this is the next generation orthogonal time-of-flight instruments developed and manufactured by Waters replacing their QTOF Premier instrument.

Wheat grain sections were prepared as previously described in section 4.7.3.3.

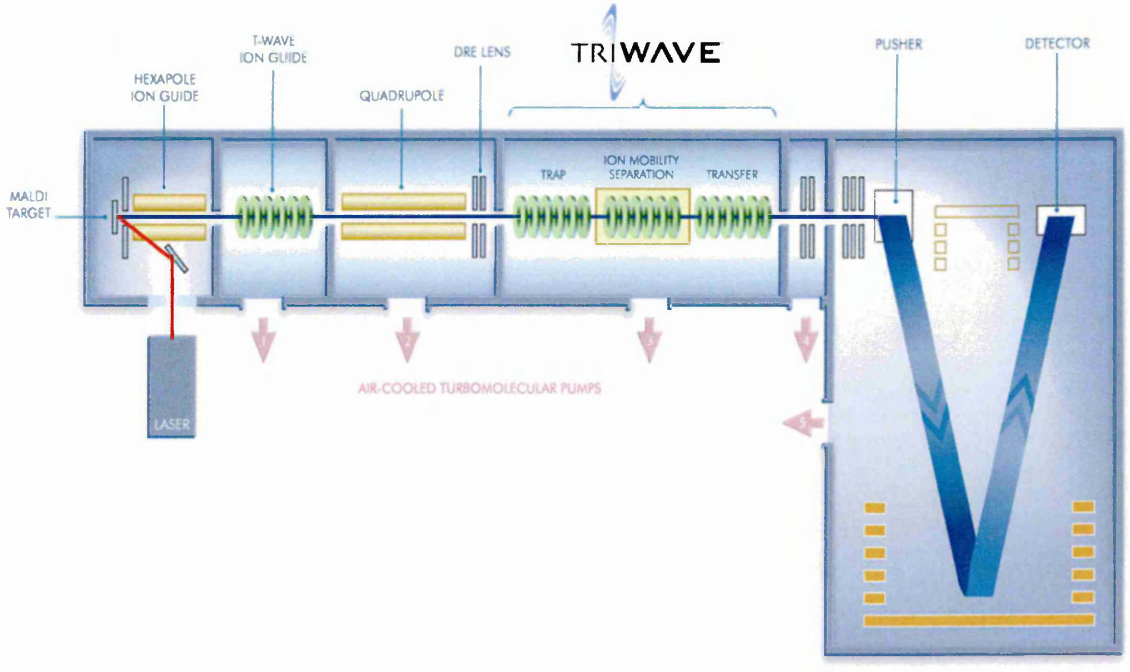

Figure 4.11: A Schematic of the Waters Corporation Synapt™ HDMS™ System.
Image supplied by Dr M. Snel, Waters, UK.

As many metabolites have masses that are exactly the same as those of other metabolites, ion mobility has been performed to try to separate metabolites according to their shape/structure. As wheat is known to contain sugars such as sucrose, ion mobility was used to investigate if sugars of the same molecular mass could be differentiated. The experiments conducted, using conventional MALDI with standards, showed that isomeric sugars could not be separated.

In another set of experiments to separate the isomeric sugars, sucrose and lactose were analysed by conventional MALDI MS analysis using α-CHCA as the matrix. Two structurally different compounds had been identified (refer to figure 4.12); however, these were later found to be sucrose and the second isotopic peak of the protonated matrix dimer occuring at m/z 381.09 (that was present in the trendline associated with the matrix).

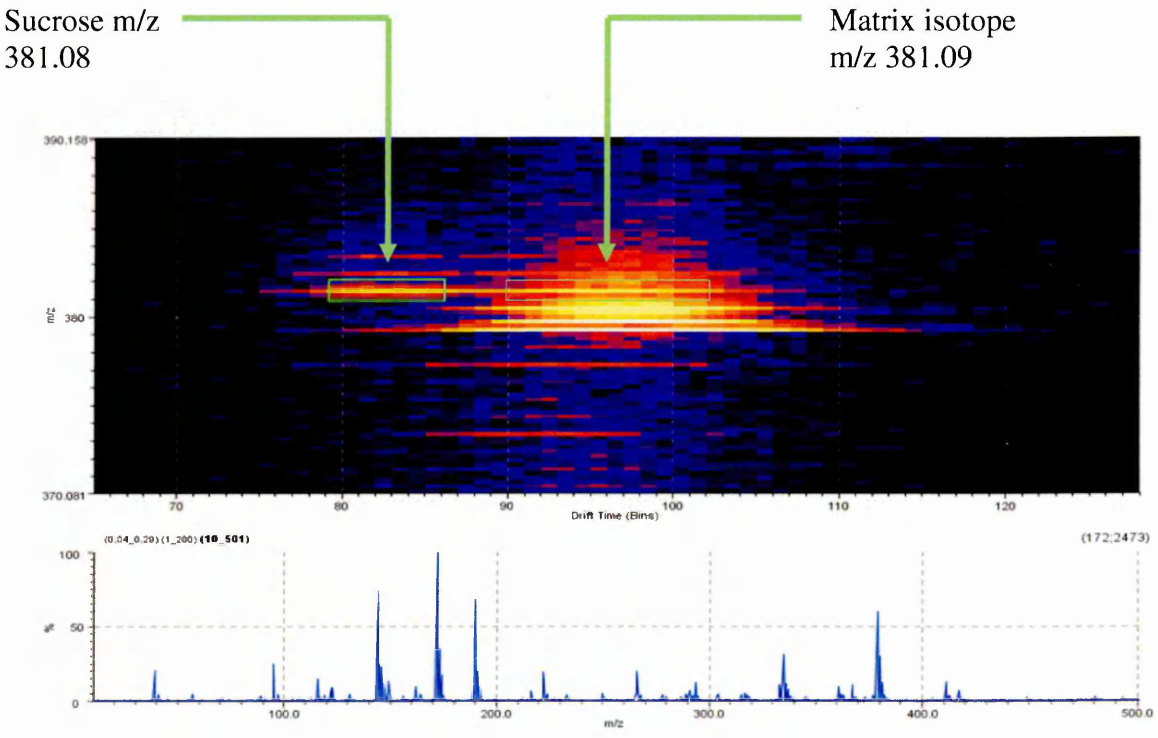

Figure 4.12: Driftscope Data Analysis of m/z 381: Isotopic separation of the potassiated sucrose ion at m/z 381.08 and the second isotope peak of the protonated matrix dimer at occuring at m/z 381.09.

The driftscope data is presented in figure 4.13, and it shows that there are three trendlines within the dataset obtained from wheat grain sections that had been prepared as previously described in section 4.7.3.3 using α-CHCA as the matrix.
The spectra in figure 4.14 show that the sugars dominate the spectra and although three different trendlines can be observed in figure 4.13, the instrument is unable to fully separate out the sugars. This is probably due to the mass resolution of the instrument [69].

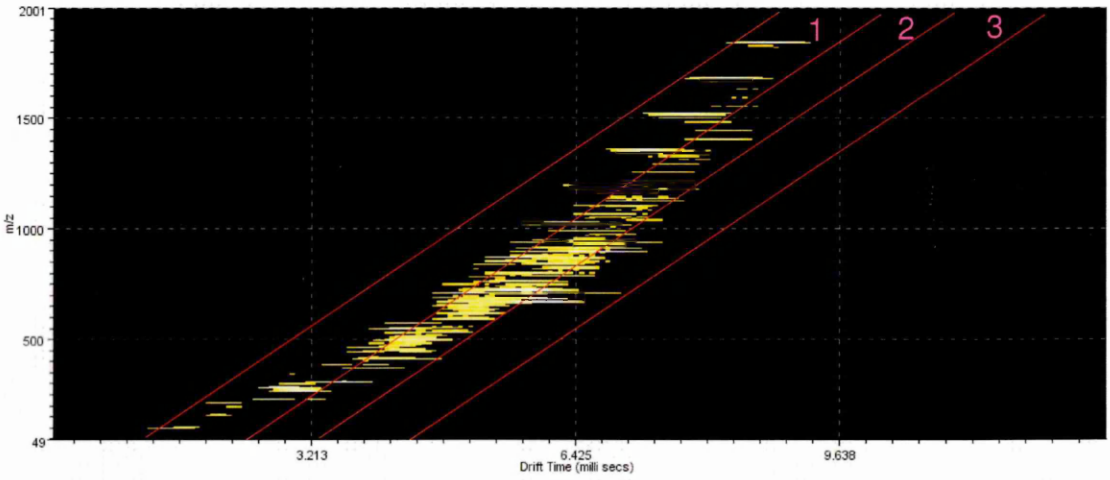

Figure 4.13: Driftscope Data Analysis of a Wheat Grain Section: There are three visible trendlines in the data; these are referred to as 1, 2 and 3.

Trendline 1 shows the sugar distribution.
Trendline 2 shows the matrix peaks.
Trendline 3 shows possible lipids.

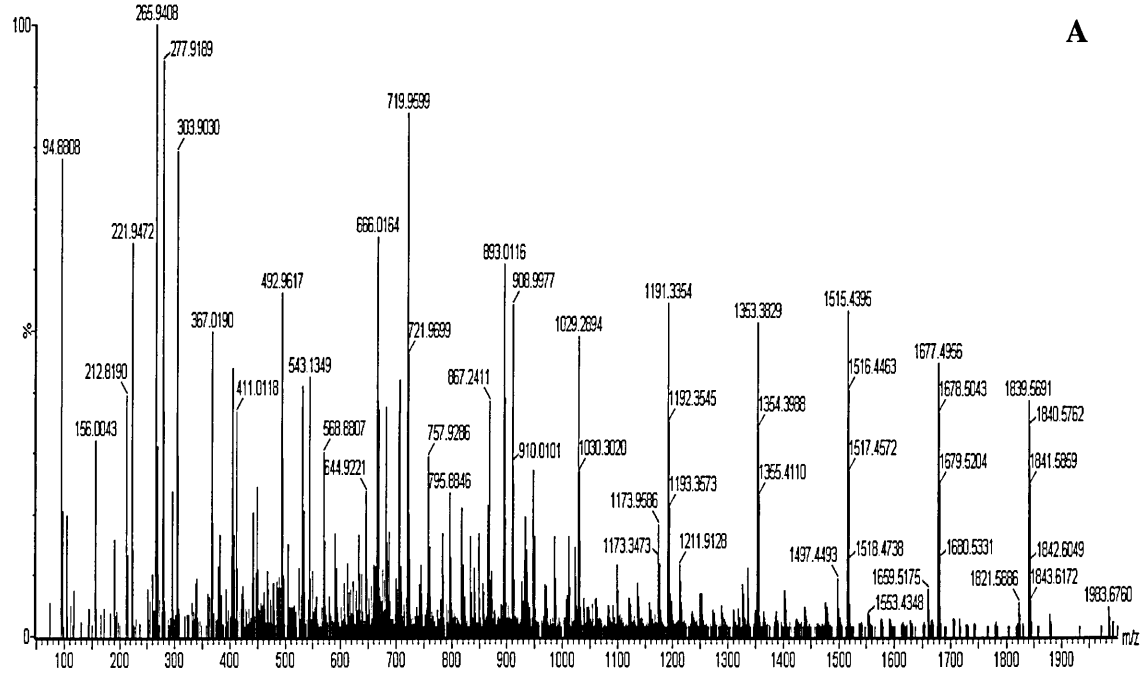
A
265.9408
277.9189
719.9599
303.9030
94.6808
666.0164
221.9472
893.0116
908.9977
492.9617
1191.3354
1353.3829
1515.4395
367.0190
1029.2694
721.9699
1677.4956
212.8190
543.1349
867.2411
1516.4463
411.0118
1192.3545
1678.5043
1839.5691
156.0043
568.8807
757.9286
1354.3988
1840.5762
910.0101
1030.3020
1517.4572
644.9221
795.8846
1355.4110
1679.5204
1841.5869
1173.9586
1193.3573
1173.3473
1211.9128
1497.4493
1518.4738
1680.5331
1842.6049
1659.5175
1821.5686
1843.6172
1553.4348
1983.6760
%
m/z
100
200
300
400
500
600
700
800
900
1000
1100
1200
1300
1400
1500
1600
1700
1800
1900
0

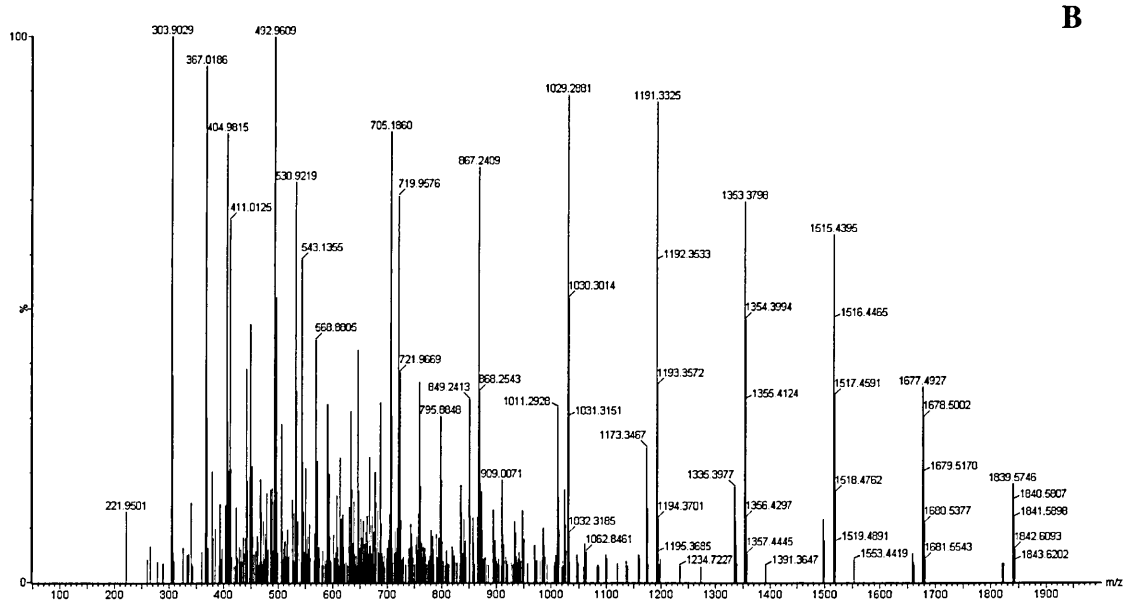
B
303.9029
492.9609
367.0186
1029.2881
1191.3325
404.9815
705.1960
867.2409
530.9219
719.9576
1353.3798
411.0125
1515.4395
543.1355
1192.3533
1030.3014
1354.3994
568.8805
1516.4465
721.9669
1193.3572
868.2543
1677.4927
849.2413
1517.4591
1011.2928
1031.3151
1355.4124
795.8848
1678.5002
1173.3467
1679.5170
1306.3977
1518.4762
1839.5746
221.9501
1194.3701
1840.5807
1356.4297
1680.5377
1032.3185
1841.5898
1062.8461
1519.4891
1357.4445
1195.3685
1842.6093
1681.5543
1553.4419
1234.7227
1391.3647
1843.6202
%
m/z
100
200
300
400
500
600
700
800
900
1000
1100
1200
1300
1400
1500
1600
1700
1800
1900
0

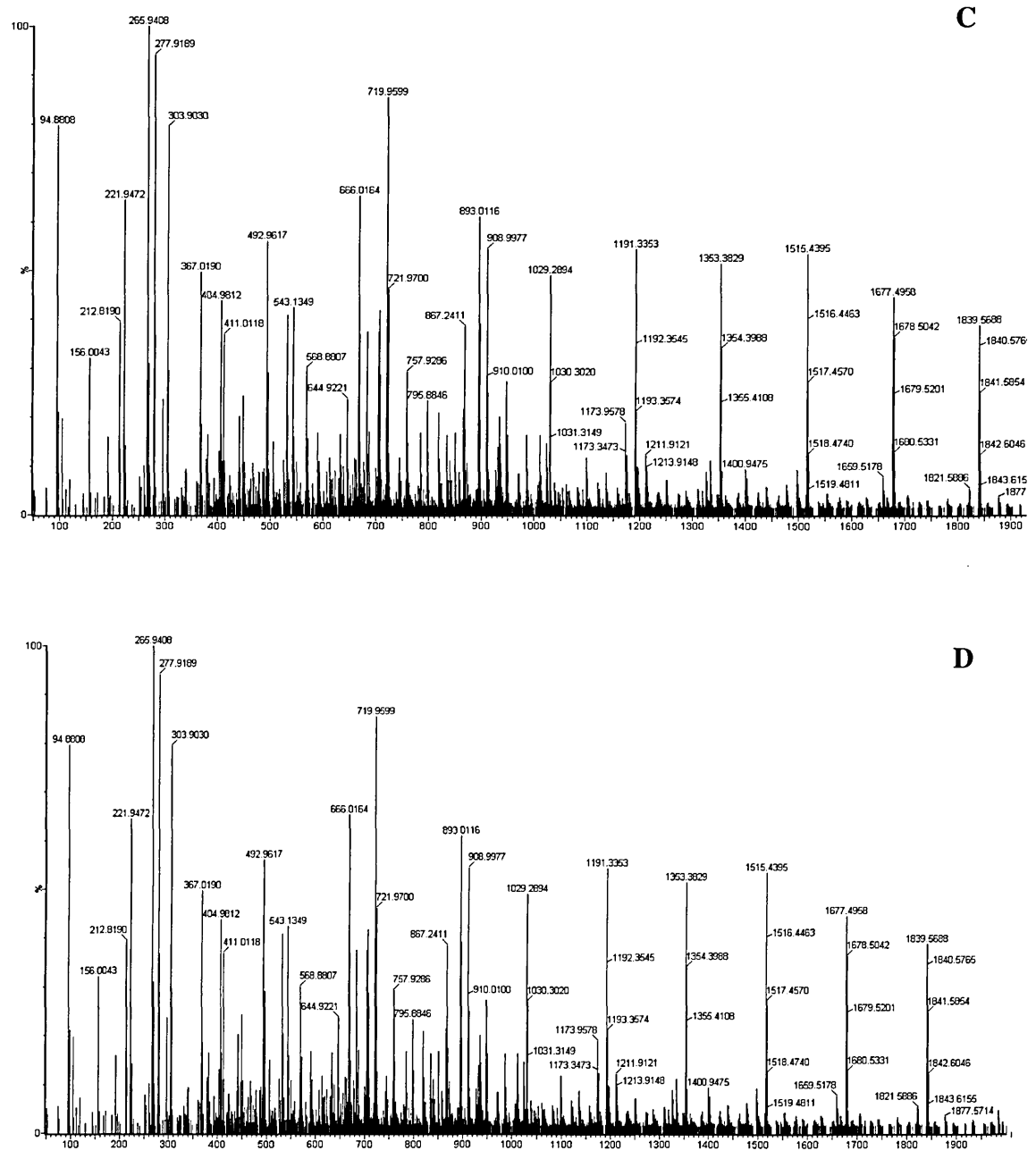

Figure 4.14: MALDI Mass Spectra of Driftscope Trendlines of Wheat Grain.
Spectrum A) represents the full dataset acquired on a wheat grain section, B) shows the trendline marked 1 (in figure 4.13) which is assigned to the presence of sugars, C) represents the data from trendline marked 2 (in figure 4.13), D) relates to the trendline marked 3 that could possibly be due to the presence of lipids.

Although isomeric separation was not achieved using ion mobility, class separation of structurally related compounds was achieved as can be seen by the three trendlines that can be clearly observed in figure 4.13 and this is useful in itself.

4.9.5 IR LDI MS

Analysis was also performed using IR LDI MS with an Er: YAG laser. This approach does not require a chemical matrix as the residual water in the sample acts as the matrix. The real elegance with this particular approach is that there are no interfering matrix peaks or matrix suppression effects and therefore all the peaks observed are sample related. There is also no risk of analyte translocation/diffusion that is sometimes observed during matrix application for UV MALDI MS. The IR laser ablates more of the sample and it was observed that it ablated through to the conductive tape on which the sample was mounted, causing contaminant peaks arising from the ionisation of the tape. Therefore, it was decided to use fresh, frozen tissue mounted onto glass slides and metabolite profiling experiments were carried out; each profile was acquired over 2 minute period. The data was recalibrated using the following sugar masses: Hex $[M+K]^+$ at m/z 219.027, Hex 2 $[M+K]^+$ at m/z 381.080, Hex 3 $[M+K]^+$ at m/z 543.133, Hex 4 $[M+K]^+$ at m/z 705.186 and Hex 5 $[M+K]^+$ at m/z 867.238. The results show that ions from the oligosaccharides dominate the spectra, the most apparent being the potassiated adducts. The mass range for the metabolite profiling experiments was limited by the quadrupole setting with the lower cut off set to m/z 150. The spectra (figures 4.15 and 4.16) show that there are clear differences between the embryo and endosperm regions of the wheat grain. The endosperm appears to contain more of the higher mass storage sugars, whereas the embryo seems to contain more of the smaller sugars, such as sucrose, which are needed for growth. Fresh frozen tissue worked better for this analysis as although the same patterns of metabolites were observed; tissue that had been freeze dried gave poor intensity spectra. Using the IR laser a very interesting effect was observed in that the signal intensity dramatically increased after the laser had fired for approximately 1 minute.

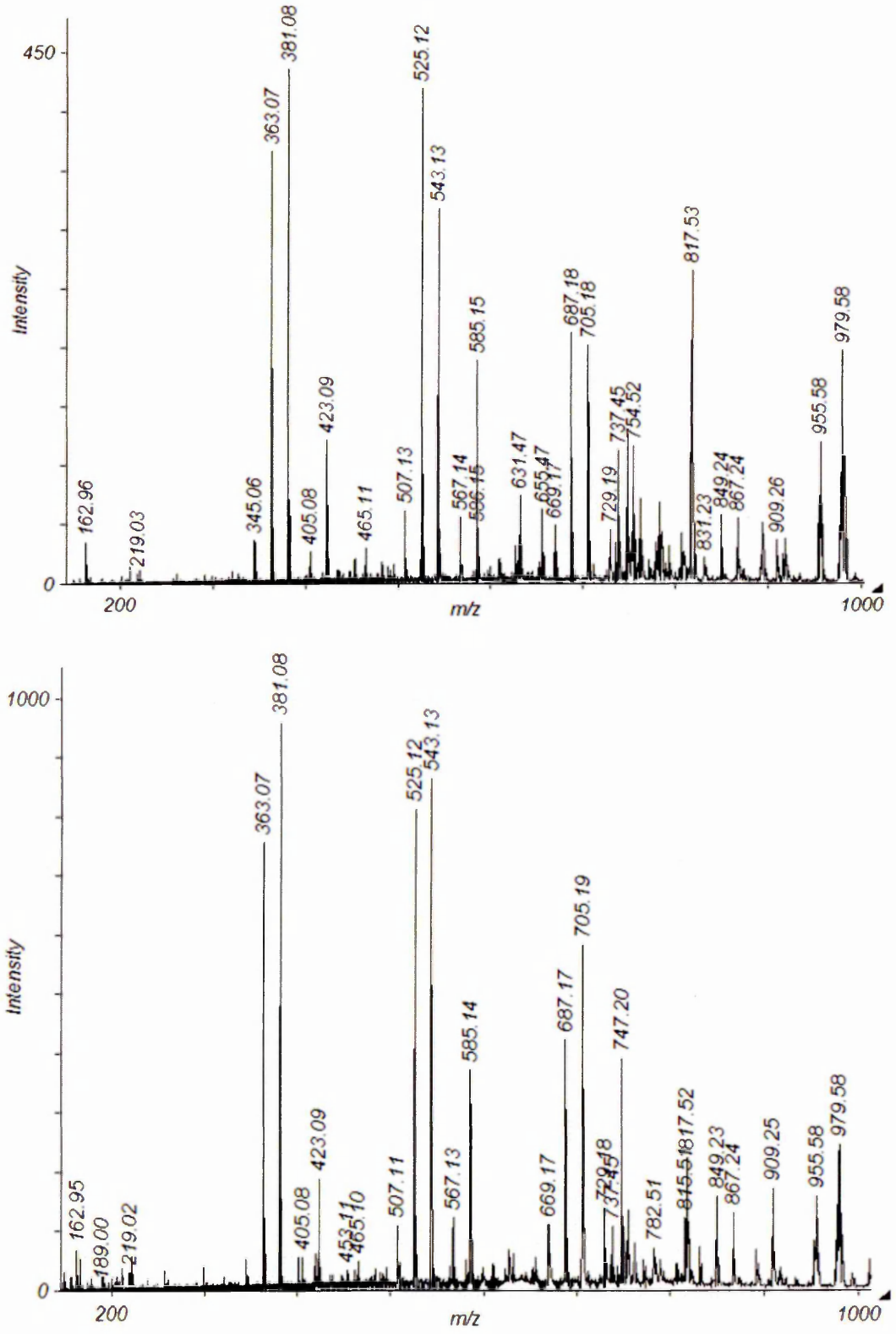

Figure 4.15: IR LDI Mass Spectra of Wheat Grain Embryos: Embryo spectra taken under the same mass spectrometry conditions from 2 different wheat grains at the same developmental stage (12 days post-anthesis).

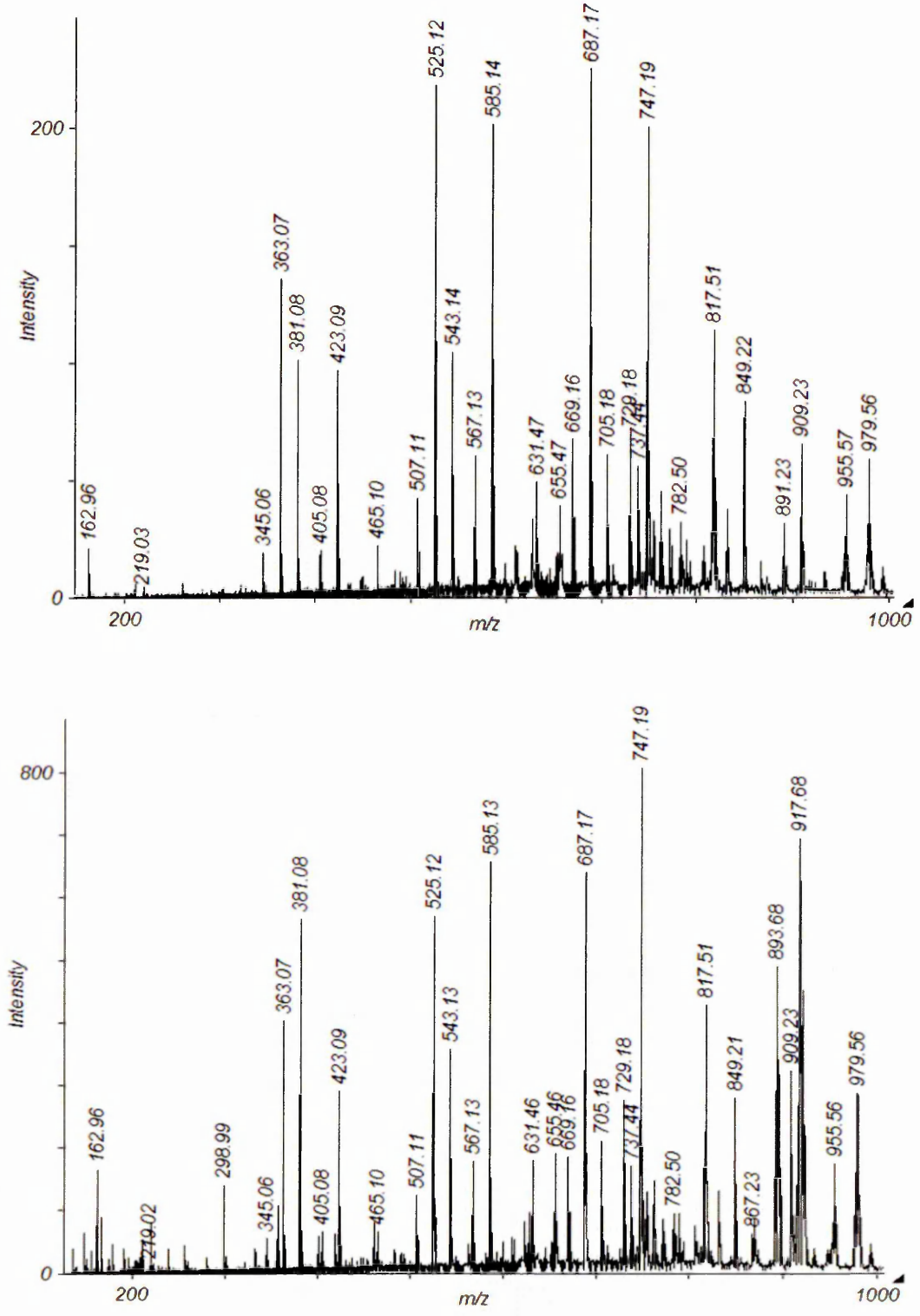

Figure 4.16: IR LDI Mass Spectra of Wheat Grain Endosperms: Endosperm Spectra – Taken under the same mass spectrometry conditions from 2 different wheat grains at the same developmental stage (12 days post anthesis).

Observed m/z	Theoretical m/z	Error mDa	Error (ppm)	Potential Metabolite	Ion detected	Possible Metabolite Pathway
185.0320	185.0329	-0.90	-4.86	Glutamine	$[M+K]^+$	Arginine biosynthesis
219.0260	219.0271	-1.10	-5.02	Hexose	$[M+K]^+$	Sugar metabolism
261.0330	261.0311	1.90	7.28	Cystathionine	$[M+K]^+$	Methionine biosynthesis
291.0470	291.0481	-1.10	-3.78	Sedoheptulose 7-phosphate	$[M+K]^+$	Pentose phosphate pathway
298.9940	298.9935	0.50	1.67	Mannose 6-phosphate	$[M+K]^+$	Ascorbate biosynthesis
363.0710	363.0693	1.70	4.68	Hex 2 ($-H_20$)	$[M+K]^+$	Sugar metabolism
381.0810	381.0799	1.10	2.89	Hex 2	$[M+K]^+$	Sugar metabolism
423.0900	423.0903	-0.30	-0.71	Sucrose 6-phosphate	$[M+K]^+$	Sucrose breakdown
525.1240	525.1211	2.90	5.52	Hex 3 ($-H_2O$)	$[M+K]^+$	Sugar metabolism
543.1300	543.1317	-1.70	-3.13	Hex 3	$[M+K]^+$	Sugar metabolism
567.1370	567.1317	5.30	9.35	Ac-Hex 3 ($-H_2O$)	$[M+K]^+$	Sugar metabolism
585.1470	585.1423	4.70	8.03	Ac-Hex 3	$[M+K]^+$	Sugar metabolism
671.1800	671.2011	-21.10	-31.44	Hex4 ($-H_2O$)	$[M+Na]^+$	Sugar metabolism
687.1760	687.1750	1.00	1.46	Hex 4 ($-H_2O$)	$[M+K]^+$	Sugar metabolism
705.1840	705.1856	-1.60	-2.27	Hex 4	$[M+K]^+$	Sugar metabolism
747.2020	747.1962	5.80	7.76	Ac-Hex 4	$[M+K]^+$	Sugar metabolism
831.2270	831.2183	8.70	10.47	Hex 5 $-(2H_2O)$	$[M+K]^+$	Sugar metabolism
849.2370	849.2289	8.10	9.54	Hex 5 ($-H_2O$)	$[M+K]^+$	Sugar metabolism
867.2400	867.2395	0.50	0.58	Hex 5	$[M+K]^+$	Sugar metabolism
909.2620	909.2501	11.90	13.09	Ac-Hex 5 ($-H_2O$)	$[M+K]^+$	Sugar metabolism

Table 4.8: Potential Metabolites Detected using IR LDI MS.

It is clear from the IR LDI data that a small number of metabolites are observed in apparently high concentrations, for example hexose sugars. The results confirm what one would assume; *viz.* that the endosperm region contains higher mass hexose sugars than the embryo region, which contains mainly sucrose. As the endosperm is the major sugar storage area of the wheat grain it would be expected to contain higher mass sugars. This distribution in sucrose also corresponds with the data obtained in negative ion mode where the sucrose distribution was predominantly in the embryo region of the wheat grain section. The oligosaccharide peaks are more apparent in the IR LDI data. This is probably because the oligosaccharides are ionised better with the infrared laser, there are no interfering matrix peaks that could suppress the sugar peaks as in UV MALDI MS, and the tissue was not freeze dried.

However, the intense oligosaccharide peaks may be suppressing other metabolites contained within the wheat grain section. A common observed modification that is apparent from the IR data is the acetylation of the sugars. The presence of sugars in a range of plant materials has also been previously reported in fruits [70] and in wheat stems [71, 72].

4.10 Conclusion

Mass spectrometry is now widely used in metabolomics studies and it has been demonstrated in this chapter that the use of UV MALDI MS alone or with imaging capabilities (MALDI MSI) can be utilized in such an area. As with any technique there are always disadvantages in this case interfering matrix peaks. When analysing plant tissue this can be very important as often some metabolites are in extremely small concentrations and any suppression effects could hinder their detection. This is apparent in mass spectrometry-based metabolomics studies when the chromatographic step seen with LC-MS and GC-MS is omitted; these techniques are still probably better for the detection of less abundant secondary metabolites. However, there are also many advantages with MALDI MSI; one of the most important is the ability to spatially locate where metabolites occur in plant sections and the ability to detect many different masses in parallel whether they are known or unknown.

Metabolomic investigations using IR LDI MS proved to be very useful and informative as all the information generated was sample related and lacked the matrix peaks and suppression effects often seen with UV MALDI MS. Using IR LDI MS the oligosaccharide peaks and the ratios between the peaks are much more visible.

There are so many variables that have been discussed within this chapter that can affect the metabolic profile/status of plant material, and a compromise between preserving the metabolic status while preparing the sample in a suitable way for the analysis to be performed must be consistently achieved. Freeze drying of the tissue was done to preserve the metabolic status of the tissue. However, this could have affected the results obtained by potentially reducing the metabolite extraction and co-

crystallisation efficiency between the matrix and metabolite molecules. To overcome this limitation the tissue could have been rehydrated or to incorporate more sample wetting in the matrix application procedure; however, this could result in the delocalisation of metabolites and therefore not produce a true biological representation. As a typical image run with a resolution of 100µm x 100µm took approximately 6 hours for image acquisition there was a need to incorporate the freeze drying step as otherwise metabolic processes could still feasibly occur in the sample while in the mass spectrometer. However, for the experiments conducted with the IR laser the freeze drying process somewhat hindered the analysis; this is not surprising as it is thought that residual water contained within the samples acts as a matrix. The more intense sugar peaks could be attributed to the use of fresh tissue as opposed to the freeze dried tissue used for UV MALDI MS experiments; the sugar peaks dominate the spectra which could suppress other less abundant metabolites within the tissue.

Data analysis can be both a complex and time-consuming process, especially for the UV MALDI data as this includes the matrix peaks.

Metabolite databases are more established for GC and LC-MS analyses. However, there are databases where masses along with their corresponding intensities can be searched. The major problem with this type of non-targeted approach is that the metabolite database may match metabolites up with the observed masses but these compounds may not be native to the type of tissue under investigation. For example, drug metabolites may be of the same mass as a plant metabolite. Therefore, an in-depth knowledge of the plant tissue investigated needs to be established before trying to match up the observed masses with potential metabolites. Metacrop, a database that contains information on crop plants, proved very useful for this purpose as it contains information regarding the metabolites in specific examples of plant tissue [41]. Another issue is that there are so many metabolites that are biologically feasible that can be supported by metabolic pathways; however, the masses that are detected often differ to an unacceptable level for mass spectrometric measurement. This is highlighted in the publication of Li *et al.* where some of the reported mass errors are up to 44mDa [66]. This factor could potentially be reduced by decreasing the mass range in an attempt to increase the sensitivity; however, this defeats the point of the

non-targeted approach and it becomes more of a selective process depending on the metabolites that are of interest.

The calibration of the instrument prior to sample analysis and the subsequent recalibration of data are very important in ensuring that data obtained is as accurate as possible. Hundreds of mass signals are obtained from a MALDI imaging experiment but assignment of masses is still limited by the lack of complete databases and standards, particularly of secondary metabolites.

The mass list obtained using α-CHCA and IR LDI MS shows the sugar distributions; however, the mass list obtained using 9-aminoacridine and F20TPP shows fewer metabolites. This could be due to the data recalibration procedure - the use of 2-3 calibration points seems to be insufficient for the mass accuracy required for metabolomic studies. This method of recalibration could be improved upon by using a spiked solution containing commercially available standards combined with matrix for both the instrument calibration prior to analysis and for the recalibration. This approach could also provide information relating to ion suppression effects as detailed by Vaidyanathan *et al.*[73].

The development of appropriate software for high throughput metabolomics using MALDI is crucial to future analyses. Software is currently available from Waters (MS^E) for LC-MS analyses that enable the user to acquire MS and MS/MS data simultaneously [74]. A similar approach would be useful for MALDI analyses as this would immediately eliminate the matrix peaks observed from the endogenous compounds contained within the sample of interest and help in the identification of unknown masses. There is a lack of complete databases for metabolomic studies. The development of metabolite searching software would be beneficial as many databases can contain metabolites that are found in many organisms and they don't always take into account the adducts that are commonly formed in MALDI analyses. Therefore, in some instances the data has to be converted into the corresponding neutral masses.

4.11 References

[1] Catchpole G. S., Beckmann M., Enot D. P., Mondhe M., Zywicki B., Taylor J., Hardy N., Smith A., King R. D., Kell D. B., Fiehn O., Draper J. Hierarchial metabolomics demonstrates substantial compositional similarity between genetically modified and conventional potato crops. Proceedings of the National Academy of Sciences of the USA, 2005, 102, 14458-62.

[2] Griffiths J. R., Stubbs M. Opportunities for studying cancer by metabolomics: preliminary observations on tumours deficient in hypoxia-inducible factor 1. Advances in Enzyme Regulation, 2003, 43, 67-76.

[3] Watkins S. M., Reifsnyder P. R., Pan H. J., German J. B., Leiter E. H. Lipid metabolome-wide effects of the PPAR gamma agonist rosiglitazone. Journal of Lipid Research, 2002, 43, 1809-1817.

[4] Watkins S. M., German J. B. Metabolomics and biochemical profiling in drug discovery and development. Current Opinion in Molecular Therapeutics, 2002, 4, 224-228.

[5] Nicholson J. K., Lindon J. C., Holmes E. "Metabonomics": understanding the metabolic responses of living systems to pathophysiological stimuli via multivariate statistical analysis of biological NMR spectroscopic data. Xenobiotica, 1999, 29, 1181-1190.

[6] Guy C., Kopka J., Moritz T. Plant metabolomics coming of age. Physiologia Plantarum, 2008, 132, 113-116.

[7] Goossens A., Hakkinen S. T., Laakso I., Seppanen -Laakso T., Biondi S., De Sutter V., Lammertyn F., Nuutila A. M., Soderlund H., Zabeau M., Inze D., Oksman-Caldentey K. M. A functional genomics approach toward the understanding of secondary metabolism in plant cells. Proceedings of the National Academy of Science USA, 2003, 100, 8595-8600.

[8] Shulaev V., Cortes D., Miller G., Mittler R. Metabolomics for plant stress response. Physiologia Plantarum, 2008, 132, 199-208.

[9] Moco S., Bino R. J., Vorst O., Verhoven H. A., de Groot J., van Beek T. A., Vervoort J., De Vos R. C. H. A liquid chromatography-mass spectrometry-based metabolome database for tomato. Plant Physiology, 2006, 141, 1205-1218.

[10] Tikunov Y., Lommen A., De Vos R. C. H., Verhoeven H. A., Bino R. J., Hall R. D., Bovy A. G. A. A novel approach for non-targeted data analysis for metabolomics. Large-scale profiling of tomato fruit volatiles. Plant Physiology, 2005, 139, 1125-1137.

[11] Sato S., Soga T., Nishioka T., Tomita M. Simultaneous determination of the main metabolites in rice leaves using capillary electrophoresis mass spectrometry and capillary electrophoresis diode array detection. Plant Journal, 2004, 40, 151-163.

[12] Roessner U., Willmitzer L., Fernie A. R. High-resolution metabolic phenotyping of genetically and environmentally diverse potato tuber systems. Identification of phenocopies. Plant Physiology, 2001, 127, 749-764.

[13] Hunter P. Reading the metabolic fine print. European Molecular Biology Organization Reports, 2009, 10, 20-23.

[14] Want E. J., Nordstrom A., Morita H., Siuzdak G. From Exogenous to Endogenous: The Inevitable Imprint of Mass Spectrometry in Metabolomics, Journal of Proteome Research 2007, 6, 459-468.

[15] Nielsen J., Oliver S. The next wave in metabolome analysis. Trends in Biotechnology, 2005, 23, 544-546.

[16] Seger C., Sturm S. Analytical Aspects of Plant Metabolite Profiling Platforms: Current Standings and Future Aims. Journal of Proteome Research 2007, 6, 480-497.

[17] Villas-Boas S. G., Roessner U., Hansen M. A. E, Smedsgaard J., Nielsen J. Metabolome Analysis: An Introduction. Wiley Interscience, 2007.

[18] Urbanczyk-Wochniak E., Baxter C., Kolbe A., Kopka A, Kopka J, Sweetlove L. J., Fernie A. R. Profiling of diurnal patterns of metabolite and transcript abundance in potato (Solanum tuberosum) leaves. Planta, 2005, 221, 891-903.

[19] Rischer H., Oksman-Caldentey K-M. Unintended effects in genetically modified crops: revealed by metabolomics. Trends in Biotechnology, 2008, 24, 102-104.

[20] Stokes T. Orcastrating plant primary and secondary metabolism. Trends in Plant Science, 2000, 9, 366-366.

[21] Theobald U., Mailinger W., Reuss M., Rizzi M. In vivo analysis of glucose-induced fast changes in yeast adenine nucleotide pool applying a rapid sampling technique. Analytical Biochemistry, 1993, 214, 31-37.

[22] Croxdale J., Brown S. S., McCauley M. Structural preservation and retention of enzymatic activity in quenched, lyophilized plant tissue. Botanical Gazette, 1982, 143, 278-285.

[23] Fiehn O. Metabolomics-the link between genotypes and phenotypes. Plant Molecular Biology, 2002, 48, 155-171.

[24] http://metacyc.org/glossary.shtml#Primary_Metabolism
Last accessed 10th May 2009.

[25] Bundy J. G., Davey M. P., Viant M. R. Environmental metabolomics: a critical review and future perspectives. Metabolomics, 2009, 5, 3-21.

[26] Reo N. V. NMR-Based Metabolomics. Drug and Chemical Toxicology, 2002, 25, 375-382.

[27] Theodoridis G., Gika H. G, Wilson I. D. LC-MS-based methodology for global metabolite profiling in metabonomics/metabolomics. Trends in Analytical Chemistry, 2008, 27, 251-260.

[28] Kanani H., Chrysanthopoulos P. K., Klapa M. I. Standardizing GC-MS Metabolomics. Journal of Chromatography B, 2008, 871, 191-201.

[29] Jopka J., Fernie A., Weckwerth W., Gibon Y., Stitt M. Metabolite profiling in plant biology: platforms and destinations. Genome Biology, 2004, 5, 109-109.9.

[30] Dettmer K., Aronov P. A., Hammock B. D. Mass Spectrometry-Based Metabolomics. Mass Spectrometry Reviews, 2007, 26, 51-78.

[31] Want E. J., Cravatt B. F., Siuzdak G. The Expanding Role of Mass Spectrometry in Metabolite Profiling and Characterization. ChemBioChem 2005, 6, 1941-1951.

[32] Hollywood K., Brison D. R., Goodacre R. Metabolomics: Current technologies and future trends. Proteomics 2006, 6, 4716-4723.

[33] Mullen A. K., Clench M. R., Crosland S., Sharples K. R. Determination of agrochemical compounds in soya plants by imaging matrix-assisted laser desorption/ionisation mass spectrometry. Rapid Communications in Mass Spectrometry, 2005, 19, 2507-2516.

[34] Robinson S., Warburton K., Seymour M., Clench M., Thomas-Oates J. Localization of water-soluble carbohydrates in wheat stems using imaging matrix assisted laser desorption ionization mass spectrometry. New Phytologist, 2006, 173, 438-444.

[35] Burrell M. M., Earnshaw C. J., Clench M. R. Imaging Matrix Assisted Laser Desorption Ionisation Mass Spectrometry: a technique to map plant metabolites at high spatial resolution. Journal of Experimental Botany 2007, 58, 757-763.

[36] http://metlin.scripps.edu/
Last accessed 10th May 2009.

[37] http://mips.gsf.de/proj/metabolomics/
Last accessed 10th May 2009.

[38] http://www.genome.jp/Kegg/
Last accessed 10th May 2009.

[39] http://metacyc.org/
Last accessed 10th May 2009.

[40] http://pgrc-35.ipk-gatersleben.de/
Last accessed 10th May 2009.

[41] Grafahrend-Belau E., Weise S., Koschutzki D., Scholz U., Junker B. H., Schreiber F. Metacrop: a detailed database of crop plant metabolism. Nucleic Acids Research, 2008, 36, 954-958.

[42] Sauter H., Lauer M., Fritsch H. Metabolic profiling of plants: a new diagnostic technique. In: Baker D.R., Fenyes J.G., Moberg W.K., American Chemical Society Symposium Series No.443, American Chemical Society, Washington DC, 1991, 288-299.

[43] Moco S., Bino R. J., De Vos R. C. H., Vervoort J. Metabolomics technologies and metabolite identification. Trends in Analytical Chemistry, 2007, 26, 855-866.

[44] Weckwerth W. Metabolomics in Systems Biology. Annual Review of Plant Biology, 2003, 54, 669-689.

[45] Stitt M., Muller C., Matt P., Gibon Y., Carillo P., Morcuende R., Scheible W.R., Krapp A. Steps toward an integrated view of nitrogen metabolism. Journal of Experimental Botany, 2002, 53, 959-970.

[46] Rochfort S. Metabolomics Reviewed: A New "Omics" Platform Technology for Systems Biology and Implications for Natural Products Research. Journal of Natural Products, 2005, 68, 1813-1820.

[47] Dettmer K., Aronov P. A., Hammaock B. D. Mass Spectrometry-Based Metabolomics. Mass Spectrometry Reviews, 2007, 26, 51-78.

[48] Roessner U., Luedemann A., Brust D., Fiehn O., Linke T., Willmitzer L., Fernie A. R. Metabolic Profiling Allows Comprehensive Phenotyping of Genetically or Environmentally Modified Plant Systems. The Plant Cell, 2001, 13, 11-29.

[49] Zorb C., Langenkamper G, Betsche T., Niehaus K., Barsch A. Metabolite Profiling of Wheat Grains (Triticum aestivum L.) from Organic and Conventional Agriculture. Journal of Agricultural and Food Chemistry, 2006, 54, 8301-8306.

[50] Tikunov Y., Lommen A., Ric de Vos C. H., Verhoeven H. A., Bino R. J., Hall R. D., Bovy A. G. A novel approach for non-targeted data analysis for metabolomics. Large-scale profiling of tomato fruit volatiles. American Society of Plant Biologists, 2005, 139, 1125-1137.

[51] Wolfender J. L., Ndjoko K., Hostettmann K. Liquid chromatography with ultraviolet absorbance-mass spectrometric detection and with nuclear magnetic resonance spectroscopy: A powerful combination for the on-line structural investigation of plant metabolites. Journal of Chromatography A, 2003, 1000, 437-455.

[52] Cohen L. H., Gusev A. I. Small molecule analysis by MALDI mass spectrometry. Analytical and Bioanalytical Chemistry, 2002, 373, 571-586.

[53] Bhalla P. L. Genetic engineering of wheat - current challenges and opprotunities. Trends in Biotechnology, 2006, 24, 305-311.

[54] Yang Z. P., Gilbert J., Somers D. J., Fedak G., Procunier J. D., McKenzie I. H. Marker assisted selection of Fusarium head blight resistance genes in two haploid populations of wheat. Molecular Breeding, 2003, 12, 309-317.

[55] Hall R. D., Brouwer I. D., Fitzgerald M. A. Plant metabolomics and its potential for human nutrition. Physiologia Plantarum, 2008, 132, 162-175.

[56] www.horizonmilling.com/wheat/images/WheatIllo.jpg
Last accessed 10th May 2009.

[57] Ayorinde F. O., Hambright P., Porter T. N., Keith Q. L. Use of meso-Tetrakis (pentafluorophenyl) porphyrin as a Matrix for Low Molecular Weight Alkylphenol Ethoxylates in Laser Desorption/ Ionisation Time-of-Flight Mass Spectrometry. Rapid Communications in Mass Spectrometry, 1999, 13, 2474-2479.

[58] Kinumi T., Saisu T., Takayama M., Niwa. Matrix-assisted laser desorption/ionization time-of-flight mass spectrometry using an inorganic particle matrix for small molecule analysis. Journal of Mass Spectrometry, 2000, 35, 417-422.

[59] Zhang H., Cha S., Yeung E. S. Colloidal Graphite-Assisted Laser Desorption/Ionization MS and MS^n of Small Molecules. 2. Direct Profiling and MS Imaging of Small Metabolites from Fruits. Analytical Chemistry, 2007, 79, 6575-6584.

[60] Schwartz S.A., Reyzer M. L., Caprioli R. M. Direct tissue analysis using matrix-assisted laser desorption/ionisation mass spectrometry: practical aspects of sample preparation. Journal of the American Society for Mass Spectrometry, 2003, 38, 699-708.

[61] Brust M., Walker M., Bethell D., Schiffrin D. J., Whyman R. Synthesis of thiol-derivitized gold nanoparticles in a 2-phase liquid-liquid system. Journal of the Chemical Society. Chemical Communications, 1994, 7, 801-802.

[62] Munro C. H., Smith W. E., Garner M., Clarkson J., White P. C. Characterization of the surface of a citrate-reduced colloid optimized for use as a substrate for surface enhanced resonance raman scattering. Langmuir, 1995, 11, 3712-3720.

[63] Weckwerth W. Metabolomics in systems biology. Annual Review of Plant Biology, 2003, 669-689.

[64] Prichard E., Mackay G. M, Points J. Trace Analysis. Royal Society of Chemistry Publishing, 1996.

[65] Palavalli L. H., Brendza K. M., Haakenson W., Cahoon R. E., McLaird M., Hicks L. M., McCarter J. P. Williams D. J., Hresko M. C., Jez J. M. Defining the role of Phosphomethylethanolamine N-Methyltransferase for Caenorhabditis elagans in Phosphocholine Biosynthesis by Biochemical and Kinetic Analysis. Biochemistry, 2006, 45, 6056-6065.

[66] Li Y., Shrestha B., Vertes A. Atmospheric Pressure Infrared MALDI Imaging Mass Spectrometry for Plant Metabolomics. Analytical Chemistry, 2008, 80, 407-420.

[67] Kanu A. B., Dwivedi P., Tam M., Matz L., Hill H. H. Jr. Ion mobility-mass spectrometry. Journal of Mass Spectrometry, 2008, 43, 1-22.

[68] http://www.waters.com/waters/nav.htm?locale=133&cid=514497. Last accessed 10th May 2009.

[69] Henry Arnoud C. Ion Mobility-Mass Spec Combo. Chemical and Engineering News, 2008, 37, 11-18.

[70] Dreisewerd K., Draude F., Kruppe S., Rohlfing A., Berkenkamp S., Pohlentz G. Molecular Analysis of Native Tissue and Whole Oils by Infrared Laser Mass Spectrometry. Analytical Chemistry, 2007, 79, 4514-4520.

[71] Robinson S., Warburton K., Seymour M., Clench M., Thomas-Oates J. Localization of water-soluble carbohydrates in wheat stems using imaging matrix-assisted laser desorption ionization mass spectrometry. New Phytologist, 2007, 173, 438-444.

[72] Robinson S., Bergstrom E., Seymour M., Thomas-Oates J. Screening of Underivitized Oligosaccharides Extracted from the Stems of Triticum aestivum Using Porous Graphitized Carbon Liquid Chromatography-Mass Spectrometry. Analytical Chemistry, 2007, 79, 2437-2445.

[73] Vaidyanathan S., Gaskell S., Goodacre R. Matrix-suppressed laser desorption/ionisation mass spectrometry and its suitability for metabolome analyses. Rapid Communications in Mass Spectrometry, 2006, 20, 1192-1198.

[74] Rainville P., Plumb R. The simultaneous acquisition of exact mass data using alternating collision cell energy: MS^E. Application note, Waters Corporation, MA, USA.

Chapter 5

Method Development for the Application of MALDI MSI to Animal Models of Disease: A Preliminary Study of Spinal Cords from Mice with Chronic Relapsing Experimental Autoimmune Encephalomyelitis

5.1 Introduction to Mammalian Metabolomics

The term metabolomics has previously been defined in chapter 4 in the context of plant tissue; in this chapter metabolomics has been applied to the study of animal tissue.

This chapter details a mammalian metabolomics approach for the study of spinal cords from mice with CREAE (Chronic Relapsing Experimental Autoimmune Encephalomyelitis), the animal model of multiple sclerosis. A non-targeted strategy was used in an attempt to discover differences between healthy and diseased tissues i.e., to identify potential biomarkers of disease. A main focus of the work presented in this chapter was to establish methodology with respect to the sample preparation procedure required for the mass spectrometric analysis of CREAE spinal cord samples.

Metabolomics is a relatively new addition to the 'omics sciences and it is gaining much interest. A major application of metabolomics is in the quest for metabolic markers of disease. In diseases such as multiple sclerosis, biomarker discovery plays a pivotal role in the development of new treatments and could eventually prevent symptoms from worsening by early disease management [1].

Metabolomics-based approaches have previously been used to study animal models of human diseases such as cancer [2], cardiovascular disease [3] and Alzheimer's disease [4].

5.2 Biomarkers

Biomarkers are compounds that are indicative of the physiological or pathological status of cells/tissues. The discovery and identification of biomarkers are important for early disease detection. Advances in molecular biology and improvements in instrumentation have allowed for more high-throughput analyses in the area of biomarker discovery [5]. The 'omics, in particular proteomics and more recently metabolomics, have become very popular in disease profiling experiments with the

ultimate aim of identifying potential biomarkers that are indicative of disease pathogenesis.

5.2.1 The Role of Mass Spectrometry in Biomarker Discovery

Mass spectrometry has a pivotal role in biomarker discovery due to its unparalled sensitivity. It allows for rapid analysis to gain qualitative and quantitative information and is operational over a large dynamic range [6]. Biomarkers of disease may be unknown, they may occur in minute quantities and they may be up or down regulated in diseased samples [7].

Until recently, the majority of biomarker related experiments have been conducted at the proteome level. Hyphenated mass spectrometry techniques such as LC-MS and LC-MS/MS have been extensively utilised for the detection and identification of protein biomarkers of disease; examples include the analysis of synovial fluid and serum from rheumatoid arthritis patients [8] and biomarkers indicative of breast cancer progression in cell lines [9]. MALDI-TOF-MS has been used to analyse cerobrospinal fluid from multiple sclerosis patients and to identify three proteins that were associated with the disease [10]. MALDI MSI has also been used to profile myelinated and demyelinated regions in mouse brain [11].

There is now increasing interest in the role of metabolomics in biomarker discovery as the biochemical pathways of metabolism can be altered in some diseases [12]. Non-targeted metabolomic experiments using LC-MS and GC-MS have been used to investigate biomarkers of drug induced nephrotoxicity with data indicating that increased levels of polyamines and amino acids were potential biomarkers [13].

SIMS and MALDI MSI have been previously used for the detection and imaging of metabolites and peptides in the spinal cords of rats [14].

5.3 Introduction to Multiple Sclerosis

Multiple sclerosis is often regarded as a disease of the western world as it is more prevalent in the northern European and North American populations; this has led

researchers to hypothesise a potential link between environmental factors and the development of multiple sclerosis. Britain is categorised as having a high incidence of multiple sclerosis with ~85 000 people suffering from the condition [15].

Multiple Sclerosis is an autoimmune condition of unknown etiology, where the white blood cells (particularly T cells) mount an attack on the central nervous system (CNS). This results in damage to the myelin sheaths that protect the nerves, resulting in demyelination and the loss of oligodendrocytes, and thus disrupting nerve signals/conduction [16, 17]. A common pathological feature associated with multiple sclerosis is the lesions that present themselves most frequently in the white matter, although they have been less commonly observed in gray matter. The lesions can be observed both in the brain and in the spinal cord [18]. It has been reported that spinal cord lesions can be present without any lesions appearing in the brain [19]. There is also evidence to support a correlation between spinal cord lesions and the level of disability in patients with multiple sclerosis [20].

5.3.1 Techniques Used for the Study of Multiple Sclerosis

The diagnosis of multiple sclerosis is not straightforward. It is based on clinical symptoms, magnetic resonance imaging (MRI) results [21] and electrophoresis of cerobrospinal fluid obtained by lumbar puncture to detect oligoclonal immunoglobulin bands [22]. This lumbar puncture is, however, an invasive procedure. In recent years there has been much research into the discovery of biomarkers of disease; these experiments are usually proteomic or metabolomic investigations. Many techniques have been adopted to study multiple sclerosis; however; the majority of studies have focussed on the more obvious disease aspects such as loss of myelin and lesion formation. Proton magnetic resonance spectroscopy has been used to obtain pathological information non-invasively from multiple sclerosis patients [23]. The benefits of this technique are that human samples can be studied, therefore avoiding the animal model versus human debate. A number of small molecule biomarkers have been previously investigated in multiple sclerosis; the most common include choline, creatine and N-acetyl aspartate [24, 25]. The published literature describes both an increase in choline [24, 26] and a decrease of

choline levels in multiple sclerosis [26]. The metabolite studies conducted by Inglese *et al.* showed from their cell culture experiments that the concentrations of choline and creatine were elevated in astrocytes and oligodendrocytes in multiple sclerosis patients [1].

5.3.2 Animal Models of Multiple Sclerosis

5.3.2.1 Chronic Relapsing Experimental Autoimmune Encephalomyelitis (CREAE)

CREAE is a T-cell mediated inflammatory, demyelinating condition of the central nervous system. CREAE is used as an animal model of multiple sclerosis to allow the pathogenesis of the disease to be studied. CREAE can be initiated by active immunisation using spinal cord homogenate or purified myelin components that are combined with adjuvants such as Freund's and *Mycobacterium Tuberculosis*. The inoculated animals go on to develop either acute monophasic or chronic relapsing disease depending on the inoculation schedule used [27]. The use of animal models that mimic human diseases is of paramount importance in gaining a greater understanding of the associated disease pathogenesis. Animal models provide a way of studying diseases which could not be directly studied in humans, for example the study of the central nervous system (CNS) in multiple sclerosis. At present three drugs for the treatment of multiple sclerosis (Glatiramer acetate, Mitoxantrone and Natalizumab) have been developed from EAE models [28].

The main advantages of using the CREAE model are as follows:

- Enables researchers to study the cellular processes underpinning multiple sclerosis in particular demyelination that may help to determine the cause of multiple sclerosis.
- Tests potential therapeutic strategies for use in the treatment of multiple sclerosis.
- As CREAE experiments most commonly use rodents, experiments are relatively short due to their fast breeding.

The disadvantages of using this animal model are:

- CREAE is an 'animal model' of multiple sclerosis and this is mainly based upon preconceived ideas on multiple sclerosis pathogenesis.
- Animal testing.

A compromise must be achieved between the number of animals used for a particular study and the statistical reproducibility. This includes the number of biological replicates as biological variability can affect the results that are obtained; however, it is apparent in many publications that repeat examinations have been performed on tissue from the same animal for evaluation of the measurement process. This provides no information on biological variability at all [29].

5.4 Experimental Part I: CREAE Induction

CREAE induction was undertaken at Queen Mary's University, London and was performed as previously described by Baker *et al.* [30] under the home office licence of Dr C. Bolton.

5.4.1 A Brief Overview of CREAE Induction

Complete Freund's adjuvant (CFA) was produced by mixing 16μg Mycobacterium tuberculosis H37Ra and 4μg Mycobacterium butyricum in 4mL of incomplete Freund's adjuvant (IFA) (all Difco Laboratoris, Detroit, Michigan, USA) and kept at 4°C. 1mL of the CFA stock was added to 11.5mL of IFA to make up 12.5mL CFA for the inoculation emulsion. Spinal cord tissue obtained from Biozzi antibody high (ABH) mice was homogenised and freeze dried; 33mg of the freeze dried tissue was reconstituted in 5mL phosphate buffered saline (PBS). The reconstituted spinal cord was added to an equal volume of CFA and then sonicated for 10 minutes at room temperature. This mixture was then drawn up and down in a 1mL syringe to emulsify the solution until it could not be dispersed further.

5.4.2 Inoculation of Biozzi ABH Mice

0.15mL of the emulsion, described previously in section 5.4.1, was injected subcutaneously into each flank of the Biozzi ABH mice at time points day 0 and day 7. Post acute phase, some of the mice spontaneously relapsed. If the mice did not relapse a further injection of 0.15mL of the emulsion was used to induce the relapse [30]. Each injection that was administered was equivalent to 1mg of lyophilised Biozzi ABH mouse spinal cord homogenate and 60μg of mycobacteria. Mice were then assessed using a CREAE score on a daily basis using the criteria shown in figure 5.1.

Weight loss was the first observed clinical sign at approximately 13-15 days post inoculation. This was followed by neurological deficit (limp tail) at approximately 15-17 days post inoculation. Acute paralysis was observed at approximately 18-20 days post inoculation, where the paralysis was sustained for approximately 4 days (days 20-24 post inoculation); mice gained weight in this period. The first remission was observed between days 24 and 28 where some tail tone was regained (not fully regained). The mice went into a spontaneous relapse between days 35 and 40 post inoculation, with the onset of rapid paralysis. In mice that did not suffer spontaneous relapse, the relapse was induced by administering a third injection of the spinal cord emulsion as previously described. Approximately 6-8 days post inoculation induced relapse was achieved and the mice developed severe paralysis from which they developed chronic disease.

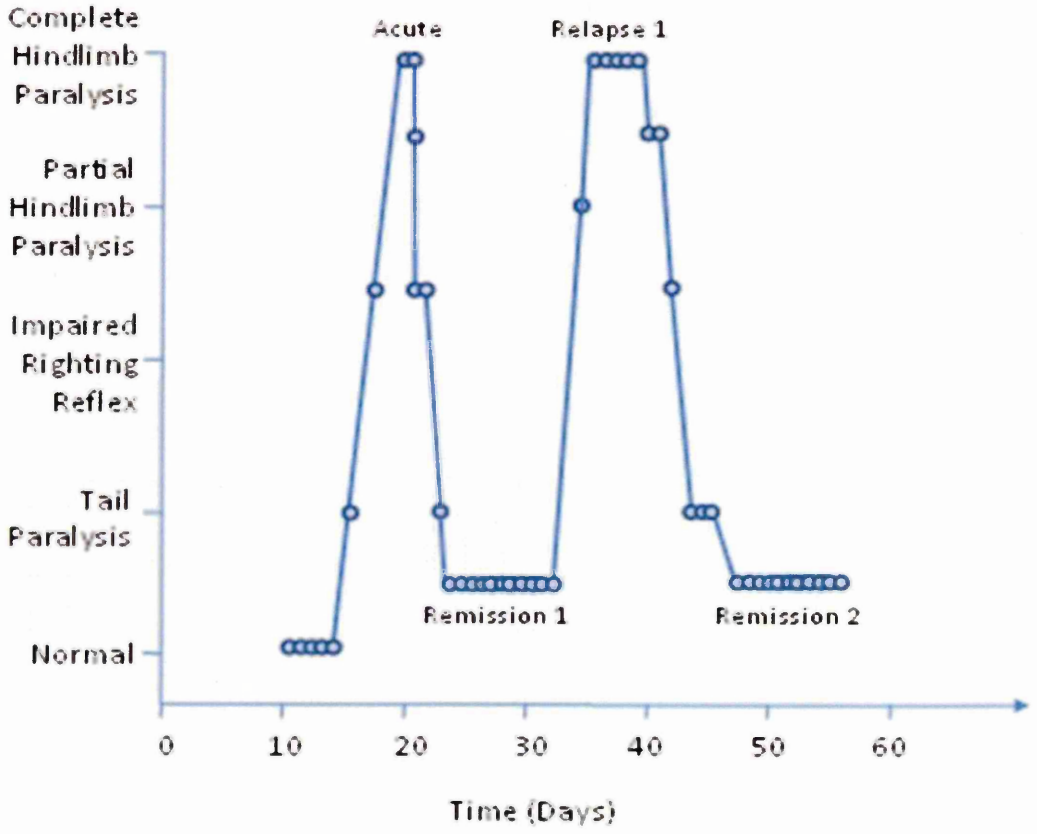

Figure 5.1: Stages and Levels of Disability Associated with CREAE: A graph to show the stages and levels of disability associated with the disease stages studied in this chapter. Adapted from [31].

5.4.3 Tissue Removal Procedure

Biozzi ABH mice were sacrificed under the schedule one method of the Home Office, UK regulations. Mice were sacrificed at the following stages: predisease, acute stage disease, relapse, first remission and second remission. Spinal cords were removed by flushing out using using approximately 1-2mL of ice cold PBS, containing Indomethacin, a cyclooxygenase inhibitor, at a concentration of 10μg/ml contained in the PBS solution (to inhibit further Prostaglandin production that occurs during the disruption of dissection). The PBS solution was made to the following concentrations by dissolving one PBS tablet in 200mL of Ultra High Quality (UHQ) water: 137mM NaCl, 2.7mM KCl and 10mM phosphate buffer solution (pH 7.4 at 25°C). Not only does the PBS aid in the removal of the spinal cords, it removes any blood from the tissue surface, which if left could interfere with the prostaglandin levels. The spinals cords were then snap frozen using isopentane and liquid nitrogen. Tissue was stored at -80°C until required.

5.5 Experimental Part II: Materials and Methods for MALDI MSI Analysis

5.5.1 Materials

Ethanol (HPLC grade), trifluoroacetic acid (TFA, HPLC grade), α-CHCA, carboxymethylcellulose (CMC), Harris's haematoxylin, eosin, DPX mounting medium, xylene, glass microscope slides and choline base standard solution were obtained from Sigma Aldrich, Gillingham, UK.

Cryomoulds were obtained from Fisher Scientific, Loughborough, UK.

5.5.2 Sample Preparation for MALDI MSI Analysis

Disease Stage	Control Animal Number (un-inoculated)	Un-inoculated Animal Weight (g)	Diseased Animal Number (inoculated)	Inoculated Animal Weight (g)
Pre-disease (group 1)	55	32.3	8	31.1
Pre-disease (group 2)	56	34.4	2	33.3
Acute (group 1)	49	30.4	25	30.6
Acute (group 2)	43	33.0	12	32.8
First Remission (group 1)	48	30.4	24	30.1
First Remission (group 2)	50	29.1	17	28.0
Relapse (group 1)	57	32.4	6	33.3
Relapse (group 2)	54	32.2	40	33.3
Second Remission (group 1)	47	31.0	38	30.0
Second Remission (group 2)	51	30.4	31	29.9

Table 5.1: Animal Sample Numbers Analysed: A summary of the animals from which the spinal cords were obtained showing the inoculated animals alongside their corresponding controls. The left hand side of the table provides information relating to the disease phase at which the spinal cord tissue was obtained. The animals have been assigned to either group 1 or group 2. Group 1 experiments were conducted first and group 2 experiments were used to assess the reproducibility. Spinal cord sections were analysed using MALDI MSI alongside their corresponding weight match control (un-inoculated).

5.5.2.1 Spinal Cord

The tops of the spinal cords (cervical section), approximately 1cm in length, were removed from the rest of the spinal cord using a disposable blade as shown in figure 5.2. They were then transferred to cryomoulds where they were embedded in carboxymethylcellulose (CMC) in order to aid the sectioning process. CMC was made to a concentration of 1mg/mL in water and forms a liquid gel-like substance. The CMC was pre-cooled and poured into the cryomould, the spinal cord was added and the cryomould was lowered carefully into liquid nitrogen to ensure that the sample did not thaw. This method ensured that the orientation of the tissue could be controlled. Sections of 12µm were obtained by cryosectioning (Leica CM1510) the

spinal cord. These sections were mounted onto an aluminium support and then affixed to a MALDI target plate for analysis.

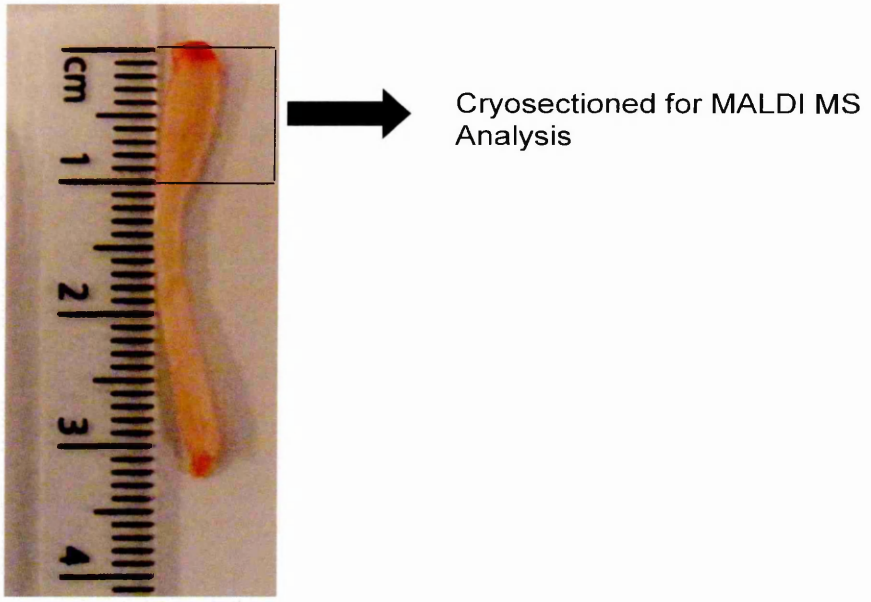

Figure 5.2: Photograph of a Spinal Cord and the Area Taken for Analysis: 1cm in length from the top of the spinal cord (cervical) was removed from the rest of the spinal cord, embedded in CMC and then cryosectioned.

5.5.2.2 Matrix Application

The matrix used was α-CHCA made to a concentration of 5mg/mL in 70% ethanol, 30% water, containing 0.1% TFA. The matrix was applied to the tissue surface using a Suncollect automated matrix sprayer that operated at 2bar (200kPa) pressure. The matrix was in 5 layers; the first layer coated the tissue applying 2μL/min; the second layer 3μL/min and the next three layers 5μL/min. This method of matrix application is thought to extract the endogenous compounds within the tissue to allow them to co-crystallise with the matrix and also allows for a homogenous covering of the sample in matrix. This improves on former manual airspraying techniques that relied on a skilled operator applying the matrix onto the tissue surface.

5.5.3 MALDI MS Images

The images presented were obtained from spinal cord sections from the cervical/partial thoracic area of 108μm depth. The resolution of each image is 150μm x150μm with a laser power of 30% (30μJ). The laser was rastered over the tissue section at set increments of 150μm acquiring data for a period of two seconds per spot. The mass spectrometer was calibrated prior to image acquisition and the data obtained was recalibrated post acquisition with the matrix peaks of α-CHCA to ensure the mass accuracy was as precise as possible.

The scale on the right hand side of the images contained within this chapter represents the ion intensity; the dark blue colour being the most intense (i.e. accounting for more ions) and the lighter blue/white colour accounting for fewer ions.

5.6 Haematoxylin and Eosin (H&E) Staining of Spinal Cord Sections

In order to confirm that the diseased animals had inflammatory cell infiltrates in the spinal cord, serial sections were collected on glass microscope slides and stained with H&E. It was found that the relapse disease stage tissue showed the most significant signs of inflammation as shown in figure 5.3.

The sections were fixed using ethanol followed by immersion in graded ethanol solutions for 1 minute periods (100%, 90% and 70%). This was followed by immersing the sections in 5% Haematoxylin solution for 40 seconds and then the sections were rinsed under running tap water to remove the excess haematoxylin stain; this was done until the water ran clear. The sections were then immersed in eosin for 40 seconds, followed by a 10 second immersion step in water. The sections were immersed in graded solutions of ethanol for 1 minute periods (70%, 90%, 100%). The slides were finally immersed in Xylene for 30 minutes and then mounted with coverslips using DPX mounting medium.

5.7 Results and Discussion

5.7.1 H&E Stained Spinal Cord Sections

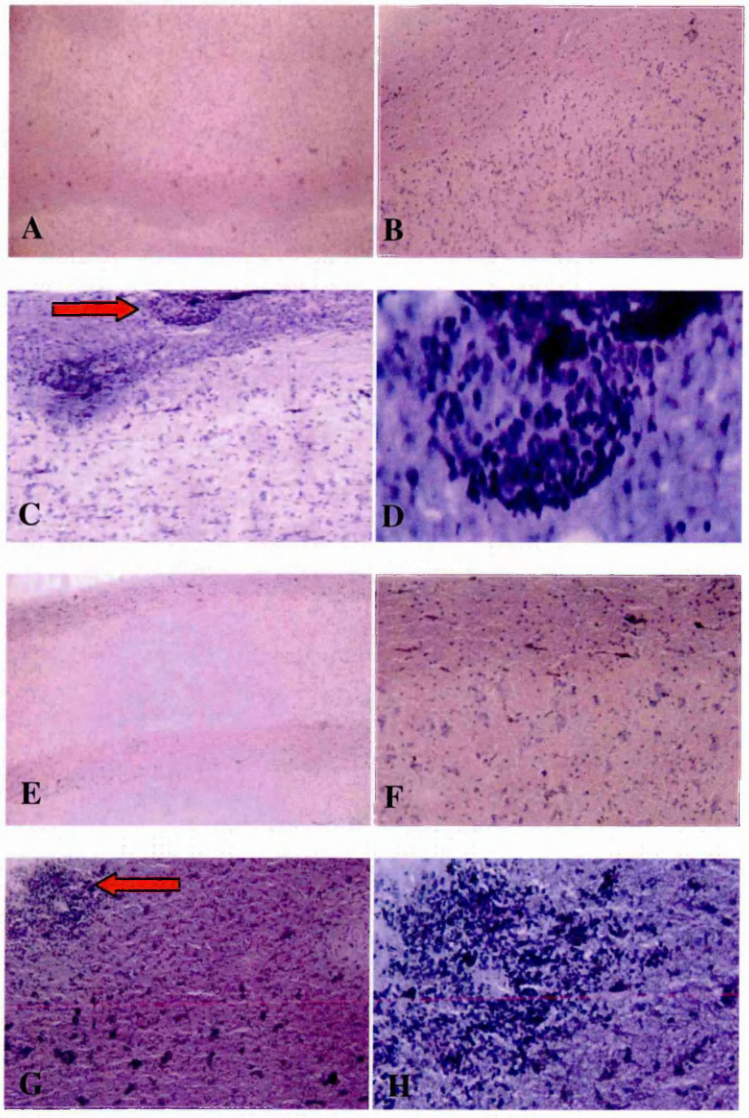

Figure 5.3: H&E Stained Spinal Cord: Representative microscope images were taken adjacent to the sections taken for MALDI MSI analysis. A: sample 54 x 40 magnification; B: sample 54 x 100 magnification; C: sample 40 x 100 magnification; D: sample 40 x 200 magnification; E: sample 57 x 40 magnification; F: sample 57 x 100 magnification; G: sample 6 x 100 magnification and H: sample 6 x 200 magnification. Inflammation was observed most significantly in the samples taken from the relapsing animals (samples 6 and 40). The meningeal perivascular cell infiltrates are shown with the red arrows. The controls showed no signs of inflammation.

5.7.2 Multivariate Analysis

Principal Component Analysis (PCA) was performed to investigate the major differences between the control samples and the diseased samples. It was found that the ion at m/z 104.11 was consistently different in the disease stages.

The data was entered into the metabolite database, Metlin [32] where it was found that the ion detected at m/z 104.11 could be from choline. Choline is an important cellular component of both plant and animal tissue; it can act as a methyl donor in metabolic processes, as a precursor for acetylcholine and play a role in lipid metabolism. Elevated choline levels in pre-lesional normal-appearing white matter in multiple sclerosis have been reported by Tartaglia *et al.* [24] using proton magnetic resonance spectroscopy (MRS). They found that changes in the myelin prior to lesion formation, with or without inflammation, can produce elevated Choline/Creatine (Cho/Cr) ratios without any related demyelination.

The PCA data presented in this chapter has been normalised against the matrix peak at m/z 190.05 and the matrix peaks were excluded from the analysis.

Confirmatory analysis was performed by MS/MS to validate the metabolite search shown in figure 5.7.

5.7.3 Investigation of Peak at m/z 104.11

The PCA data presented in sections 5.7.6 and 5.7.7 show that the ion at m/z 104.11 appears to be the most significant difference between the healthy and the diseased tissues. Conventional MALDI MS experiments were conducted to investigate if this peak was a matrix related peak. It was found that there was a matrix-related ion at m/z 104.10, as shown in figure 5.4c. However, a peak at 104.11 was detected from the tissue surface as shown in figure 5.4a and b.

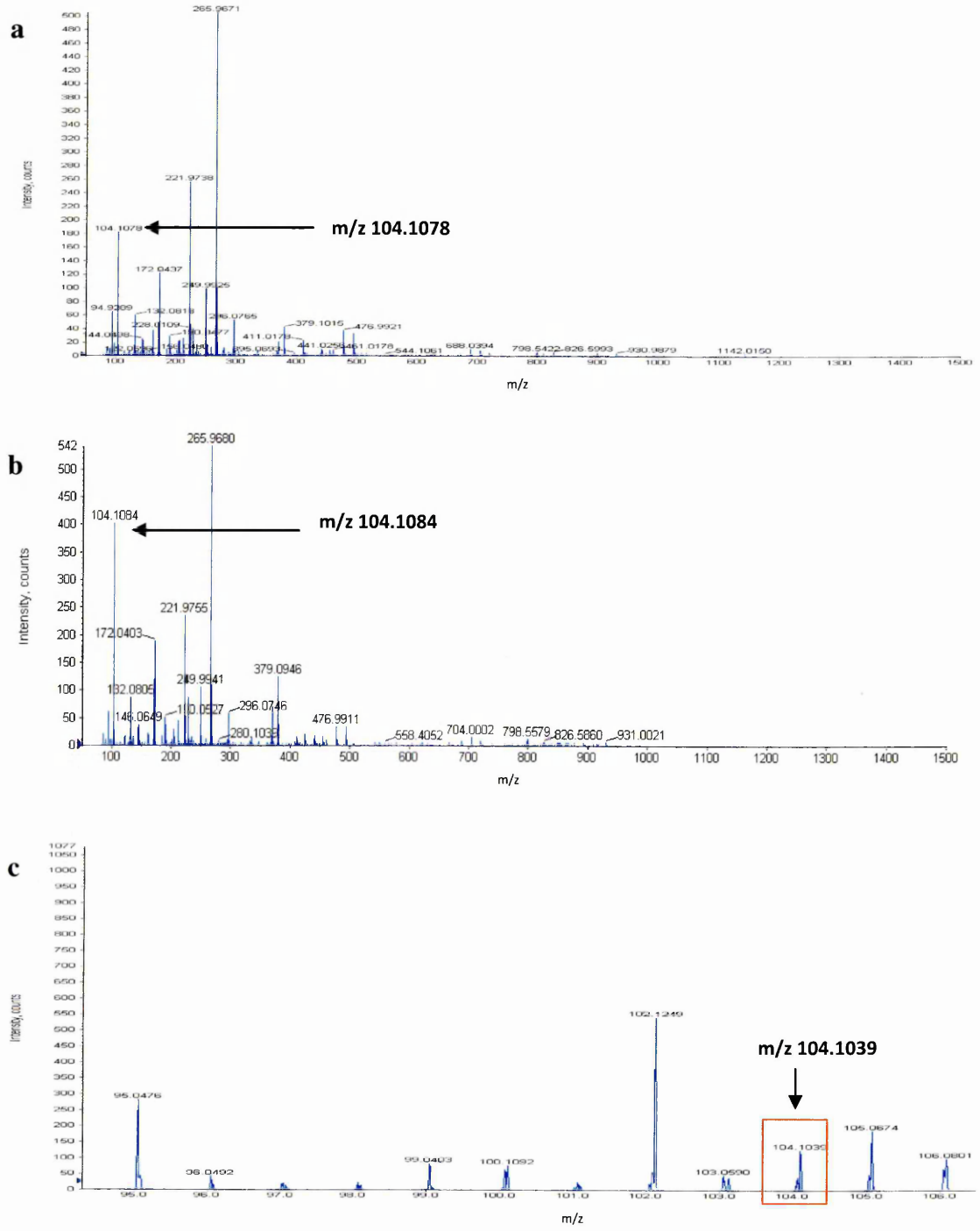

Figure 5.4: MALDI-MS Spectra of Relapse Stage Spinal Cord: Example spectra for the relapse disease phase: (a) spectrum recorded from sample 6 (inoculated mouse); (b) the corresponding control – sample 57 (un-inoculated mouse); (c) matrix blank showing that a peak is present at m/z 104.10

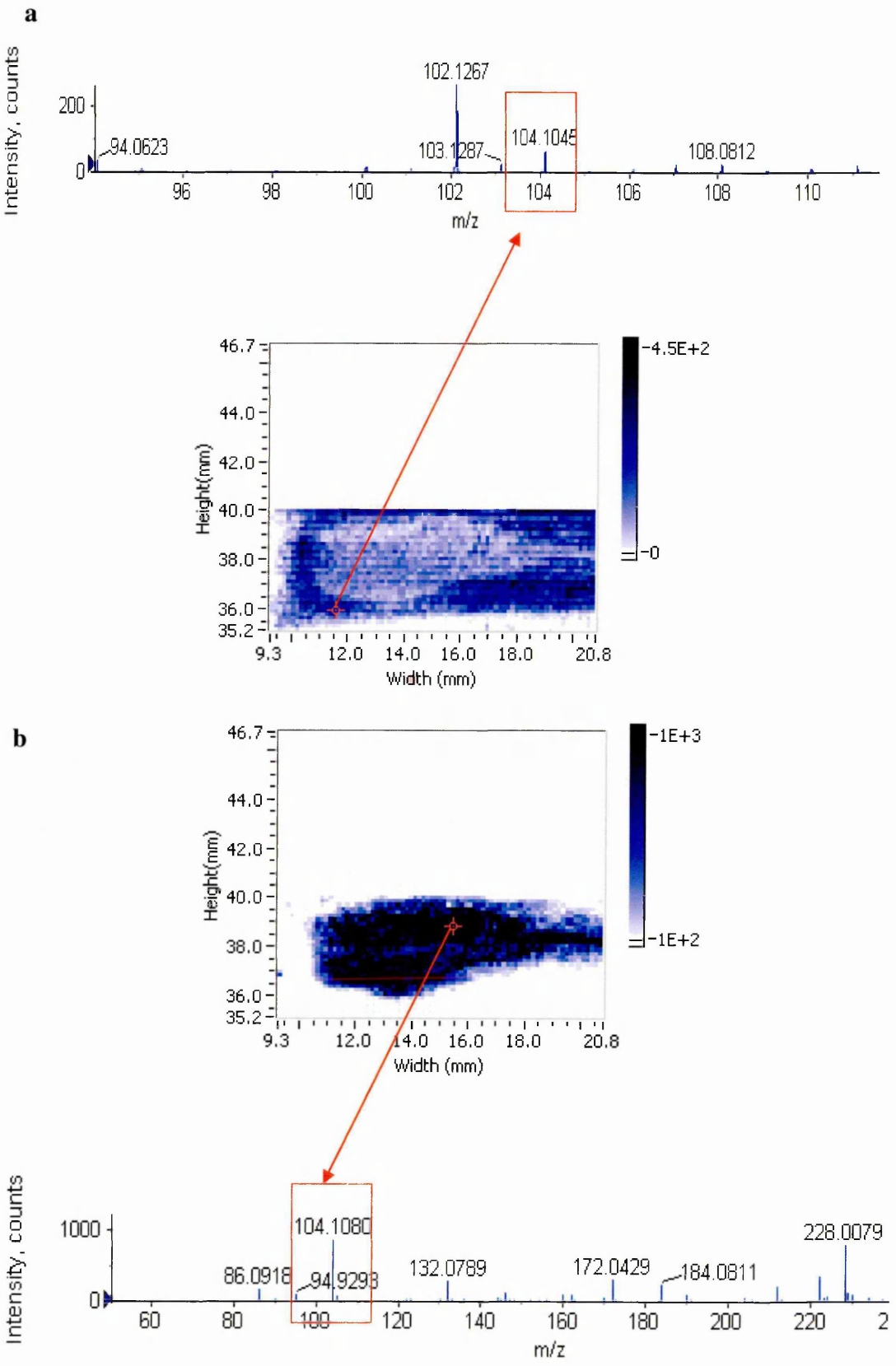

Figure 5.5: MALDI-MS Spectra and Images to Investigate m/z 104: (a) shows the matrix peak present at m/z 104.1045; (b) shows the more intense peak observed on the spinal cord section at m/z 104.1080.

5.7.4 MS/MS Analysis

The observed mass at m/z 104.11 appeared to differ in ion intensity in the diseased animals compared with the healthy controls; this was highlighted in the PCA data. The use of a chemical matrix can present problems in metabolomic analyses as discussed in chapter 4. However, to allocate the observed mass with a potential metabolite MS/MS was performed. A matrix peak occurs at m/z 104.10 and therefore MS/MS analysis was performed to differentiate between the matrix and other possible metabolites.

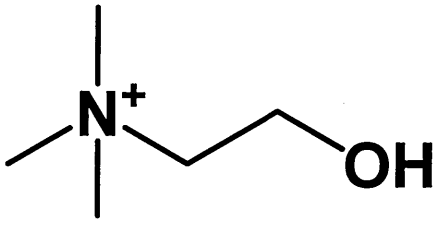

Figure 5.6: The Chemical Structure of Choline:

Formula: $C_5H_{14}NO^+$

RMM: 104.11

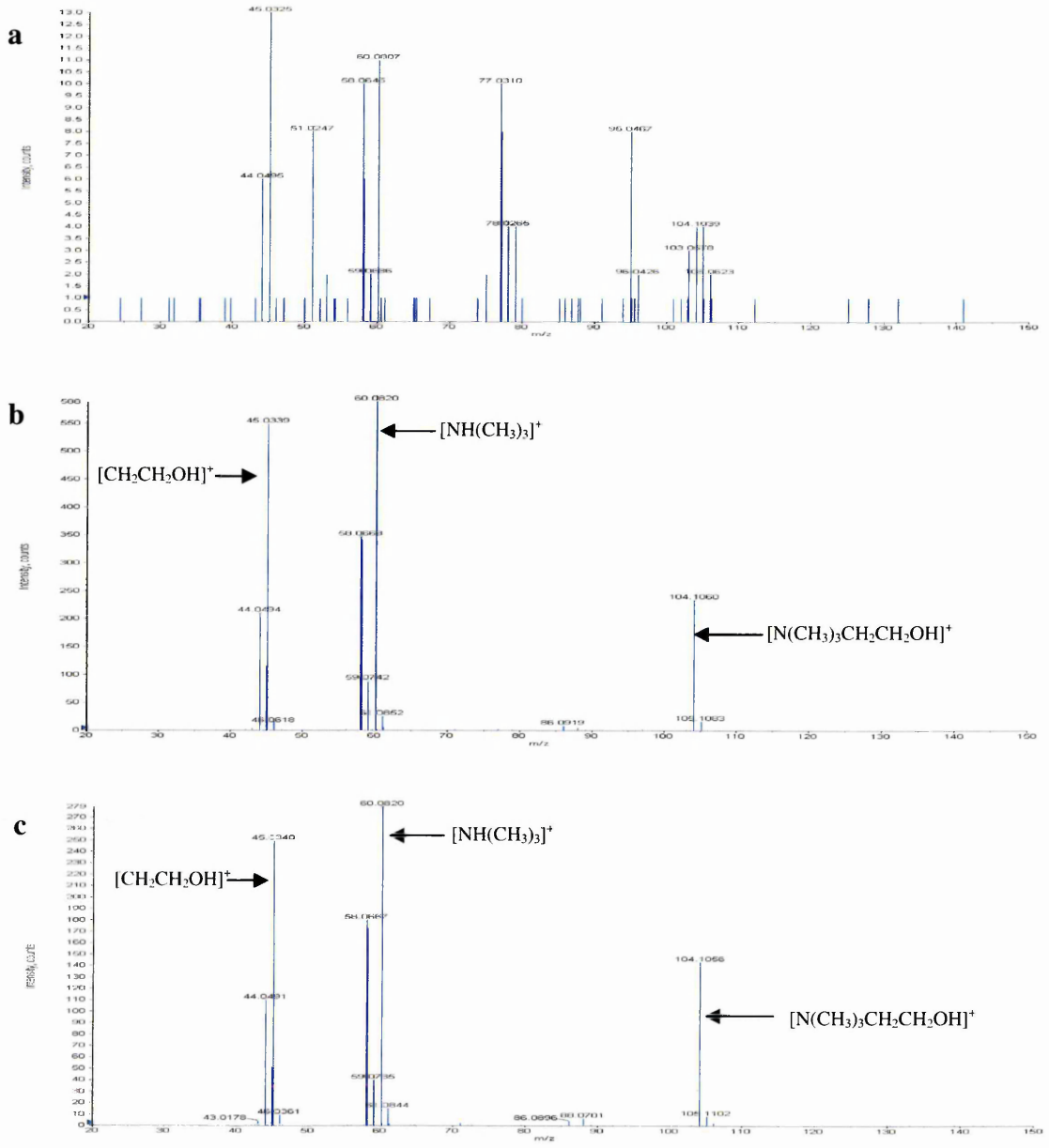

Figure 5.7: MALDI MS/MS Analysis of m/z 104: Product ion spectra for the verification of the mass observed at m/z 104.11: (a) the product ion spectrum showing the fragmentation pattern of the matrix peak observed at m/z 104.10; (b) the product ion spectrum showing the fragmentation pattern observed when choline (m/z 104.11) standard was ionised off spinal cord tissue; (c) the product ion spectrum showing the fragmentation pattern for m/z 104.11 present in spinal cord tissue.

5.7.5 Assessment of the Matrix Coverage

Matrix coverage is an important aspect of successful MALDI MS analyses. The overall aim of the optimal sample preparation procedures is to obtain a homogenous coating of matrix across the sample surface. This is generally achieved using automated matrix applicators as this allows for the matrix application procedure to be consistent and reproducible. The presence of endogenous compounds and salts may vary across the surface of biological tissue; therefore image normalisation is required. Figure 5.8 shows the coverage of the protonated matrix peak of m/z 190.05. The reduced signal intensity of the matrix ion on the surface of the spinal cord section indicates that endogenous compounds within the tissue are suppressing the matrix ion signal at m/z 190.05. To account for this, image data was normalised against this matrix peak to account for any slight differences in matrix coverage. The left hand side of each image represents the top of the spinal cord.

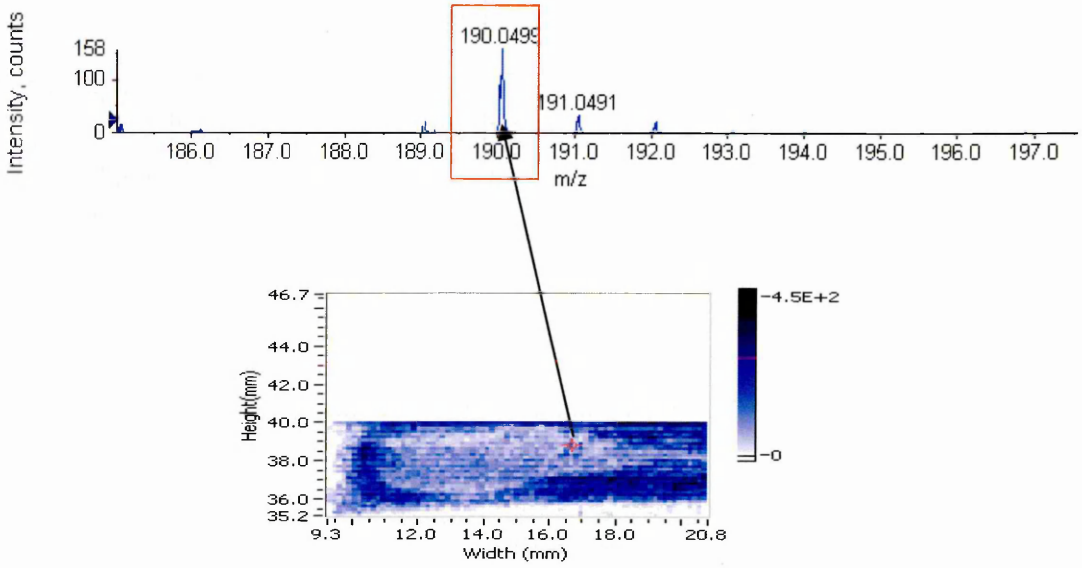

Figure 5.8: Assessment of Matrix Coverage at m/z 190.05: The matrix distribution appears to be relatively homogenous over the tissue surface. However, it is apparent that endogenous compounds contained in the tissue are suppressing the matrix co-crystallisation process. This can be seen in the image presented by a reduction in the matrix signal intensity over the tissue surface. To account for differences/unevenness in matrix coverage the data was normalised against the matrix peak at m/z 190.05.

5.7.6 MALDI MSI and PCA Results for Spinal Cord Sections (Group 1)

For the PCA analysis and statistical analysis five spectra were randomly selected across the spinal cord tissue. The results from the PCA support the image data, therefore this was deemed a sufficient dataset for this particular study.

The results presented for the first group of experiments show that the ion detected at m/z 104.11, assigned tentatively to choline is significant in the acute, relapse and potentially the second remission tissue samples although in the latter group there is slight overlap between the control and disease. This observation is supported in the images by either increased ion intensity (i.e. 104.11 is more abundant in the tissue sample) or decreased ion intensity (i.e. 104.11 is less abundant in the tissue sample) and by the statistical comparisons in figure 5.14. The data that was used for the PCA was also used to deduce any statistical relevance. It was found that in both the acute stage tissue and the relapse tissue the presence of m/z 104.11 was significant.

5.7.6.1 Pre-Disease Stage Tissue

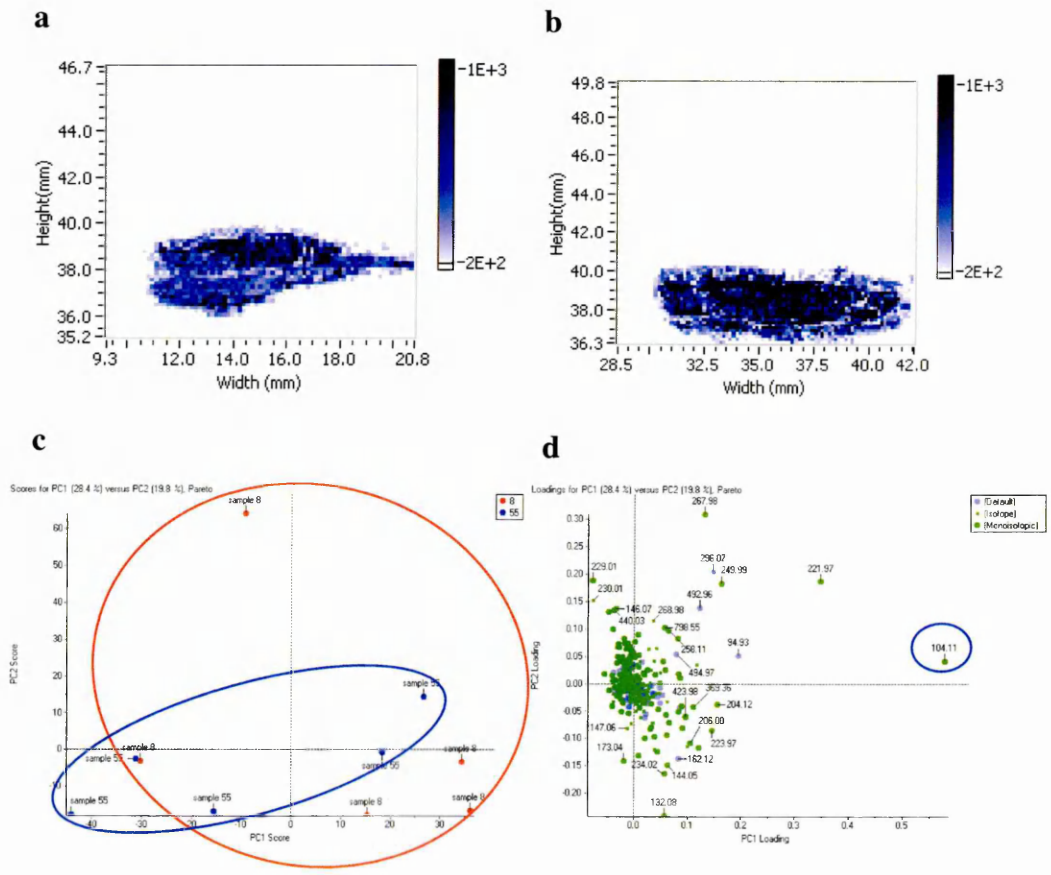

Figure 5.9: MALDI MS Images and Multivariate Analysis of Pre-disease Stage Samples (Group 1): (a) the distribution of m/z 104.11 in the spinal cord section taken from the inoculated mouse (sample 8); (b) the corresponding m/z 104.11 distribution image from the spinal cord tissue obtained from the healthy un-inoculated control (sample 55); PCA results: (c) There is almost total overlap between the diseased and control sample; however, it is clear from the scores plot and (d) the corresponding loadings plot that sample 55 (un-inoculated control) groups more towards m/z 104.11. Thus the difference between the samples is brought about by the compound, potentially choline, at m/z 104.11.

5.7.6.2 Acute Stage Tissue

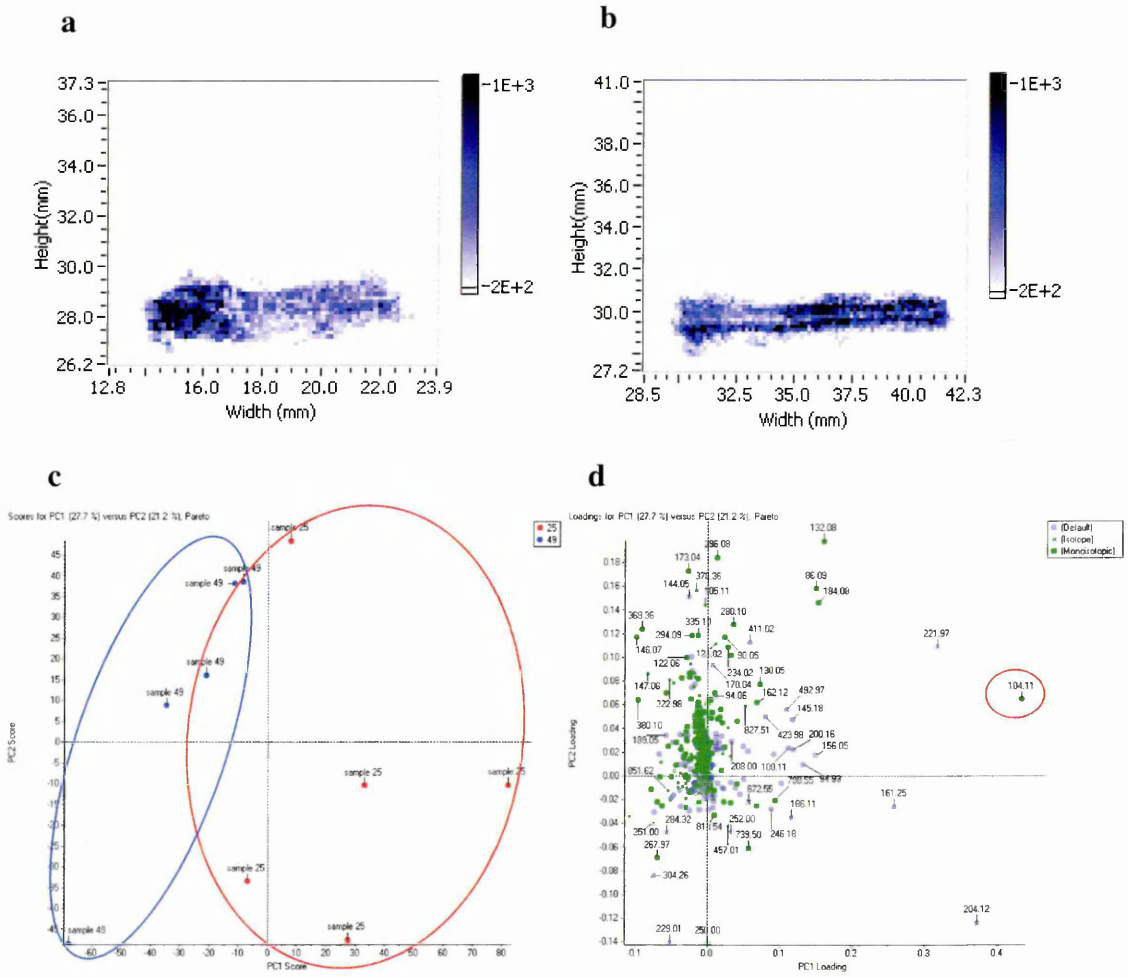

Figure 5.10: MALDI MS Images and Multivariate Analysis of Acute Stage Disease Samples (Group 1): (a) the distribution of m/z 104.11 in the spinal cord section taken from the inoculated mouse (sample 25); (b) the corresponding m/z 104.11 distribution image from the spinal cord tissue obtained from the healthy un-inoculated control (sample 49); PCA results: (c) the scores plot shows that there is grouping of the data between the diseased and healthy samples (d) the corresponding loadings plot shows that sample 25 (inoculated control) groups more towards m/z 104.11.

5.7.6.3 First Remission Stage Tissue

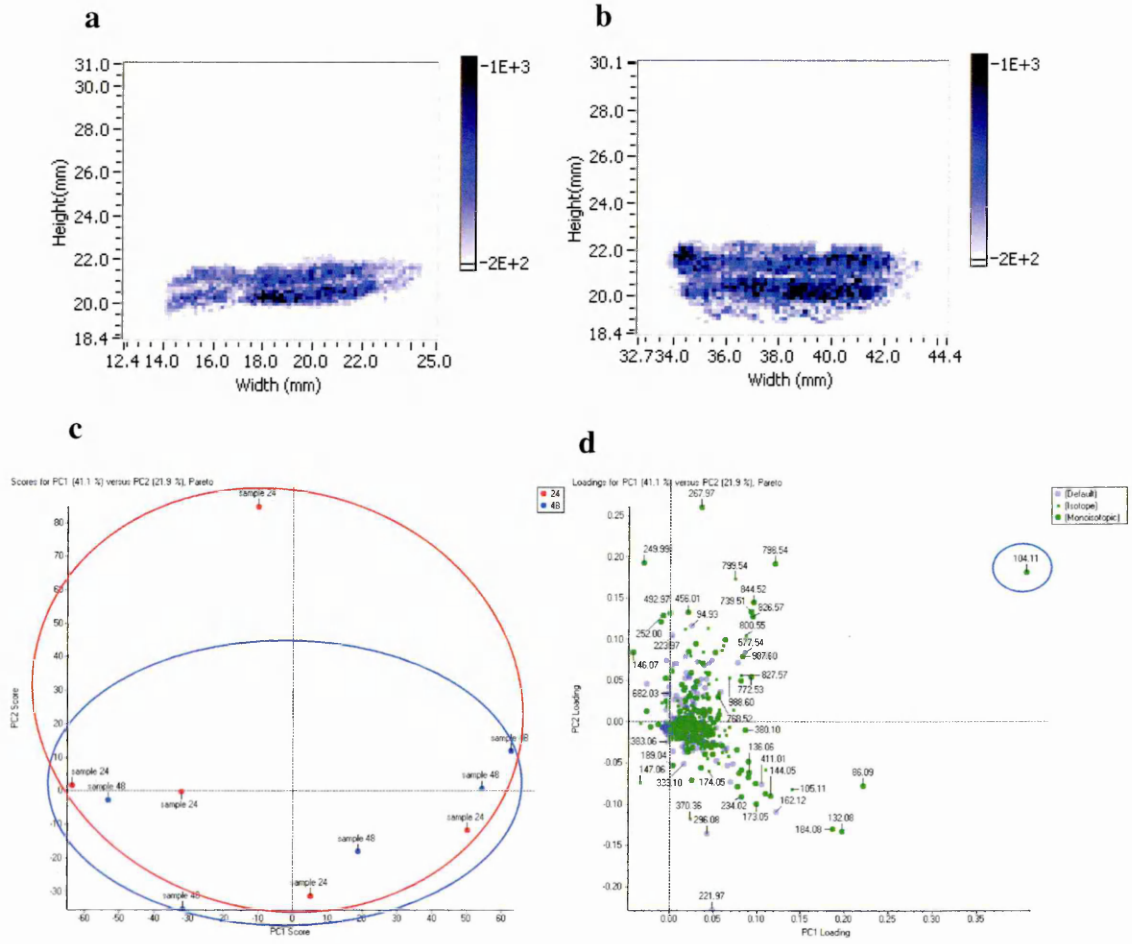

Figure 5.11: MALDI MS Images and Multivariate Analysis of First Remission Stage Disease Samples (Group 1): (a) the distribution of m/z 104.11 in spinal cord section taken from the inoculated mouse (sample 24); (b) the corresponding m/z 104.11 distribution image from the spinal cord tissue obtained from the healthy un-inoculated control (sample 48); PCA results: (c) data showing overlap between the diseased and corresponding control sample, (d) the corresponding loadings plot

5.7.6.4 Relapse Stage Tissue

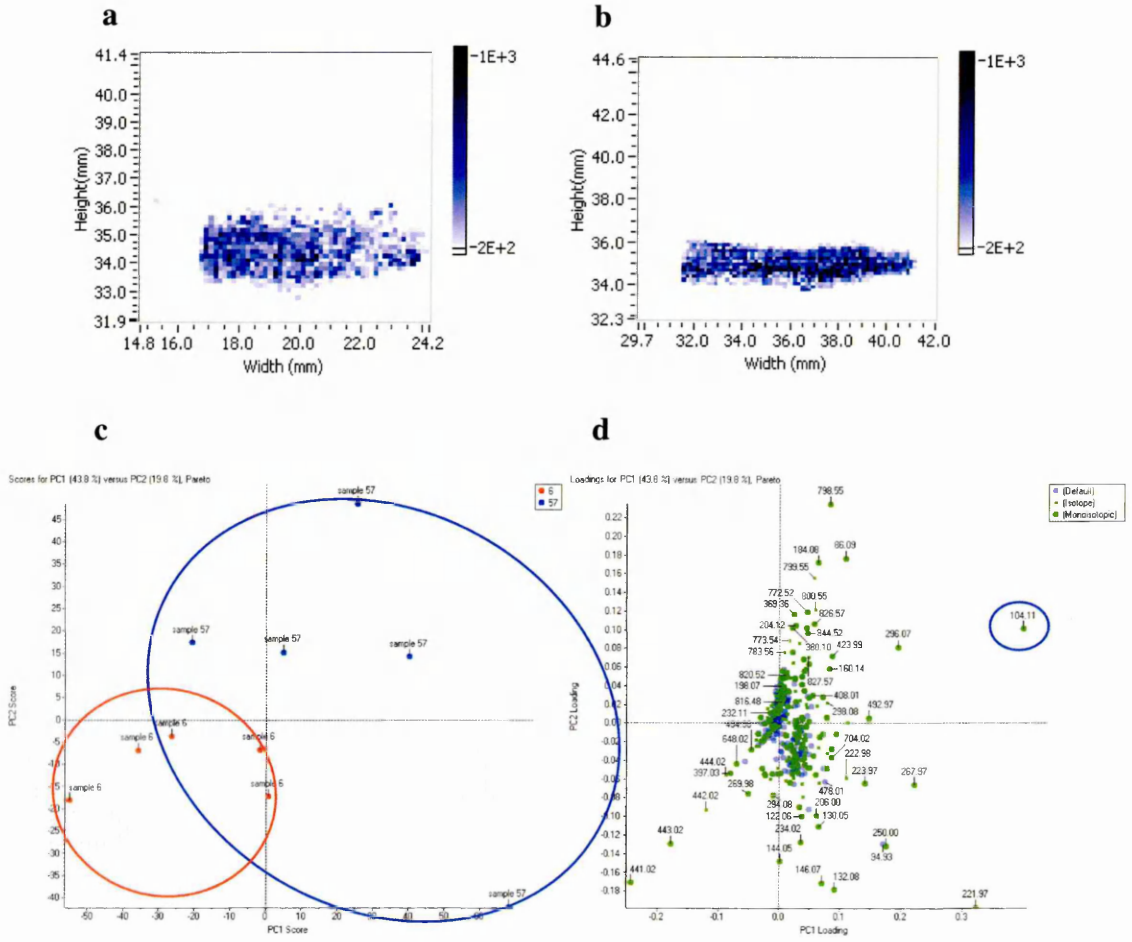

Figure 5.12: MALDI MS Images and Multivariate Analysis of Relapse Stage Disease Samples (Group 1): (a) the distribution of m/z 104.11 in spinal cord section taken from the inoculated mouse (sample 6); (b) the corresponding m/z 104.11 distribution image from the spinal cord tissue obtained from the healthy un-inoculated control (sample 57); PCA results: (c) shows significant grouping between the diseased and corresponding control sample. The scores plot and the corresponding loadings plot (d) show this difference to be brought about by the presence of m/z 104.11 as sample 57 groups more towards the m/z 104.11 in the loadings plot.

5.7.6.5 Second Remission Stage Tissue

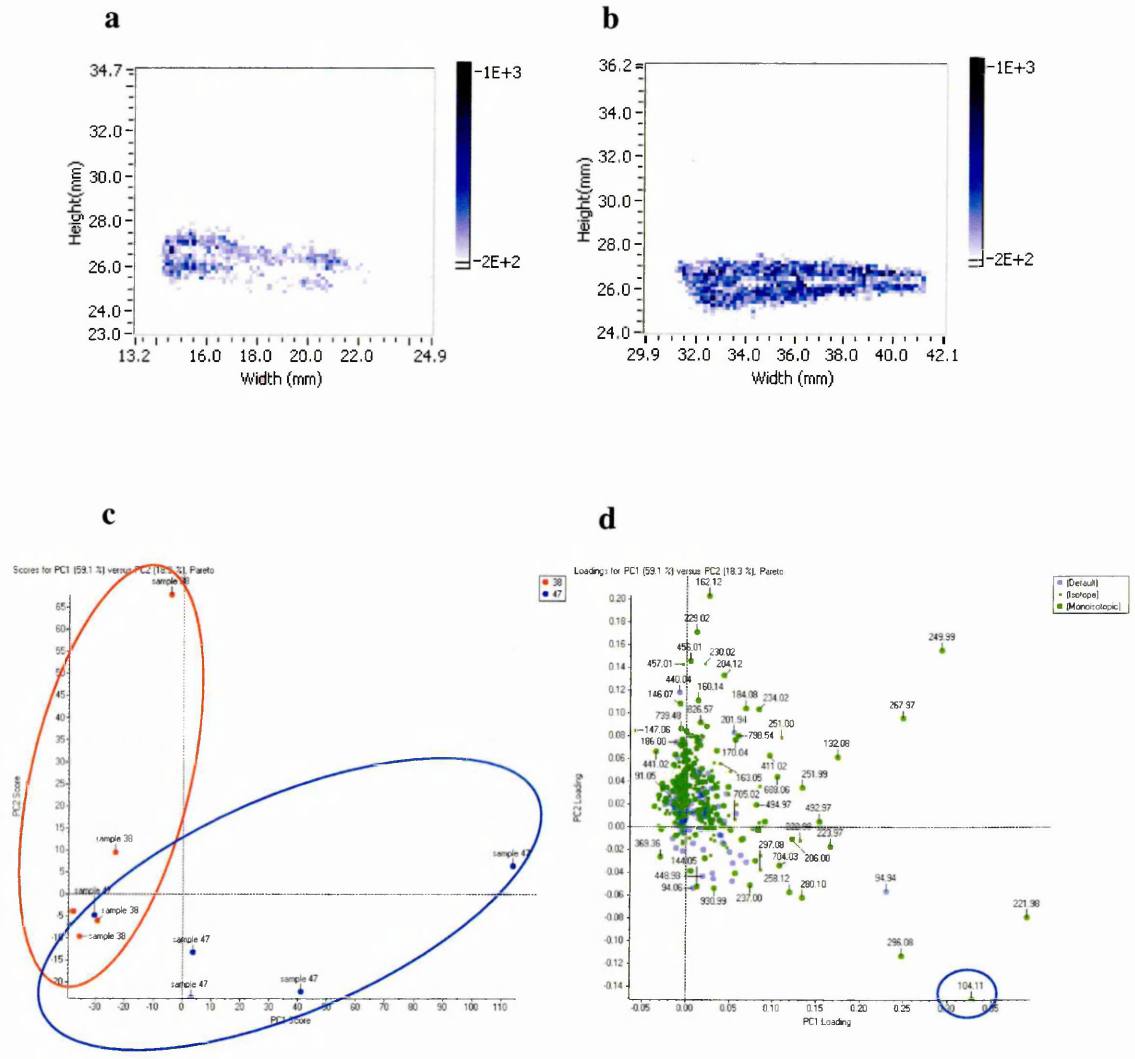

Figure 5.13: MALDI MS Images and Multivariate Analysis of Second Remission Stage Disease Samples (Group 1): (a) the distribution of m/z 104.11 in spinal cord section taken from the inoculated mouse (sample 38); (b) the corresponding m/z 104.11 distribution image from the spinal cord tissue obtained from healthy un-inoculated control (sample 47); PCA results: (c) data showing significant grouping between the diseased and corresponding control sample. The scores plot and (d) the corresponding loadings plot show this difference to be brought about by m/z 104.11 as sample 47 groups more towards the m/z 104.11 in the loadings plot.

5.7.6.6 Statistical Comparisons

A Kolmogorov-Smirnov test revealed that the sample is normally distributed: Z = 0.147; p>0.05. An independent-samples t test was used to assess the significance of differences between disease and matched control sample means for each stage of EAE progression.

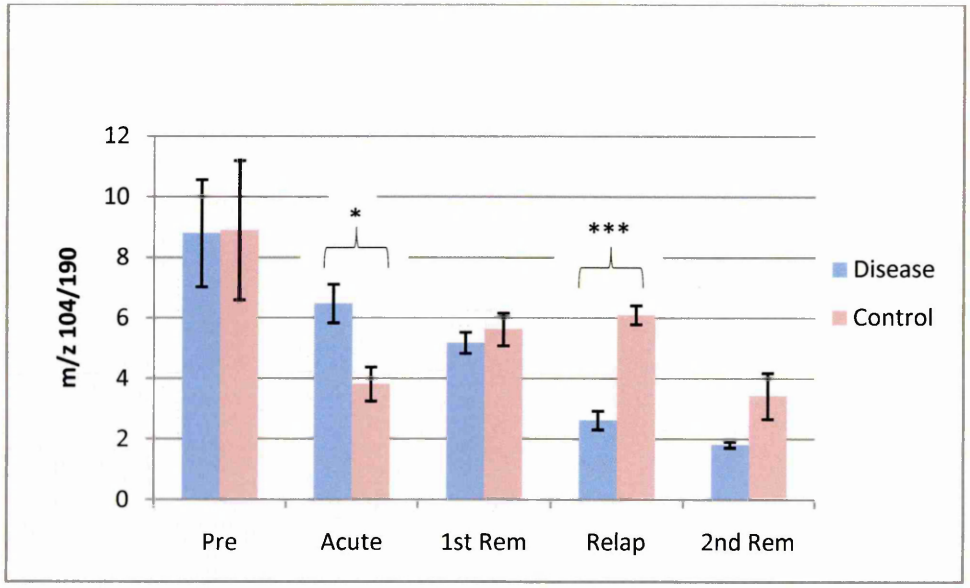

Figure 5.14: Group 1 Disease Stage Comparisons: A graph to show the differences between the diseased samples and the corresponding weight-matched controls (Mean ± SEM). The most significant differences in the levels of choline detected can be seen at acute and relapse stages of disease. This graph was produced using the same five spectra that were used for PCA analysis. (*=P<0.05, **=P<0.01, ***=P<0.001).

Disease Stage	t statistic	Significant?
Pre-disease	-0.03	No
Acute	3.12	Yes*
1st remission	-0.69	No
Relapse	-7.86	Yes***
2nd Remission	-2.10	No

Table 5.2: t-test Results for Group 1 Disease Stage Comparisons: Data relates to figure 5.14 and corresponding significance (*=P<0.05, **=P<0.01, ***=P<0.001).

The results for the first group of experiments show that the most significant changes occur at acute phase and relapse stages of disease; this is supported with significant separation between the groups being observed with the PCA analysis and the t-test results.

5.7.7 MALDI MSI and PCA Results for Spinal Cord Sections (Group 2)

The results presented for group two analysis conflict with the first group of results generated in that the pre-disease, acute, relapse and second remission stage samples appear to show that there are differences related to the abundance of m/z 104.11 between the healthy and the diseased samples. However, the statistical analysis performed in section 5.7.7.6 show only pre-disease, acute and second remission samples to be significantly different. After closer inspection of the PCA data for the relapse stage it appears that some of the grouping of the datasets shown in the scores plot could be due to not only the m/z 104.11 but also by the presence of additional masses that appear to be lipids.

5.7.7.1 Pre-Disease Stage Tissue

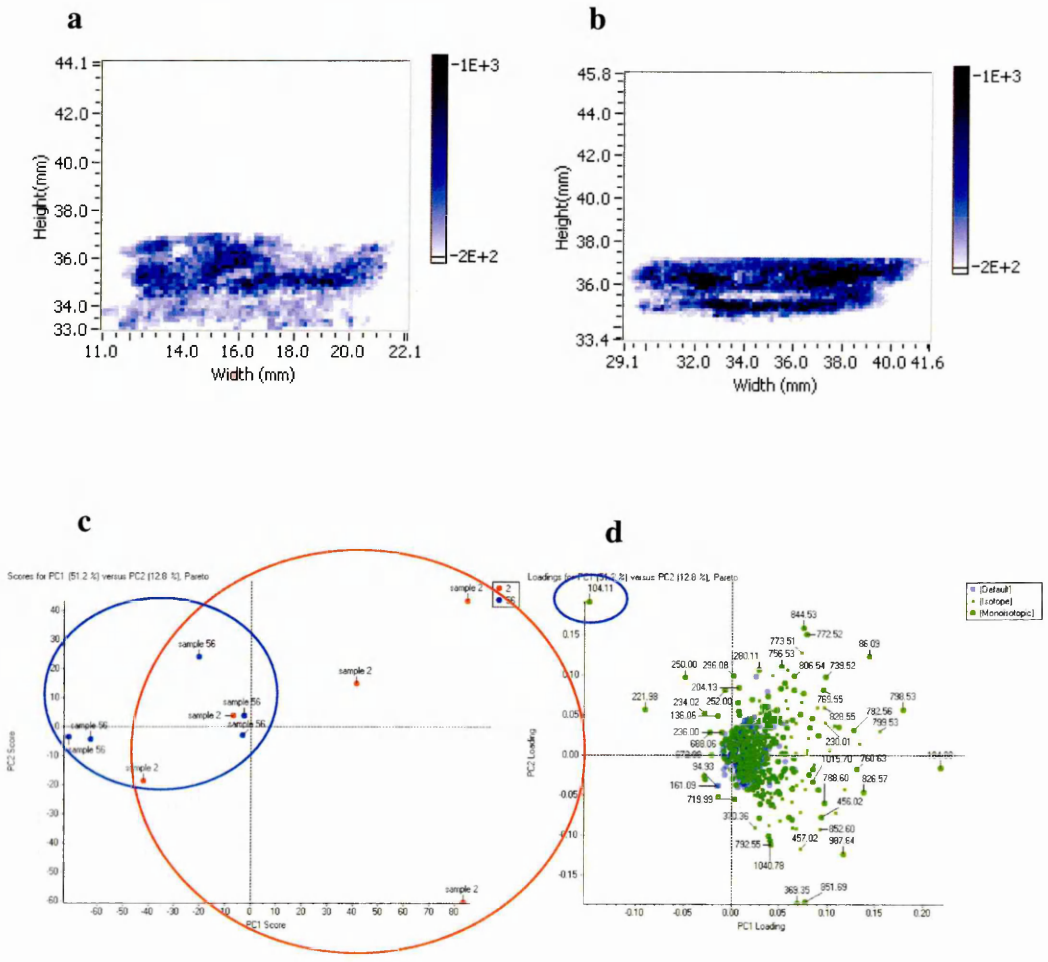

Figure 5.15: MALDI MS Images and Multivariate Analysis of Pre-disease Stage Samples (Group 2): (a) the distribution of m/z 104.11 in the spinal cord section taken from the inoculated mouse (sample 2); (b) the corresponding m/z 104.11 distribution image from the spinal cord tissue obtained from the healthy un-inoculated control (sample 56); PCA results: (c) there is some overlap between the diseased and control sample; however, it is clear from the scores plot and (d) the corresponding loadings plot that sample 56 (un-inoculated control) groups more towards m/z 104.11.

5.7.7.2 Acute Stage Tissue

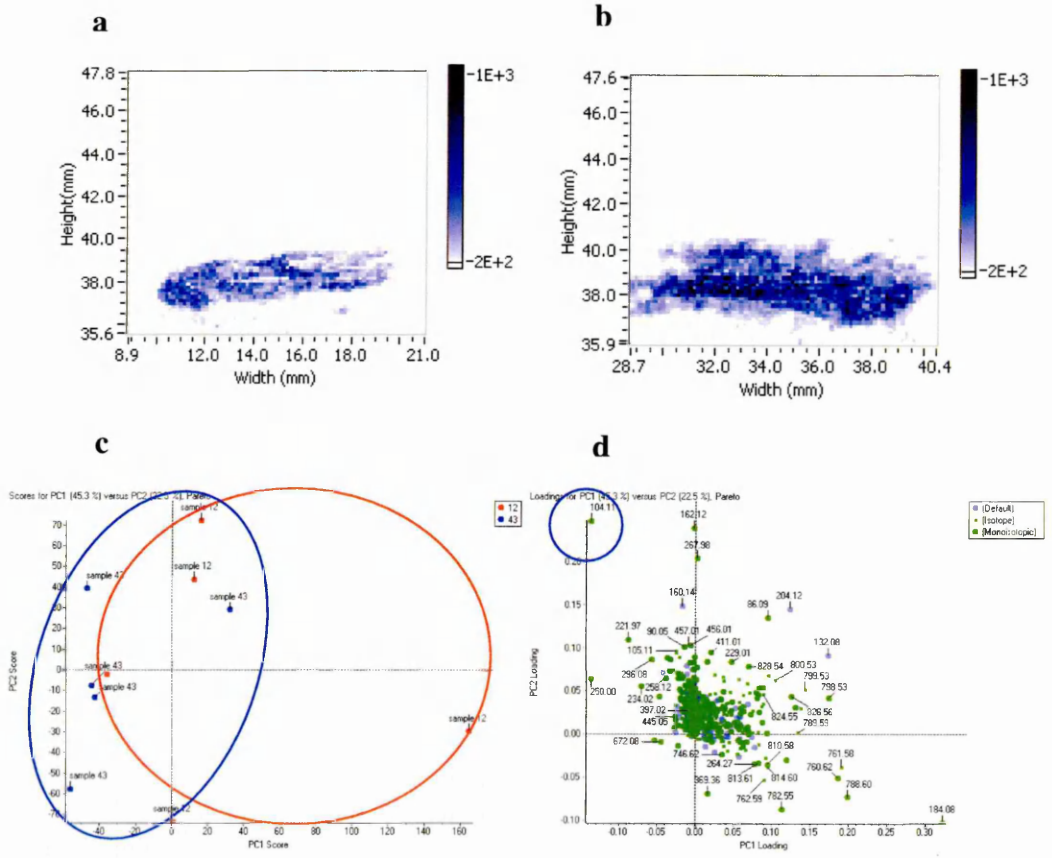

Figure 5.16: MALDI MS Images and Multivariate Analysis of Acute Stage Disease Samples (Group 2): (a) the distribution of m/z 104.11 in the spinal cord section taken from the inoculated mouse (sample 12); (b) the corresponding m/z 104.11 distribution image from the spinal cord tissue obtained from the healthy un-inoculated control (sample 43); PCA results: (c) there is some overlap between the diseased and control sample; however, it is clear to see from the scores plot and (d) the corresponding loadings plot that sample 43 (un-inoculated control) groups more towards m/z 104.11.

5.7.7.3 First Remission Stage Tissue

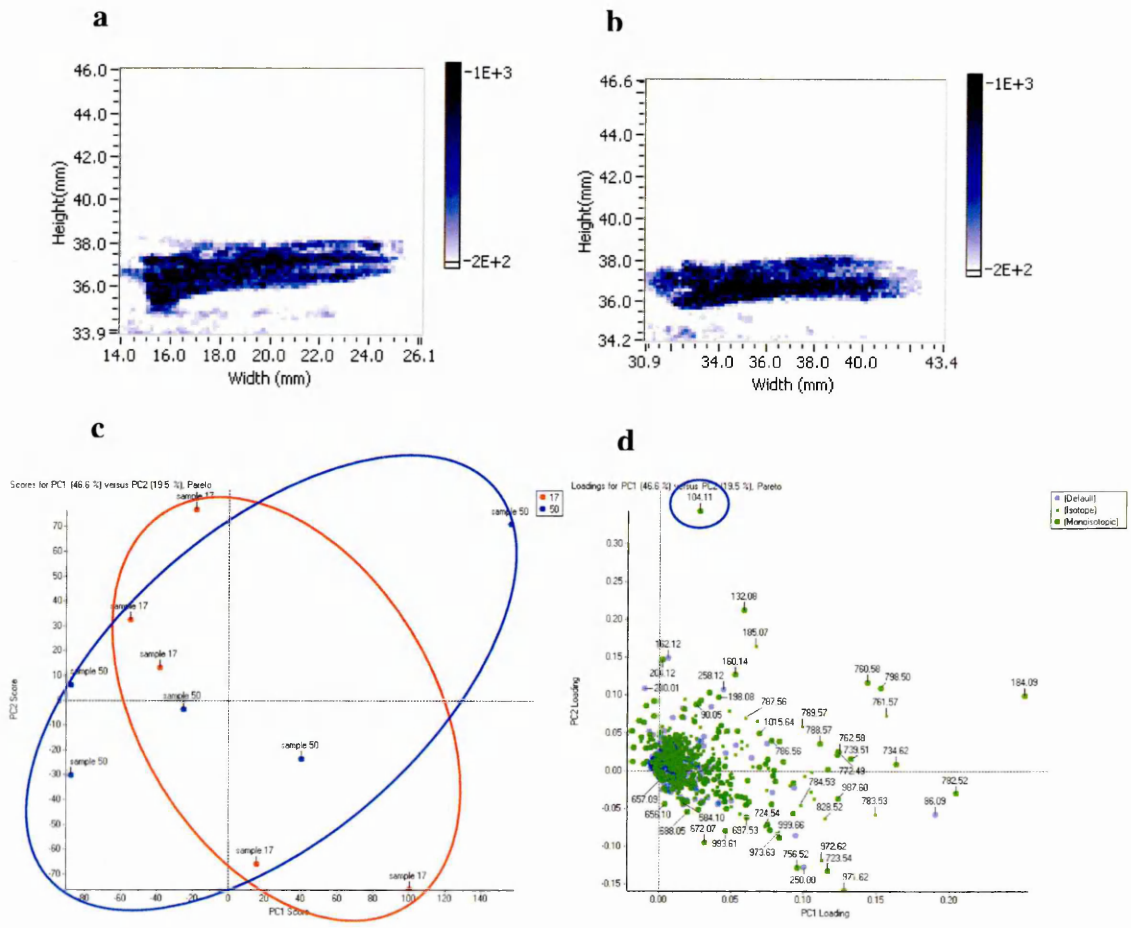

Figure 5.17: MALDI MS Images and Multivariate Analysis of First Remission Stage Disease Samples (Group 2): (a) the m/z 104.11 distribution in the spinal cord section taken from the inoculated mouse (sample 17); (b) the corresponding m/z 104.11 distribution image from the spinal cord tissue obtained from the healthy un-inoculated control (sample 50); PCA results: (c) There is some overlap between the diseased and control sample; however, it is clear from the scores plot and (d) the corresponding loadings plot that sample 50 (un-inoculated control) groups more towards m/z 104.11.

5.7.7.4 Relapse Stage Tissue

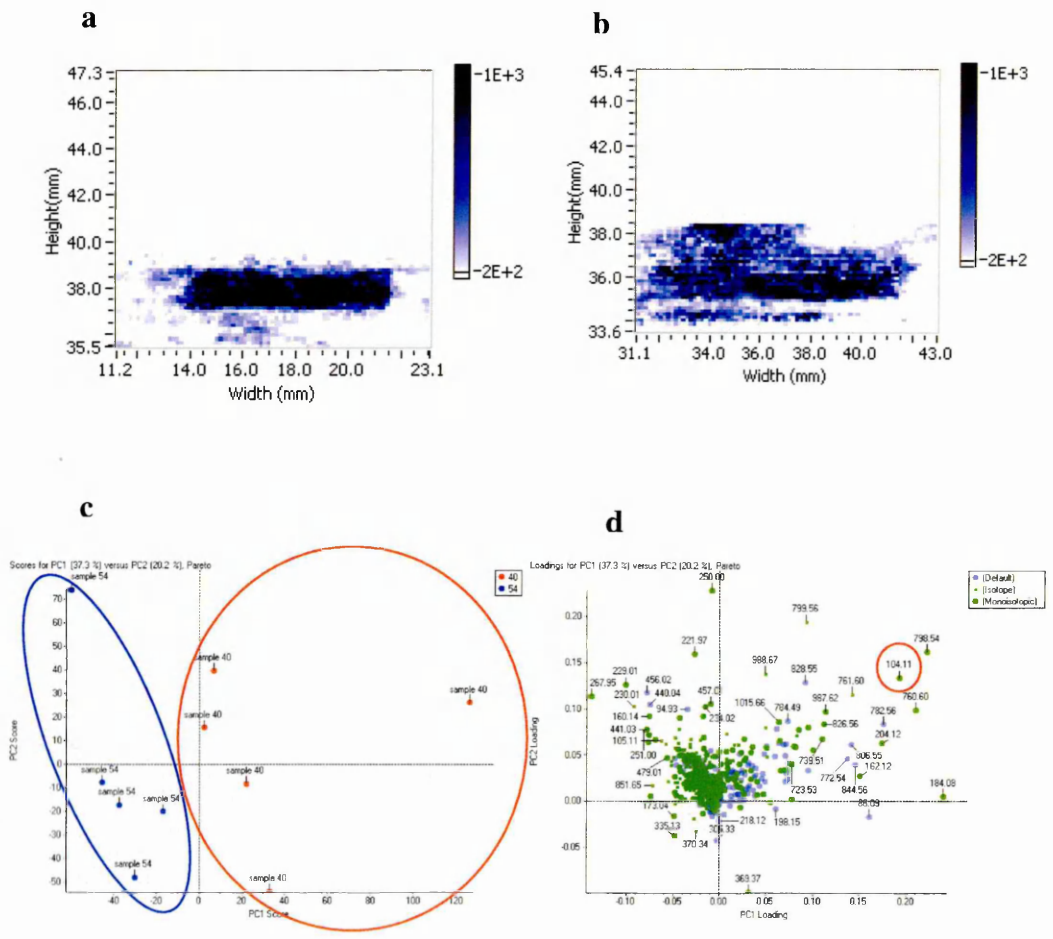

Figure 5.18: MALDI MS Images and Multivariate Analysis of Relapse Stage Disease Samples (Group 2): (a) the m/z 104.11 distribution in the spinal cord section taken from the inoculated mouse (sample 40); (b) the corresponding m/z 104.11 distribution image from the spinal cord tissue obtained from the healthy un-inoculated control (sample 54); PCA results: (c) There is significant grouping between the diseased and control sample; however, it is clear from the scores plot and the corresponding loadings plot (d) that sample 40 (inoculated control) groups more towards m/z 104.11.

5.7.7.5 Second Remission Stage Tissue

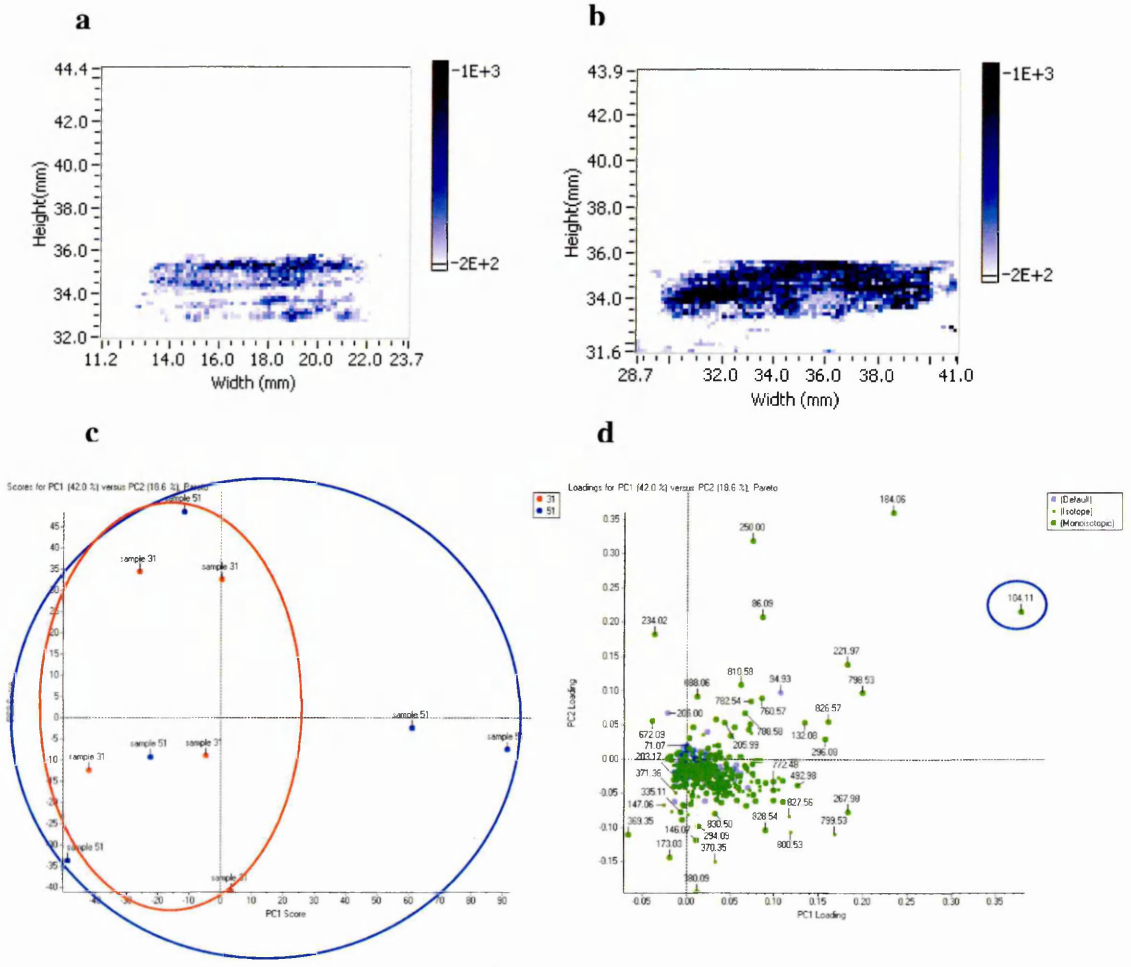

Figure 5.19: MALDI MS Images and Multivariate Analysis of Second Remission Stage Disease Samples (Group 2): (a) the m/z 104.11 distribution in the spinal cord section taken from the inoculated mouse (sample 31); (b) the corresponding m/z 104.11 distribution image from the spinal cord tissue obtained from the healthy un-inoculated control (sample 51); PCA results: (c) there is some overlap between the diseased and control sample; however, it is clear from the scores plot and (d) the corresponding loadings plot that sample 51 (inoculated control) groups more towards the m/z 104.11.

5.7.7.6 Statistical Comparisons

A Kolmogorov-Smirnov test revealed that the sample is normally distributed: Z = 0.8346; p>0.05. An independent-samples t-test was used to assess the significance of differences between disease and matched control sample means for each stage of CREAE progression.

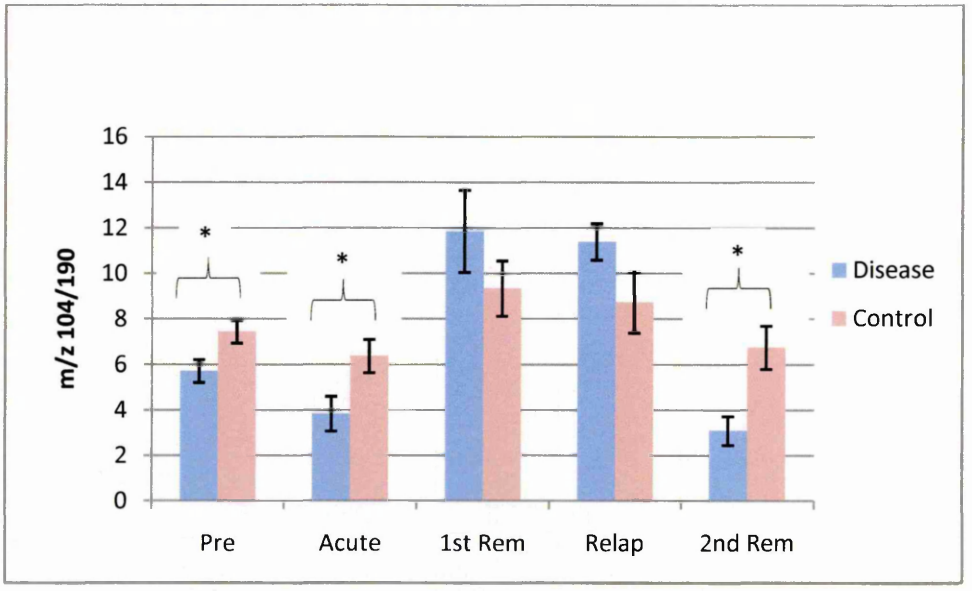

Figure 5.20: Group 2 Disease Stage Comparisons: A graph to show the diffrences between the diseased and control tissue samples. The main differences are observed to be at the acute, relapse and second remission stages. (*=P<0.05, **=P<0.01, ***=P<0.001).

Disease Stage	t statistic	Significant?
Pre-disease	-2.43	Yes*
Acute	-2.39	Yes*
1st remission	1.15	No
Relapse	1.64	No
2nd Remission	-3.20	Yes*

Table 5.3: t-test Results for Group 2 Disease Stage Comparisons. Data relates to figure 5.20 and corresponding significance (*=P<0.05, **=P<0.01, ***=P<0.001).

Group 2 experiments were undertaken to assess the reproducibility; however, the data generated did not support the first group of data. The t-test indicated that pre-disease, acute and second remission were significant; however, it seems unlikely that the predisease samples should differ as there was no sign of inflammation in these samples when the histology was undertaken. This would need to be further investigated and could potentially be attributed to matrix interference. However, lesions where there are changes in the myelin without any evidence of inflammation have been reported [33]. Thus these apparent changes in choline may be a marker for this early type of lesion.

As the controls indicate that there are natural fluctuations in choline levels between the animals, biological variability between different animals is also significant and has made the interpretation of data from this small preliminary study tentative at present.

5.7.8 Combined Analysis (Group 1 & Group 2)

A Kolmogorov-Smirnov test on the combined data revealed that the sample is normally distributed: $Z = 0.147$; $p>0.05$. An independent-samples t test was used to assess the significance of differences between disease and matched control sample means for each stage of EAE progression with the pooled data from groups 1 and 2.

The pooling of the data from both group 1 and group 2 experiments shows that the abundance of the m/z 104.11 is only significant in the second remission samples.

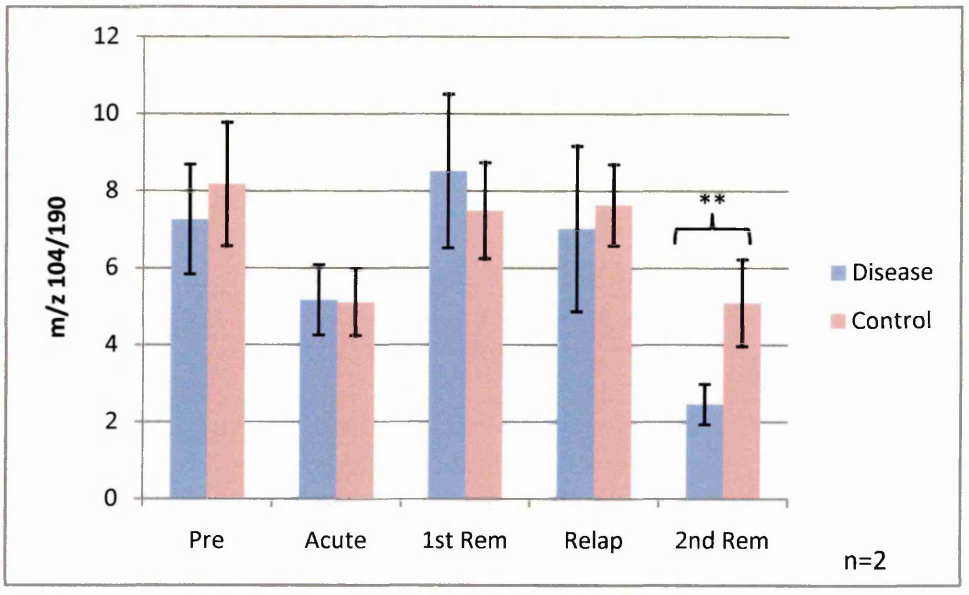

Figure 5.21: Combined Disease Stage Comparisons: A graph to show the diffrences between the diseased and control tissue samples where the data from groups 1 and 2 are pooled. The only significant difference was observed at the second remission stage. Any previous significance from the individual groups was lost (*=P<0.05, **=P<0.01, ***=P<0.001).

Disease Stage	t statistic	Significant?
Pre-disease	-0.60	No
Acute	0.08	No
1st remission	0.62	No
Relapse	-0.36	No
2nd Remission	-2.99	Yes**

Table 5.4: T-test Results for Combined Disease Stage Comparisons. Data relates to figure 5.21 and corresponding significance (*=P<0.05, **=P<0.01, ***=P<0.001).

In section 5.7.6 and 5.7.7 the results have been presented separately (i.e. the data has not been pooled for all the experiments) as the two sets of data generated do not support each other. By combining the data from experimental groups 1 and 2, significance between disease stage tissue and corresponding controls seen in the individual groups (as assessed by t-test statistic) was lost. Averaging the observed changes created greater variability within the different stages. This meant that differences were no longer statistically significant, as seen previously with acute, relapse (group1) and predisease, acute (group 2) disease stages (see figures 5.14, 5.20 and 5.21).

This highlights the importance of reproducibility between samples and the consideration of individual differences within animal populations, and emphasises the need for larger 'n' numbers when stating differences between biological samples. The use of larger 'n' numbers reduces the possibility of drawing false conclusions from experimental observations. The significance of biological variability has been acknowledged by Lay *et al.* stating that even in in-bred mice there is often significant biological variability [34].

Within this preliminary data, however, the second remission disease stage of CREAE retained statistical significance for the normalised choline intensity, as compared with healthy control tissue, when the groups were combined. The lower level of choline in this stage of the disease may be of potential biological and clinical relevance as lower choline levels have previously been reported [26].

5.9 Conclusion

The use of MALDI MSI generated some interesting results; however, the presence of interfering matrix peaks in the spectral region of interest proved to be a problem. The tandem mass spectrometric (MS/MS) analysis confirmed that it is possible that the peak at m/z 104.11 could be attributed to the presence of choline within the tissue section. However, the mass of the matrix peak and the choline mass are very close and therefore, although the images have been generated for m/z 104.11 and normalised against the matrix peak at m/z 190.05, any fluctuations in the matrix ion

also at m/z 104 could potentially produce a misleading image. This could be further investigated by acquiring images in MS/MS mode i.e.; this preliminary non-targeted study could be further investigated using a targeted approach.

The sample preparation procedure, with a particular emphasis on the embedding of the tissue prior to cryosectioning, may also need to be re-evaluated as a few of the images appear not to be as well defined as other images generated. This could be due to the transfer of choline, a water soluble compound to the CMC, as the CMC was prepared in water. This would need to be further investigated. However, a more likely explanantion is the possible interference from the matrix peak as the imaging software only permits images to be accurate to two decimal places. Therefore any fluctuations in the measured mass of the matrix peak at m/z 104.10 could produce the ill-defined edges observed around the edge of the spinal cord.

Another point of discussion is whether the choline detected and confirmed by MS/MS experiments is free choline or a fragment ion arising from choline-containing phospholipids by the laser energy settings used for these experiments. Therefore, the data is very preliminary for the reasons previously stated and further experimentation would be required in order to confidently reach any conclusions from this study.

The preliminary data presented shows that MALDI MSI can be used for the imaging of spinal cord sections. The results of the PCA show that there are other masses that appear to be different in the inoculated and un-inoculated. These masses could be further investigated in order to establish the compound identification and to ensure that there is no interfering matrix peaks in the spectral region of interest.

Further experiments could be performed on the rest of the spinal cord; this could establish if there are differences in metabolite levels down the length of the spinal cord. This would be particularly difficult to achieve in the diseased animals as the spinal cord is very weak towards the bottom and often falls to pieces prior to snap freezing. It would therefore be very difficult to cryosection the spinal cord samples and maintain the same orientation between the controls and the diseased animals. Experiments could also be performed on the brain tissue of the same animals to

establish if the observed metabolites in the spinal cord correspond with those that are present in the brain.

A proteomics strategy could also be used to complement the results obtained with the non-targeted metabolomics to assess the distribution of small molecules in areas of demyelination. This could be achieved by performing a tryptic digest on the spinal cord section prior to mass spectrometric analysis as the proteins have masses of approximately 30kDa [35] and the cytokines that are associated with inflammation have masses around 20kDa [36].

The results from this preliminary study demonstrate that MALDI MS is a suitable technique to directly analyse tissue samples. Due to time constraints, in this preliminary study the combined data of n=2 is not sufficient enough to make any significant biological conclusions and the analysis of many more samples is required.

5.10 References

[1] Inglese M., Li B. S. Y., Rusinek H., Babb J. S., Grossman R. I., Gonen O. Diffusely elevated cerebral choline and creatine in relapsing-remitting multiple sclerosis. Magnetic Resonance in Medicine, 2003, 50, 190-195.

[2] Griffin J. L., Kauppinen R. A. Tumour metabolomics in animal models of human cancer. Journal of Proteome Research, 2007, 6, 498-505.

[3] Griffin J. L. Understanding mouse models of disease through metabolomics. Current Opinion in Chemical Biology, 2006, 10, 309-315.

[4] Barba I., Fernandez-Montesinos R., Garcia-Dorado D., Pozo D. Alzheimer's disease beyond the genome era: nuclear magnetic resonance (NMR) spectroscopy-based metabolomics. Journal of Cellular and Molecular Medicine, 2008, 12, 1477-1485.

[5] Bischoff R., Luider T. M. Methodological advances in the discovery of protein and peptide disease markers. Journal of Chromatography B, 2004, 803, 27-40.

[6] Dunn W. B., Ellis D. I. Metabolomics: Current analytical platforms and methodologies. TrAC Trends in Analytical Chemistry, 2005, 24, 285-294.

[7] Pendyala G., Want E. J., Webb W., Siuzdak G., Fox H. S. Biomarkers for NeuroAIDS: The widening scope of metabolomics. Journal of Neuroimmunology and Pharmacology, 2007, 2, 72-80.

[8] Liao H., Wu J., Kuhn E., Chin W., Chang B., Jones M. D., O'Neil S., Clauser K. R., Karl J., Hasler F., Roubenoff R., Zolg W., Guild B. C. Use of mass spectrometry to identify protein biomarkers of disease severity in the synovial fluid and serum of patients with rheumatoid arthritis. Arthritis and Rheumatism, 2004, 50, 3792-3803.

[9] Mbeunkui F., Metge B. J., Shevde L. A., Pannel L. K. Identification of differentially secreted biomarkers using LC-MS/MS in isogenic cell lines representing a progression of breast cancer. Journal of Proteome Research, 2007, 6, 2993-3002.

[10] Stoop M. P., Dekker L. J., Titulaer M. K., Burgers P. C., Sillevis Smitt P. A. E., Luider T. M., Hintzen R. Q. Multiple sclerosis-related proteins identified in cerobrospinal fluid by advanced mass spectrometry. Proteomics, 2008, 8, 1576-1585.

[11] Ceuppens R., Dumont D., Van Brussel L., Van de Plas B., Daniels R., Noben J-P., Verhaert P., Van der Gucht E., Robben J., Clerens S., Arckens L. Direct profiling of myelinated and demyelinated regions in mouse brain by imaging mass soectrometry. International Journal of Mass Spectrometry, 2007, 260, 185-194.

[12] Wikoff W. R., Gangoiti J. A., Barshop B. A., Siuzdak G. Metabolomics identifies perturbations in human disorders of propionate metabolism. Clinical Chemistry, 2007, 53, 2169-2176.

[13] Boudonck K. J., Mitchell M.W., Nemet L., Keresztes L., Nyska A., Shinar D., Rosenstock M. Discovery of metabolomics biomarkers for early detection of nephrotoxicity. Toxicological Pathology, 2009, 37, 280-292.

[14] Monroe E.B., Annangudi S. P., Hatcher N. G., Gutstein H. B., Rubakhin S. S., Sweedler J. V. SIMS and MALDI MS imaging of the spinal cord. Proteomics, 2008, 8, 3746-3754

[15] http://www.mssociety.org.uk/about_ms/index.html
Last accessed 10th May 2009.

[16] http://www.mssociety.org.uk/about_ms/what_is_ms/index.html
Last accessed 10th May 2009.

[17] Bruck W. The pathology of multiple sclerosis is the result of focal inflammatory demyelination with axonal damage. Journal of Neurology, 2005, 252, v3-v9.

[18] Compston A., Coles A. Multiple Sclerosis. The Lancet, 2002, 359, 1221-31.

[19] Bot J. C. J, Barkof F., Lycklama, Nijehalt G., van Schaardenburg D., Voskuyl A. E, Ader H. J, Pijnenburg J. A. L., Polman C. H., Uitdehaag B. M. J., Vermeulen E. G. J., Castelijn J. A. Differentiation of multiple sclerosis from other inflammatory

disorders and cerebrovascular disease: value of spinal MR imaging. Radiology, 2002, 223, 46-56.

[20] Tartaglino L. M., Friedman D. P., Flanders A. E., Lublin F. D., Knobler R. L., Liem M. Multiple sclerosis in the spinal cord: MR appearance and correlation with clinical parameters. Radiology, 1995, 195, 725-732.

[21] Miller D. H., Grossman R. I., Reingold C., McFarland H. F. The role of magnetic resonance techniques in understanding and managing multiple sclerosis. Brain, 1998, 121, 3-24.

[22] Imrell K., Greiner E., Hillert J., Masterman T. HLA-DRB1*15 and cerobrospinal-fluid specific oligoclonal immunoglobulin G bands lower age at attainment of important disease milestones in multiple sclerosis. Journal of Neuroimmunology, 2009, 210, 128-130.

[23] Kendi A. T. K, Tan F. U., Kendi M., Huvaj S., Tellioglu S. MR spectroscopy of cervical spinal cord in patients with multiple sclerosis. Neuroradiology, 2004, 46, 764-769.

[24] Tartaglia M. C., Narayanan S., De Stefano N., Arnaoutelis R., Antel S. B., Francis S. J., Santos A. C., Lapierre Y., Arnold D. L. Choline is increased in pre-lesional normal appearing white matter in multiple sclerosis. Journal of Neurology, 2002, 249, 1382-1390.

[25] Chard D. T., Griffin C. M., McLean M. A., Kapeller P., Kapoor R., Thompson A. J., Miller D. H. Brain metabolite changes in cortical grey and normal-appearing white matter in clinically early relapsing-remitting multiple sclerosis. Brain, 2002, 125, 2343-2352.

[26] Gustafsson M. C., Dahlqvist O., Jaworski J., Lundberg P., Landtblom A. M. Low choline concentrations in normal-appearing white matter of patients with multiple sclerosis and normal MR imaging brain scans. American Journal of Neuroradiology, 2007, 28, 1306-1312.

[27] Heremans H., Dillen C., Groenen M., Martens E., Billiau A. Chronic relapsing experimental autoimmune encephalomyelitis (CREAE) in mice: enhancement by monoclonal antibodies against interferon-γ. European Journal of Immunology, 1996, 26, 2393-2398.

[28] Steinman L., Zamvil S. S. How to successfully apply animal studies in experimental allergic encephalomyelitis to research on multiple sclerosis. Annals of Neurology, 2006, 60, 12-21.

[29] Rock D. M. Design and analysis of experiments with high throughput biological assay data. Seminars in Cell and Developmental Biology. 2004, 15, 703.

[30] Baker, D., O'Neill, J.K., Gschmeissner, S.E., Wilcox, C.E., Butter, C., Turk, J.L.,. Induction of chronic relapsing experimental allergic encephalomyelitis in Biozzi mice. Journal of Neuroimmunology, 1990, 28, 261-270.

[31] Baker D., Jackson S. J. Models of Multiple Sclerosis. Advances in Clinical Neuroscience and Rehabilitation, 2007, 6, 10-12.

[32] http://metlin.scripps.edu/metabo_search.php
Last accessed 10th May 2009.

[33] Kornek B., Storch M. K., Weissert R., Wallstroem E., Stefferi A., Olsson T, Linington C., Schmidbauer M., Lassmann H. Multiple Sclerosis and Chronic Autoimmune Encephalomyelitis. American Journal of Pathology, 157, 267-276.

[34] Lay Jr J. O., Borgmann S., Liyanage R., Wilkins C. L. Problems with the "omics." Trends in Analytical Chemistry, 2006, 25, 1046-1056.

[35] van der Goes A., Boorsma W., Hoekstra K., Montagne L., de Groot C. J. A., Dijkstra C. D. Determination of the sequential degradation of myelin proteins by macrophages. Journal of Neuroimmunology, 2005, 161, 12-20.

[36] Murphy F. J., Hayes I, Cotter T. G. Targeting inflammatory disease via apoptotic mechanisms. Current Opinion in Pharmacology, 2003, 3, 412-419.

Chapter 6

Conclusion and Suggestions for Future Work

6.0 Conclusion and Suggestions for Future Work

The work presented in this thesis demonstrates the versatility of MALDI MSI for a range of different samples. Methodology has been developed for the analysis of pharmaceutical compounds (Chapters 2 and 3) and for the application of MALDI MSI as a potentially new technique for metabolomic studies (Chapters 4 and 5). The quality of the data obtained from MALDI MS is dependent on many factors; the most influential of which are related to the type of sample to be analysed, for example the type of tissue to be analysed and the sample preparation procedures employed prior to the analysis.

The analysis of anti-asthmatic drugs in lung tissue proved to be quite a challenging experiment due to the ion suppression brought about from the endogenous compounds contained within this type of tissue such, for example relatively high salt concentrations. Also, the type of compound to be analysed was a major factor in the overall success of an experiment as some compounds ionise more readily than others; this was observed with Fluticasone Propionate and GSK256066B. Drug distribution studies can provide valuable information relating to the overall drug efficiency, for example it has been reported in the literature that Fluticasone Propionate has been observed to accumulate in the lung undissolved; this is clearly an issue in terms of how effective the drug is in relieving the symptoms of the patient. As there were problems with the co-crystallisation process with the organic matrix α-CHCA on the surface of the lung tissue due to the presence of endogenous compounds such as high salt concentrations, a blotting approach was used as an alternative in an attempt to analyse the drugs that couldn't be detected directly. Particle suspension matrices were also investigated as an alternative to the more conventional organic acid matrices as they work via a thermal effect in contrast to the co-crystallisation that occurs between organic acid matrices and the sample. Future studies in this area could involve derivatisation of the anti-asthmatic compounds to make them more easily ionisable, this could be achieved through the matrix application by modifying the matrix, thus derivatising the compound of interest in situ.

Another type of pharmaceutical analysis was performed in chapter 3 whereby tablet pharmaceutical formulations were analysed in an attempt to obtain information relating to the homogeneity of the active drug throughout the excipients contained within tablet formulations. This can provide valuable information that relates back to the manufacture of the tablet, this is especially important in slow release formulations. The importance of the sample preparation procedure is highlighted with regard to the sample morphology. It was found that tablets with a curved surface produced poor quality images due to a potential laser focussing problem resulting in the doughnut effect that can be clearly seen in the data. Future experiments could be undertaken to investigate the optimum laser positioning for such studies.

In Chapters 4 and 5 MALDI MSI has been assessed for its contribution to existing techniques that are used to study metabolomics. The concept of metabolomics arose primarily from the analysis of plant tissue and is gaining prominence in the area of biomarker discovery. The requirements for high throughput techniques that can detect metabolites in parallel make MALDI MSI a logical consideration to provide complementary information to existing techniques such as LC-MS. The work presented in chapter 4 details a metabolomics approach to study the metabolites contained within wheat grains. Aspects of the sample preparation procedure in relation to preserving the metabolic status of the tissue section have been discussed. A major problem with this type of analysis was not surprisingly the interference of matrix peaks in the spectral regions of interest and the suppression of the metabolites due to the presence of intense matrix peaks. However, the matrix peaks can also act as internal calibrants that are useful for the recalibration of data for accurate mass measurement. A range of matrices were tested in an attempt to increase the achievable sensitivity. F20TPP matrix peaks occur at around m/z 800 - m/z 1000; however, this matrix did not appear to ionise the endogenous metabolites contained within the section as well as α-CHCA and appeared to suppress the ionisation of the sugars that were observed using α-CHCA. The use of gold and silver nanoparticles was also investigated but did not yield good results. This is probably because they do not co-crystallise with the sample and thus extract the metabolites; this is also true of the particle suspension matrices that have also been investigated. As consistency

with sample preparation is a critical factor in achieving high quality reproducible data, a number of commercially available devices have been developed in order to control the variability in the matrix application procedure, however their use is generally not suited to the use of particle suspension matrices and nanoparticles due to problems encountered with devices that use a small diameter needle to apply the matrix as these matrices can block the needle.

The IR LDI MS data obtained from the collaboration with the University of Munster provided a matrix free option to obtain data that was purely sample related. This is because the IR laser emits at a different wavelength to UV lasers such as Nd: YAG and Nitrogen lasers that is also the wavelength at which water molecules absorb, thus residual water contained within samples acts as an endogenous matrix promoting the ionisation of molecules from the sample surface. The sugar ions dominate the spectra and this could have potentially suppressed the ionisation of the less abundant smaller mass metabolites. However, a compromise had to be reached between the preparation of the plant tissue and the associated instrumental parameters; the use of freeze dried tissue did not produce good results but this isn't surprising considering that the freeze drying process removes the residual water from the tissue. Rehydrating experiments could be used to help combat this problem, however this would result in the delocalisation of the metabolites and results generated from profiling/imaging experiments would potentially be misleading.

The establishment of methodology for plant material in Chapter 4 led into the animal work described in Chapter 5 where MALDI MSI was used to investigate the animal model of multiple sclerosis (chronic relapsing experimental autoimmune encephalomyelitis) in an attempt to discriminate at the metabolomics level between healthy controls and the corresponding diseased tissue at five different stages of the disease progression. The images obtained correlated with the multivariate analysis obtained by performing principal component analysis on the data generated. The results obtained showed that potentially choline levels can fluctuate from animal to animal as can be observed from the control samples. However, at the specified stages in the disease process it was found that the levels of choline detected were different to those of the control samples. The data presented in this chapter is very

preliminary and to draw any significant biological conclusions from the data obtained more samples would need to be analysed.

Metabolomics experiments generate large volumes of data and it is not feasible to conduct MS/MS experiments for every mass that is detected at present using MALDI MSI, especially in non-targeted metabolomics experiments. The development of appropriate software for high throughput metabolomics using MALDI is crucial to the future analyses. Software is currently available from Waters (MS^E) for LC-MS analyses that acquire both MS and MS/MS data simultaneously; a similar approach would be useful for MALDI analyses as this would immediately eliminate the matrix peaks observed from the endogenous compounds contained within the sample of interest and help in the identification of unknown masses. There is a lack of complete databases for metabolomic studies, the development of metabolite searching software would be beneficial as many databases can contain metabolites that are found in many organisms and they don't always take into account the adducts that are commonly formed in MALDI analyses, therefore in some instances the data has to be converted into the corresponding neutral masses.

Mass spectrometry is becoming increasingly popular due to its expanding role in the biosciences. It is an unparalled technique in many ways owing to its excellent sensitivity, specificity, speed, it can be applied to many classes of compound and it can be coupled to separation techniques if required. With advancements in mass spectrometers and data processing applications, the role of mass spectrometry is ever increasing and will be adopted furthermore in the advancement of biomedical research.

Appendices

Appendix 1

Oral Presentations

"Imaging the Distribution of Endogenous Compounds in Biological Tissue"
ASMS, Seattle Applied Biosystems Luncheon (May 2006).

Presented a workshop on data analysis using BioMap software. Society for Experimental Biology, University of Kent (April 2006).

Poster Presentations

"Matrix-Assisted Laser Desorption Ionisation Mass Spectrometry Imaging of Small Molecules in Brain Tissue"
BMSS, York 2008.

"Tablet Imaging Using Matrix-Assisted Desorption Ionisation Mass Spectrometry"
(updated version 2), ASMS, Denver 2008 and BMSS, Edinburgh 2007 (version 1).

"Metabolite Profiling of Wheat Grains by Imaging Matrix-Assisted Laser Desorption Ionisation Mass Spectrometry"
Imaging Mass Spectrometry Conference, Sanibel and the Royal Society of Chemistry Analytical Research Forum (RSC ARF), Glasgow 2007.

"Investigating the Distribution of Metabolites in Wheat by Imaging Matrix-Assisted Laser Desorption Ionisation Mass Spectrometry"
ASMS, Seattle, International Mass Spectrometry Conference (IMSC), Prague and RSC ARF, Cork 2006.

Appendix 2

Publications

Earnshaw C. J., Atkinson S. J., Burrell M. M., Clench M. R. **Matrix Assisted Laser Desorption Ionisation Mass Spectrometry Imaging – Principles and Applications.** Metabolomics, Metabonomics and Metabolite Profiling. Griffith W. J. (editor), November 2007.

Burrell M. M., Earnshaw C. J., Clench M. R. **Imaging Matrix Assisted Laser Desorption Ionisation Mass Spectrometry: a technique to map plant metabolites within tissues at high spatial resolution.** Journal of Experimental Botany, 2007; 58: 757-763.